General Motors Corporation
Legal Staff

Facsimile
(586) 492-2928

Telephone
(586) 947-9212

MAY 10 2002

L. Robert Shelton,
Executive Director
NATIONAL HIGHWAY TRAFFIC
SAFETY ADMINISTRATION
400 Seventh Street, S.W., Room 5220
Washington, DC 20590

Dear Mr. Shelton:

Re: **Settlement Agreement**
Section B. Fire Safety Research

On August 31, 2001, GM submitted a final report for Project B.3 (Fire Initiation and Propagation Tests), entitled, "Evaluation of Motor Vehicle Fire Initiation and Propagation/Part 6: Propagation of an Underbody Gasoline Pole Fire in a 1997 Rear Wheel Drive Passenger Car." This letter supplements that report.

A technical error was recently identified on page 8, second paragraph, of the B.3 final report. Specifically, one of the units of measurement referenced on that page was incorrect. The report states, "The needle valve was adjusted to give a flow rate of approximately 500 cm^3/s, measured before the test by collecting the gasoline effluent in a graduated container for a specified period of time." The actual flow rate was approximately 500 cm^3/min.

Enclosed is a corrected replacement page for your records. I apologize for any confusion this error may have caused.

Yours truly,

D.K. Nowak-Vanderhoef

Deborah K. Nowak-Vanderhoef
Attorney

Enclosure

Mail Code: 480-210-225
Vehicle Engineering Center 30001 Van Dyke Avenue Warren, Michigan 48090-9020

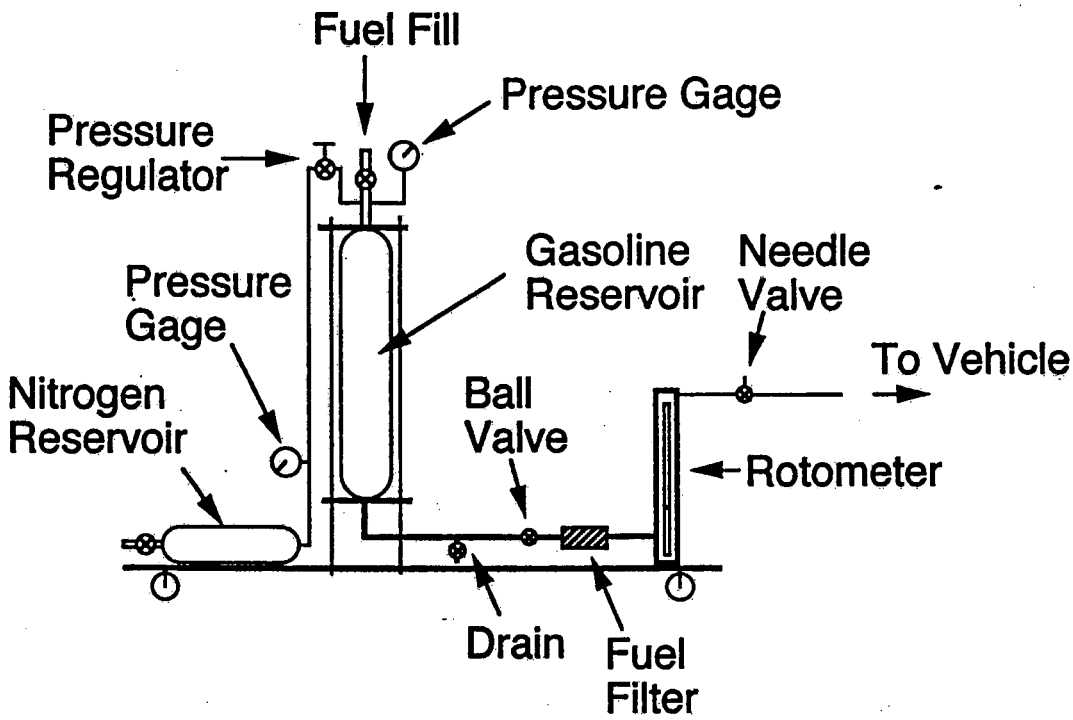

Figure 5. Fire Test F971001. Schematic diagram of the external gasoline reservoir and delivery system used to artificially supply gasoline to the test during this test.

The outlet of the tube was located at the lower left edge of the fuel tank, below the area where the fuel filler tube enters the fuel tank. The outlet of the tube was fitted with a flow restrictor (i.d. = 0.125") to reduce vaporization of gasoline by maintaining some back-pressure in the delivery tube.

Gasoline (4 L) was added to a steel fluid reservoir (4 L). The gas reservoir was filled with dry nitrogen gas. The pressure regulator was adjusted to maintain a head pressure of 275 kPa (25.0 psi) in the fluid reservoir. Before the test, the delivery tube was purged with gasoline before the start of the test to eliminate air. The needle valve was adjusted to give a flow rate of approximately 500 cm^3/min, measured before the test by collecting the gasoline effluent in a graduated container for a specified period of time.

A valve approximately 3 feet from the outlet of the gasoline delivery tube was mounted to the right outer quarter panel and opened to start the flow of gasoline during this test. The flow rate of gasoline through the delivery tube was determined from readings taken from the rotometer. The

B.3

General Motors Corporation
Legal Staff

Facsimile
(810) 492-2928

Telephone
(810) 947-9212

AUG 31 2001

L. Robert Shelton,
Executive Director
NATIONAL HIGHWAY TRAFFIC
SAFETY ADMINISTRATION
400 Seventh Street, S.W., Room 5220
Washington, DC 20590

Dear Mr. Shelton:

Re: **Settlement Agreement**
Section B. Fire Safety Research

Enclosed is a final report prepared by Jeffrey Santrock of General Motors Corporation, entitled, "Evaluation of Motor Vehicle Fire Initiation and Propagation/Part 6: Propagation of an Underbody Gasoline Pool Fire in a 1997 Rear Wheel Drive Passenger Car."

This report relates to Project B.3 (Fire Initiation and Propagation Tests).

Yours truly,

D. K. Nowak-Vanderhoef

Deborah K. Nowak-Vanderhoef
Attorney

Enclosure

Mail Code: 480-206-335
Cadillac Building 30009 Van Dyke Avenue Warren, Michigan 48090-9055

Evaluation of Motor Vehicle Fire Initiation and Propagation Part 6: Propagation of an Underbody Gasoline Pool Fire in a 1997 Rear Wheel Drive Passenger Car

Jeffrey Santrock
General Motors Corporation

ABSTRACT

This report describes a vehicle fire propagation test conducted pursuant to the GM/DOT Settlement Agreement. This fire test was conducted on September 30, 1997. The test vehicle was a crash-tested 1997 Chevrolet Camaro. In the crash test, the test vehicle was stationary and struck in the rear by a moving barrier. No leaks were detected in the fuel system of the test vehicle during the crash test or the subsequent roll test performed after the crash test. No fire was observed during the crash test, nor was there evidence of fire present in the test vehicle after the crash test. To create a gasoline pool under the test vehicle for the fire test, a gasoline delivery system consisting of a gasoline reservoir, compressed nitrogen reservoir, a pressure regulator, and a flow regulator was used to deliver liquid gasoline under the test vehicle during this test. The flow rate of gasoline delivered by this system was 515 ± 20 cm^3/s. A hand-held propane torch was used to ignite the gasoline. The fire was allowed to burn until flames spread into the passenger compartment and along the headlining panel to the front of the passenger compartment. Flames appear to have entered the passenger compartment through seam openings around the left rear wheelhouse, a gap under the driver's door, and through a floor pan drain hole. Heating of the carpet by conduction through the floor pan also appears to have played a role in flame-spread into the passenger compartment. The carpet, the interior left quarter trim finishing panel, and the left rear seat cushion were burning 170 seconds after the gasoline pool was ignited. Flames started to spread forward along the lower surface of the headlining panel between 180 and 190 seconds after ignition. Fire suppression started approximately 210 after ignition.

Table of Contents

Appendices

Evaluation of Motor Vehicle Fire Initiation and Propagation Part 6: Propagation of an Underbody Gasoline Pool Fire in a 1997 Rear Wheel Drive Passenger Car

Jeffrey Santrock
General Motors Corporation

ABSTRACT

This report describes a vehicle fire propagation test conducted pursuant to the GM/DOT Settlement Agreement. This fire test was conducted on September 30, 1997. The test vehicle was a crash-tested 1997 Chevrolet Camaro. In the crash test, the test vehicle was stationary and struck in the rear by a moving barrier. No leaks were detected in the fuel system of the test vehicle during the crash test or the subsequent roll test performed after the crash test. No fire was observed during the crash test, nor was there evidence of fire present in the test vehicle after the crash test. To create a gasoline pool under the test vehicle for the fire test, a gasoline delivery system consisting of a gasoline reservoir, compressed nitrogen reservoir, a pressure regulator, and a flow regulator was used to deliver liquid gasoline under the test vehicle during this test. The flow rate of gasoline delivered by this system was 515 $\pm$ 20 cm^3/s. A hand-held propane torch was used to ignite the gasoline. The fire was allowed to burn until flames spread into the passenger compartment and along the headlining panel to the front of the passenger compartment. Flames appear to have entered the passenger compartment through seam openings around the left rear wheelhouse, a gap under the driver's door, and through a floor pan drain hole. Heating of the carpet by conduction through the floor pan also appears to have played a role in flame-spread into the passenger compartment. The carpet, the interior left quarter trim finishing panel, and the left rear seat cushion were burning 170 seconds after the gasoline pool was ignited. Flames started to spread forward along the lower surface of the headlining panel between 180 and 190 seconds after ignition. Fire suppression started approximately 210 after ignition.

Table of Contents

Appendices

List of Figures

Report

Appendices

List of Tables

Report

Appendices

1 Introduction and Test Summary

This report describes a full-scale vehicle fire test conducted on September 30, 1997. This test was conducted by General Motors (GM) pursuant to an agreement between GM and the U.S. Department of Transportation. As part of this agreement, General Motors and the National Highway Traffic Safety Administration (NHTSA) jointly have developed 13 separate vehicle fire safety research projects. One of these projects, entitled "Fire Initiation and Propagation Tests", involves conducting vehicle crash tests to investigate potential ignition events that occur in vehicle crashes, and subsequent vehicle fire tests to characterize fire propagation in these crash-tested vehicles. The vehicle models to be tested, and the crash- and fire-test methods to be used for Project B.3 are described in another report [1]. The objectives of these fire tests are:

- To determine the principal fire paths and time-lines for flame propagation into the passenger compartment under the test conditions;
- To identify which components burn and to measure the thermal environments around those components associated with their ignition under the test conditions; and
- To measure air temperatures, heat fluxes, and combustion gas concentrations in the passenger compartment under the test conditions.

The vehicle used in that test was a 1997 Chevrolet Camaro (VIN: 2G1FP22K1V219145) with the following options: 3.8 liter 6-cylinder engine, a 4-speed automatic transmission, air conditioning, a six-way power driver's seat, and 16-inch aluminum wheels.

The test vehicle was crash tested on January 8, 1997 at the General Motors Proving Ground in Milford, Michigan [2]. In the crash test, this vehicle was stationary and was struck in the left rear (driver's side) by a moving barrier. The barrier had a deformable aluminum honeycomb face similar to that described in FMVSS214 [3]. The test vehicle was parked with the brakes on and positioned so that the longitudinal midline of the test vehicle was parallel to the direction of motion (velocity vector) of the barrier. The mass of the test vehicle, including Anthropomorphic Test Devices and test instrumentation, was 1,811 kg (3,992 lbs.). The mass of the barrier was 1370 kg (3020 lbs.).

The barrier impacted the rear of the test vehicle speed at 84.7 km/h (52.6 mph). The longitudinal center-line of the test vehicle was parallel to the direction of motion of the barrier. The test vehicle was offset to the right so that approximately 70% of the barrier face overlapped the rear of the test vehicle. The maximum change in velocity of the test vehicle was 38 km/h (23.6 mph). The fuel system of the test vehicle did not leak at any time during the crash or subsequent static roll test

performed as specified in MVSS301 [4]. A detailed description of this test can be found in another report [2].

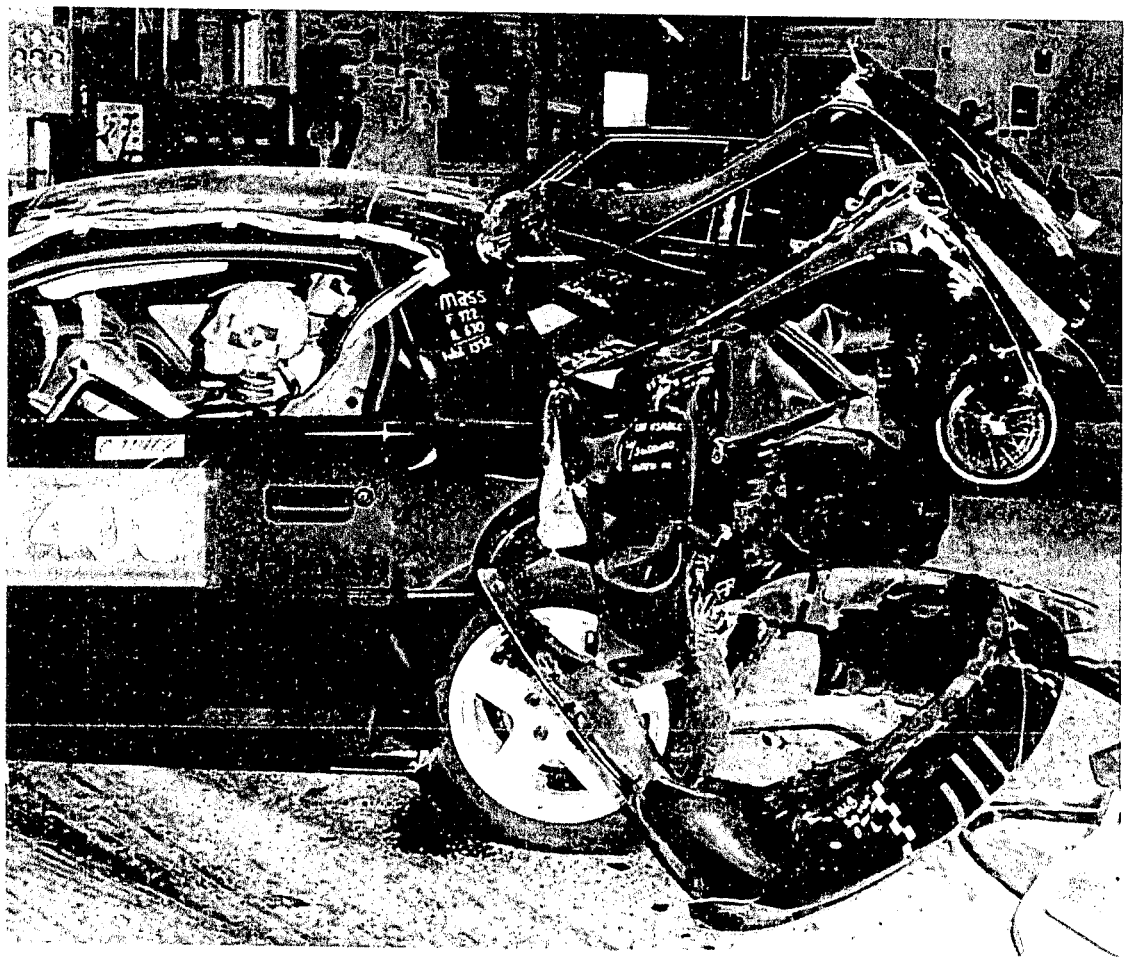

Figure 1. Fire Test F971001. Photograph of the test vehicle after the crash test.

Figure 1 is a photograph of the test vehicle after the crash test. The residual crush to the test vehicle was 1080 mm on the left side of the test vehicle and 610 mm on the right side of the test vehicle. The left side door window shattered during the crash test. The rear compartment lift window panel was broken and the rear compartment lift window was glass shattered. The left quarter interior trim finishing panel was dislodged and pushed forward (Fig. 1). The left door was pushed outward slightly creating a gap between the bottom of the door and the lower section of doorframe (Fig. 1). The carbon absorbant from the evaporative emission canister, which ruptured during the crash test, spilled onto the ground in front of the left rear tire (Fig. 1).

Figure 2 is a photograph showing a side-view of the area around the left rear wheelhouse of the test vehicle after the crash test. Figure 3 is a photograph showing a front-view of the area around the left rear wheelhouse of the test vehicle after the crash test. A seam opening between the rear floorpan panel and left inner quarter panel is visible in the photographs shown in both of these figures. The fuel filler tube splash shield and left rear tire are visible through the seam opening (Fig. 3).

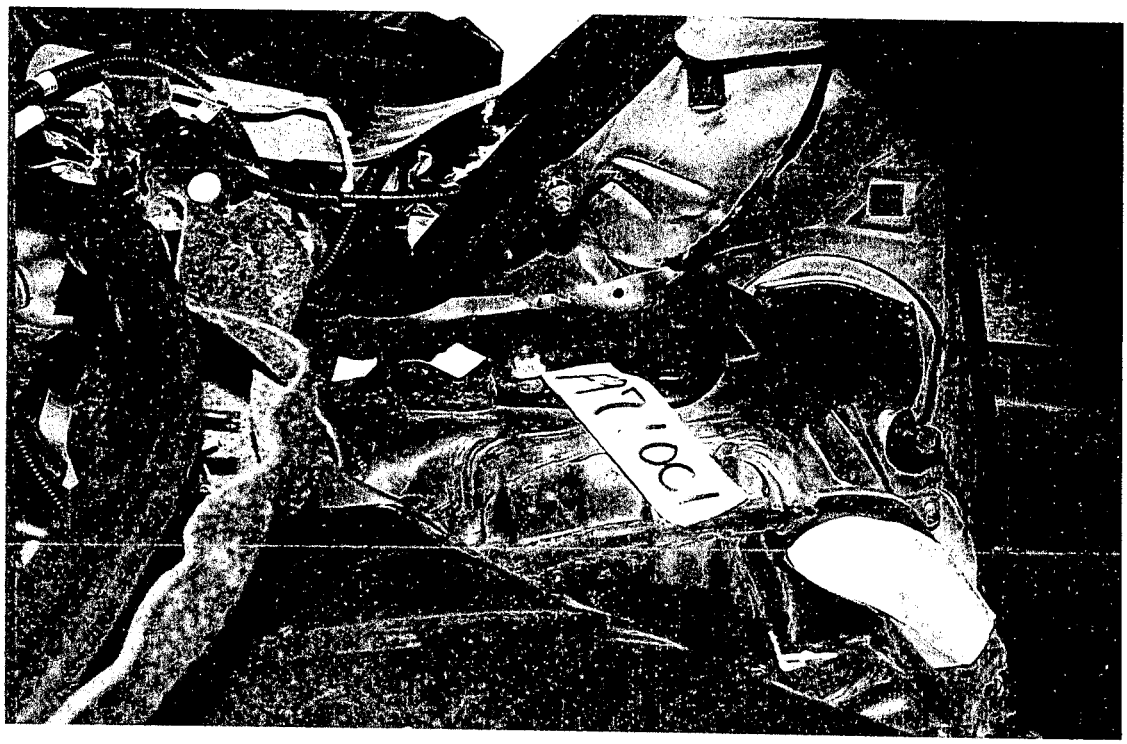

Figure 2. Fire Test F971001. Photograph of the area around the left rear wheelhouse of the test vehicle after the crash test.

The fire test was designed to study propagation of an under-body gasoline pool fire into the passenger compartment. Table 1 summarizes the timing of flame-spread into the passenger compartment along these pathways. Table 1 also includes estimated times of ignition of selected interior components.

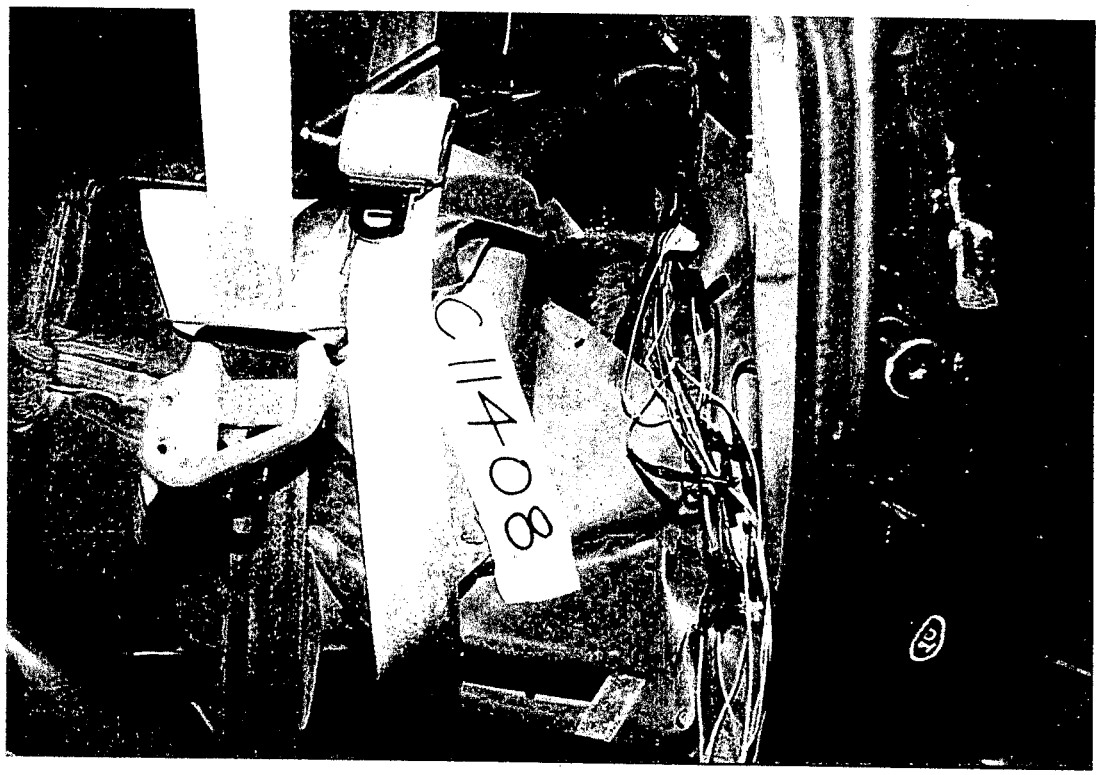

Figure 3. Fire Test F971001. Photograph showing a front-view of the area around the left rear wheelhouse of the test vehicle after the crash test. The left rear tire and a section of the left rear wheelhouse lining is visible through the seam opening.

The fuel system in the test vehicle did not leak as a result of the crash test. An artificial method of creating an underbody gasoline pool was used in this test. Gasoline was pumped continuously from an external reservoir onto the ground under the rear of the test vehicle during the fire test. The gasoline was ignited with a propane torch and allowed to burn until flames were observed spreading across the headlining panel in the test vehicle. Flames entered the passenger compartment through (i) seam openings around the left rear wheelhouse, (ii) a floor pan drain hole in the left rear section of the floor pan panel, and (iii) the gap between the bottom of the left door and the door frame. The signal to end the test and begin fire suppression was given 199 seconds after the gasoline was ignited.

Table 1

Summary of Fire Development during in Fire Test F971001

Time[1] (sec)	Event
-30	Start of gasoline flow
0	Gasoline vapor under the test vehicle was ignited using a propane torch
5	The temperature recorded by the thermocouple on top of the floor pan drain hole plug under the left rear seat cushion started to increase
7	Flames from the burning gasoline pool entered the passenger compartment through the seam opening around the left rear wheel house
12	Flames from the burning gasoline were visible in the left rear corner of the test vehicle
40 to 45	The fire plume disappeared from the left rear corner of the test vehicle
100 to 110	Flames from the burning gasoline pool ignited the rear bumper energy absorber
150 to 170	Ignition of the left quarter interior trim finishing panel
160	Flames burned through the floor pan drain hole plug located under the rear left seat cushion
175	Flames began to reach the left rear corner of the headlining panel
188	Flames burned through the carpet in the area between the rear seat cushions
199	Signal to begin fire suppression

[1]Time after ignition of the gasoline pool.

2 Vehicle Condition and Test Protocol

The fire test described in this report was conducted at the Factory Mutual Test Center in West Glocester, Rhode Island. The crash-tested vehicle was prepared for the fire tests at the General Motors Research and Development Center (GM R&D Center) in Warren, Michigan, and shipped to the Factory Mutual Test Center. The test vehicle was returned to the GM R&D Center after the fire test, where it was systematically disassembled to permit closer inspection of the fire damage and identification of fire spread paths that were not obvious during the tests.

A description of the video cameras used in during this test is in **APPENDIX A**. A description of the infrared cameras used in this test is in **APPENDIX B**. A description of the thermocouples installed in the test vehicle and data from these thermocouples are in **APPENDIX C**. A description of the aspirated thermocouples used in this test and date from these aspirated thermocouples are in **APPENDIX D**. A description of the heat flux transducer/radiometer assemblies installed in the test vehicle and data from these devices are in **APPENDIX E**. Descriptions of the pressure and airflow measurement equipment and analysis procedures, and data from these measurements are in **APPENDIX F**. A description of the Fire Products Collector at the Factory Mutual Global Test Center and analysis procedures, and data from this device are in **APPENDIX G**. A description of the Fourier Transform Infrared Gas Analysis System used during this test and results from this device are in **APPENDIX H**. Descriptions of the Gas Chromatography/Mass Spectrometry equipment and analysis procedures, and the results of these analyses are in **APPENDIX I**. Descriptions of the particulate sampling equipment and analysis procedures, and the results of these analyses are in **APPENDIX J**.

The test vehicle was placed in the center of the fluid containment pan (Fig. 4). All doors were closed. The left side door and rear glasses were broken in the crash test, and were not replaced for the fire test. The right side door window was raised to its fully closed positions. All components in the vehicle were at ambient temperature at the start of the fire test.

Charcoal was removed from a vapor recovery canister for a 1997 Chevrolet Camaro and soaked for approximately 10 minutes in 50 mL of gasoline. Residual liquid gasoline was decanted from the charcoal. The charcoal saturated with gasoline was placed on the surface of the cement board just in front of the left rear tire approximately 5 minutes before beginning of this fire test.

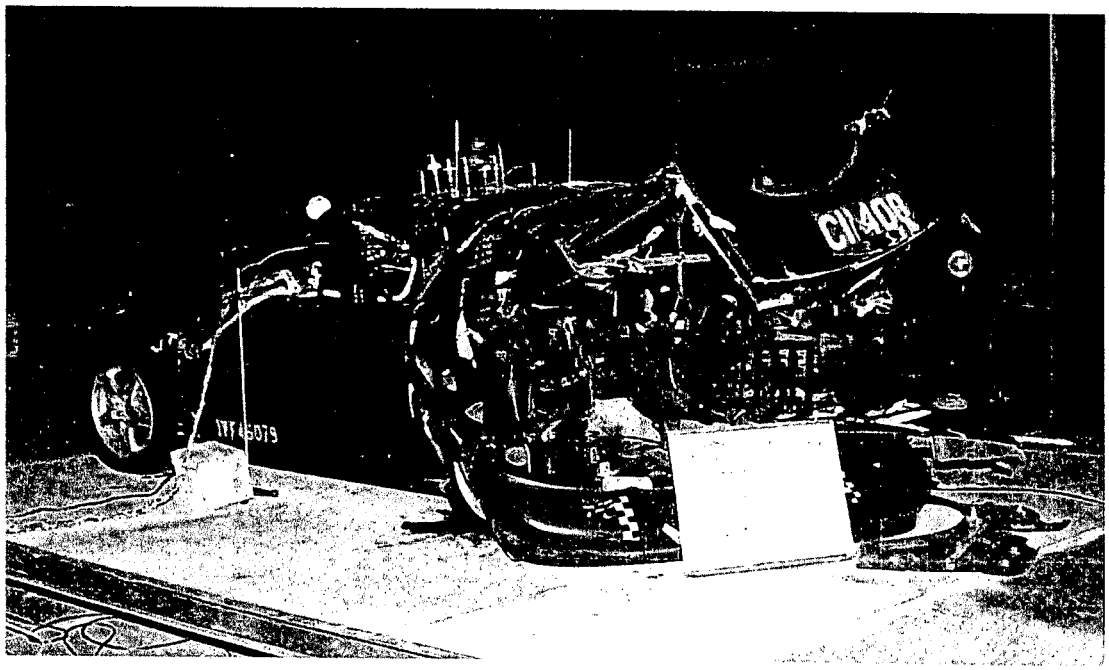

Figure 4. Fire Test F971001. Photograph of the test vehicle in the fluid containment pan before the fire test.

An air horn was sounded to signal three events during the test: (1) the start of gasoline flow, (2) ignition of the gasoline pool by the propane torch, and (3) the end of the test and start of fire suppression. The air horn was used to synchronize the data acquisition systems used in this test. The air horn was audible on the videotapes and infrared imaging systems. One channel of the data acquisition system for vehicle instrumentation monitored a normally open switch, which was depressed at each sounding. The real-time clock in the FTIR data system was synchronized to the real-time clock in the vehicle instrumentation data system.

Gasoline was delivered from a pressurized external reservoir at a constant flow rate during this test. Technical personnel from the Building and Fire Research Laboratory of the National Institutes of Standards and Technologies designed, built, and operated the gasoline delivery system used in this test. Figure 5 shows a schematic diagram of the gasoline delivery system used in this test. This system consisted of two stainless steel cylinders. One cylinder functioned as a fluid reservoir and had a capacity of 4 L, while the other cylinder functioned as a pressurized gas reservoir. A pressure regulator in the line connecting the gas reservoir to the fluid reservoir controlled the head pressure in the fluid reservoir. The outlet line of the fluid reservoir contained a ball valve that was used to turn on and off the flow of gasoline during the test, a rotometer to indicate the flow of gasoline during the test, and a needle valve to control the flow of gasoline.

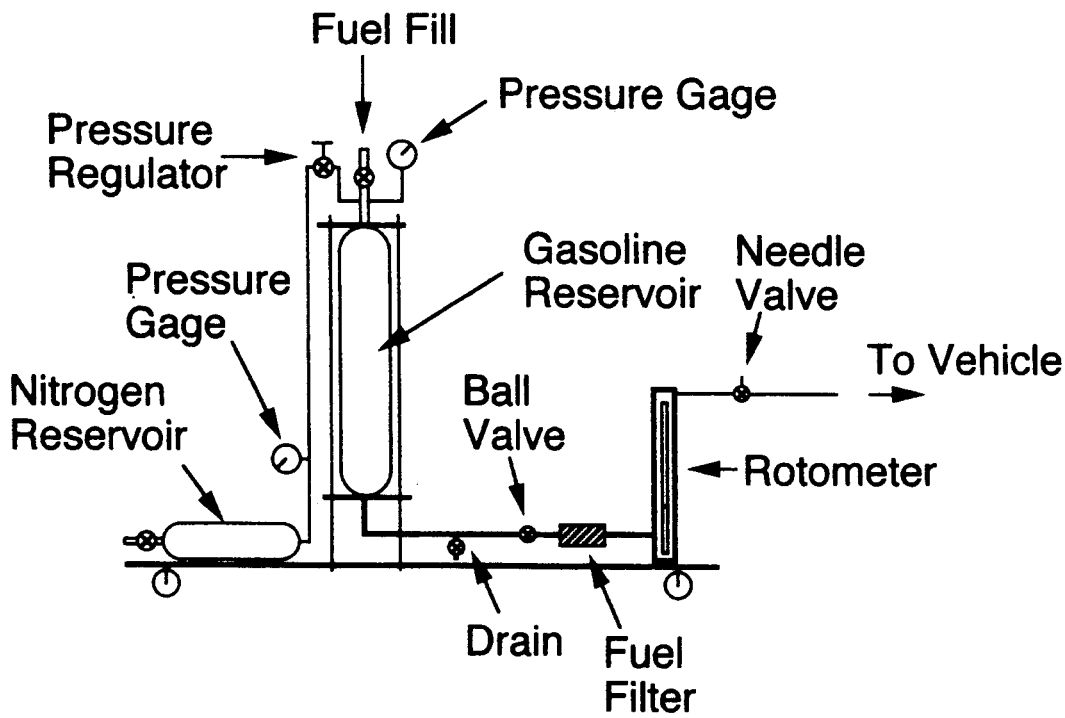

Figure 5. Fire Test F971001. Schematic diagram of the external gasoline reservoir and delivery system used to artificially supply gasoline to the test during this test.

The outlet of the tube was located at the lower left edge of the fuel tank, below the area where the fuel filler tube enters the fuel tank. The outlet of the tube was fitted with a flow restrictor (i.d. = 0.125") to reduce vaporization of gasoline by maintaining some back-pressure in the delivery tube.

Gasoline (4 L) was added to a steel fluid reservoir (4 L). The gas reservoir was filled with dry nitrogen gas. The pressure regulator was adjusted to maintain a head pressure of 275 kPa (25.0 psi) in the fluid reservoir. Before the test, the delivery tube was purged with gasoline before the start of the test to eliminate air. The needle valve was adjusted to give a flow rate of approximately 500 cm^3/s, measured before the test by collecting the gasoline effluent in a graduated container for a specified period of time.

A valve approximately 3 feet from the outlet of the gasoline delivery tube was mounted to the right outer quarter panel and opened to start the flow of gasoline during this test. The flow rate of gasoline through the delivery tube was determined from readings taken from the rotometer. The

head pressure in the fluid reservoir and ball position in the rotometer was checked at 30 second intervals during the test to determine if the initial flow rate of gasoline had changed. The pressure regulator and needle valve were adjusted as necessary to maintain a constant flow rate of gasoline during the test.

The test was ended after objects in the rear of the passenger compartment had ignited and flames were observed spreading forward along the headlining panel. A water mist was used to extinguish the flames after the flow of gasoline was stopped.

3 Ignition

Figures 6 through 8 contain a series of video stills from Cameras 5 and 8 at 35, 15, and 5 seconds before ignition. These series of video stills show the gasoline pool spreading spreading laterally along a seam between the cement boards lining the fluid containment pan before gasoline vapor above the pool was ignited with a propane torch. The video stills in Figure 6 show the area under the test vehicle approximately 4 seconds before the start of gasoline flow and were included in this series of figures for reference. Charcoal absorbant from a vapor recovery canister that was poured onto the surface of the cement board in front of the left rear tire is visible in both video stills in Figure 6. Figure 7 shows the gasoline pool spreading laterally along a seam between the cement boards lining the fluid containment pan after about 15 seconds of flow. Figure 8 shows the gasoline pool approximately 5 seconds before it was ignited with a propane torch.

Gasoline was allowed to flow onto the cement board surface under the test vehicle for approximately 31 seconds before it was ignited. The average flow rate of gasoline from the delivery system for the time period before ignition was determined to have been 515 ± 20 cm^3/s.[1] The shape of the gasoline pool on the cement board surface was not symmetrical. A seam between two of the cement boards appeared to channel the flow of gasoline on the surface laterally between the two rear wheels (Fig.'s 7 and 8). The shallow view-angle of Cameras 5 and 8, low lighting conditions under the test vehicle, and the irregular shape of the gasoline pool made it impossible to estimate the actual dimensions of the gasoline pool from these videotapes. Because of these unanticipated technical difficulties in determining the dimensions of the gasoline pool accurately from analysis of the video tapes, no attempt was made to estimate flow rate from pool size before ignition.

Gasoline vapor above the liquid gasoline pool was ignited with a propane torch approximately 31 seconds after the start of gasoline flow (Fig.'s 9 and 10). Ignition occurred at the rear of the test vehicle beyond (rearward of) the boundary of the gasoline pool (Fig. 9). Flames spread concentrically from the point of ignition (Fig. 10) so that gasoline vapor under most of the rear section of the test vehicle was burning within a few seconds of ignition.

[1] A series of measurements was performed after this test to determine the flow rate of gasoline from the delivery system during this test. In this series of measurements, 4 L of gasoline was added to the reservoir and the pressure regulator was adjusted to maintain a head pressure of 275 kPa (25.0 psi) in the fluid reservoir. The rotometer was adjusted to match the readings recorded during the test. The volume flow rate of gasoline from the system was determined by collecting the effluent from the outlet in a graduated cylinder for a measured period of time.

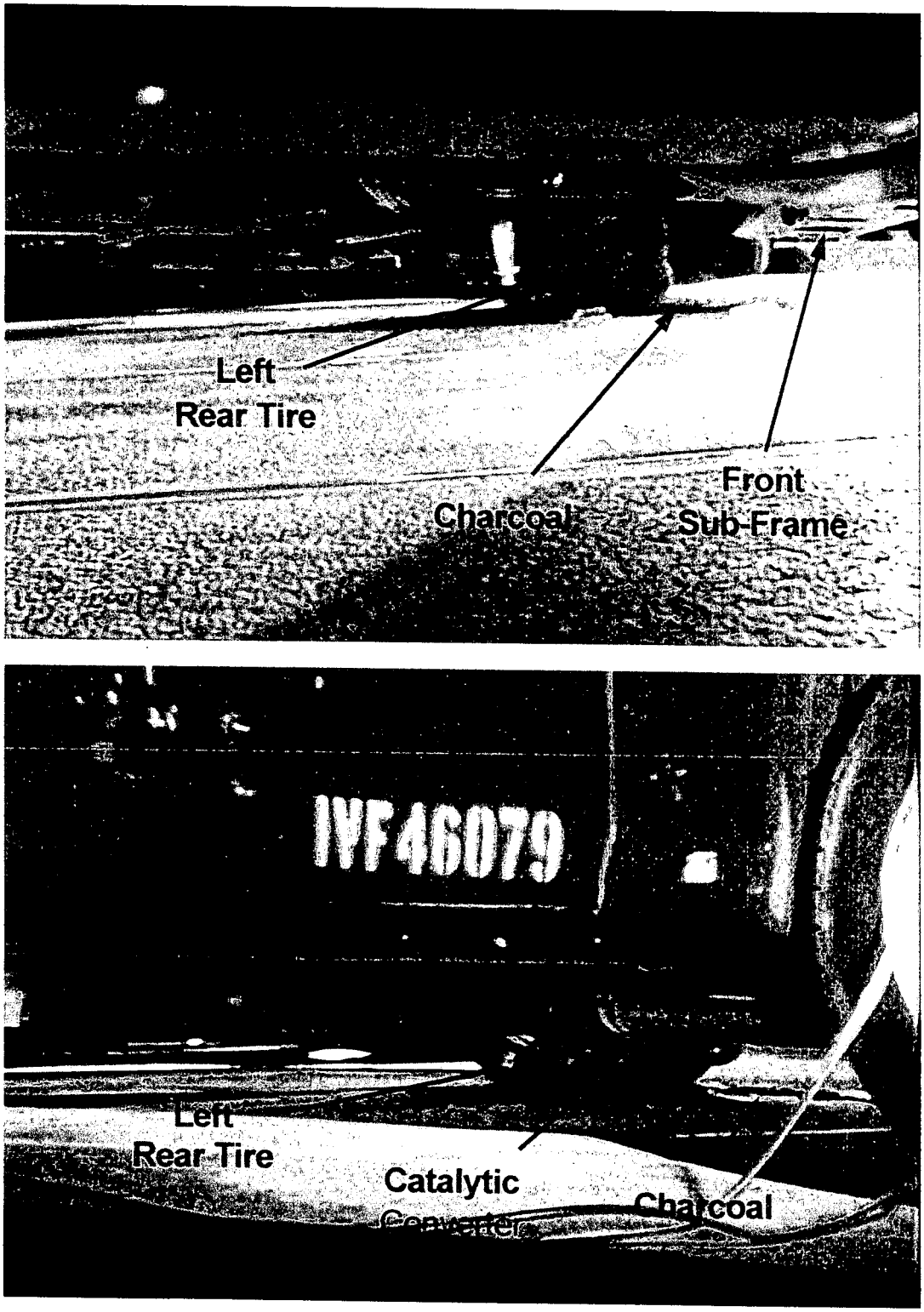

Figure 6. Fire Test F971001. Video stills from Camera 5 (upper) and Camera 8 (lower) at 35 seconds before ignition (4 seconds before the start of gasoline flow) showing the underbody of the test vehicle and the surface of the cement board below the rear of the test vehicle.

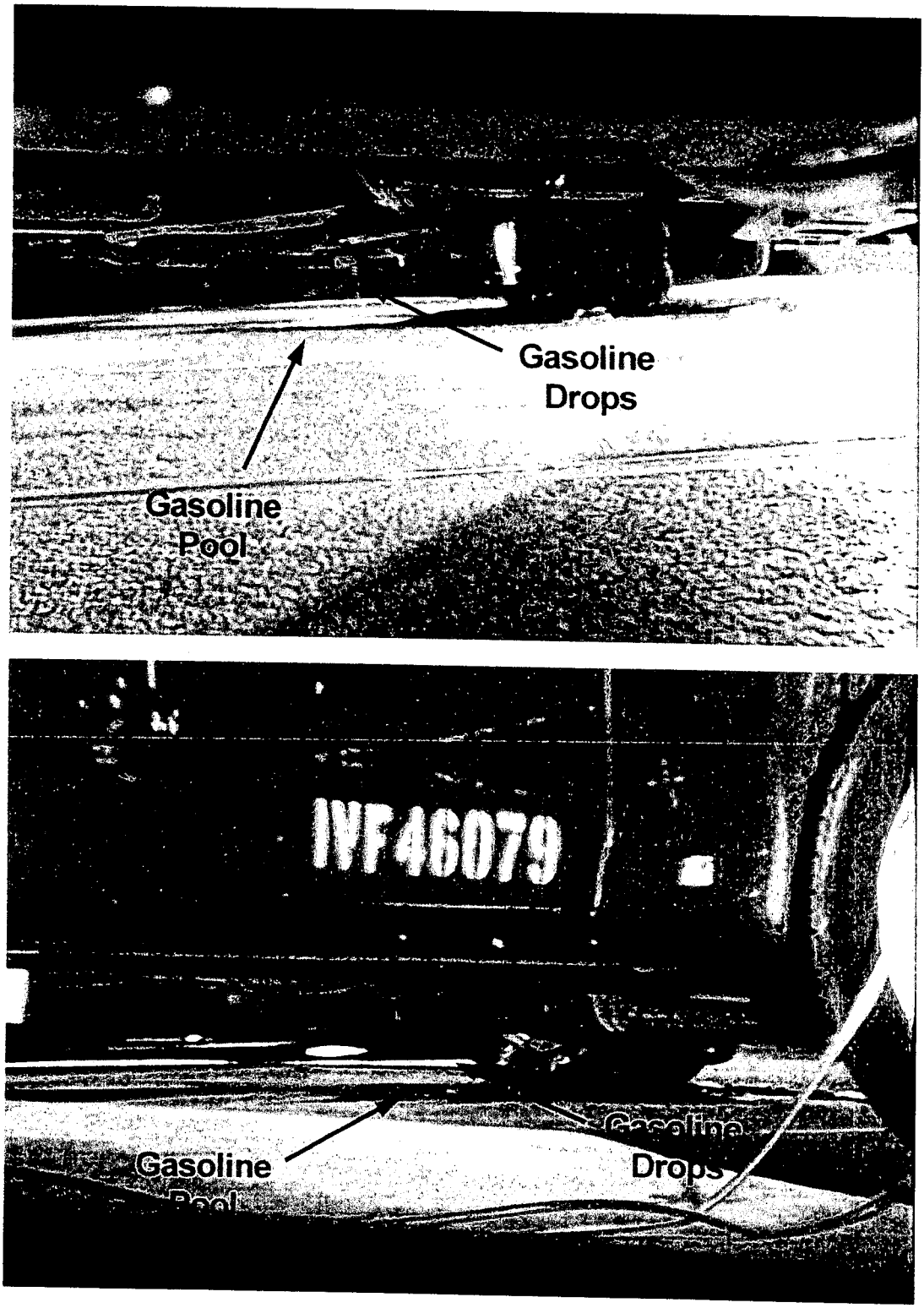

Figure 7. Fire Test F971001. Video stills from Camera 5 (upper) and Camera 8 (lower) at 15 seconds before ignition (16 seconds after the start of gasoline flow) showing gasoline dripping from the outlet of the delivery tube and pooling on the surface of the cement board below the rear of the test vehicle.

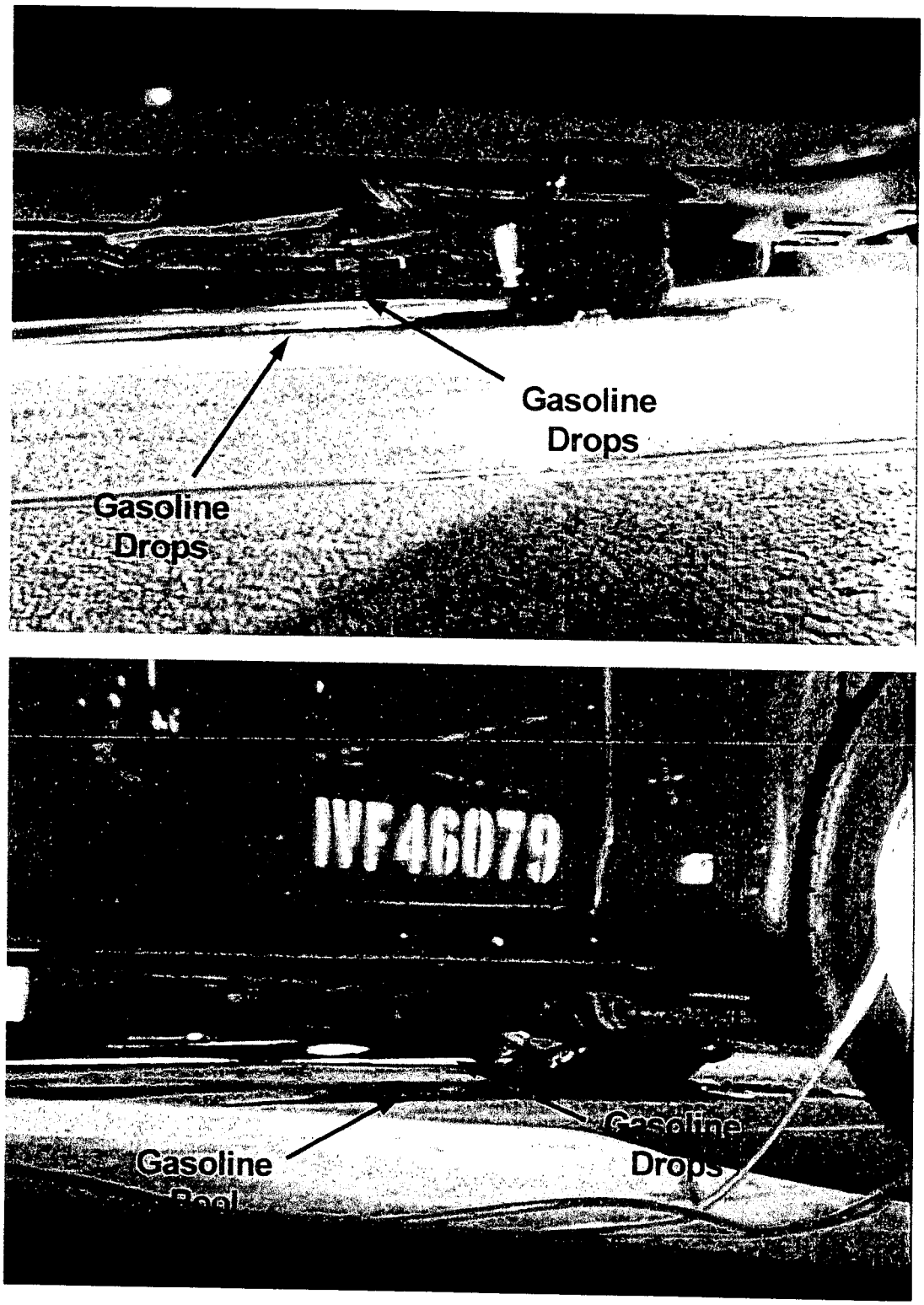

Figure 8. Fire Test F971001. Video stills from Camera 5 (upper) and Camera 8 (lower) at 5 seconds before ignition (26 seconds after the start of gasoline flow) showing gasoline dripping from the outlet of the delivery tube and pooling on the surface of the cement board below the rear of the test vehicle.

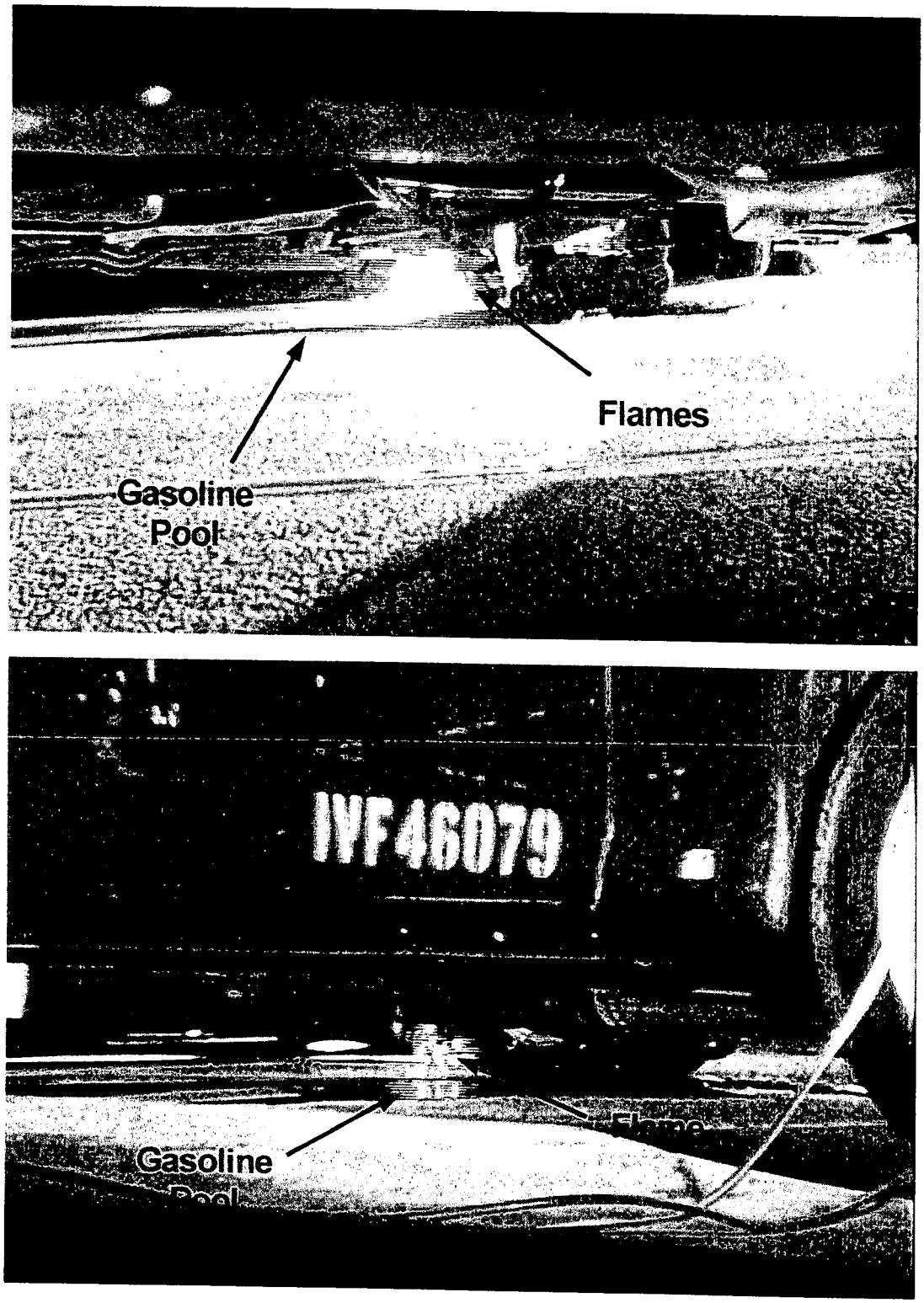

Figure 9. Fire Test F971001. Video stills from Camera 5 (upper) and Camera 8 (lower) at the time of ignition (31 seconds after the start of gasoline flow) showing flames on the gasoline pooling on the surface of the cement board below the rear of the test vehicle.

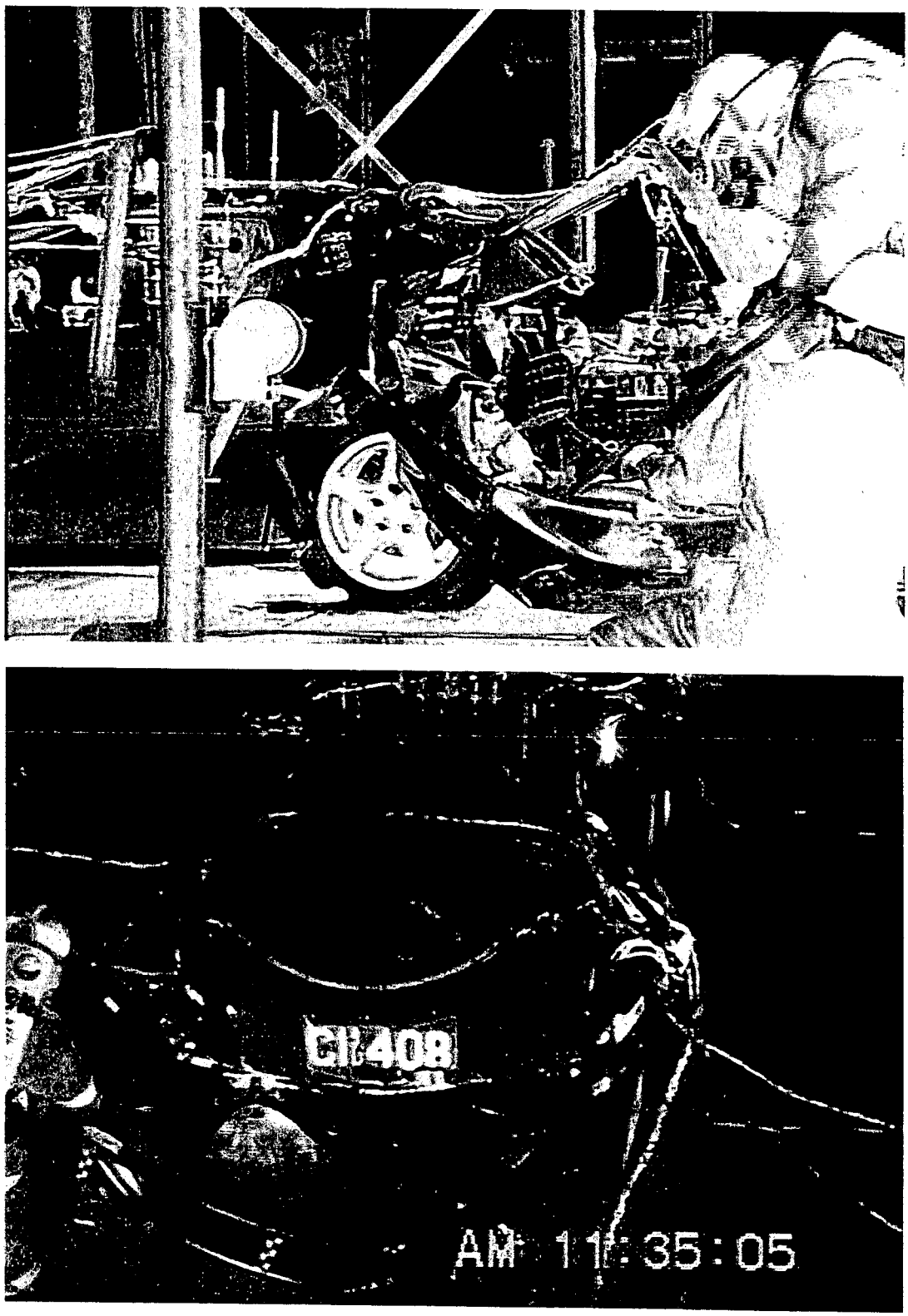

Figure 10. Fire Test F971001. Video stills from Camera 2 (upper) and Camera 4 (lower) at the time of ignition (0 seconds post-ignition) showing ignition of the gasoline pool by a propane torch.

4 Behavior of the Underbody Gasoline Pool Fire in this Test

The flow rate of gasoline was maintained at approximately 515 cm^3/min throughout the test. After ignition, the length of the burning gasoline pool was estimated from the videotapes from Cameras 5 and 8. Figure 11 shows plots of the estimated length of the gasoline pool at five-second intervals from the time of ignition to approximately 210 seconds post-ignition. The uncertainty in the estimated pool size was ± 5 cm.

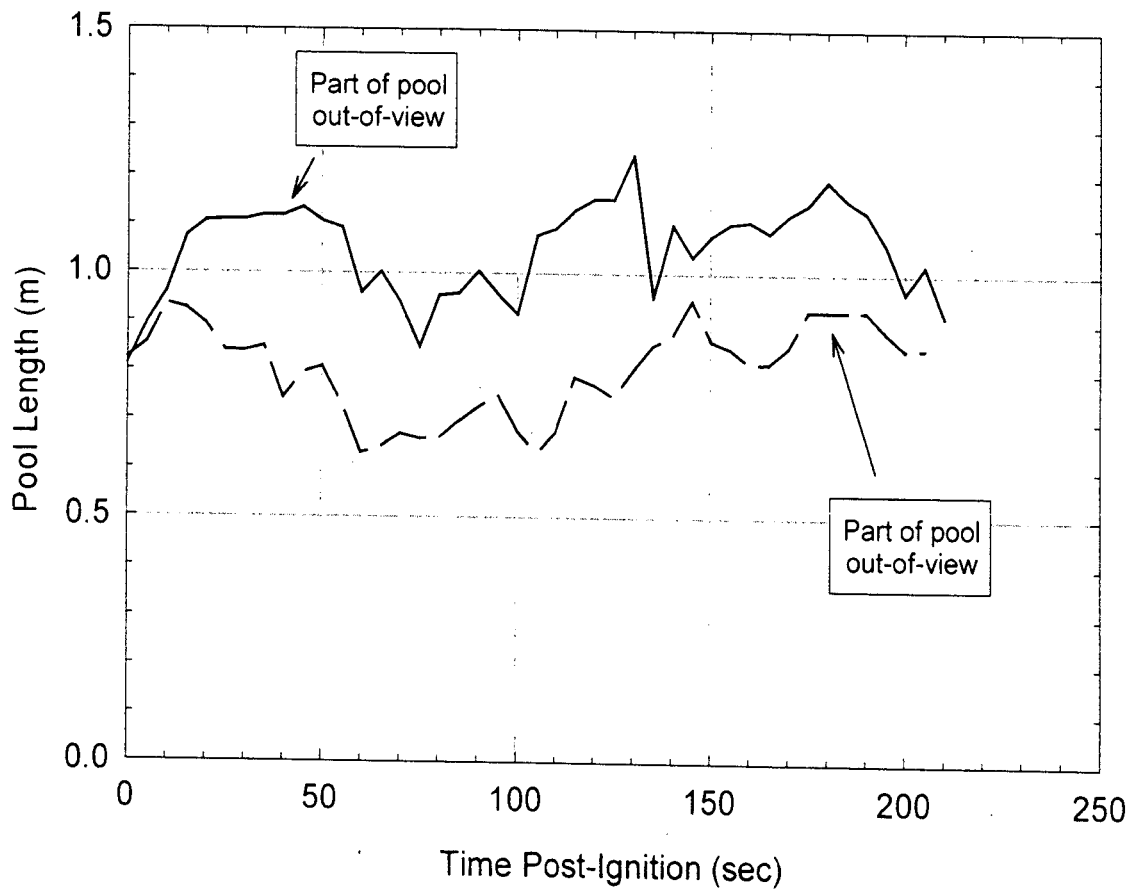

Figure 11. Fire Test F971001. Estimates of the length of the gasoline pool under the test vehicle obtained by analysis of the videotapes from Cameras 5 (——) and 8 (— —).

The physical characteristics of the surface in the bottom of the fluid retention pan effected the shape of the gasoline pool and its distribution under the test vehicle, which effected the area of the underbody exposed to flames. The gasoline pool was elongated, spreading out along a seam between two of the cement boards under and parallel to the rear axle of the test vehicle. Figures 12 through 19 show a series of video stills from Cameras 5 and 8 at 25 second intervals between 25 and 200 seconds post-ignition. Both Cameras 5 and 8 viewed the long axis of the gasoline pool, which was roughly aligned with the rear axle of the test vehicle. Camera 5 viewed the pool

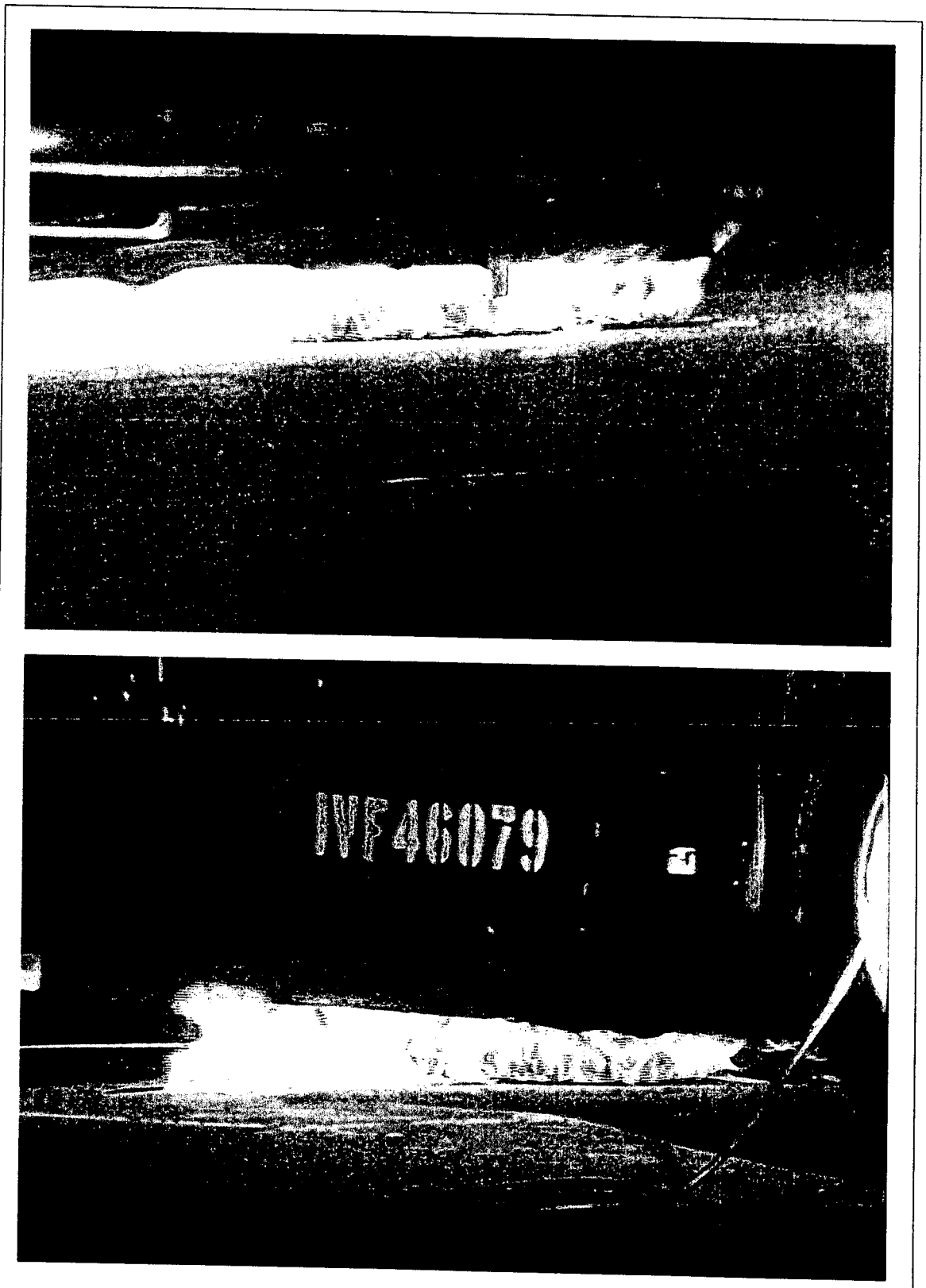

Figure 12. Fire Test F971001. Video stills from Camera 5 (upper) and Camera 8 (lower) at 25 seconds post-ignition showing of the burning gasoline pool under the test vehicle.

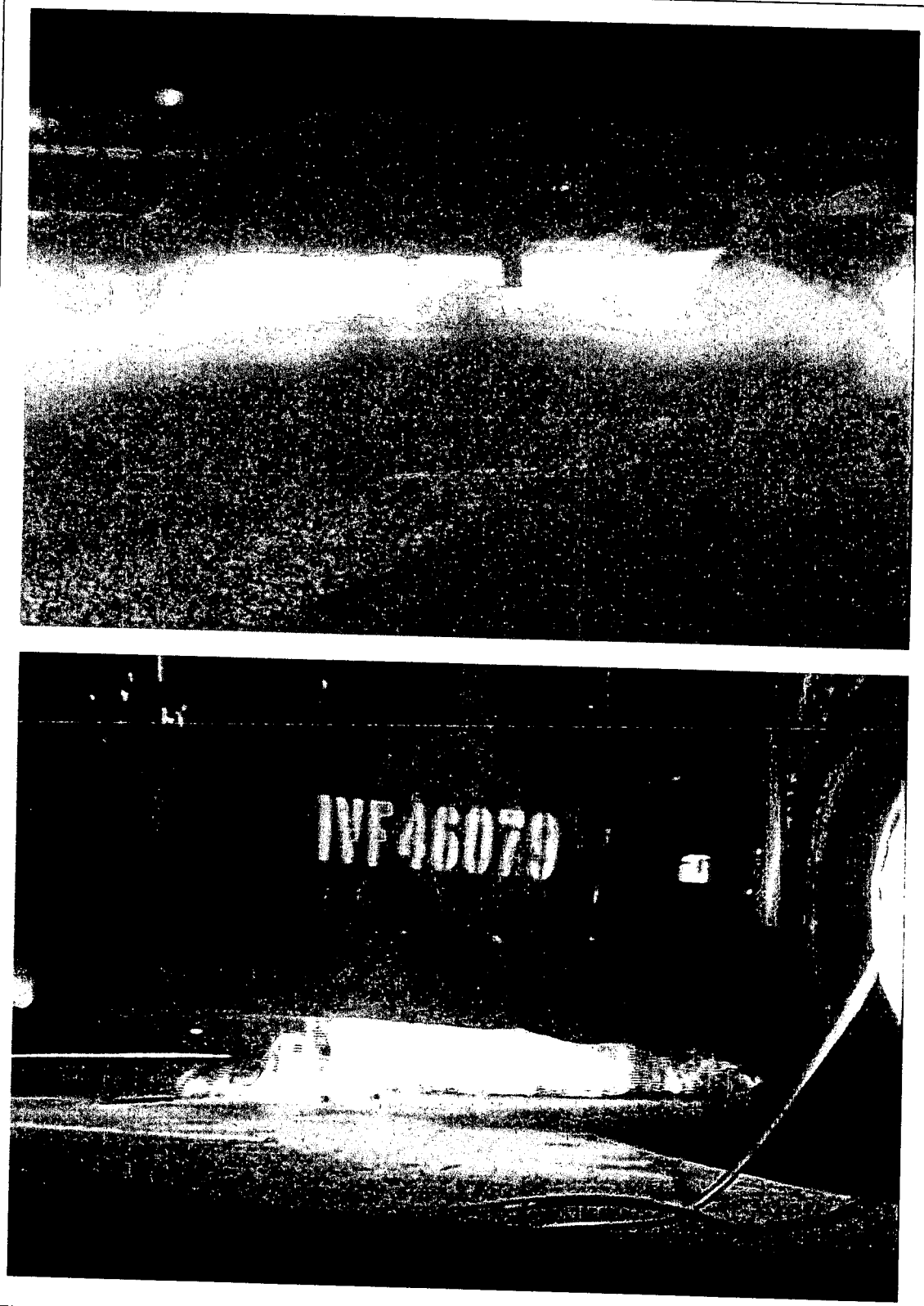

Figure 13. Fire Test F971001. Video stills from Camera 5 (upper) and Camera 8 (lower) at 50 seconds post-ignition showing of the burning gasoline pool under the test vehicle.

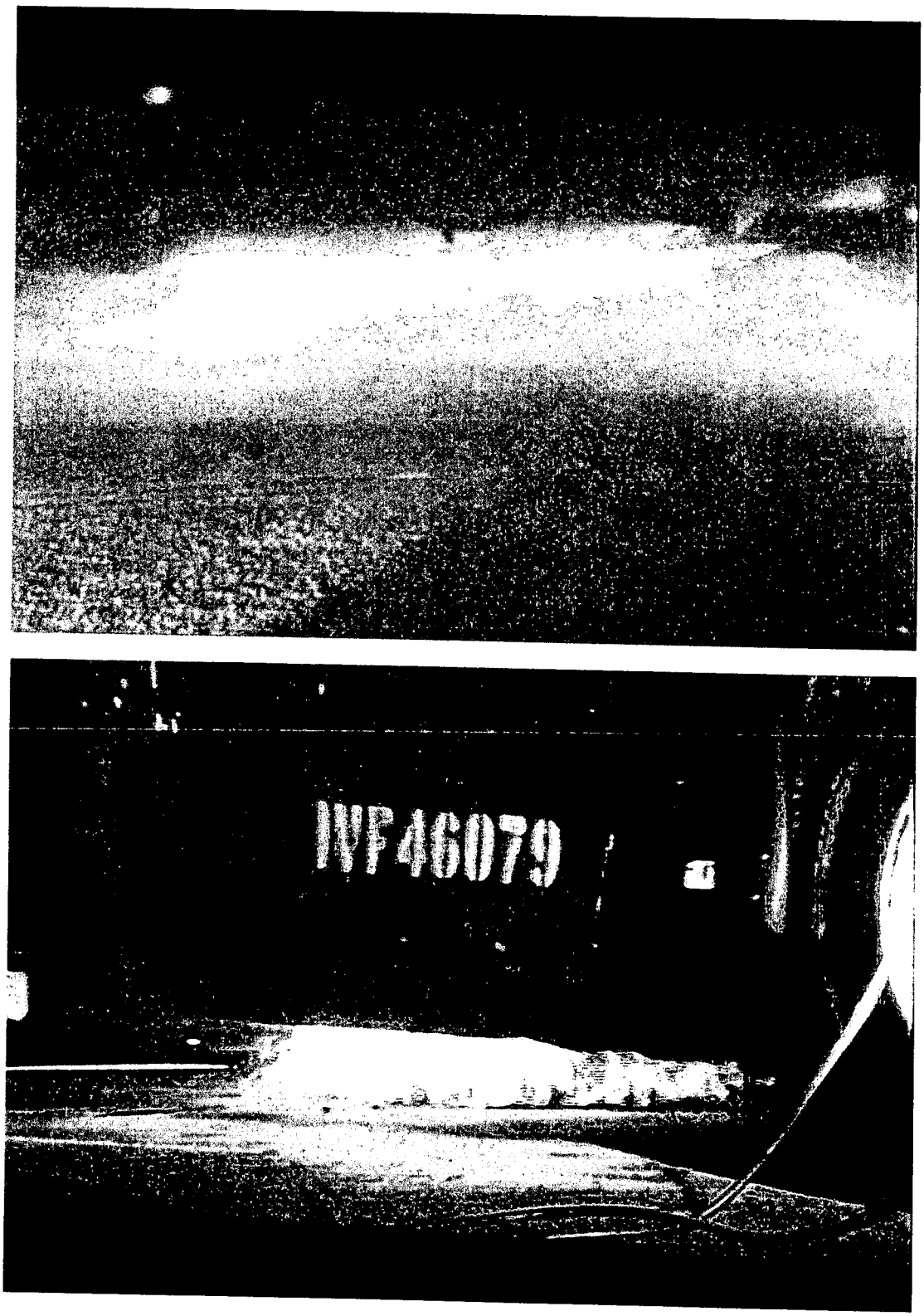

Figure 14. Fire Test F971001. Video stills from Camera 5 (upper) and Camera 8 (lower) at 75 seconds post-ignition showing of the burning gasoline pool under the test vehicle.

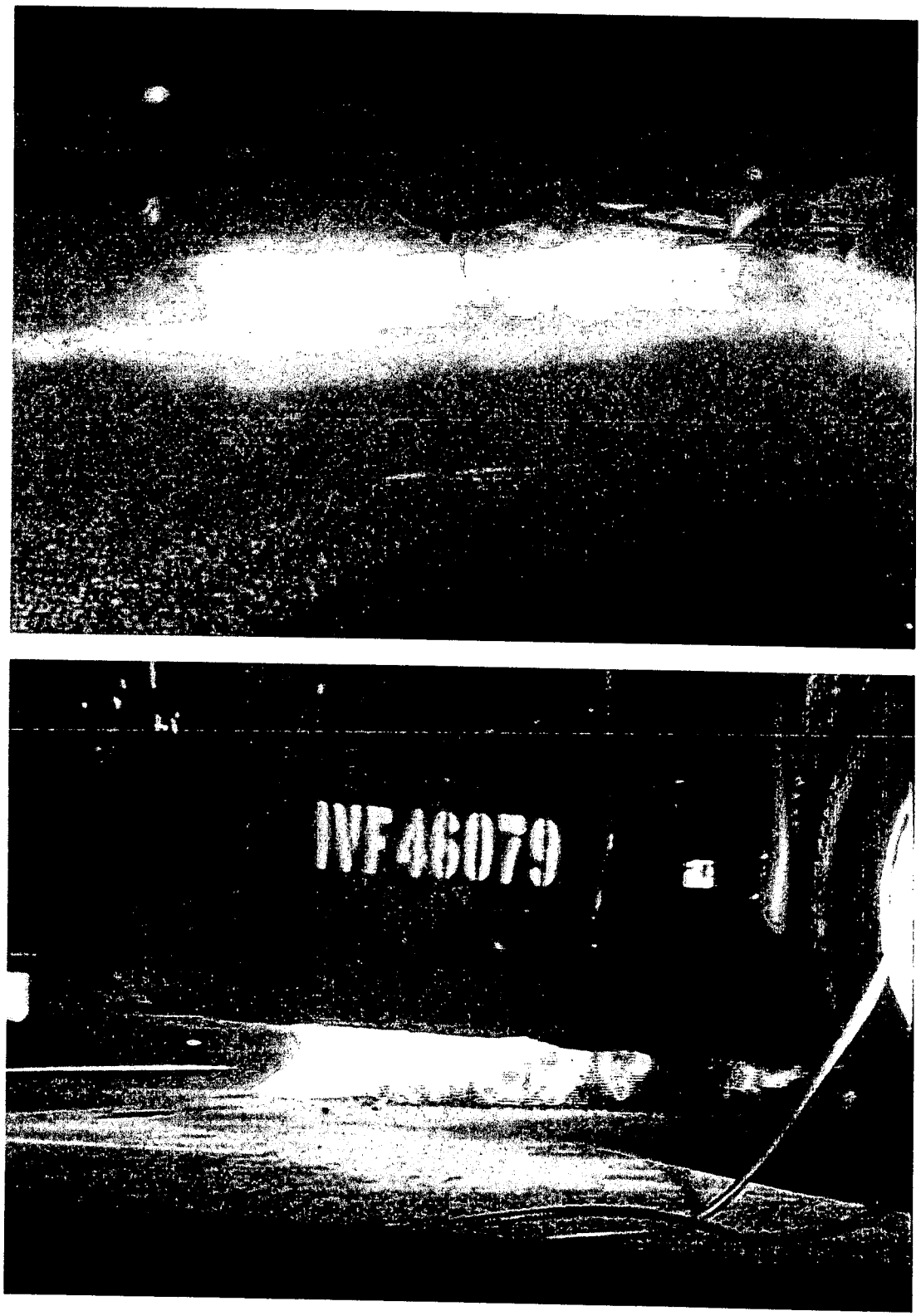

Figure 15. Fire Test F971001. Video stills from Camera 5 (upper) and Camera 8 (lower) at 100 seconds post-ignition showing of the burning gasoline pool under the test vehicle.

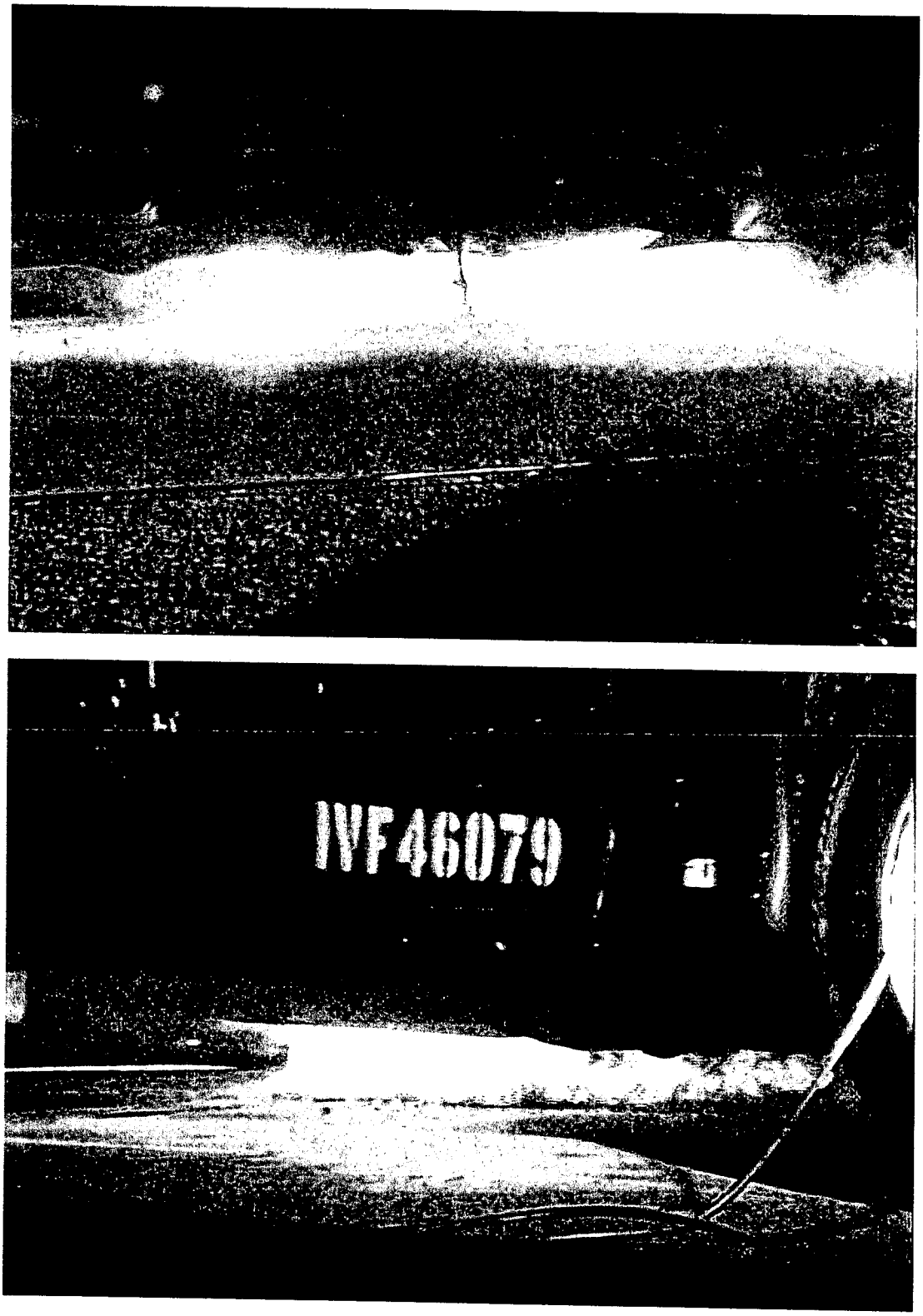

Figure 16. Fire Test F971001. Video stills from Camera 5 (upper) and Camera 8 (lower) at 125 seconds post-ignition of the burning gasoline pool under the test vehicle.

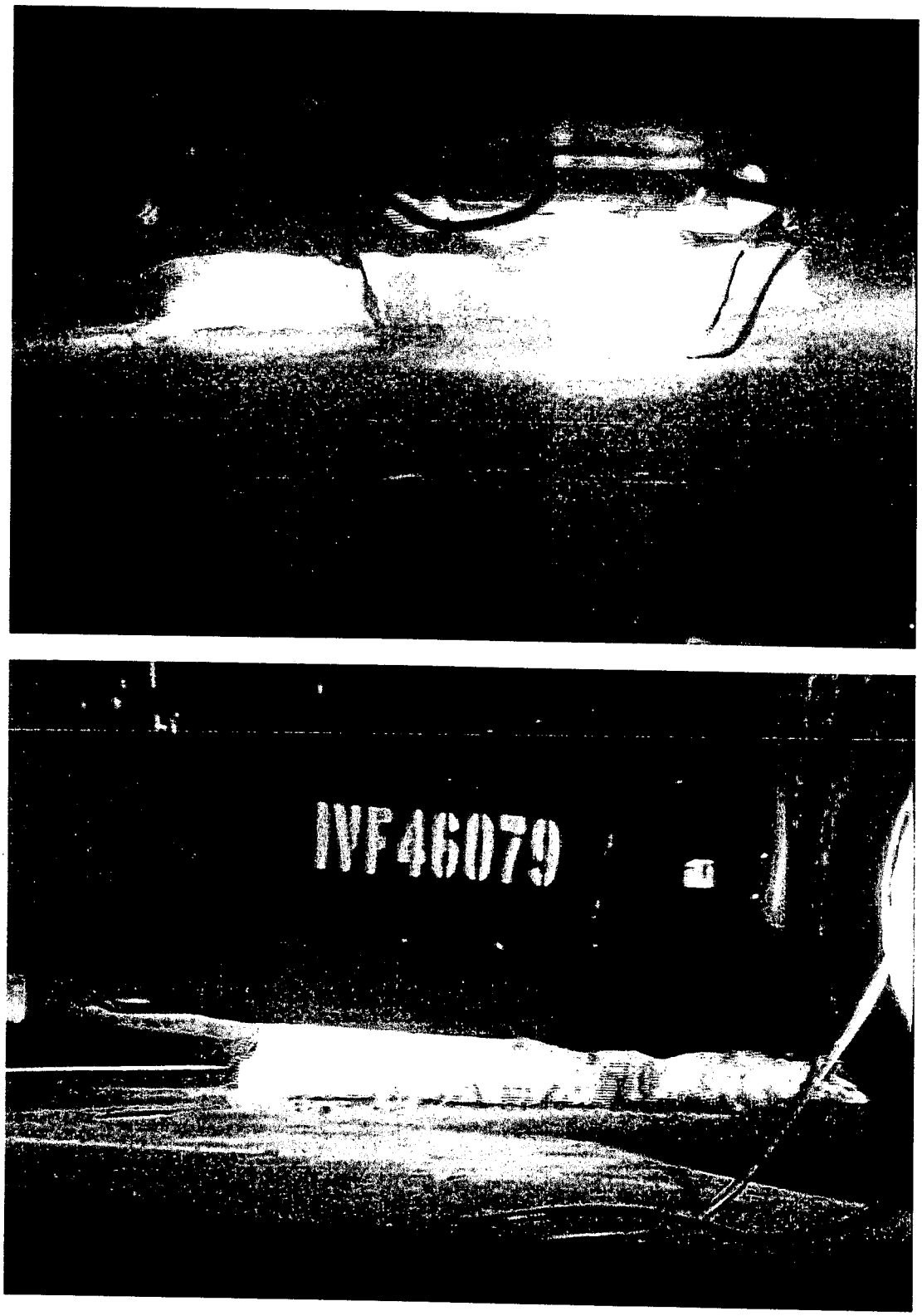

Figure 17. Fire Test F971001. Video stills from Camera 5 (upper) and Camera 8 (lower) at 150 seconds post-ignition of the burning gasoline pool under the test vehicle.

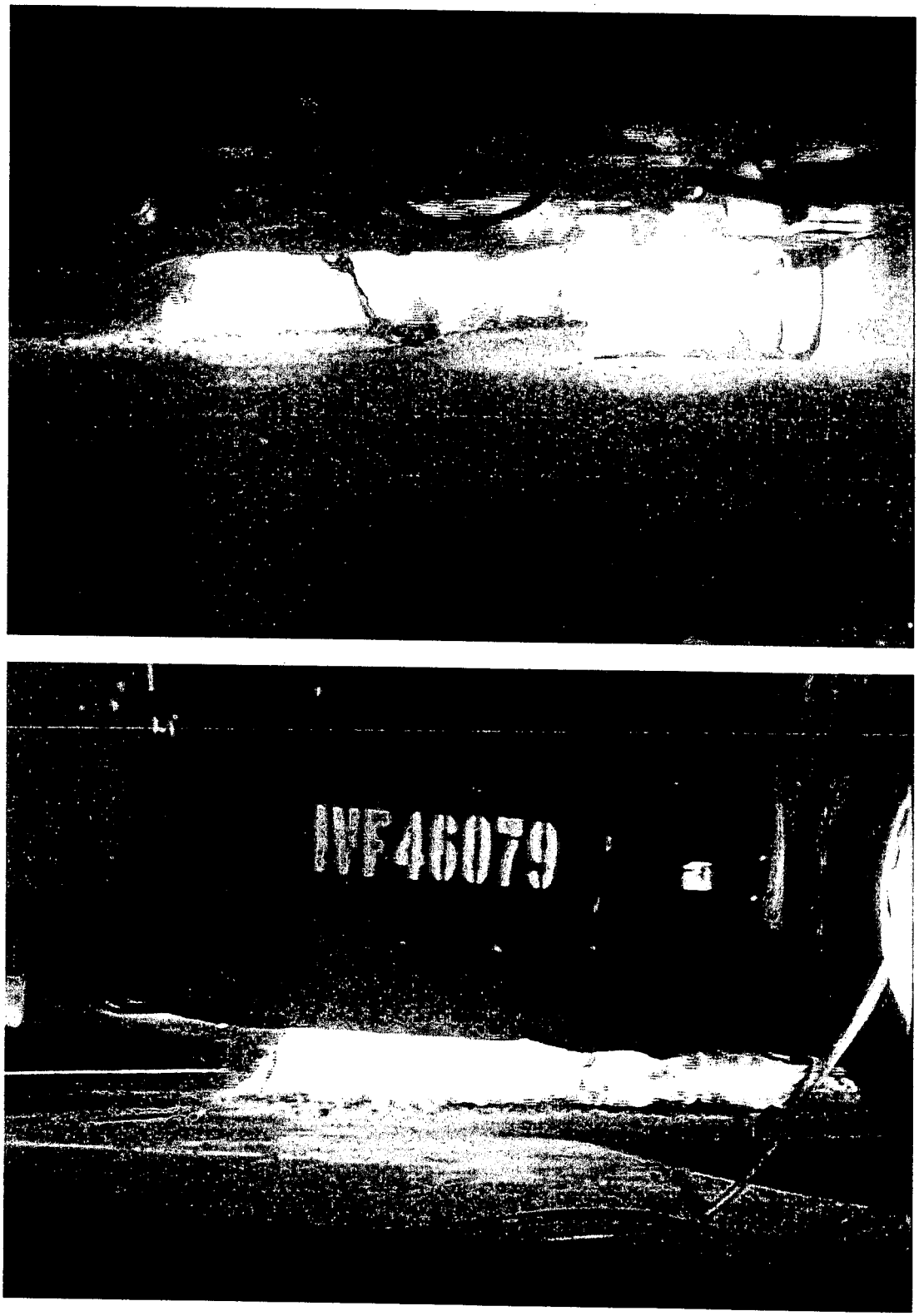

Figure 18. Fire Test F971001. Video stills from Camera 5 (upper) and Camera 8 (lower) at 175 seconds post-ignition of the burning gasoline pool under the test vehicle.

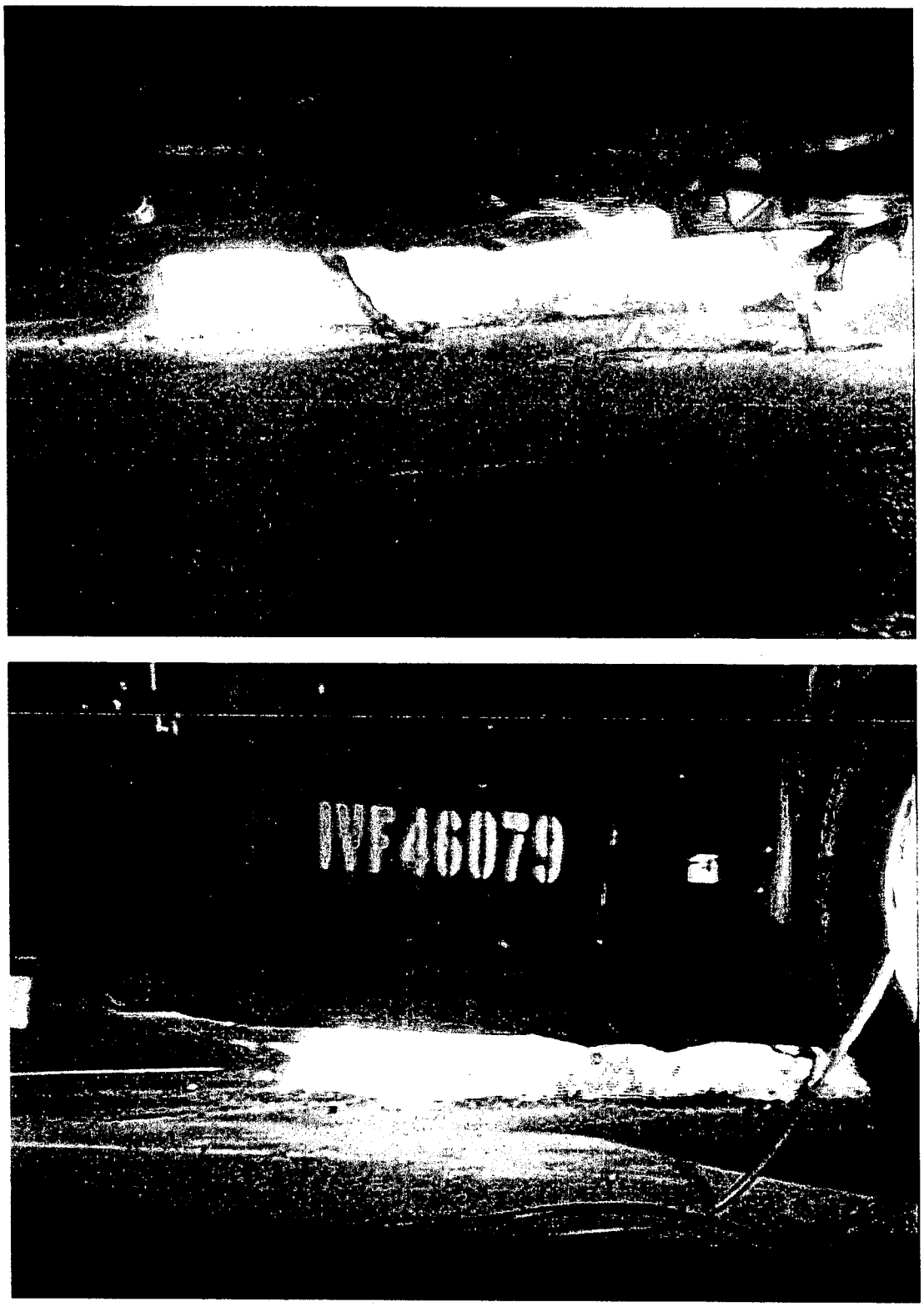

Figure 19. Fire Test F971001. Video stills from Camera 5 (upper) and Camera 8 (lower) at 200 seconds post-ignition of the burning gasoline pool under the test vehicle.

nearly head-on (perpendicular to its long axis). Camera 8 viewed the gasoline pool at approximately a 45° angle to its long axis. The difference in the two estimates of gasoline pool length shown in Figure 11 were the result of the different view-angles of Cameras 5 and 8. These estimates indicate that the gasoline pool was between 60 and 120 cm long, with an average length of between 90 and 100 cm (Fig. 11). The pool was estimated to have been less 12 cm wide. It was not possible to estimate the lateral extension of flames along the underbody of the test vehicle accurately from the videos from Cameras 5 and 8 because the low clearance under the test vehicle did not allow good views of the underbody of the test vehicle.

Isothermal contour plots of temperatures below the test vehicle were estimated from data recorded from thermocouples located below the floor pan panel.[2] Figure 20 shows some of the structures forming the underbody of the test vehicle after the crash test. The approximate locations of the floor panel drain hole plugs, and outlines of the body, tires, fuel tank, and rear compartment floor pan rails (frame rails) are also shown in this diagram. Thermocouples were placed in pairs on the floor panel and the section of the rear compartment front panel around the rear left wheelhouse. One thermocouple of each pair was adhered to the upper surface of the metal with thermally conducting ceramic cement. The other thermocouple in each pair was positioned approximately 1 cm below the metal panel. The number of thermocouples on the rear compartment front panel and rear compartment rear panel was not sufficient to allow accurate estimation of isothermal contours under the section of the test vehicle rearward of the rear seat backs. For this reason, only isothermal contours under the floor panel are shown.

The distribution of flames under the test vehicle[3] was indicated by isothermal contours with $t \geq 600°C$ (Fig. 21). These plots indicate that heated gases started to spread forward along the left side of the floor panel at about the time of ignition. The natural buoyancy of the hot gases in the fire plume caused the flames to move upward toward the highest points in the floor panel, which appeared to be a pocket under the rear left seat created as the floor panel buckled during the crash test. The left rocker panel and left rear compartment floor panel rail (frame rail) appeared to limit lateral extension of flames to the edge of the left side of the floor panel. Heated gases and flames appeared to accumulate in the rear section of the drive train tunnel, but not to have spread

---

[2] Isothermal contours of the temperature below the floor panel were estimated from the temperature data recorded from the F-Thermocouples located below the floor panel using a three-dimensional interpolation algorithm available in SigmaPlot for Windows Version 4.00 [**5**]. This algorithm uses an inverse distance method to generated temperature values for points on a uniformly spaced Cartesian grid from the [x,y,t] triple data from these thermocouples. Refer to **APPENDIX C** for the approximate locations of the F-thermocouples on the floor panel and the data recorded from the F-thermocouples.

[3] As in previous reports, a value of 600°C was used in this report as the threshold to indicate the presence of flame.

beyond to the right side of the floor panel. The driveshaft and differential housing in the rear axle may have impeded the flow of air and gasses under the test vehicle, thus limiting extension of flames to the about the longitudinal midline of the test vehicle.

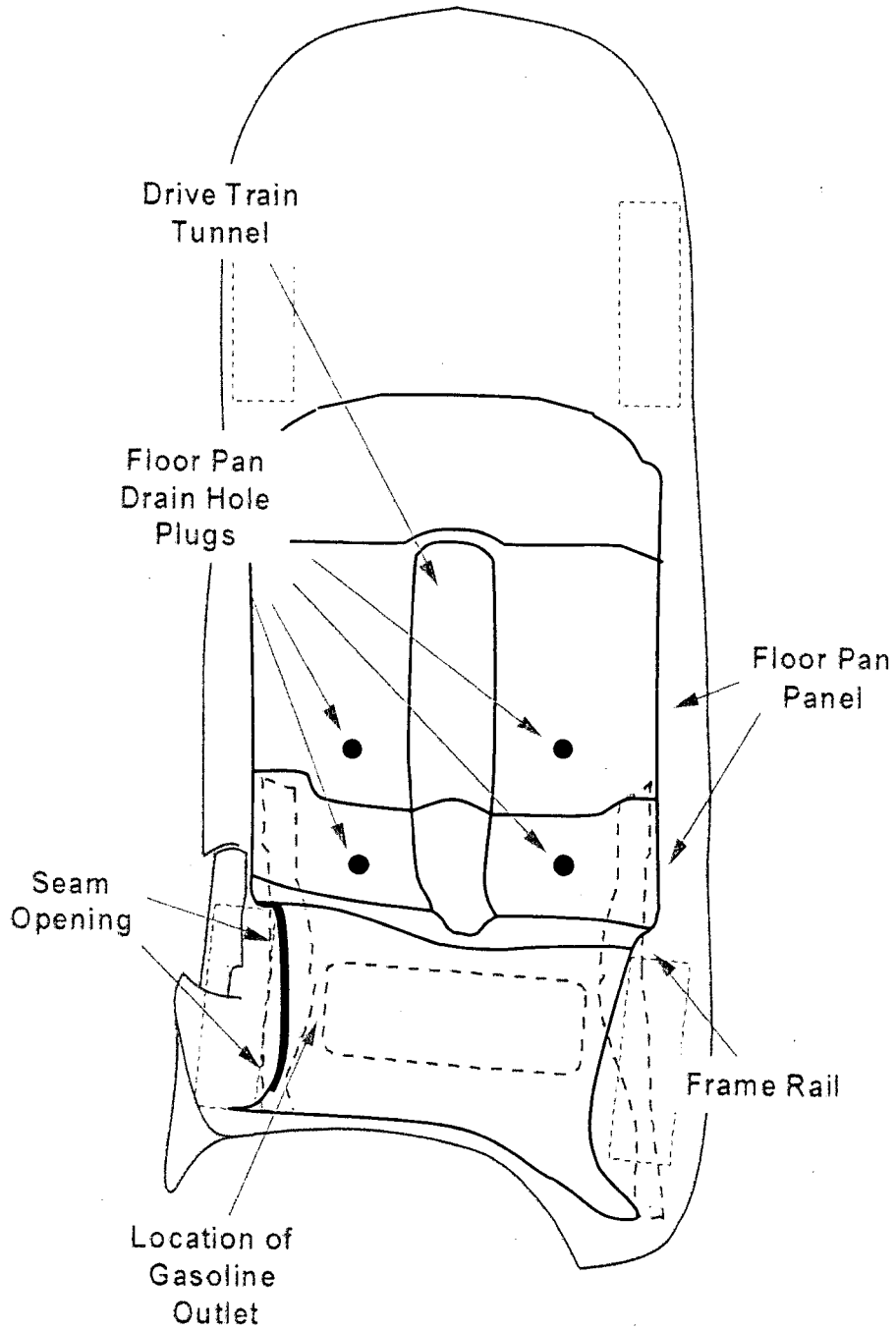

Figure 20. Fire Test F971001. View from above the test vehicle showing the floor panel, rear compartment front panel, and rear compartment rear panel.

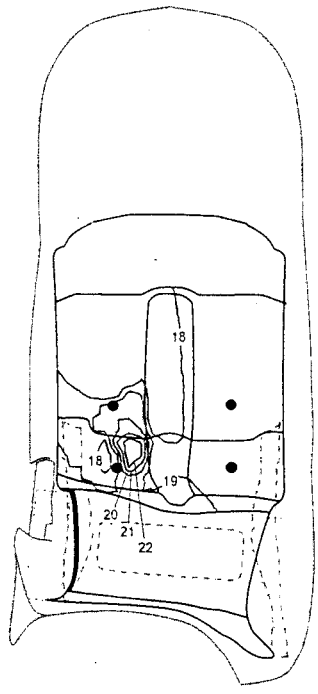

-10 seconds post-ignition

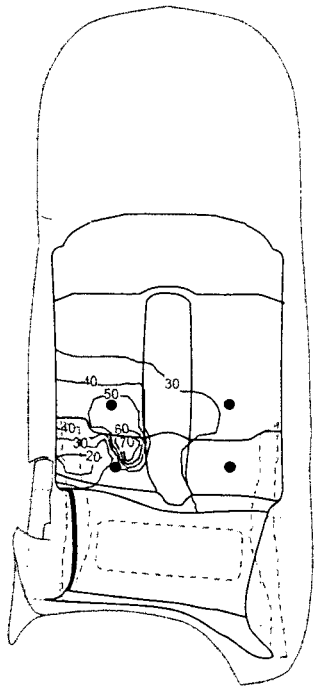

0 seconds post-ignition

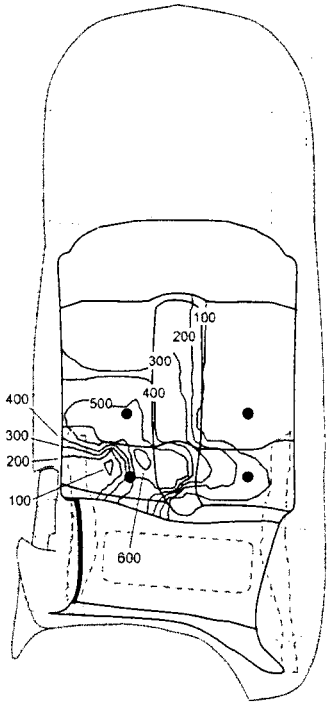

25 seconds post-ignition

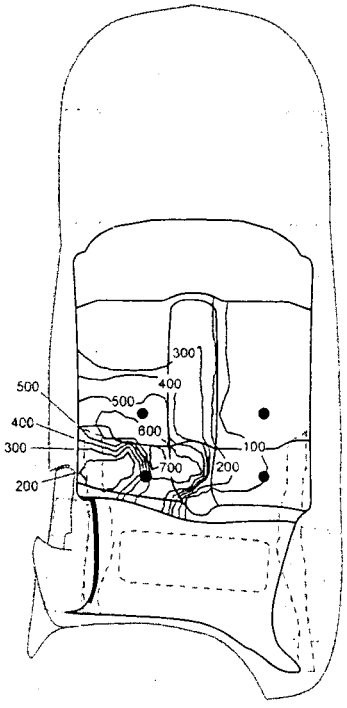

50 seconds post-ignition

Figure 21. Fire Test F971001. Isothermal contour plots showing estimated temperatures below the floor panel at –10, 0, 25, 50, 75, 100, 125, 150, 175, and 200 seconds post-ignition.

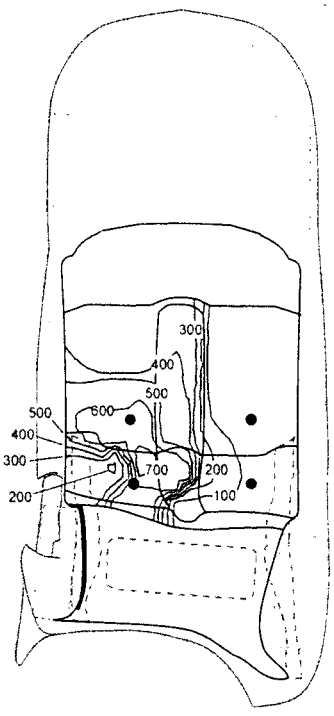

75 seconds post-ignition

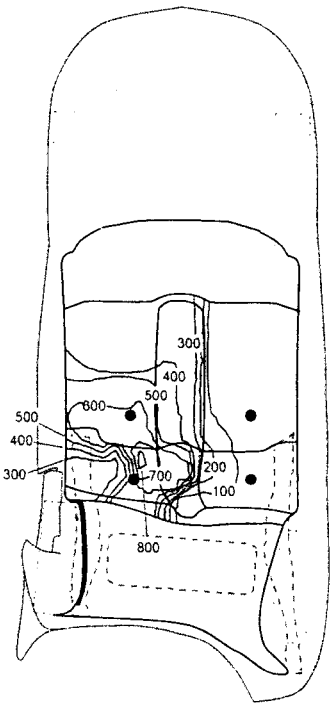

100 seconds post-ignition

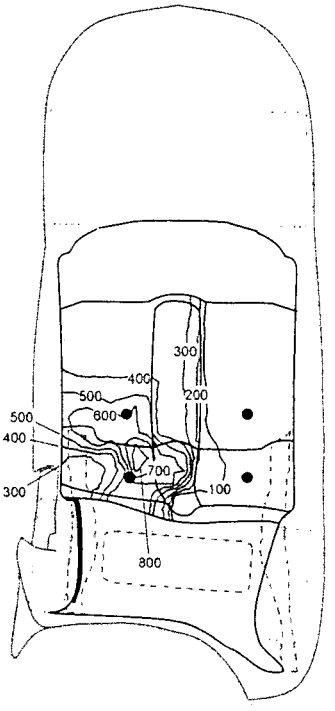

125 seconds post-ignition

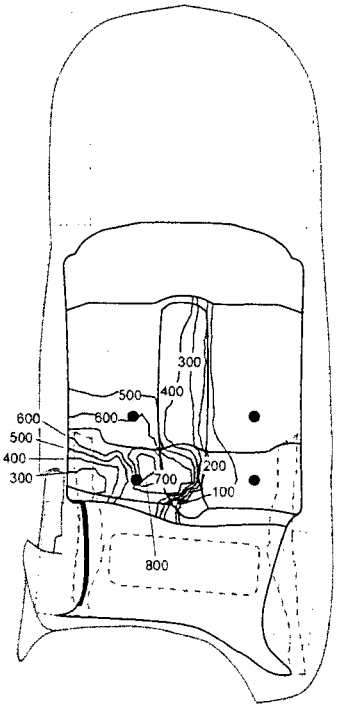

150 seconds post-ignition

Figure 21, continued. Fire Test F971001. Isothermal contour plots showing estimated temperatures below the floor panel at –10, 0, 25, 50, 75, 100, 125, 150, 175, and 200 seconds post-ignition.

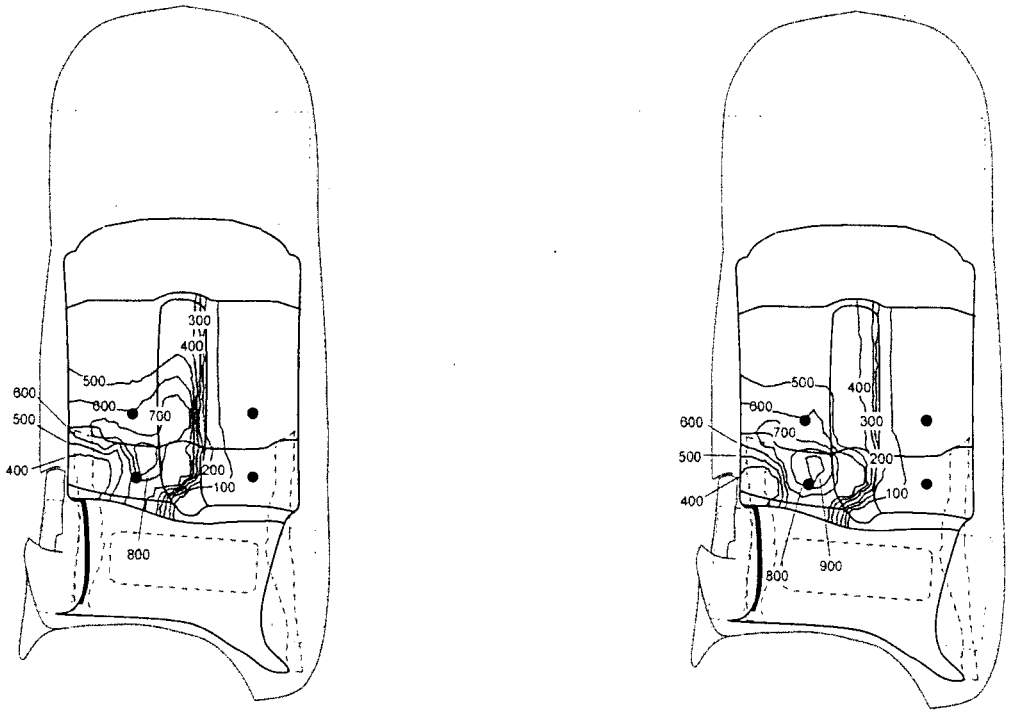

Figure 21, continued. Fire Test F971001. Isothermal contour plots showing estimated temperatures below the floor panel at –10, 0, 25, 50, 75, 100, 125, 150, 175, and 200 seconds post-ignition.

Thermocouples located below the floor panel under the inboard half of the rear left seat cushion recorded temperatures exceeding 600°C at approximately 25 seconds post-ignition (Fig. 21), indicating that flames were below this section of the floor panel at this time. By 50 seconds post-ignition, the isothermal contour plots indicate that the area of the floor panel exposed to flames increased to include an adjacent section of the drive train tunnel and a section just forward of the rear left seat cushion (Fig. 21). The distribution of flames on the floor panel inferred from the isothermal contour plots could not be confirmed by the direct observation of flames contacting specific areas of the underbody (Fig.'s 12 through 19).

The video tapes from Cameras 5 and 8 did not show clearly the areas of the floor panel that were exposed to flames between 25 and 50 seconds post-ignition (Fig.'s 12 and 13). By 75 seconds post-ignition, flames were discernable on a section of floor panel just forward of the rear left seat well (Fig. 14). The video record also showed that a section of flexible nylon fuel pipe[4] under the rear left seat started to sag and burn by 100 seconds post-ignition (upper still, Fig. 15). Flames

[4] The flexible nylon fuel pipe was 0.375 in. i.d. Nylon 12 tubing.

spread forward along the fuel lines to the in-line fuel filter[5], also located under the rear left seat, which separated from its mounting bracket and fell onto the surface of the fluid containment pan by 150 seconds post-ignition (upper video still, Fig. 17).

[5] The in-line fuel filter had a steel shell and paper filter element.

5 Flame-Spread into the Passenger Compartment

The data presented in this section indicates that flame-spread into the passenger compartment progressed simultaneously along three pathways. These pathways included crash-induced seam openings between the rear floor pan panel and left rear inner quarter panel, a gap between the back of the driver's door and door frame that was created by damage to the test vehicle sustained during the crash test, and a drain hole in the floor panel. Flame-spread along these p[athways appeared to be a consequence of the elongated shape and location of the gasoline pool under the test vehicle, which resulted in these three areas being exposed to flames during this test. The following sections contain an analysis of the test data to determine the timing and locations of flame spread into the passenger compartment.

5.1 Flame-Spread into the Left Rear Corner of the Test Vehicle

Flames first entered the passenger compartment in the area behind the displaced left quarter interior trim finishing panel between 10 and 20 seconds post-ignition, at which time flames appeared along the top edge of the trim panel (Fig. 22). By 30 seconds post-ignition, the flames had reached the left rear corner of the headlining panel and had started to spread forward and to the right along its lower surface. By 45 seconds post-ignition, no flames were visible inside the passenger compartment of the test vehicle (Fig. 23).

Figures 24 through 27 show a series of video, temperature plots, and Infrared thermograms of the interior of the test vehicle at 0, 15, 30, and 45 seconds post-ignition. In each figure, Panel A is a video still from Camera 6, which was located inside the passenger compartment on top of the instrument panel. Its field-of-view included sections of the driver's and rear seat backs, the displaced quarter trim finishing panel, an exposed section of the inner quarter panel, and the left rear corner of the headlining (A, Fig. 24). Panel B is a video still from Camera 7, which was mounted on a tripod adjacent to the drivers door and focused through the window. Its field-of-view included the upper corners of the driver's and rear seat backs, a section of the forward edge of the displaced quarter trim finishing panel, and a section of the seal for the driver's window (B, Fig. 24). The left quarter interior trim finishing panel was displaced forward in the crash. The rear compartment lift window was broken in the crash. Both were visible in these video stills. Panel C is a line drawing showing isothermal contour plots estimated from thermocouple data (C, Fig. 24).

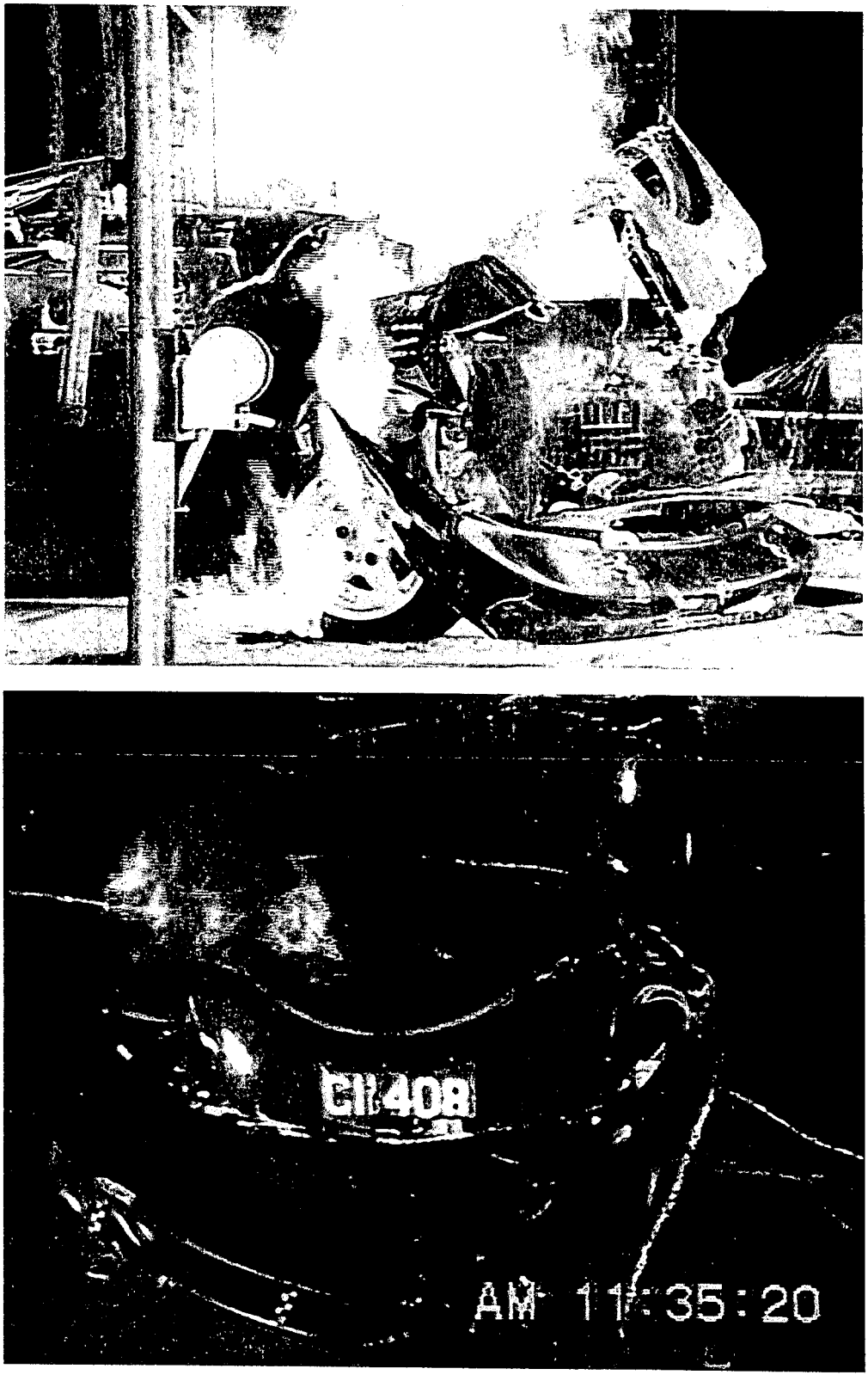

Figure 22. Fire Test F971001. Video still from Cameras 2 (upper) and 4 (lower) at 15 seconds post-ignition.

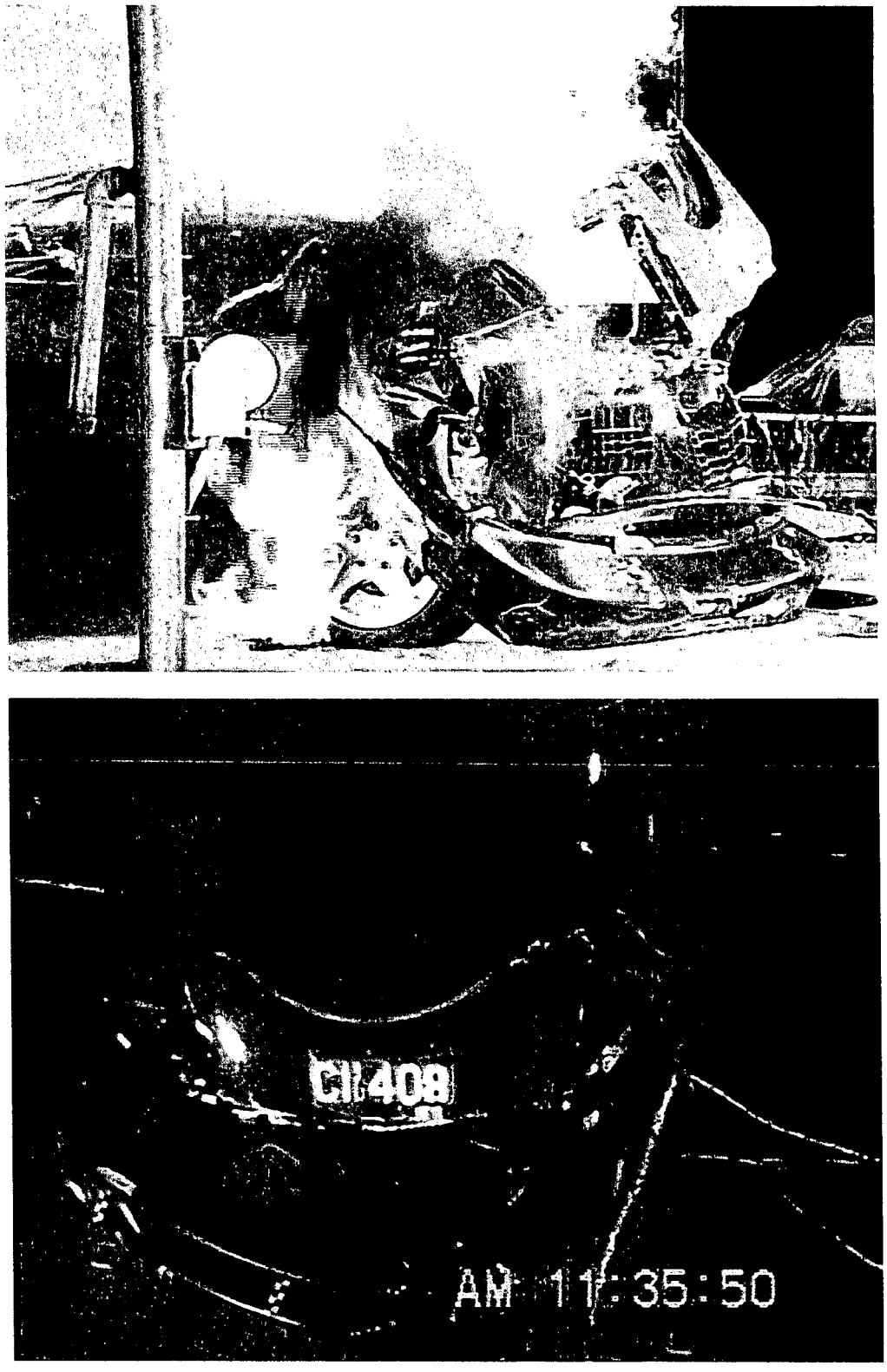

Figure 23. Fire Test F971001. Video still from Cameras 2 (upper) and 4 (lower) at 45 seconds post-ignition.

The isothermal contours represent temperatures below the headlining panel and behind the interior quarter trim finishing panel[7]. The solid lines indicate estimated isothermal contours in front of the inner quarter panel or below the headlining panel. The dashed lines indicate estimated isothermal contours behind the quarter trim finishing panel. The number of thermocouples on the quarter trim panel was not adequate to estimate temperatures behind the entire panel. Only isothermal contours where the thermocouple coverage allowed interpolation are shown in these figures. Panel D is an Infrared thermogram from IR6, which was suspended from a threaded rod mounted to the roof of the test vehicle above the driver's seat cushion (D, Fig. 24). Its field-of-view included sections of the driver's seat back, front passenger's seat back, rear seat back, left quarter trim finishing panel, and the headlining panel. As these objects were not easily discernable in most of the thermograms shown in these figures, a line drawing was over-laid on the thermograms for reference.

The video stills, isothermal contour plot, and Infrared thermogram in Figure 24 show the interior of the test vehicle at the time of ignition (0 seconds post-ignition). Some of the interior components are labeled for reference. Figure 25 shows the video stills, isothermal contour plot, and Infrared thermogram at 15 seconds post-ignition. Flames were visible at the top of the left quarter trim finishing panel (A, Fig. 25) and behind the test vehicle through the rear compartment opening (B, Fig. 25). The isothermal contour plot (C, Fig. 25) indicates that the fire plume had not contacted the roof of the test vehicle at this time as the temperatures along the headlining panel were between 100 and 250°C, with the hottest area just above the rear of the drivers door. The infrared thermogram shows that the temperature in the left rear of the test vehicle was > 174°C (the upper limit the range IR6 was set to at that time). This is 25 to 100°C than the temperatures shown in the isothermal contour plots, and was attributed to hot gases and airborne particulate in this space, which also emitted infrared radiation detected by IR6.

The fire plume had reached the headlining by 30 seconds post-ignition (A and B, Fig. 26). The temperature along an area of the headlining panel just above the upper edge of the left quarter trim finishing panel was > 600°C (C, Fig. 26).

[7] Isothermal contours of the temperature behind the displaced quarter trim finishing panel, and along the inner quarter panel and headlining panels were estimated from the temperature data recorded from the H- and T-Thermocouples. A three-dimensional interpolation algorithm available in SigmaPlot for Windows Version 4.00 was used for these estimations [**5**]. This algorithm uses an inverse distance method to generated temperature values for points on a uniformly spaced Cartesian grid from the [x,y,t] triple data from these thermocouples.

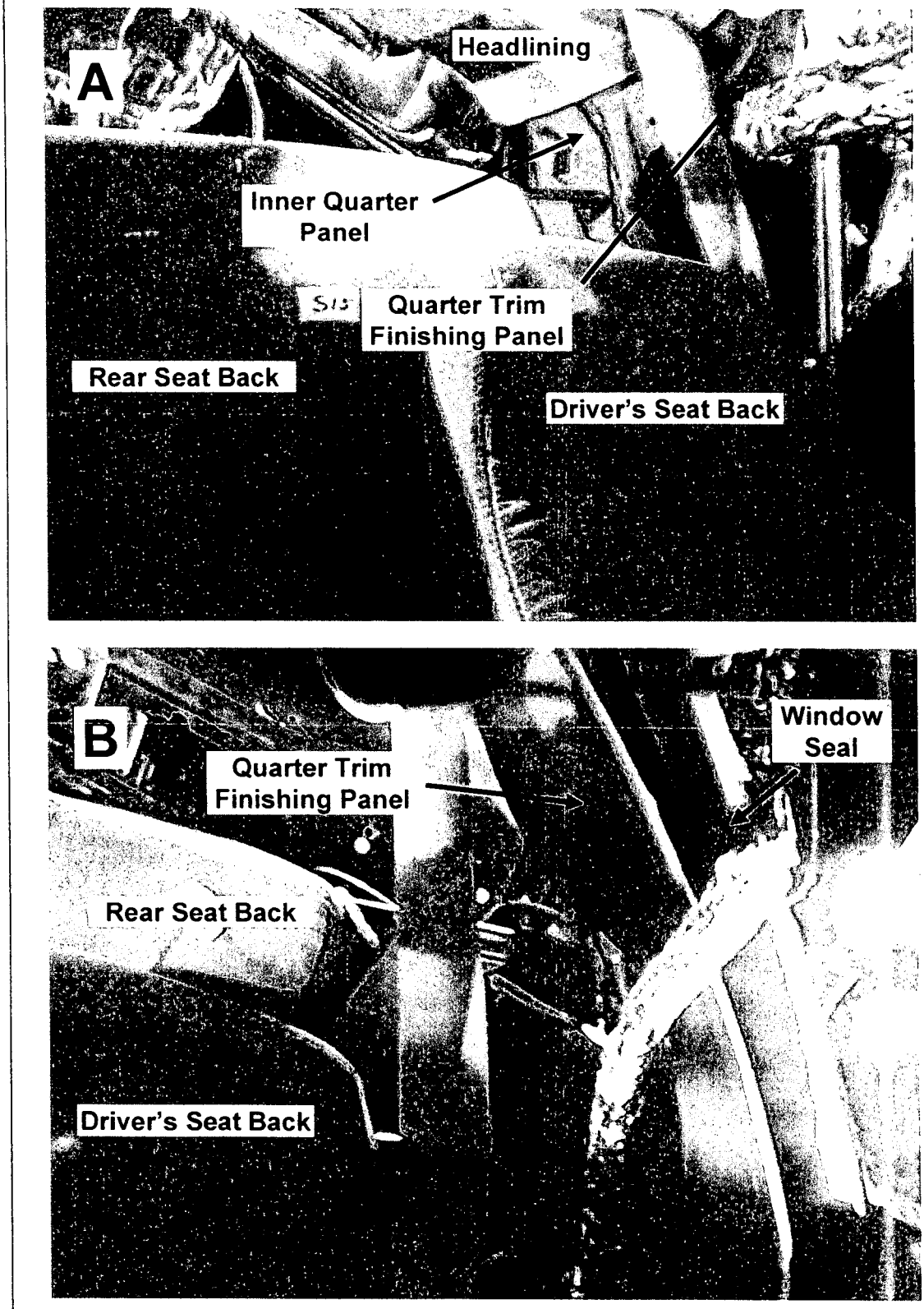

Figure 24. Fire Test F971001. Video stills from Cameras 6 (A) and 7 (B) showing the rear left corner of the test vehicle at the time of ignition (0 seconds post-ignition).

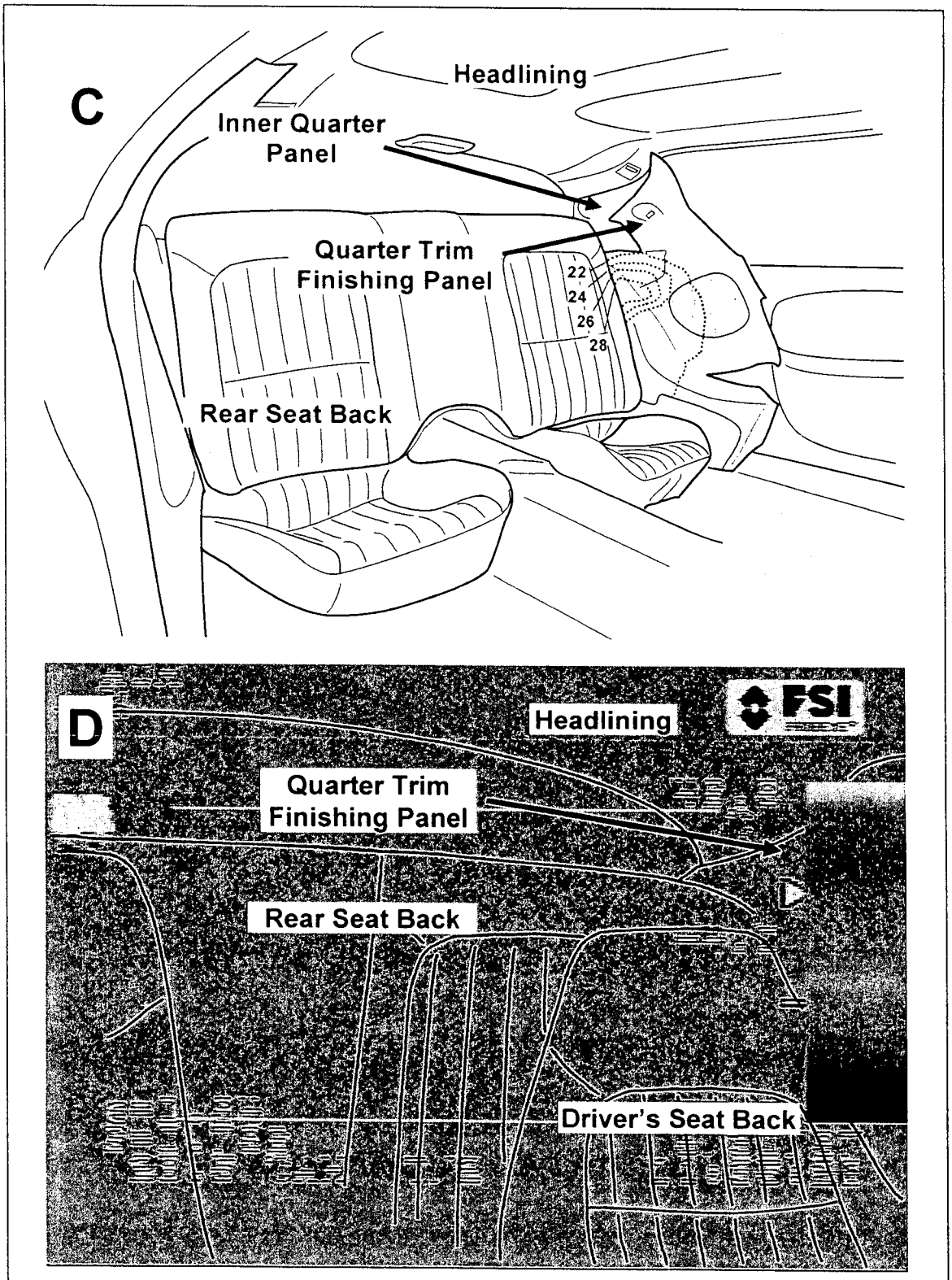

Figure 24, continued. Fire Test F971001. Estimated isothermal contour plot (C) and Infrared thermogram (lower) from IR6 (D) showing temperatures in the rear left corner of the test vehicle at the time of ignition (0 seconds post-ignition).

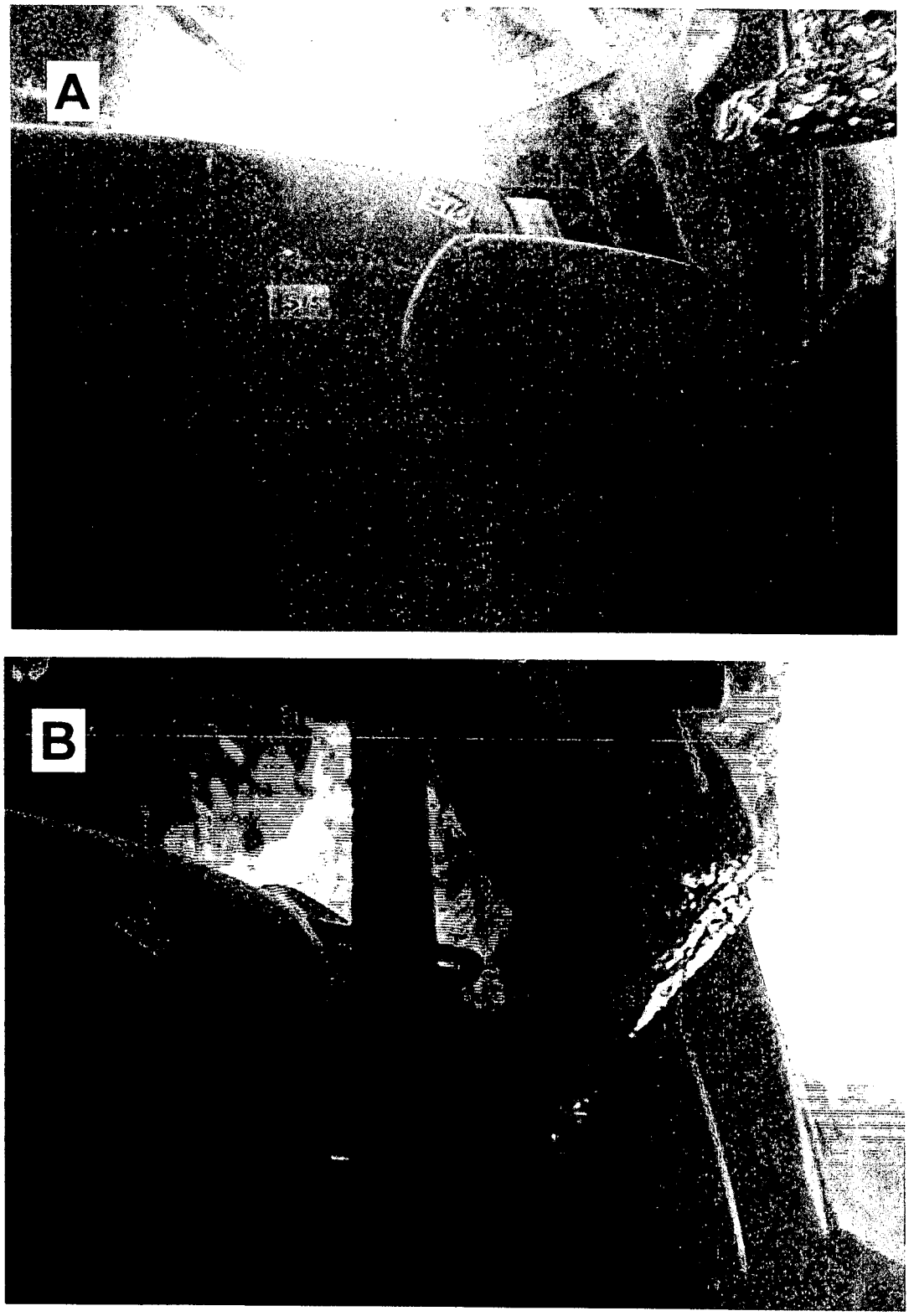

Figure 25. Fire Test F971001. Video stills from Cameras 6 (A) and 7 (B) showing the rear left corner of the test vehicle at 15 seconds post-ignition.

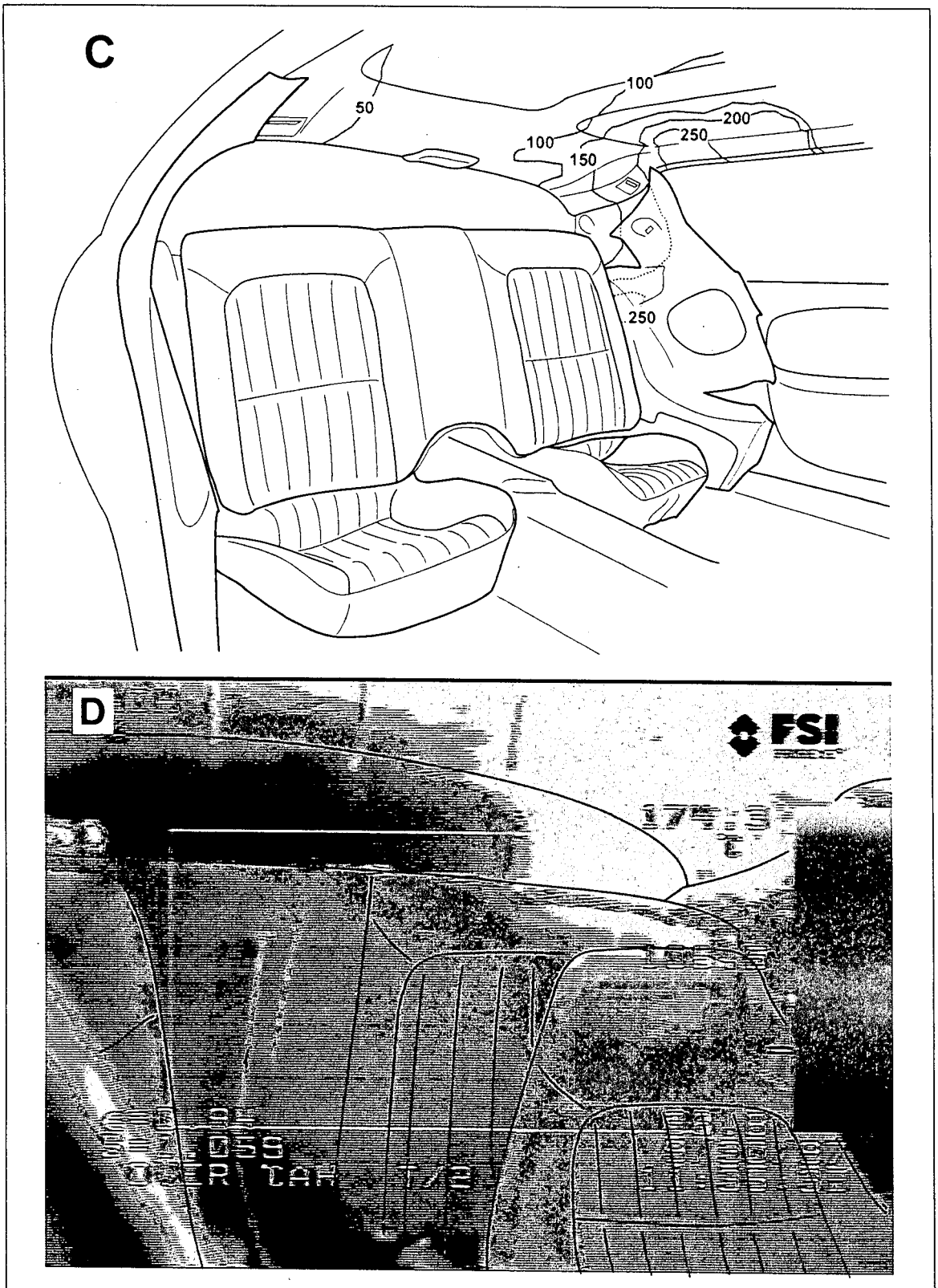

Figure 25, continued. Fire Test F971001. Estimated isothermal contour plot (C) and Infrared thermogram from IR6 (D) showing temperatures in the rear left corner of the test vehicle at 15 seconds post-ignition.

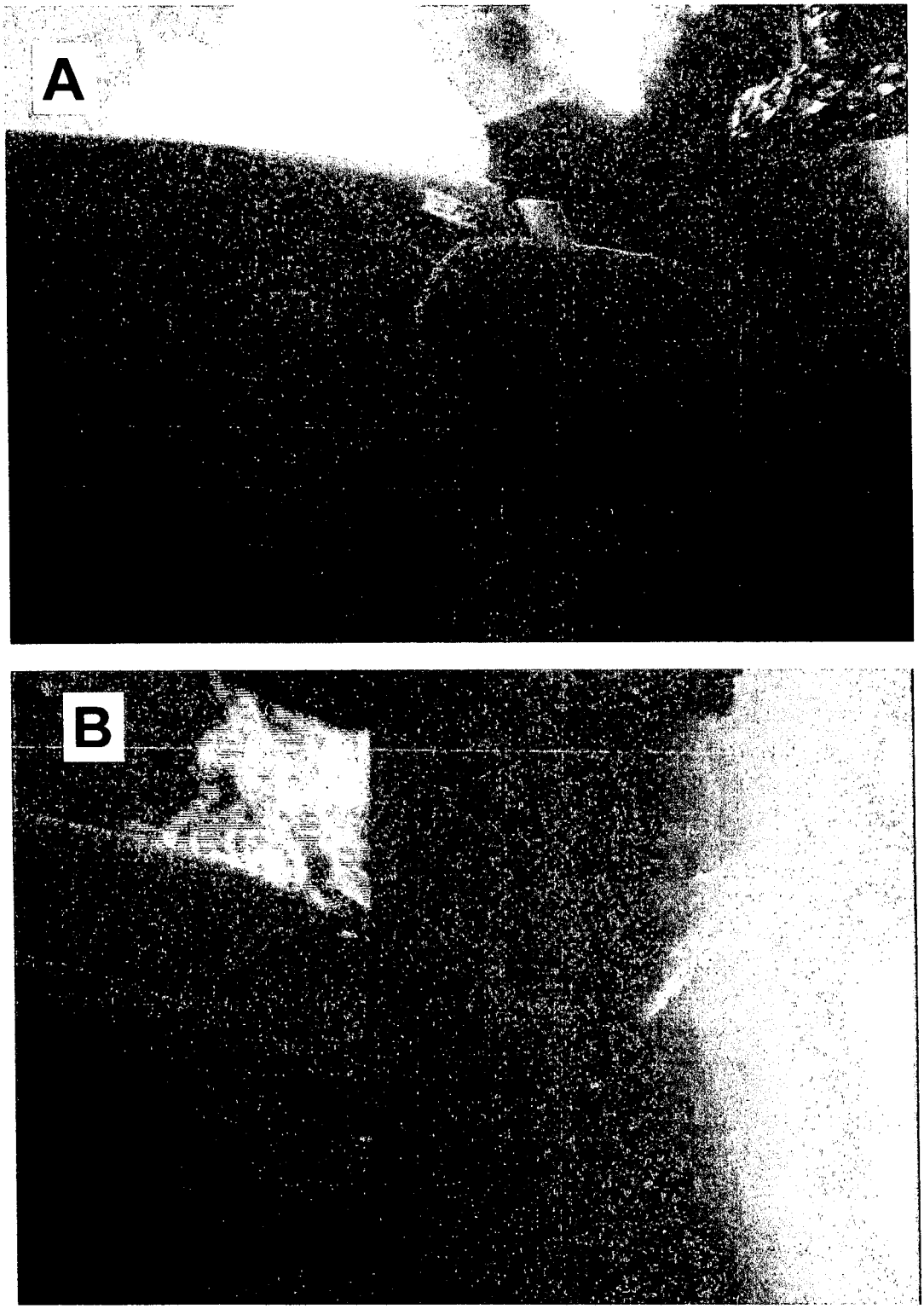

Figure 26. Fire Test F971001. Video stills from Cameras 6 (A) and 7 (B) showing the rear left corner of the test vehicle at 30 seconds post-ignition.

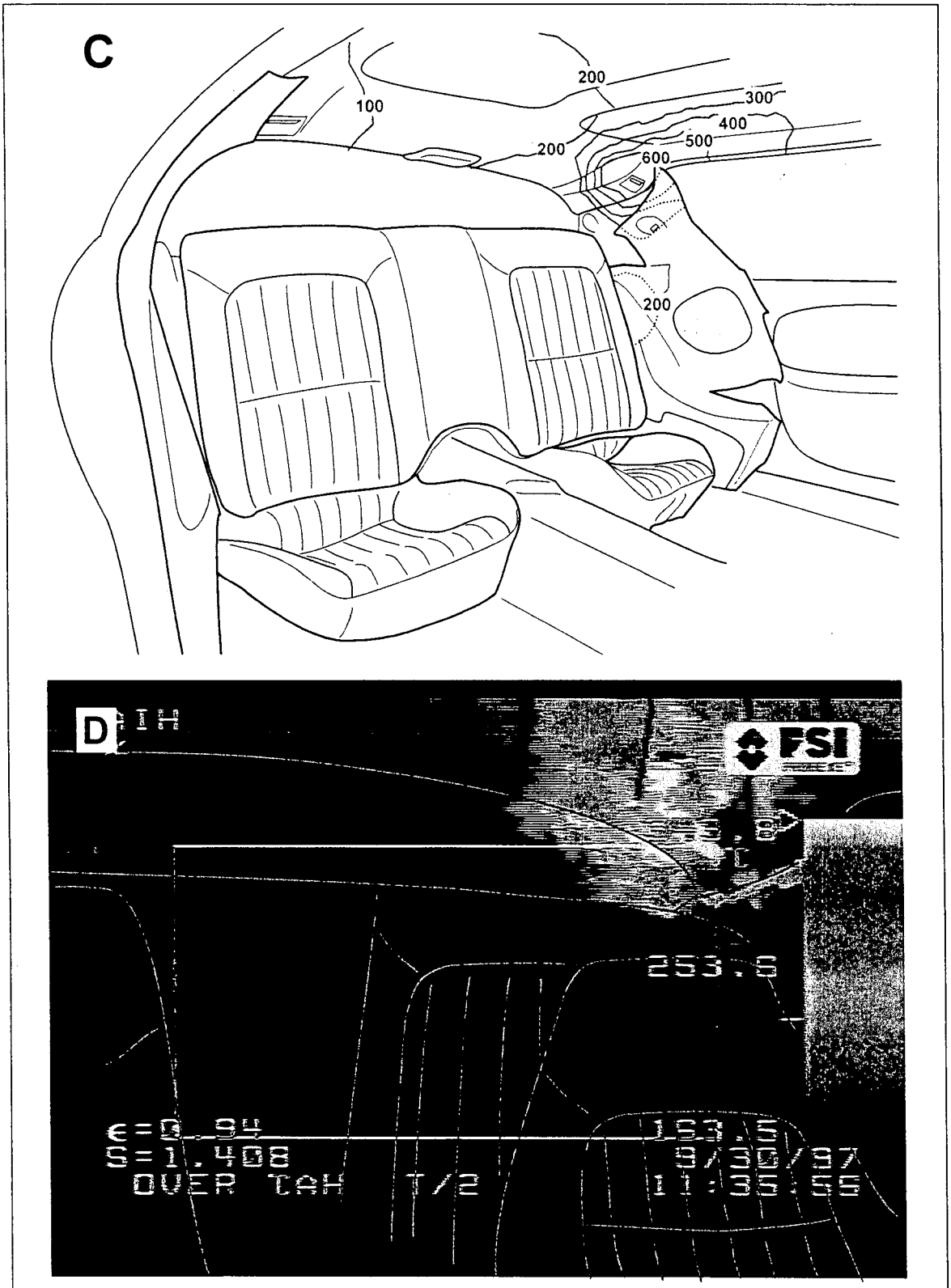

Figure 26, continued. Fire Test F971001. Estimated isothermal contour plot (C) and Infrared thermogram from IR6 (D) showing temperatures in the rear left corner of the test vehicle at 30 seconds post-ignition.

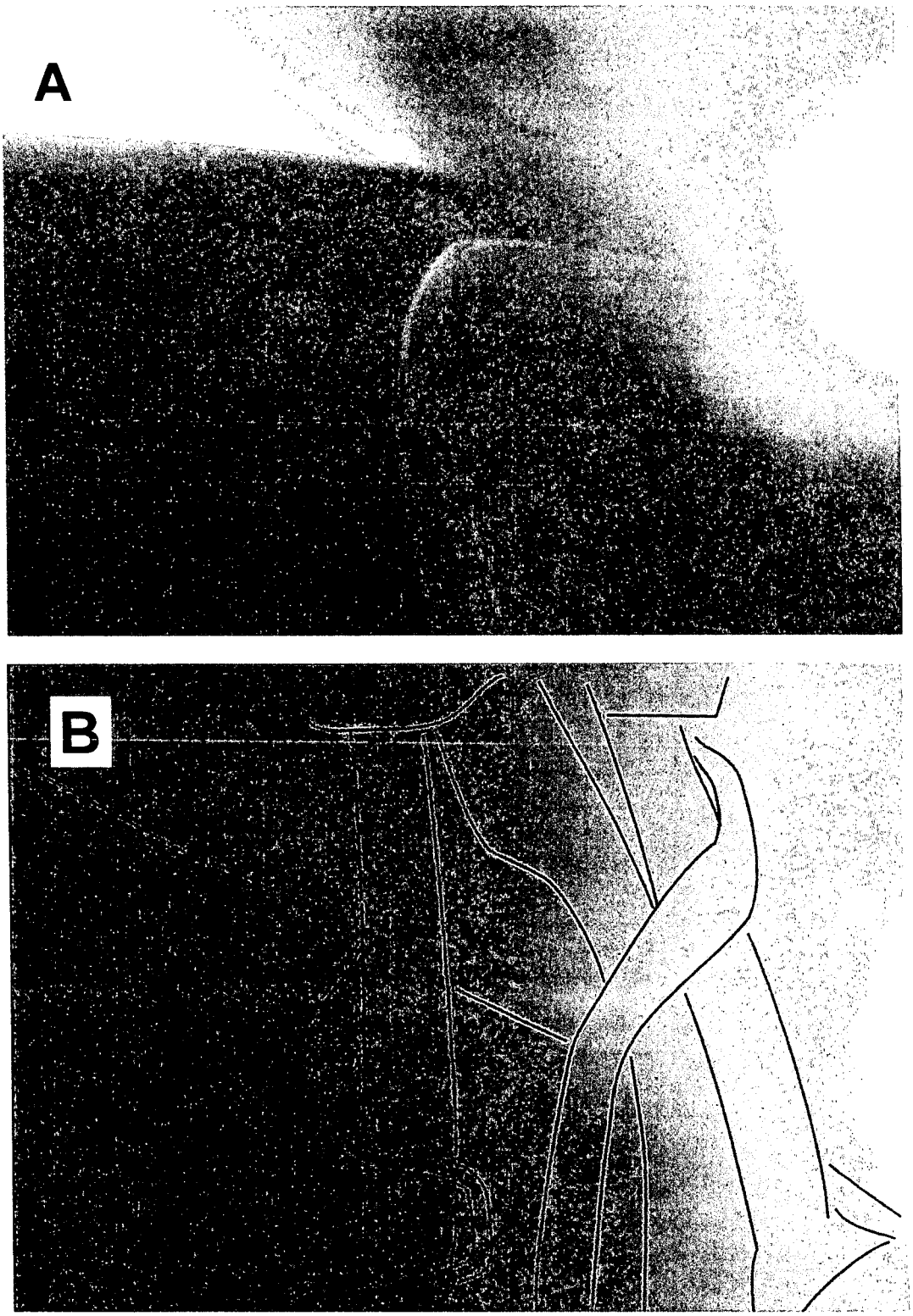

Figure 27. Fire Test F971001. Video stills from Cameras 6 (A) and 7 (B) showing the rear left corner of the test vehicle at 45 seconds post-ignition.

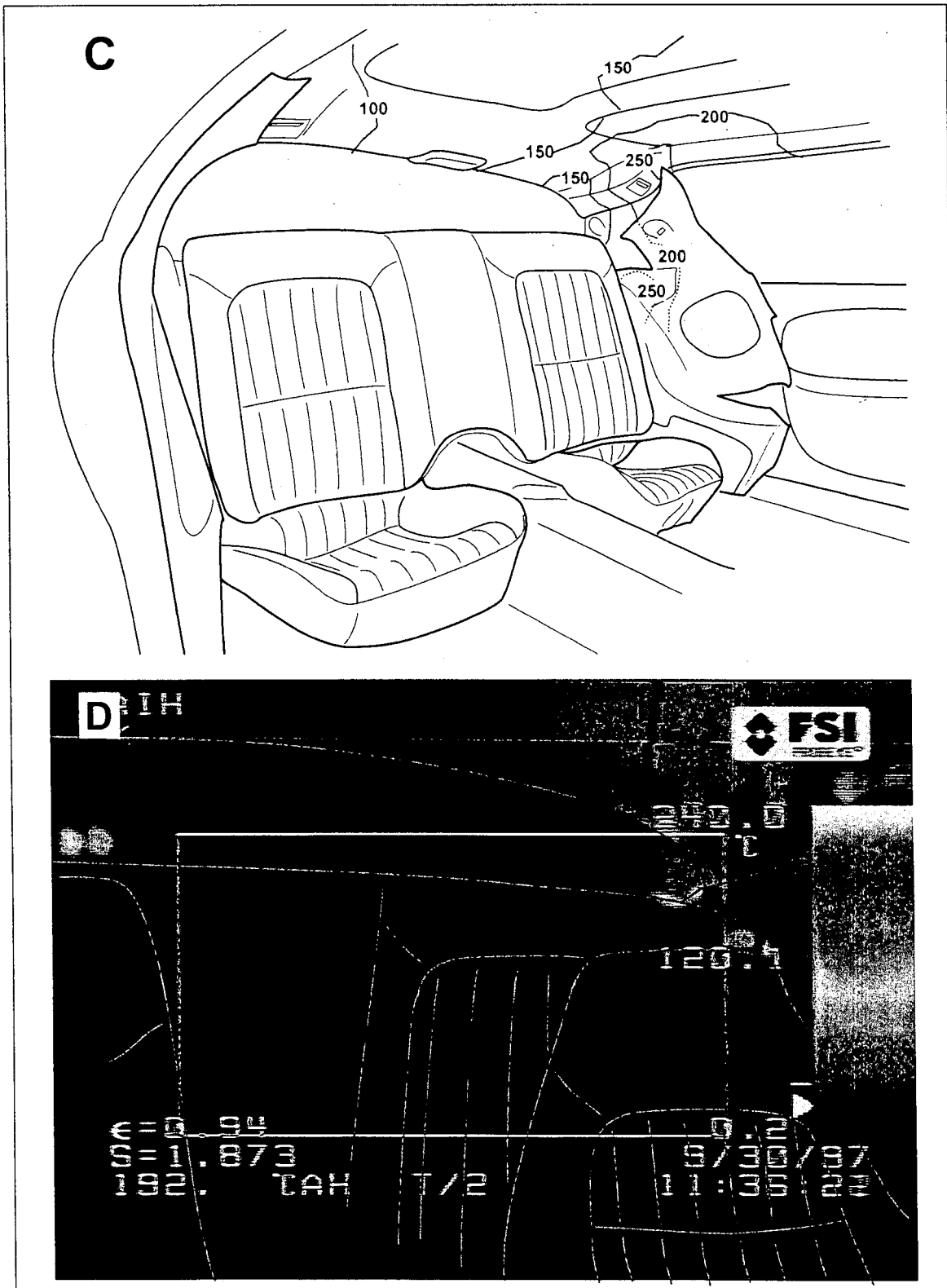

Figure 27, continued. Fire Test F971001. Estimated isothermal contour plot (C) and Infrared thermogram from IR6 (D) showing temperatures in the rear left corner of the test vehicle at 45 seconds post-ignition.

The infrared thermogram from IR6 at this time (D, Fig. 26) shows temperatures in this area were greater than 444°C (the upper temperature limit of IR6 at that time). By 45 seconds post-ignition, the fire plume had disappeared (A and B, Fig. 27). Temperatures along the headlining panel and behind the quarter trim panel less than 300 °C at this time (C and D, Fig. 27).

Flames were observed in the area behind the displaced left interior quarter trim finishing panel between 160 and 170 seconds post-ignition. Figures 28 through 33 show a series of video stills from Cameras 6 and 7, estimated isothermal contour plots, and Infrared thermograms from IR6 at 160, 170, 180, 190, 200, and 210 seconds post-ignition. Comparison of the video stills in Figures 28 and 29 shows that flames became visible along the forward edge of the left interior quarter trim finishing panel between 160 and 170 seconds post-ignition (B, Fig.'s 28 and 29). Flames were not visible along its upper edge at this time (A, Fig.'s 28 and 29). The isothermal contour plots (C, Fig.'s 28 and 29) and infrared thermograms (D, Fig.'s 28 and 29) in these figures indicate that flames did not contact the headlining panel during this time. By 180 seconds post-ignition, flames were visible between the front of the left interior quarter trim finishing panel and the drivers seat back (B, Fig. 30). Temperatures along the lower surface of the of the left rear corner of the headlining panel were between 300 and 400°C at 180 seconds post-ignition (C, Fig. 30), indicating that heated gases were spreading outward below the roof of the test vehicle at this time. Flames were not visible around the upper and rear edges of the displaced interior quarter trim finishing panel at this time (A, Fig. 30). The thermocouple data indicate that flames were present along the top edge of the left interior quarter trim finishing panel between 180 and 190 seconds post-ignition (C, Fig. 31). Flames had started to spread forward and to the right along the headlining panel by 190 seconds post-ignition (Fig. 31).

The time of ignition, the rate of flame spread, or the area of the on the left interior quarter trim finishing panel that had burned could not be determined precisely from the data acquired during this test. For example, the video stills from Camera 6 at 200 and 210 post-ignition, and from Camera 7 and 200 seconds post-ignition show flames in front of much of the left rear quarter of the test vehicle (Fig.'s 32 and 33), suggesting that the entire trim panel had ignited. The accompanying isothermal contour plots calculated using data recorded from thermocouples located on the inner and outer surfaces of the trim panel show temperatures less that 500°C between 190 and 200 seconds post-ignition (see **APPENDIX C**), suggesting that the trim panel had not ignited at this time. One possible explanation for this apparent discrepancy is that this area of the trim finishing panel had not ignited at this time and flames observed in the video stills from Cameras 6 and 7 at 200 and 210 seconds post-ignition were from burning objects below the fields of view of these cameras. Another possible explanation is that the thermoplastic trim panel

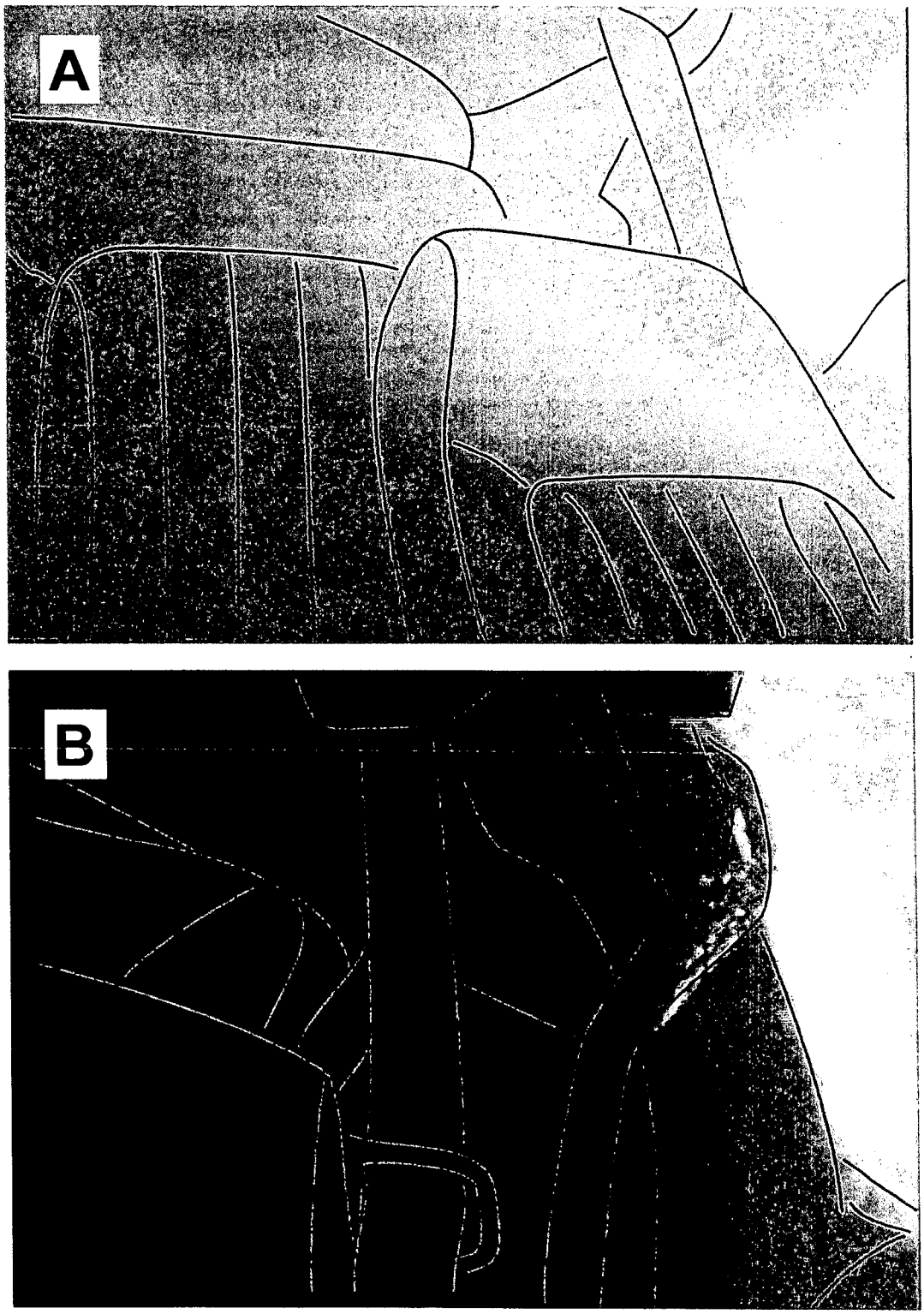

Figure 28. Fire Test F971001. Video stills from Cameras 6 (A) and 7 (B) showing the rear left corner of the test vehicle at 160 seconds post-ignition.

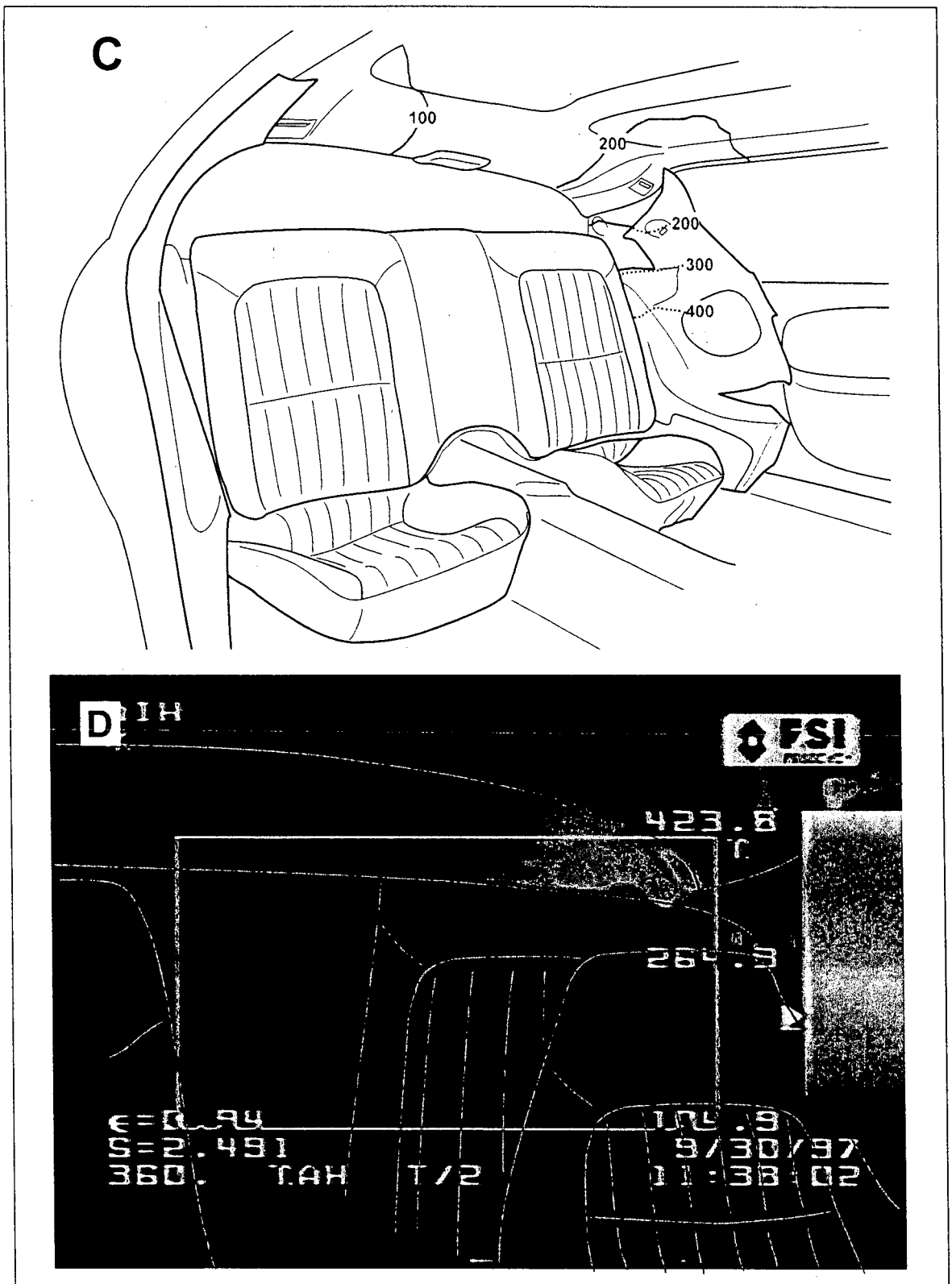

Figure 28, continues. Fire Test F971001. Estimated isothermal contour plot (C) and Infrared thermogram from IR6 (D) showing temperatures in the rear left corner of the test vehicle at 160 seconds post-ignition.

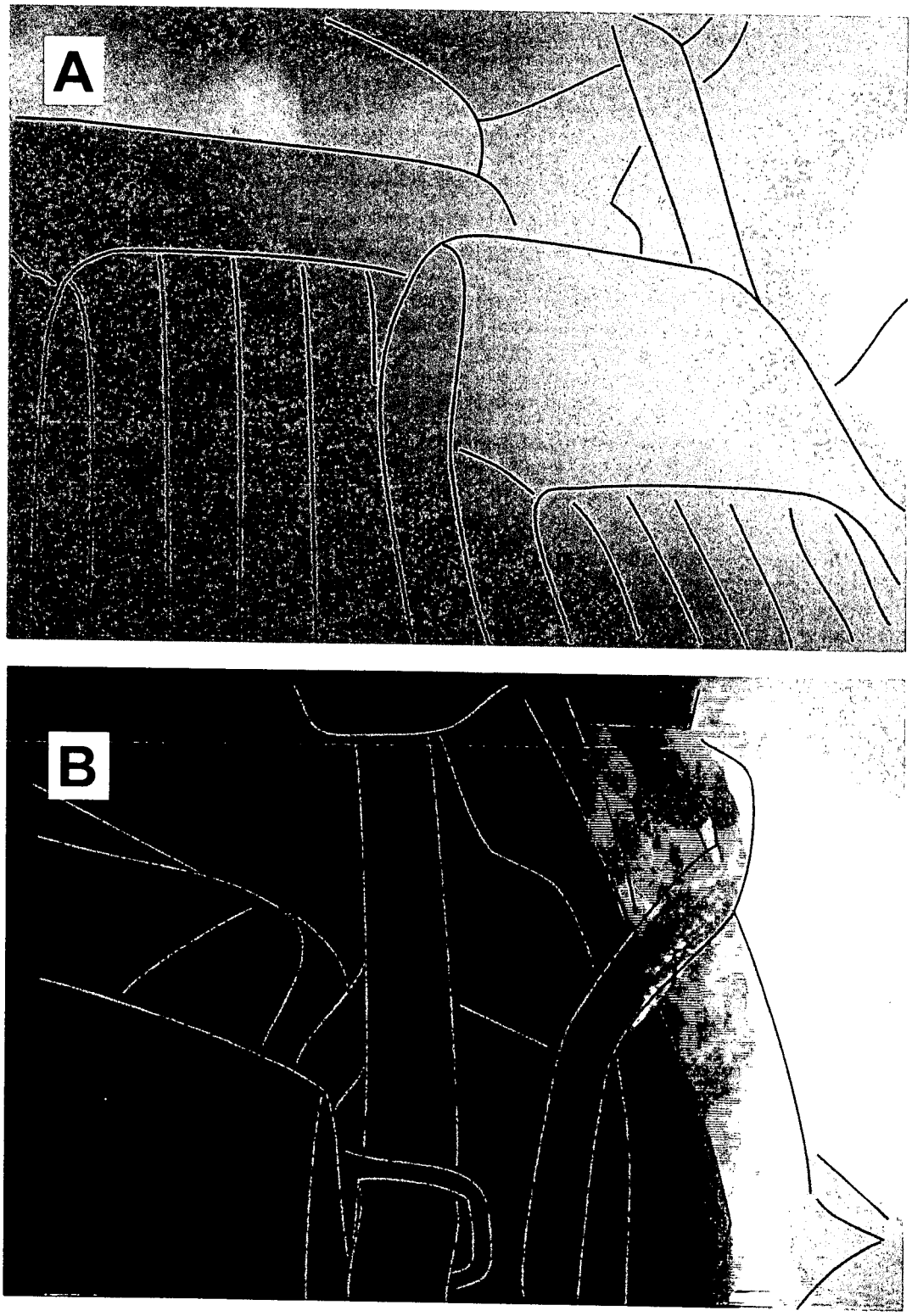

Figure 29. Fire Test F971001. Video stills from Cameras 6 (A) and 7 (B) showing the rear left corner of the test vehicle at 170 seconds post-ignition.

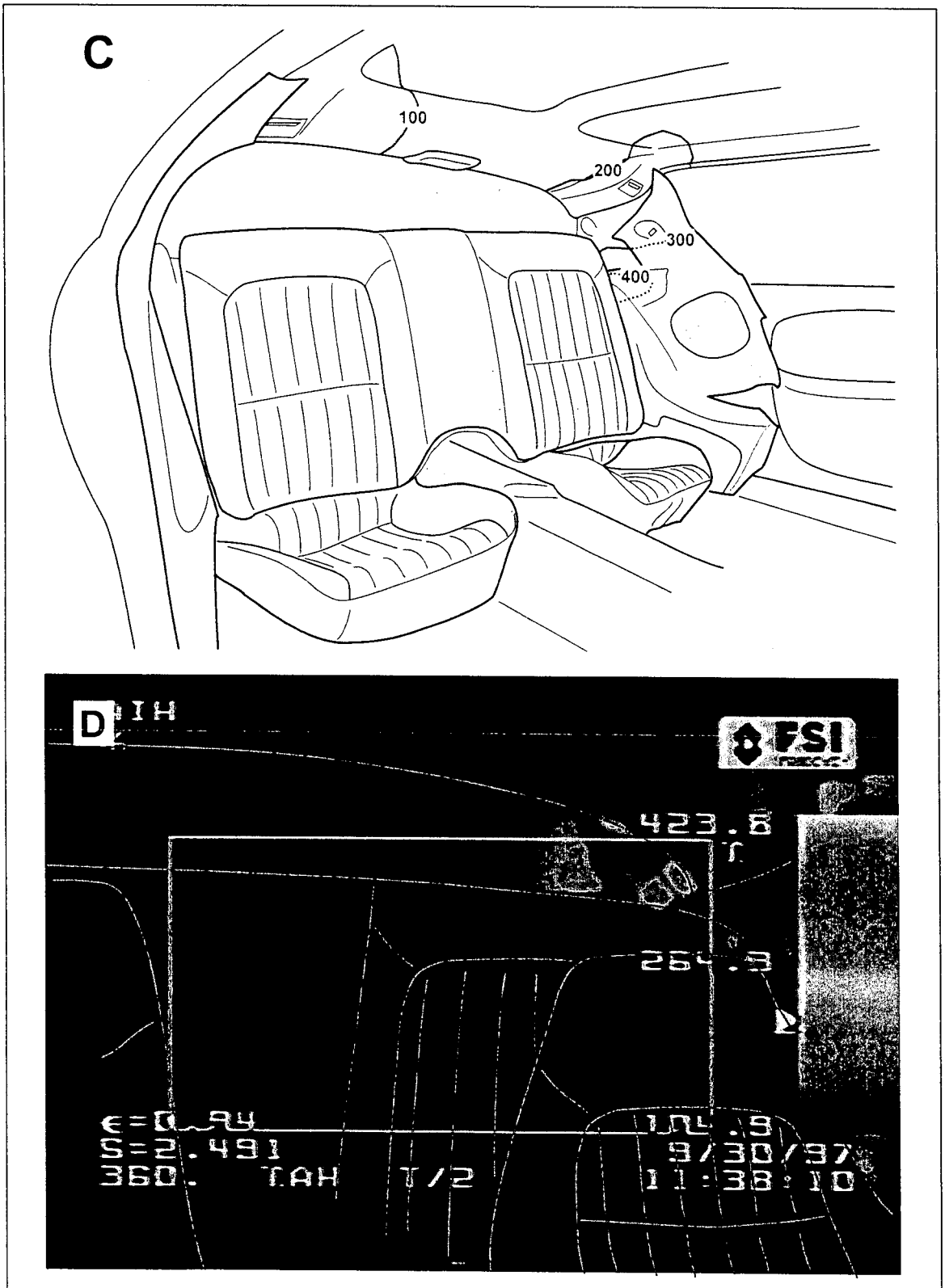

Figure 29, continues. Fire Test F971001. Estimated isothermal contour plot (C) and Infrared thermogram from IR6 (D) showing temperatures in the rear left corner of the test vehicle at 170 seconds post-ignition.

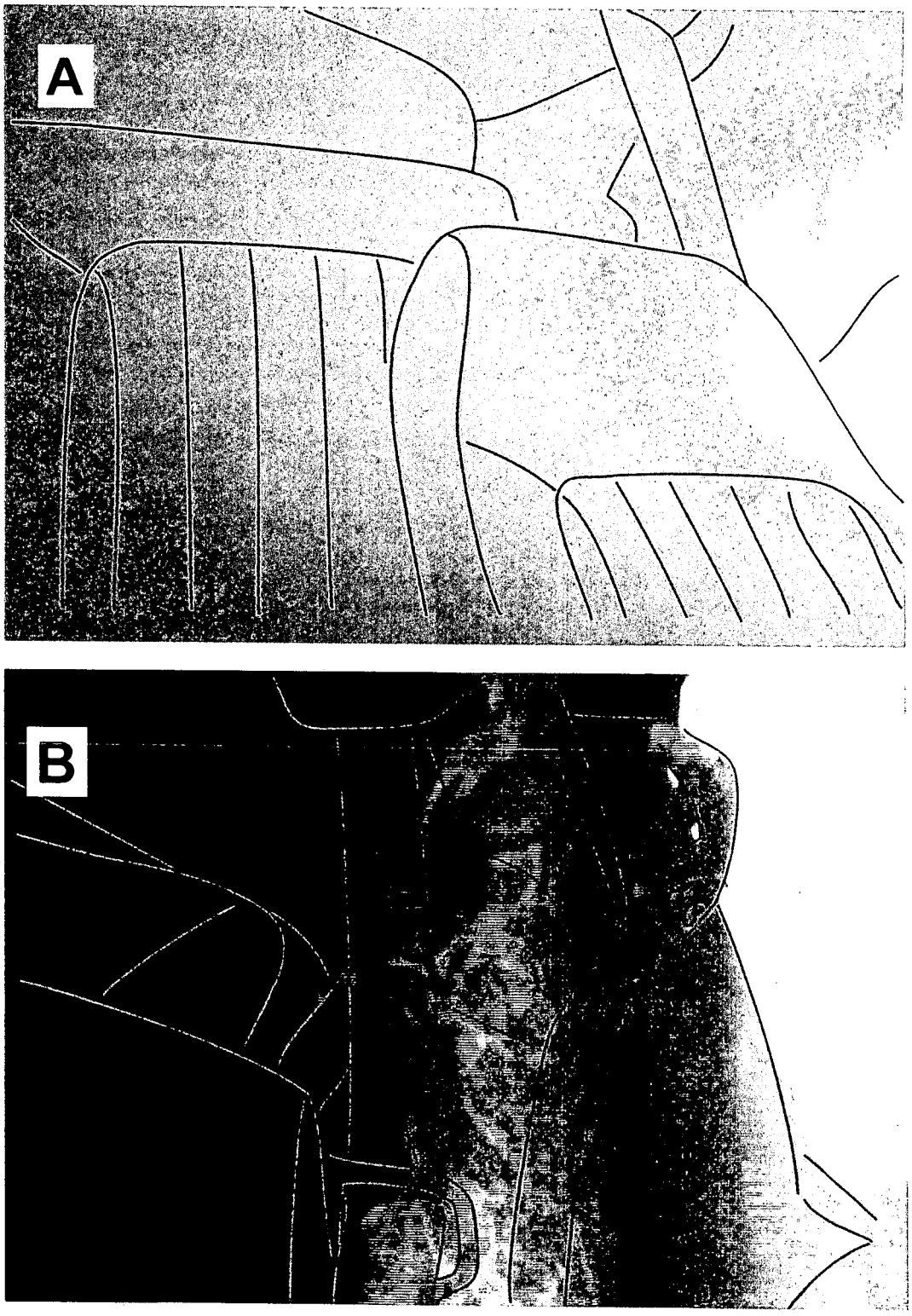

Figure 30. Fire Test F971001. Video stills from Cameras 6 (A) and 7 (B) showing the rear left corner of the test vehicle at 180 seconds post-ignition.

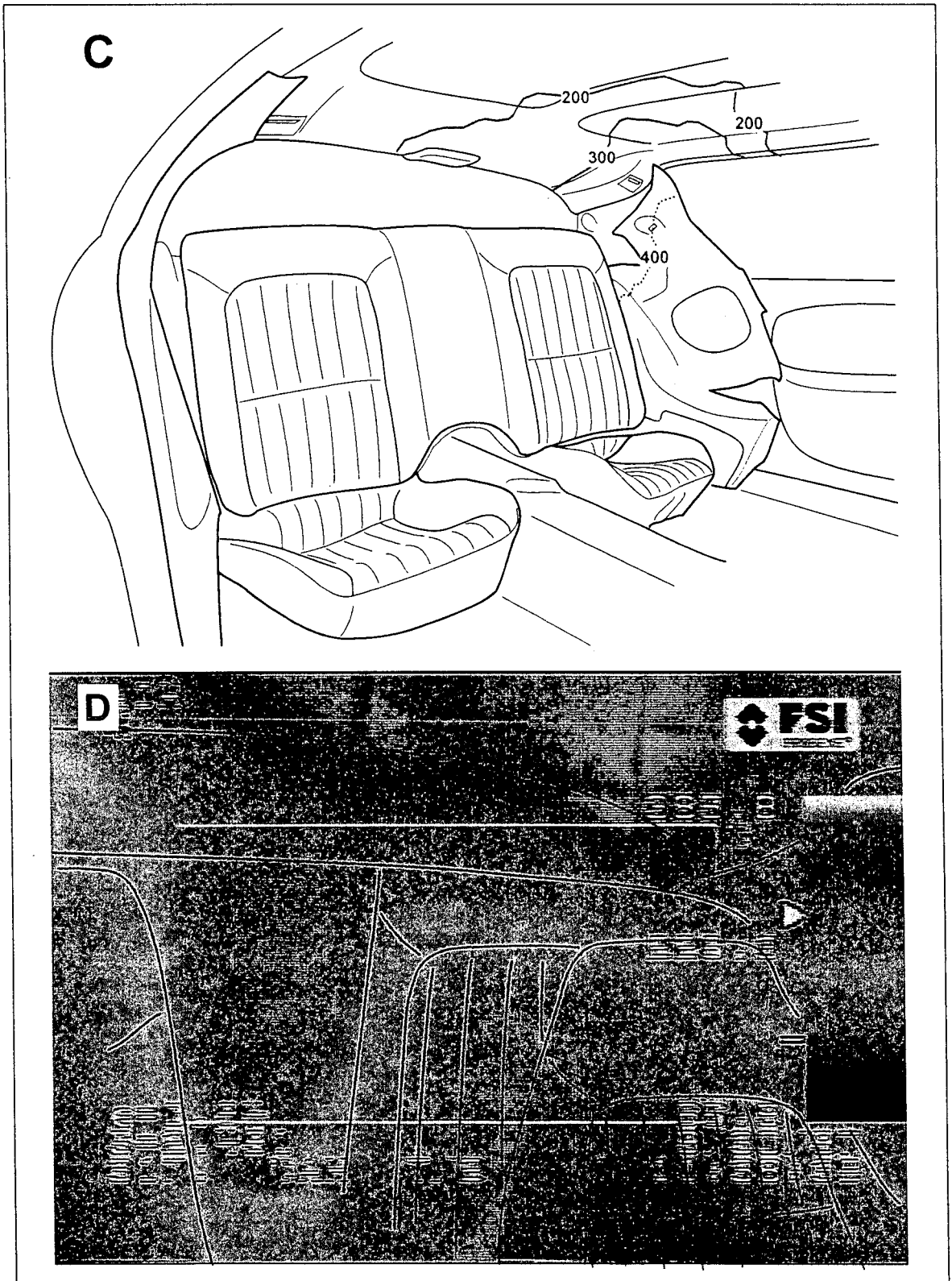

Figure 30, continued. Fire Test F971001. Estimated isothermal contour plot (C) and Infrared thermogram (lower) from IR6 (D) showing temperatures in the rear left corner of the test vehicle at 180 seconds post-ignition.

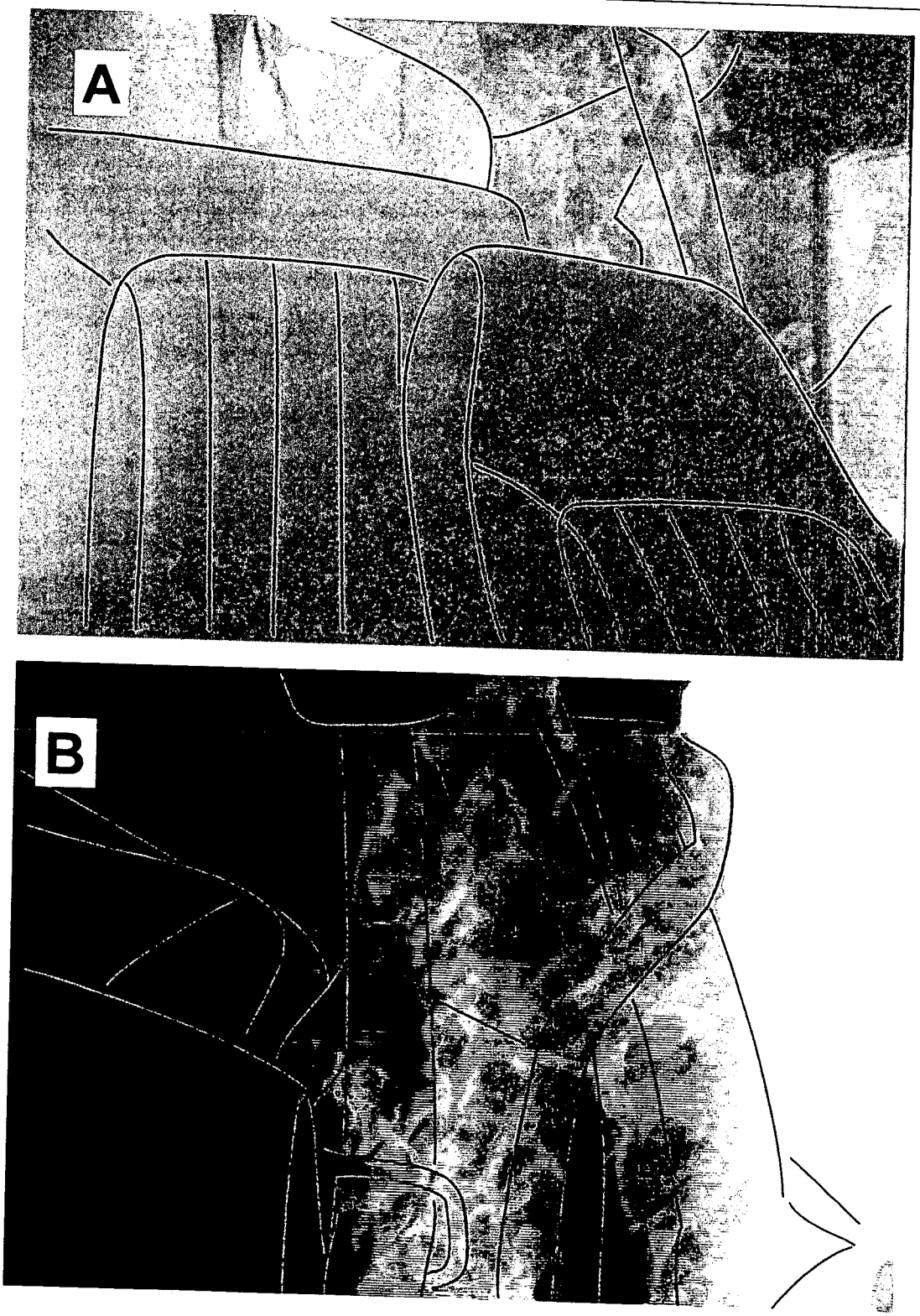

Figure 31. Fire Test F971001. Video stills from Cameras 6 (A) and 7 (B) showing the rear left corner of the test vehicle at 190 seconds post-ignition.

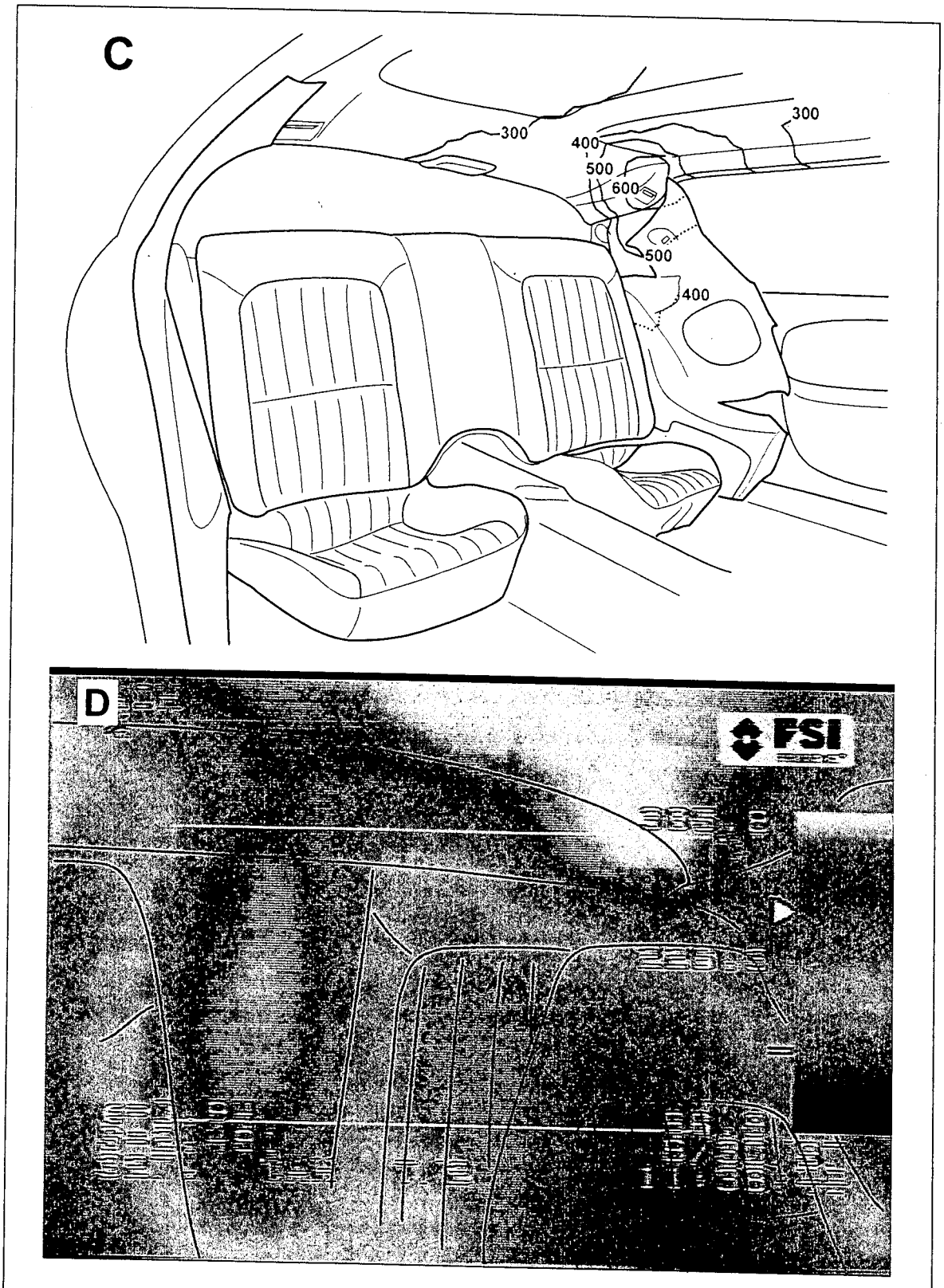

Figure 31, continued. Fire Test F971001. Estimated isothermal contour plot (C) and Infrared thermogram from IR6 (D) showing temperatures in the rear left corner of the test vehicle at 190 seconds post-ignition.

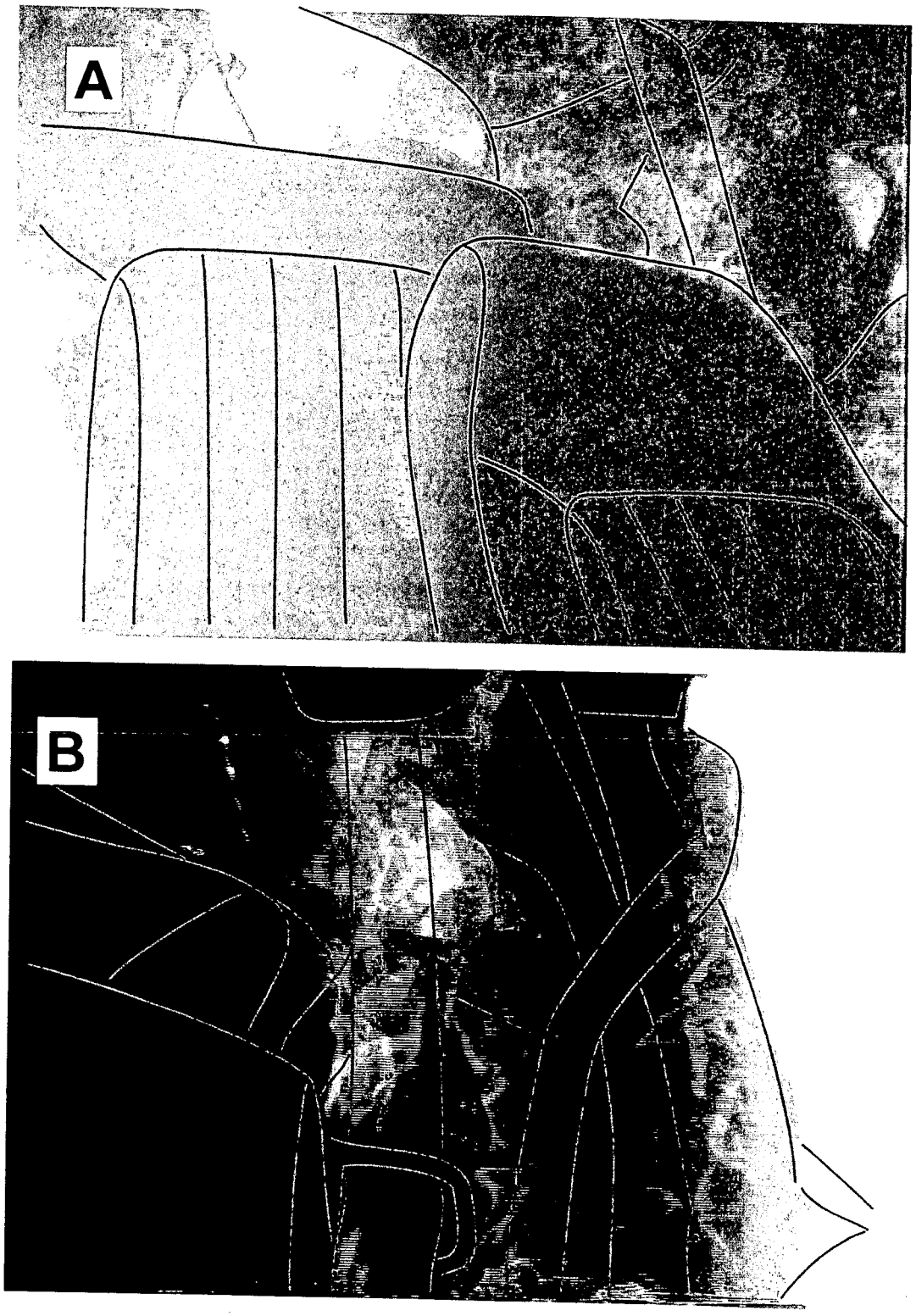

Figure 32. Fire Test F971001. Video stills from Cameras 6 (A) and 7 (B) showing the rear left corner of the test vehicle at 200 seconds post-ignition.

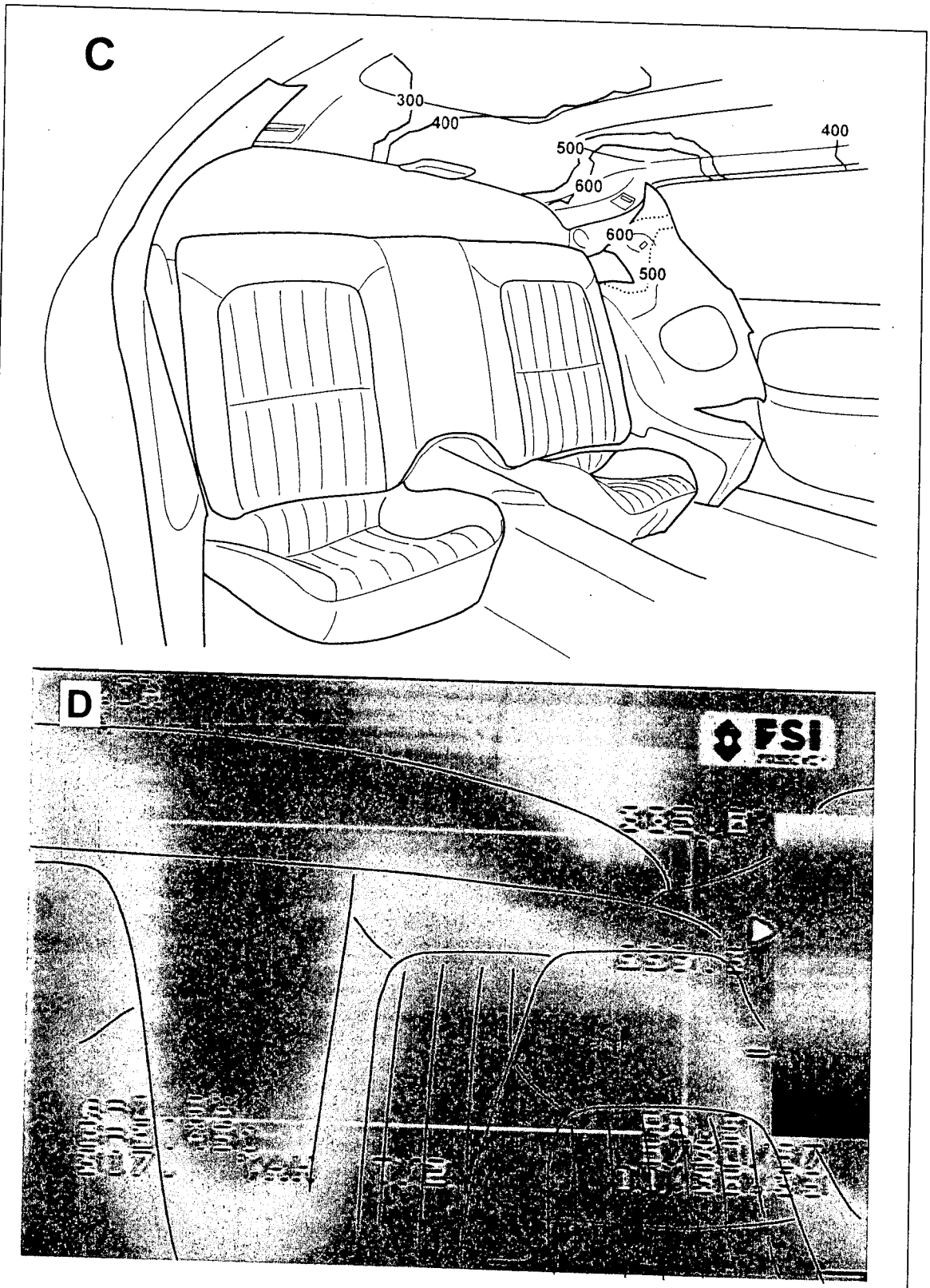

Figure 32, continued. Fire Test F971001. Estimated isothermal contour plot (C) and Infrared thermogram from IR6 (D) showing temperatures in the rear left corner of the test vehicle at 200 seconds post-ignition.

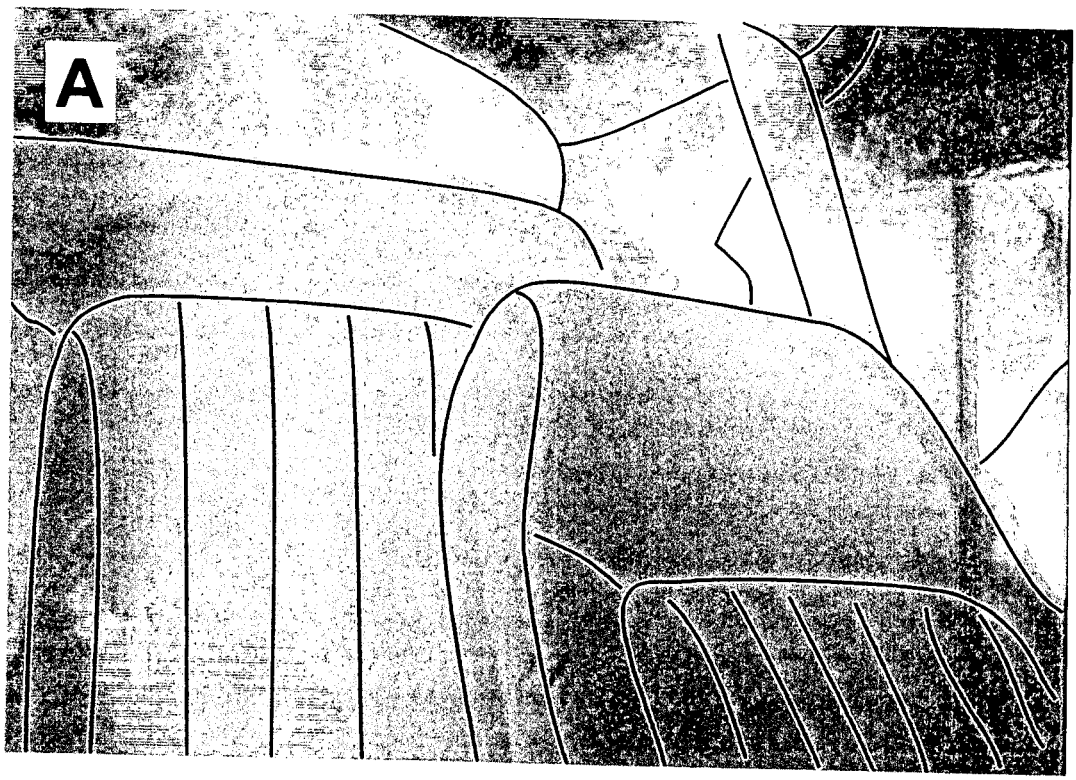

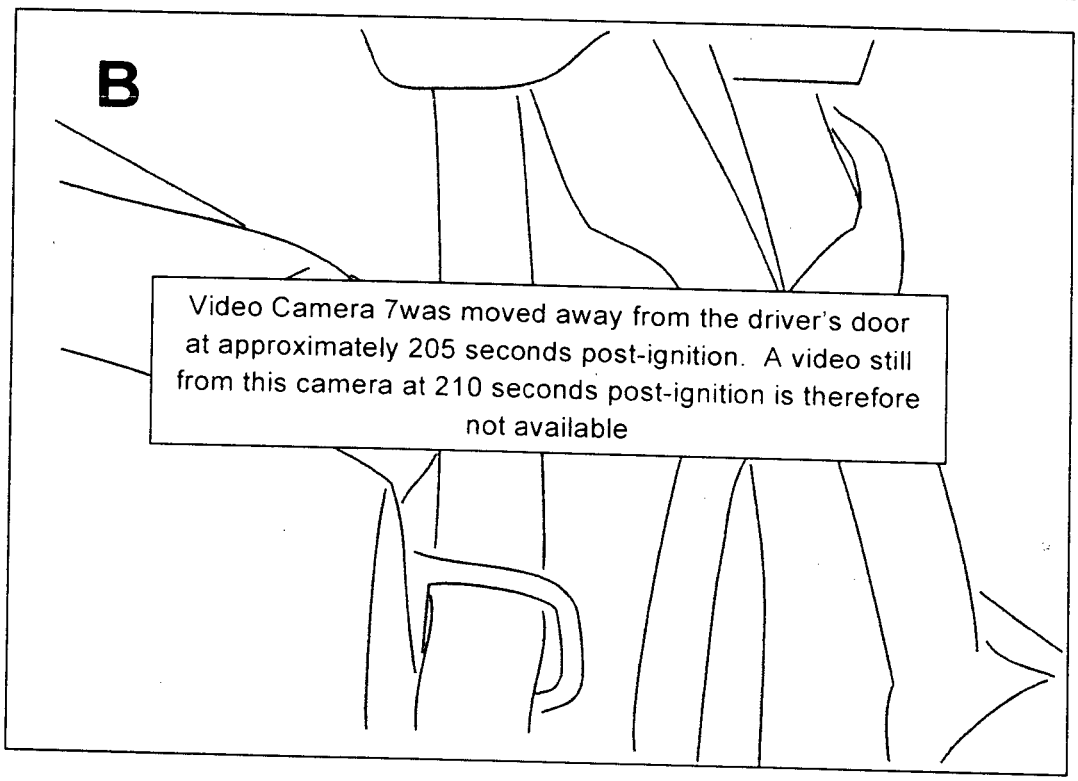

Figure 33. Fire Test F971001. Video stills from Cameras 6 (A) and 7 (B) showing the rear left corner of the test vehicle at 210 seconds post-ignition.

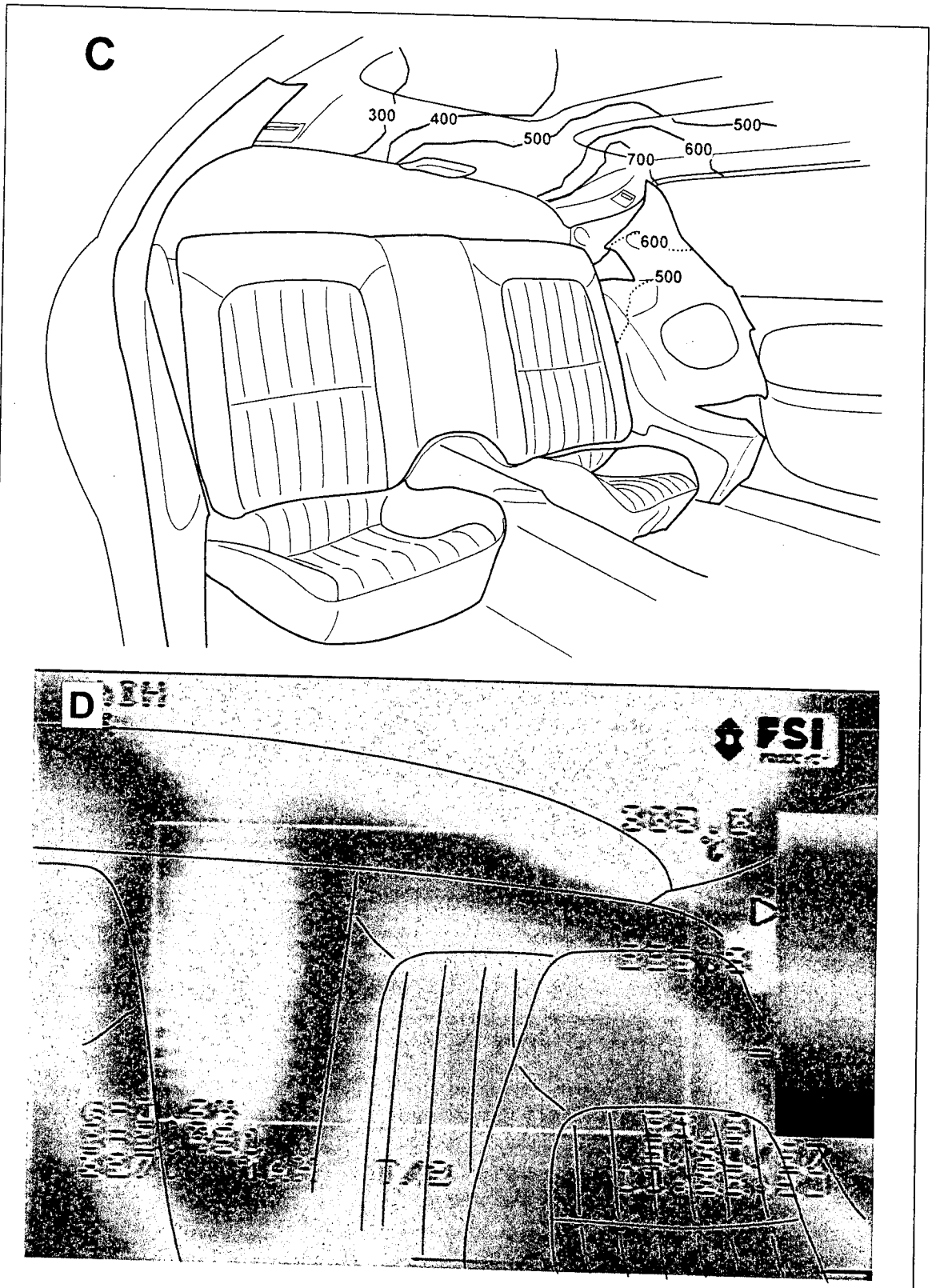

Figure 33, continued. Fire Test F971001. Estimated isothermal contour plot (C) and Infrared thermogram from IR6 (D) showing temperatures in the rear left corner of the test vehicle at 210seconds post-ignition.

may have started to melt and sag around this time, causing some of the thermocouples that were attached to trim panel to change position or to become detached and move out of the flames.

One of the possible pathways for flame-spread into the area behind the interior quarter trim finishing panel was through the seam openings around the left rear wheelhouse. The preceding discussion showed that flames were present in this area briefly during the first 30 after ignition, and again at between 150 to 160 seconds post-ignition which lead to ignition of the quarter trim panel and the left rear section of the headlining panel. The following analysis of the test data indicates that flames entered in the left rear wheelhouse and the seam openings around the wheelhouse between 200 to 210 seconds post-ignition.

Two thermocouples were installed in the wheelhouse just below the inner wheelhouse panel and above the left rear tire (Fig. 34). One thermocouple also was on the filler splash shield, which was folded on top of the tire. One heat flux transducer was installed in the top of the inner wheelhouse panel facing downward, and one heat flux transducer was installed in a seam opening at the front of the wheelhouse and facing rearward.

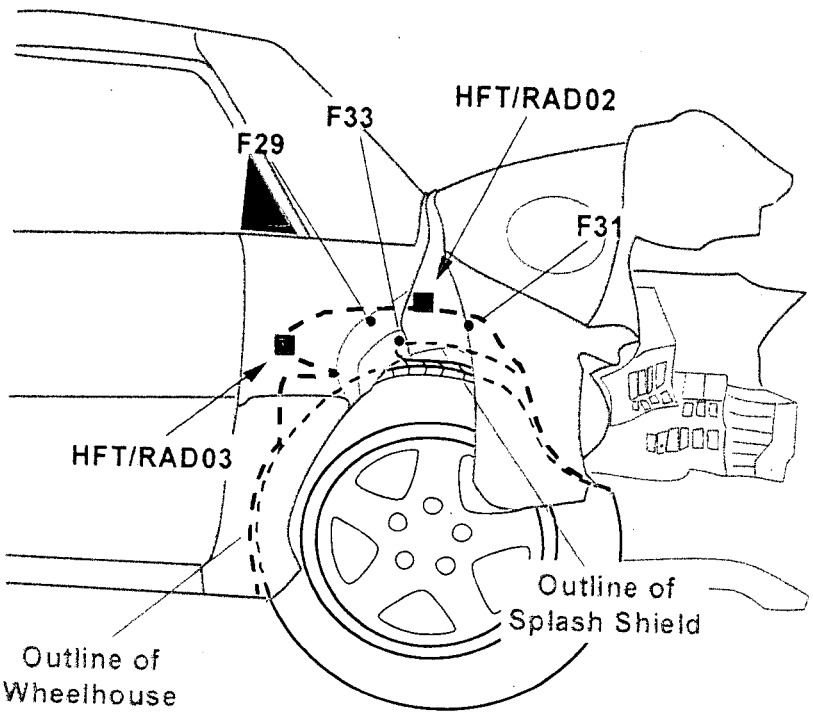

Figure 34. Fire Test F971001. Left side view of the test vehicle. Thermocouples F29 and F31 were located inside the wheelhouse approximately 1 cm below the wheelhouse inner panel (see also Fig. C1). Thermocouple F33 was located inside the wheelhouse on the filler splash shield (see also Fig. C1). HFT/RAD02 was located in the left rear wheelhouse inner panel and facing downward (see also Fig. E1). HFT/RAD03 was located in a seam opening at the front of the left rear wheelhouse and facing rearward (see also Fig. E1).

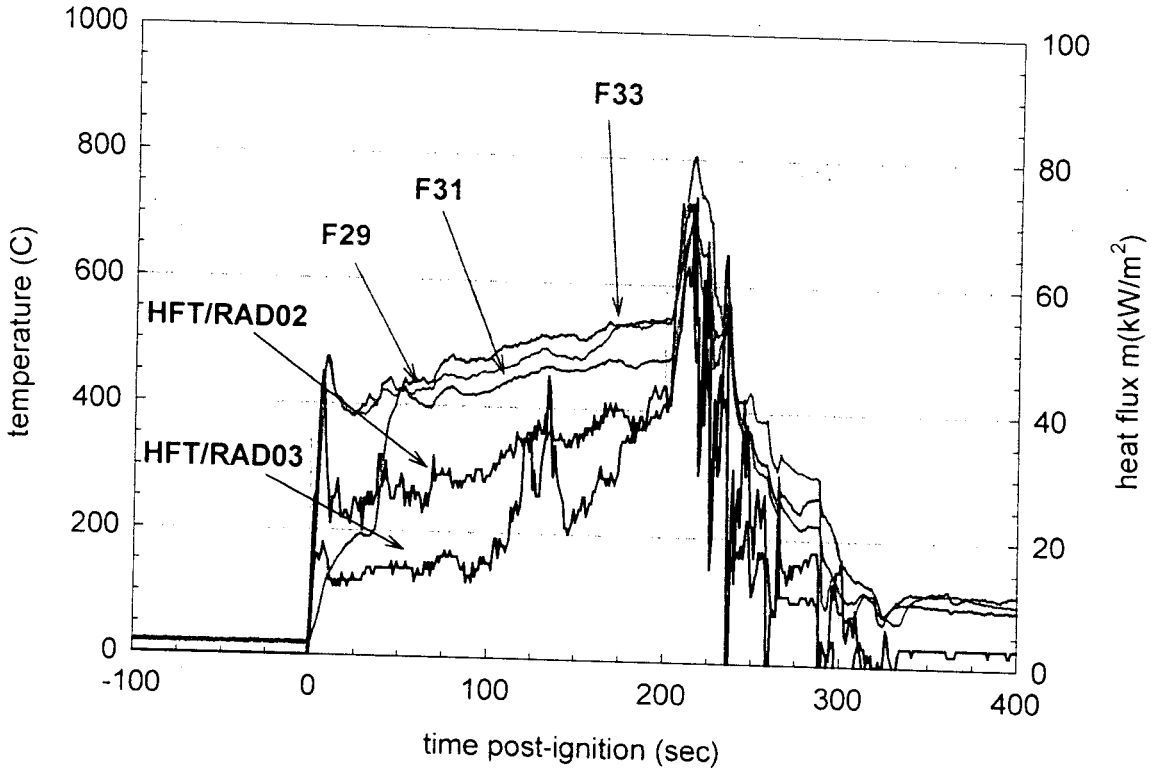

Figure 35. Fire Test F971001. Plots of data recorded from Thermocouples F29, F31, and F33, and Heat Flux Transducers HFT/RAD02 and HFT/RAD03.

The temperature data recorded from Thermocouples F29 and F31 before 200 seconds post-ignition were less than 600°C (Fig. 35), indicating that neither of these thermocouples were exposed directly to flames during this time (see footnote 4). The increase in temperature from 500 – 550°C to 650 – 700°C recorded from these thermocouples between 200 and 215 seconds post-ignition indicates that flames entered the top of the wheelhouse at this time. The simultaneous increase in the temperatures recorded from Thermocouple F33 from greater than 550°C to approximately 700°C suggests that flames were contacting the splash shield between 200 and 215 seconds post-ignition (Fig. 35).

The heat flux to a horizontal surface above a burning gasoline pool was measured in a separate laboratory study [6]. A horizontal metal sheet was placed over a burning gasoline pool, where the height of the metal sheet above the gasoline pool was less than the unobstructed flame height. Flames made contact with the sheet above the center of the burning pool, but not above the periphery of the burning pool. The measured heat flux to the metal sheet directly above the center of the burning gasoline pool was in the range of 60 to 80 kW/m^2 [6]. The heat flux to the sheet at the periphery of the burning pool was 10 to 30 kW/m^2 [6].

The total heat flux data recorded from HFT/RAD02 and HFT/RAD03 followed similar trends to the temperatures recorded from Thermocouples F29 and F31 (Fig. 35). The heat fluxes recorded

from both transducers were < 45 kW/m^2 for the first 200 seconds post-ignition. The heat fluxes recorded from both transducers increased from 40 – 45 kW/m^2 to greater than 60 kW/m^2 between 200 and 215 seconds post-ignition. And except for two transient peaks, the heat flux recorded from HFT/RAD03 was less than the heat flux recorded from HFT/RAD02 before 200 seconds post-ignition. As with the temperature data recorded from Thermocouples F29 and F31, the heat flux data recorded from HFT/RAD02 indicated that flames entered the part of the left rear wheelhouse between 200 and 215 seconds post-ignition (Fig. 35). The heat flux data recorded from HFT/RAD03 indicates that flames entered the passenger compartment through the seam opening at the front of the left rear wheelhouse between 200 and 215 seconds post-ignition (Fig. 35).

The timing of flame-spread into the rear left wheelhouse and through the seam opening at the front of the wheelhouse determined from the recorded test data is not consistent with the timing of the appearance of flames around the left quarter interior trim finishing panel. This discrepancy suggests that there may have been other fire propagation pathways into the passenger compartment that were not evident in the temperature and heat flux data. Before installation of thermocouples and heat flux transducers for the fire test, the crash-tested vehicle was disassembled and evaluated for potential fire propagation pathways into the passenger compartment. Thermocouples and heat flux transducers were then installed in the test vehicle along all potential fire propagation pathways identified during the post-crash-test vehicle inspection. As this test demonstrates, prediction of all fire propagation pathways during the post-crash-test physical inspection may be impossible. In this test for example, the crushed and folded sheet metal in the rear left quarter may have formed channels that allowed gasoline vapor to enter the passenger compartment in the area behind the displaced left interior quarter trim finishing panel. Fire propagation pathways such as these channels, if they existed, were not discovered because they were hidden in sections of the deformed metal structure of the test vehicle which was not altered while evaluating this vehicle after the crash test or preparing it for this fire test.[8]

Physical inspection of the test vehicle after the fire test revealed evidence of flame-spread at the rear of the driver's door. Figure 36 is a photograph of the interior of the test vehicle after this fire

[8] In conducting these fire propagation tests, an attempt was made to avoid affecting the results of the tests by substantially altering the test vehicle from the condition it was in immediately after the crash test. Practically, it was necessary to remove certain components from the test vehicle after the crash test to allow physical inspection of the crash-tested vehicle and installation of test equipment for the fire propagation test. In the test vehicle used in this test, none of the metal structures or body panels were altered during the post-crash-test physical inspection or in preparing the test vehicle for this fire propagation test. Only components that could be re-installed in the test vehicle to their post-crash conditions were removed during these operations. These components included the front and rear seats, the carpet, some of the interior trim panels, the headlining panel, the hood, the liftgate, and the bumper fascias. As a consequence, some potential fire pathway may not have been identified during the post-crash-test physical inspection or in preparing the test vehicle for this fire propagation test.

test. This photograph shows that the headlining panel was burned and charred in areas where the estimated temperature at 210 seconds post-ignition was greater than 500°C (C, Fig. 33). The left side of the driver's seat back was burned, as was the left side and top of the rear seat back (Fig. 36). The section of the interior trim panel on the driver's door that was behind the displaced interior quarter trim finishing panel was burned. The interior quarter trim finishing panel was not visible in this photograph.

Figure 36. Fire Test F971001. Photograph of the interior of the test vehicle after the fire test.

Figure 37 is a photograph of the interior of the test vehicle with the driver's seat, rear seat back, and rear seat cushions removed. The upper section of the interior quarter trim finishing panel appeared to have melted and burned. Solidified polymer resin from the interior quarter trim finishing panel[9] was observed on the lower portion of the inner quarter panel, the carpet on the vertical section of floor pan behind the rear seat back (Arrows A, Fig. 37), and the package shelf in the rear compartment (Arrow B, Fig. 37). Some of this polymer residue appeared to have softened and sagged downward without burning. Some of this residue was charred and contained what appeared to be gas bubbles trapped in the molten resin as it cooled and solidified, indicating that this section of the trim panel had ignited. Temperature data recorded from

[9] The interior quarter trim finishing panels were made from a propylene/ethylene copolymer.

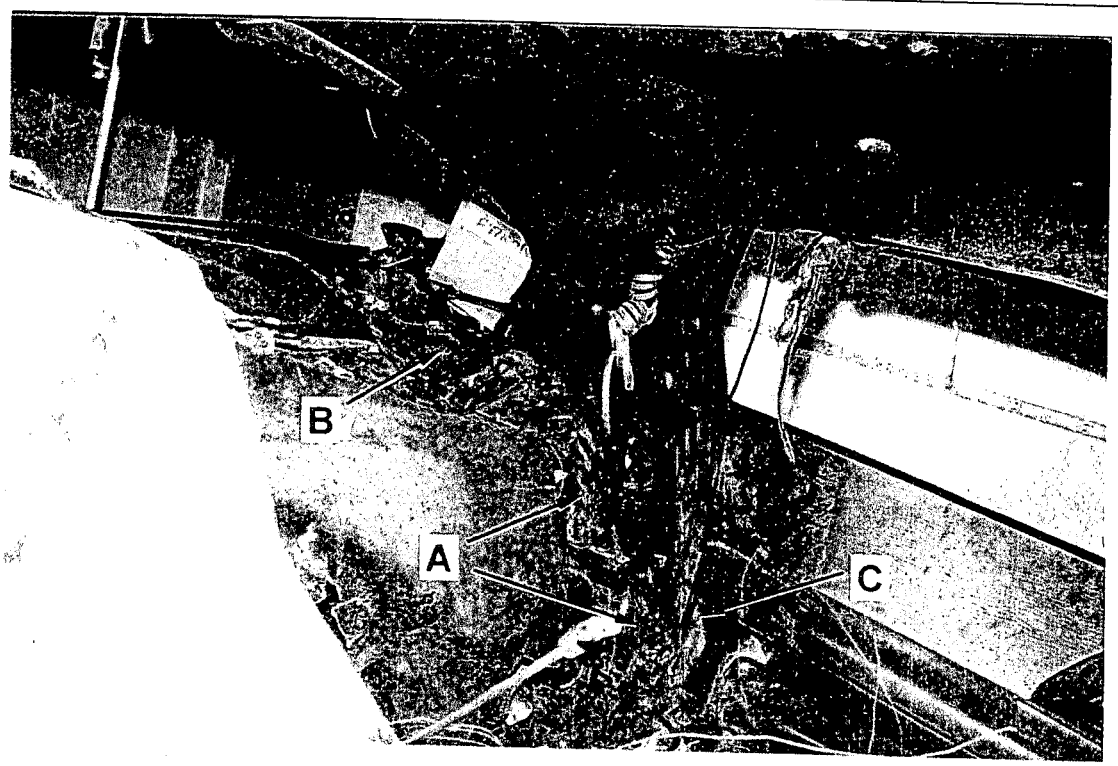

Figure 37. Fire Test F971001. Photograph of the interior of the test vehicle after the fire test with the driver's seat, the rear seat back, and rear seat cushions removed. The arrows point to the following: (A) plastic resin from the section of the left interior quarter trim finishing panel that ignited and burned; (B) the upper section of the left interior quarter trim finishing panel that sagged and fell onto the package shelf in the rear compartment; and (C) a hole where the weather seal at the back of the driver's door had burned-through.

thermocouples on the upper section of the interior quarter trim finishing panel indicate that it was exposed to flames starting at about 190 seconds post-ignition (C, Fig. 31). The video record shows flames attached to the upper section of the interior quarter trim finishing panel by 210 seconds post-ignition, when it was observed sagging downward. The quarter inner rear trim finishing panel on the package shelf behind the rear seat back (and under the fallen piece of interior quarter trim finishing panel) was not burned (Fig. 37).

Physical inspection of the test vehicle after the fire test revealed that a section of the weather seal at the rear of the driver's door was burned-through (Arrow C, Fig. 36 and Arrow B, Fig. 38). Areas of the interior door trim panel adjacent to and above the hole in the weather seal were burned and charred (Arrow C, Fig. 37). Black soot was observed the door latch reinforcement panel and section of the outer quarter panel that form the door jam at the rear of the driver's door (Fig. 38).

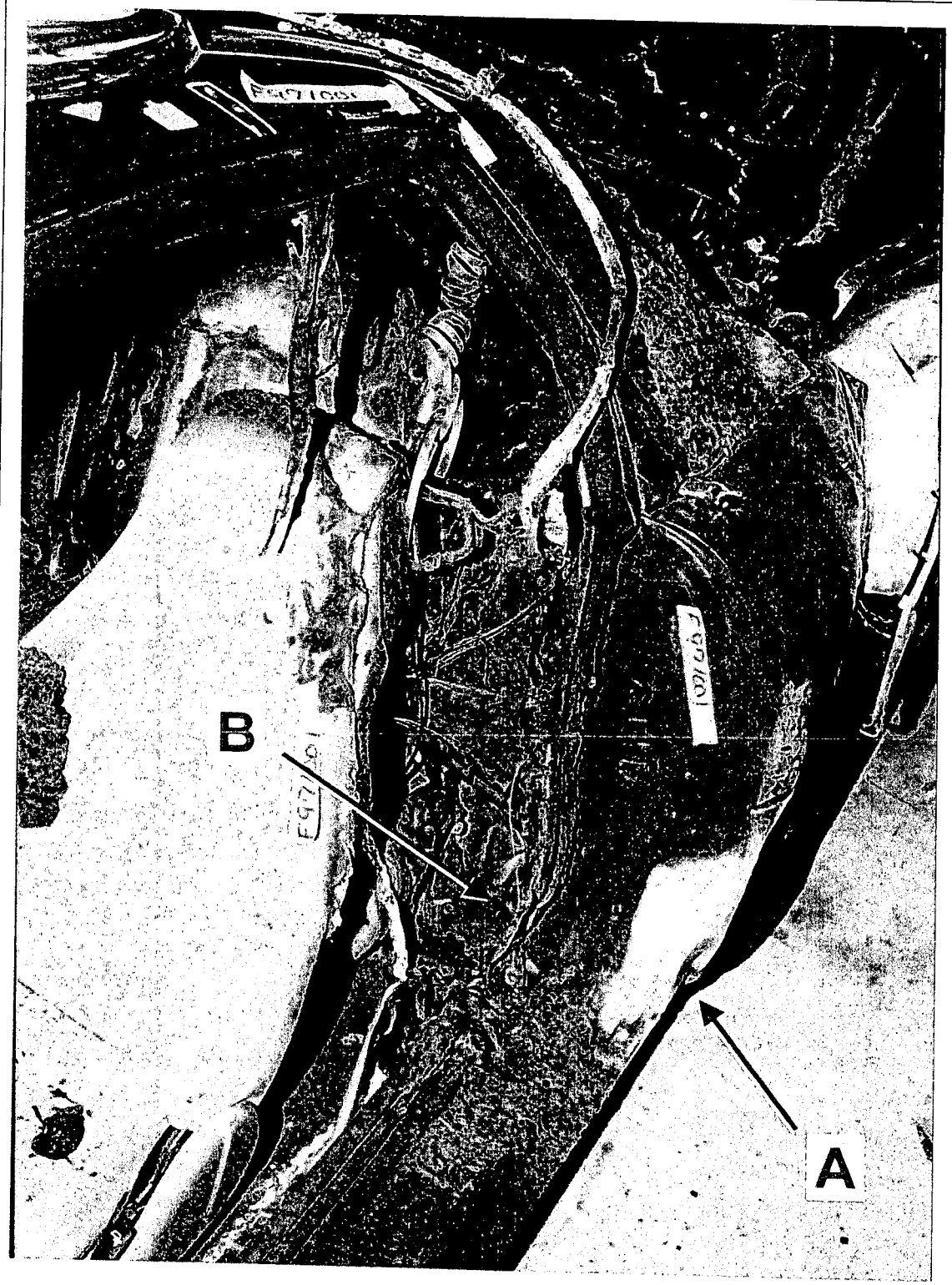

Figure 38. Fire Test F971001. Photograph of the driver's door opening of the test vehicle after the fire test. Arrow A points to areas on the lower front corner of the left outer quarter panel and the lower rear corner of the door frame were the surface of the metal contained a white oxide layer. Arrow B points to the section of weather seal at the rear of the driver's door frame that burned-through.

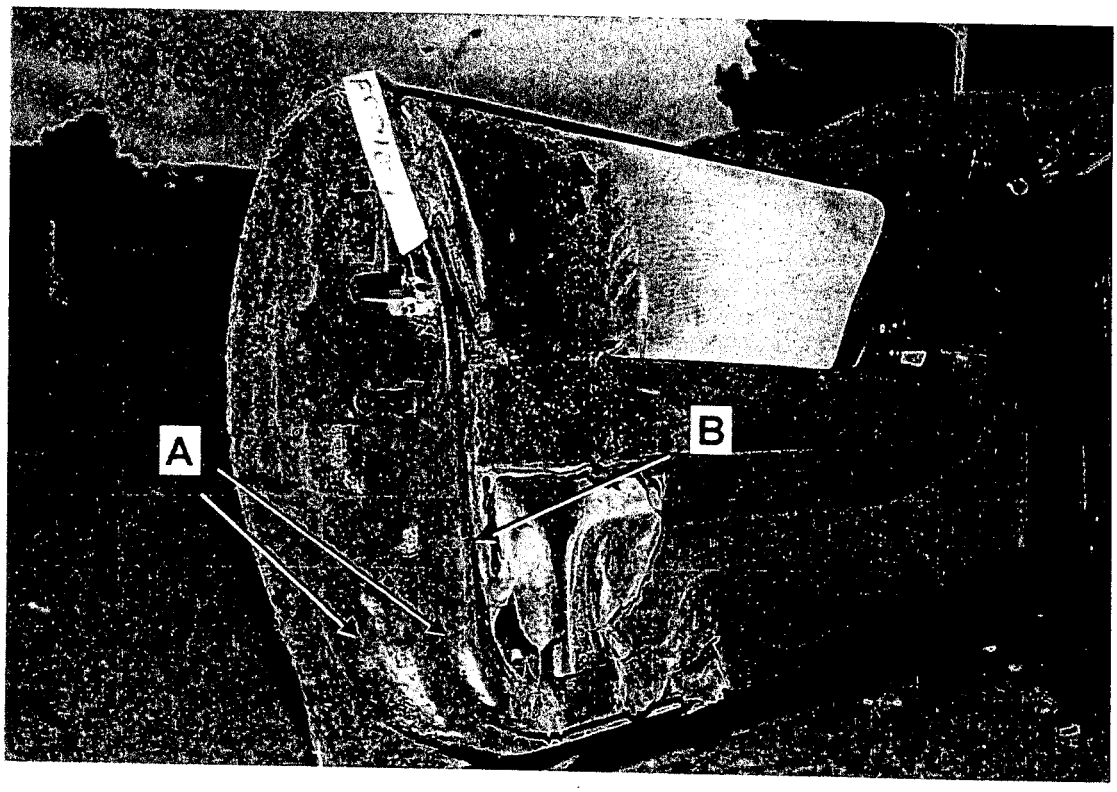

Figure 39. Fire Test F971001. Photograph of the driver's door of the test vehicle after the fire test.

A white oxide layer was observed on exposed metal surfaces at the lower rear corner of the door frame and the lower front corner of the outer quarter panel (Arrow A, Fig. 39). The polymer resin[7] in the driver's door had burned (Fig. 39). Glass fibers were exposed in two areas at the lower rear corner of the driver's door (Arrows A, Fig. 39) and in one area along the inner edge of the door where it contacted the burned-through weather seal (Arrow B, Fig. 39).

This evidence suggests that flames spread into the passenger compartment at the back of the driver's door between the door and door frame. The video stills from Camera 2 show flames along the left rocker panel in front of the rear tire by 15 seconds post-ignition (Fig. 22), with a portion of the flames apparently entering the space behind the lower and rear edges of the driver's door (Fig. 22 and 23). Figures 28 through 33 show that flames were visible were between the displaced interior quarter trim panel and the rear of the driver's door by 170 seconds post-ignition

[7] The exterior panel and frame in the doors of the test vehicle were made from Sheet Molding Compound, a styrene cross-linked aromatic polyester filled with calcium carbonate and glass fibers.

(B, Fig. 29). This was approximately 30 seconds before the thermocouple and heat flux transducer data indicated that flames were present in the left rear wheelhouse or in the seam opening at the front of the left rear wheelhouse. Data from thermocouples on the headlining panel indicated an area directly above the back of the driver's door where temperatures were greater than 600°C by 190 seconds post-ignition (panel C, Fig. 31), which is consistent with flame spread at the back of the driver's door. Neither thermocouples nor heat flux transducers were installed on the driver's door or the interior quarter trim panel in this area. Thus, the recorded thermocouple and heat flux transducer/radiometer data could not be used either to confirm flame-spread at the back of the door or to determine the timing of flame-spread along this pathway.

5.2 Flame-Spread through a Floor Pan Drain Hole

The video from Camera 4 showed that flames were visible in front of the middle of the rear seat back between 185 and approximately 210 seconds post-ignition (Fig. 40). Physical inspection of the underbody of the test vehicle after this test revealed that flames had burned-through a drain hole plug in the front floor pan panel (Fig. 41). Three other drain hole plugs in the front floor pan

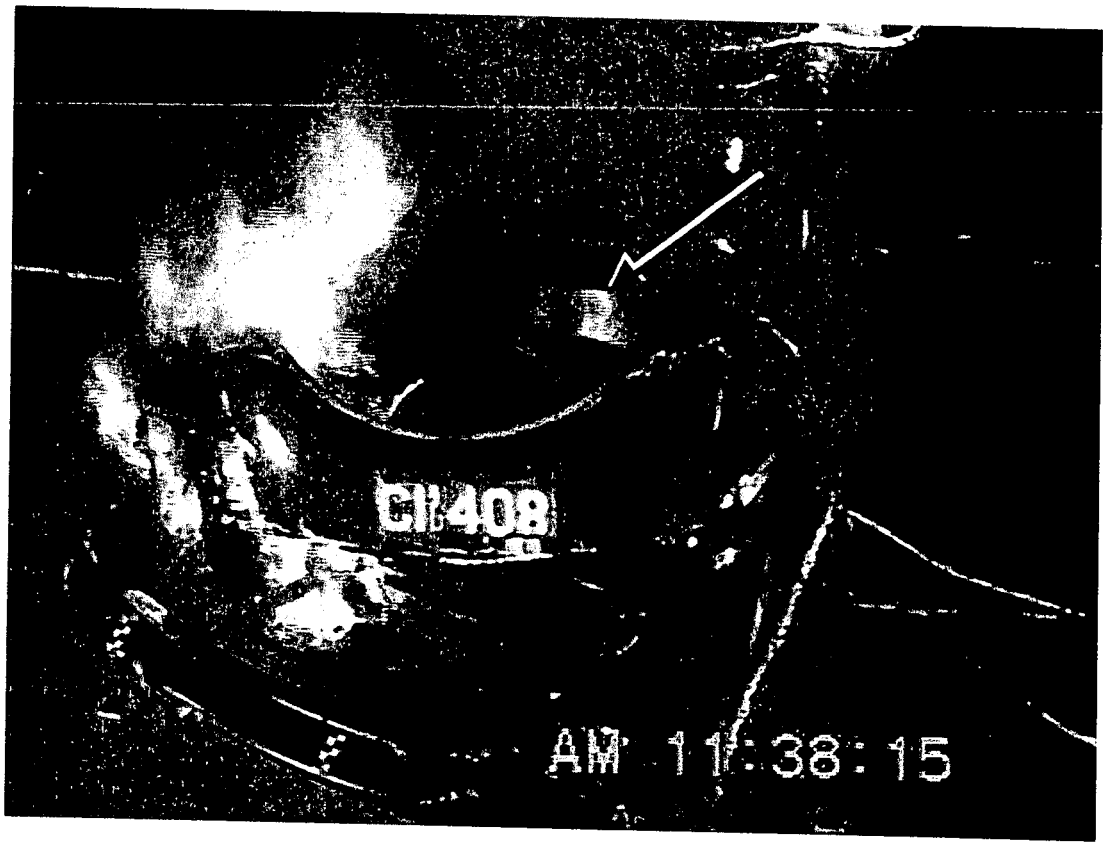

Figure 40. Fire Test F971001. Video Still from Camera 4 at 189 seconds post-ignition. The arrow indicated a fire plume in front of the middle section of the rear seat back.

panel of the test vehicle were in place after this test. Paint had burned away from an area at the rear of the left side of the front floor pan panel (Fig. 41). This area corresponded roughly to the area where the estimated temperatures below the floor pan were greater than about 600°C at the end of this test (Fig. 21). The lower surface of the floor pan panel in this area contained charred paint and exposed metal with a red or white oxide layer (Fig. 41).

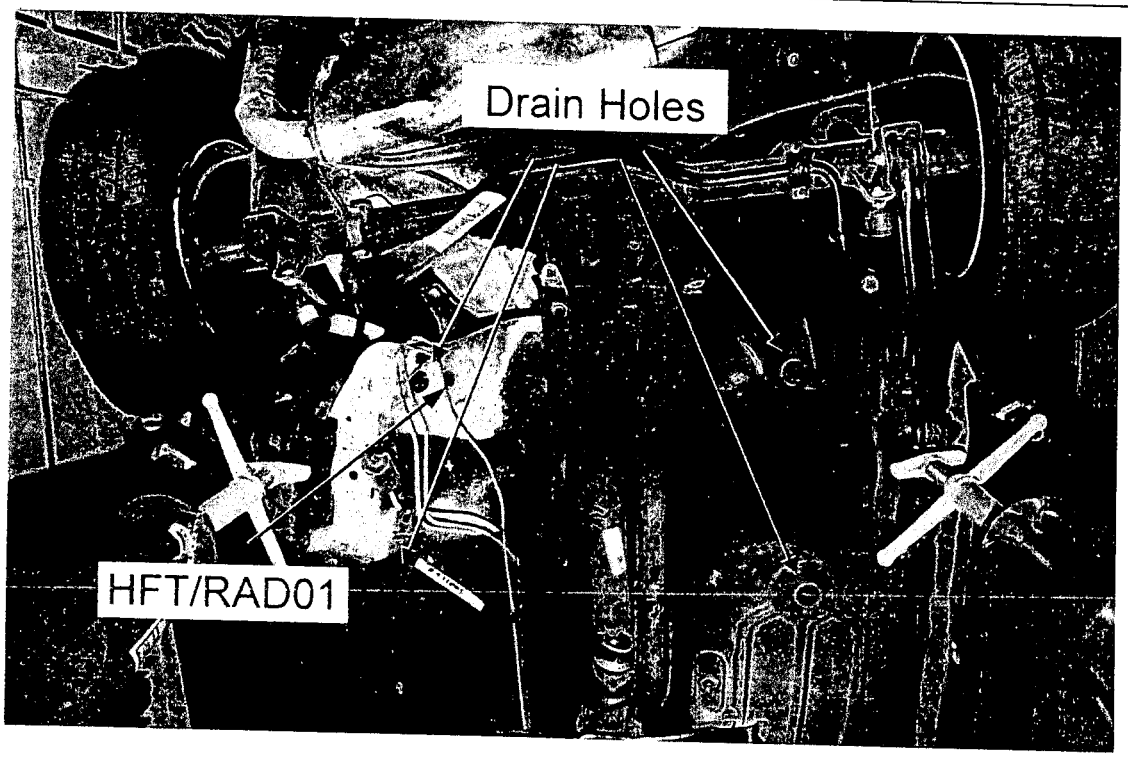

Figure 41. Fire Test F971001. Photograph of the rear underbody test vehicle after this fire test.

The temperature and heat flux data acquired during this test indicate that the section of the floor pan around the drain hole under the left rear seat was exposed to flames from about 15 seconds post-ignition until the end of the test (Fig. 42). The temperature data recorded from Thermocouple F19, located below the floor pan panel adjacent to the drain hole plug under the left rear seat cushion, increased from ambient temperature before ignition to 670°C at 16 seconds post-ignition (Fig. 42). After decreasing to 570°C at 22 seconds post-ignition, the temperature recorded from Thermocouple F19 increased steadily to a maximum temperature of 940°C at 202 seconds post-ignition. The heat flux to this area of the floor pan followed a trend similar to the temperature data recorded from Thermocouple F19 (Fig 42). The heat flux to the floor pan increased from 0 kW/m^2 before ignition to 69 kW/m^2 at 13 seconds post-ignition, decreased to 44 kW/m^2 at 18 seconds post-ignition, and reached a maximum of 116 kW/m^2 at 202 seconds post-

ignition (Fig. 42). The estimated isothermal contour plots in Figure 21 indicate that the fire plume extended forward onto the foot well in front of the left rear seat and to the right into the rear section of the transmission tunnel.

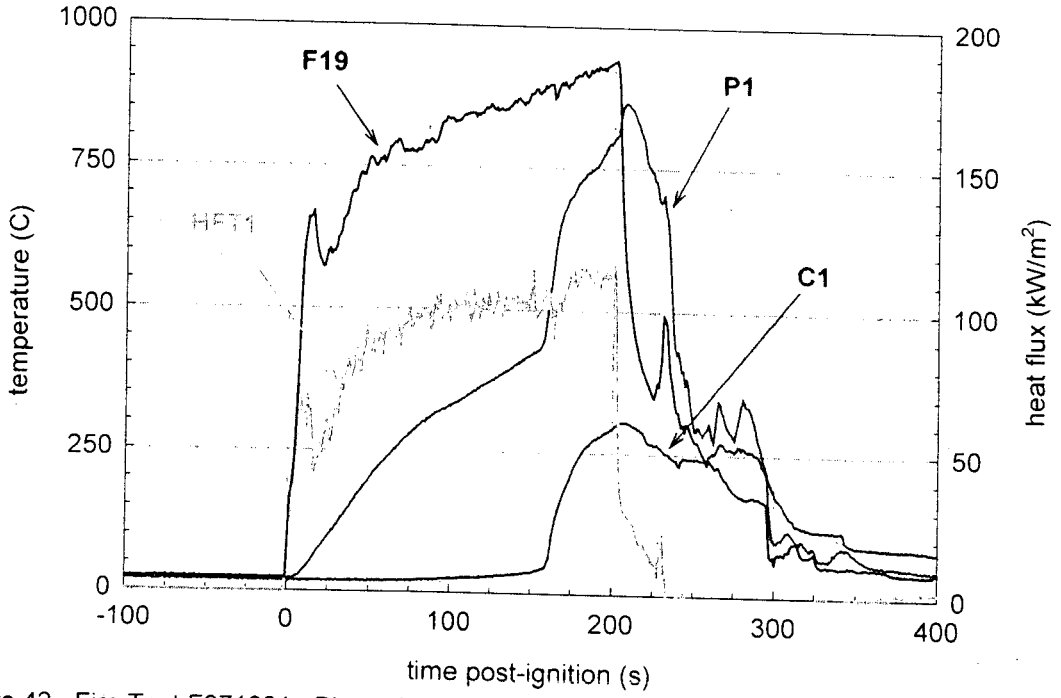

Figure 42. Fire Test F971001. Plots of temperatures recorded from Thermocouples F19, P1, and C1, and the Heat flux recorded from Heat Flux Transducer HFT1. Thermocouple F19 was located below an area of the floor pan adjacent to this drain hole. Thermocouple P1 was located above the center of this floor pan drain hole plug. Thermocouple C1 was located above the section of carpet over this drain hole plug. Heat Flux Transducer HFT1 was located in the floor pan adjacent to this drain hole (HFT1).

Temperature data recorded from Thermocouple P1 indicates that the left rear floor pan drain hole plug burned through between 155 and 170 seconds post-ignition, when recorded temperature increased from approximately 430 to 680°C (Fig. 42). Heated gases and flames that entered the drain hole appeared to have followed channels between the floor pan and carpet that were created when the floor pan deformed during the crash test. The pattern of char and soot deposits on the carpet (upper photograph, Fig. 43) and on the interior surfaces of the floor pan (lower photograph, Fig. 43) indicate that flames entered the drain hole under the left rear seat cushion. Flames then spread between the carpet and floor pan to the right and upward along the vertical section of the pan behind the rear seat back. These areas of the carpet were covering an upward sloping section of the drive train tunnel (upper photograph, Fig. 43). A section of the carpet directly above the drain hole plug was not burned or charred (upper photograph, Fig. 43).

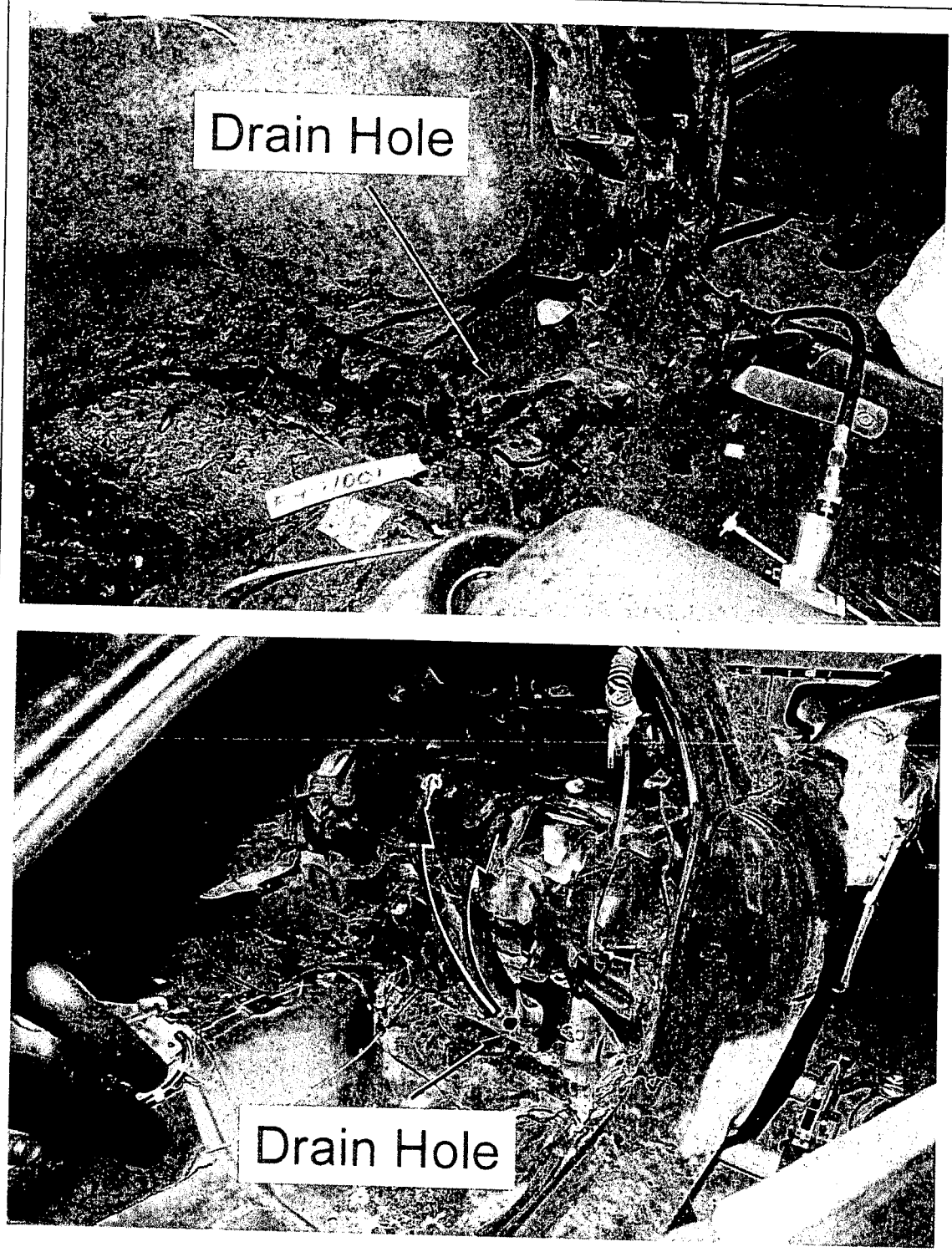

Figure 43. Fire Test F971001. Photographs of the carpet with the rear seat back and cushions removed (upper) and the floor pan with the carpet removed (lower) in the rear left corner of the test vehicle after this fire test. The arrows in the lower photograph indicated the probable directions of flame-spread under the carpet indicated by the pattern of char and soot deposits on the interior surfaces of the floor pan panels.

Temperature data recorded from Thermocouple C1, located on the upper surface of the carpet just above the drain hole plug, reached a maximum of 306°C at 208 seconds post-ignition (Fig. 42). This temperature data also indicated that flames did not burn through the section of carpet directly above the drain hole.

Flames appeared to have burned-through the inboard side of the left rear seat cushion (arrow A, upper photograph, Fig. 44). The fabric cover and foam pad in the rear seat back and rear seat cushions were charred and discolored above areas of the carpet that were burned and charred (upper photograph, Fig. 44). The carpet covering the drive train tunnel between the rear seat cushions had melted onto the floor pan. The fabric cover and foam pad in the rear seat back were charred and contained soot deposits above the drive train tunnel (arrow B, upper photograph, Fig. 45) and along the exterior face of the middle section (lower photograph, Fig. 45). As most of the middle of the rear seat back was out of its field-of-view, the video stills from Camera 6 could not be used to determine when flames first appeared in this area or if the rear seat back had ignited. For example, the video still from Camera 4 at 189 seconds post-ignition shows flames in front of the middle of the rear seat back (Fig. 40). No flames were visible on the rear seat back in the video still from Camera 6 at 190 seconds post-ignition (A, Fig. 31). Although flames were visible in front of the rear seat back in the video still from Camera 6 at 200 seconds post-ignition (A, Fig. 32), it was not possible to determine what was burning. The series of infrared thermograms in Figures 28 through 33 shows that the temperature of the middle section of the rear seat back was between 300 and 400°C from about 190 to 210 seconds post-ignition. These thermograms cannot distinguish between flames attached to this area of the seat back and heated gases and flames produced by burning objects below the field-of-view of this infrared camera.

Sections of the under-side of the left rear seat cushion were coated with dark soot (Fig. 45). The foam pad had pulled away from the support wire, and the foam was charred in several places along the inboard and rear edges of the seat cushion (Fig. 45). Temperatures recorded from thermocouples located under the seat cushion did not exceed 505°C during the test (**APPENDIX C**), which is below the 600°C used here to establish the presence of flames. But the physical evidence appears to indicate that the under-side of the foam pad did ignite along the inboard edge of the seat cushion. The spaces between the floor pan and carpet and under the left rear seat cushion were not open to the surroundings. Airflow into these spaces may have been limited and insufficient for well-ventilated combustion of these materials, slowing flame-spread and reducing flame temperatures in these spaces. It was not possible to determine unambiguously the timing of flame-spread in this space or the timing of ignition of the carpet, rear seat back, and left rear seat cushion from the test data.

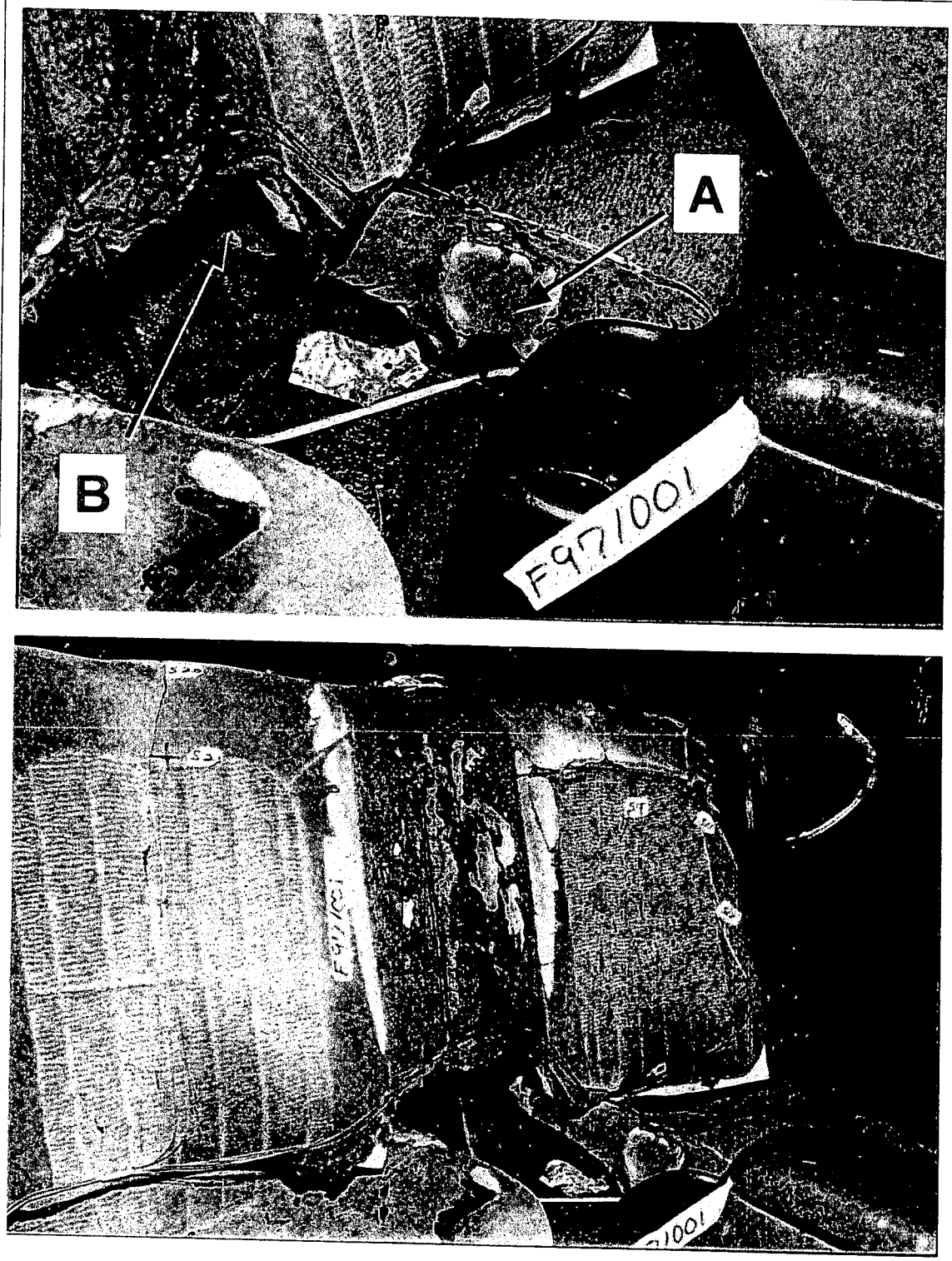

Figure 44. Fire Test F971001. Photographs of the carpet (upper) and floor pan (lower) in the rear left corner of the test vehicle after this fire test. The arrows in the upper photograph indicated areas where the seat cushion (Arrow A) and the seat back (Arrow B) appear to have been exposed to flames.

Figure 45. Fire Test F971001. Photograph of the under-side of the left rear seat cushion from the test vehicle after this fire test.

The pressure difference across the rear of the floor pan panel was estimated from the pressure data recorded from pressure gauges P3 and P7 (Fig. 46). Pressure Tap P3 was located above the carpet in the foot-well in front of the left rear passenger's seat. Pressure Tap P7 was located directly above the burning gasoline pool on the lower surface of the middle floor pan panel where it forms the package shelf behind the rear seat. The plot of the pressure difference shown in Figure 46 indicates that the pressure along the lower surface of the rear of the floor pan panel was greater that the pressure along the upper surface of the floor pan panel from the time of ignition until approximately 240 seconds post-ignition. After ignition of the gasoline, the flames below the test vehicle created an area of high pressure relative to atmosphere along the lower surface of the floor pan. Airflow into the fire plume caused air to be drawn out of the test vehicle through the rear opening, resulting in low pressure relative to atmosphere along the upper surface of the floor pan. Accumulation of buoyant heated gases in the pocket formed by the middle floor pan panel and the rear wheel houses would have caused the pressure to have been higher than where hot gases could flow unobstructed from under the test vehicle, such as below

the rear seat cushions. Thus, the pressure curve shown in Figure 46 is an upper bound for the pressure difference across the floor pan under the left rear seat cushion.

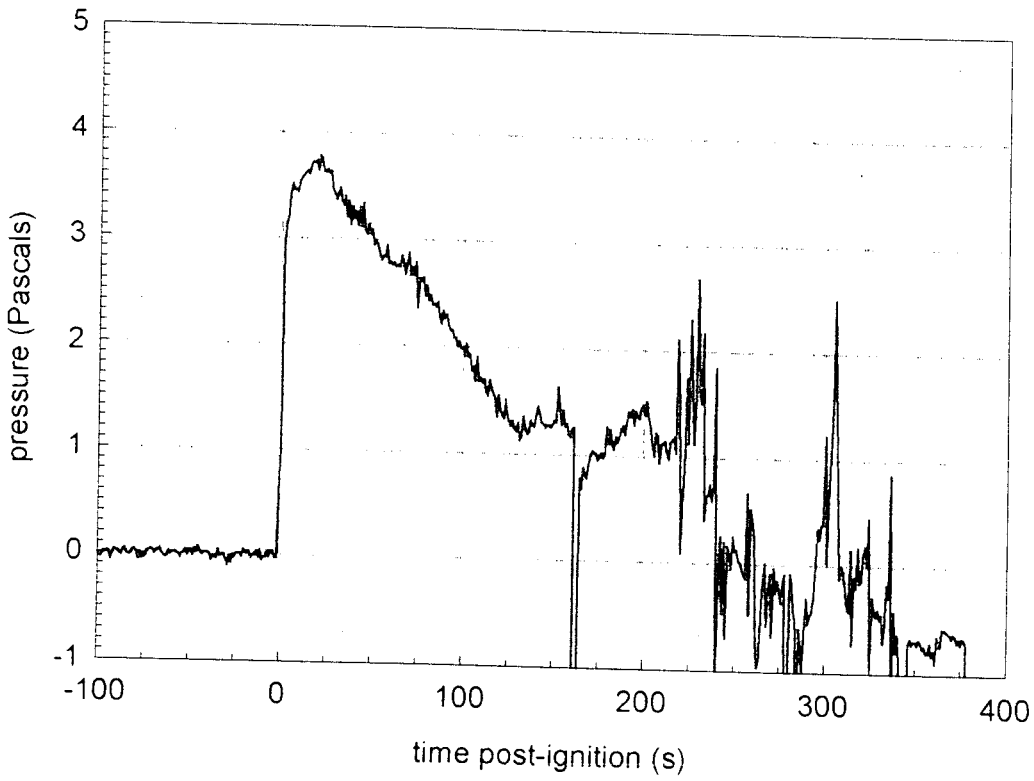

Figure 46. Fire Test F971001. Plot of the difference in pressures measured by Pressure Taps P7 and P3. P3 was located in the foot well in front of the left rear seat. P7 was located below the lower surface of the middle floor pan panel where it forms the package shelf behind the rear seat.

The maximum estimated pressure across the front floor pan panel at this time was about 1.5 Pascals,[8] which would have resulted in a maximum volume flow rate of about 3.4 L/s (7.2 cfm) through the drain hole.[9]

[8] The timing of the negative pressure transient at about 160 seconds post-ignition correlates with the timing of gases venting from the left rear shock absorber and appeared to have been unrelated to flame-spread through the drain hole.

[9] An orifice diameter of 1.5 in. and a gas temperature of 750°C were used in this estimation of the maximum volume flow rate.

5.3 Conduction through the Floor Pan

Conduction through the floor pan may have been a factor in the thermal degradation and ignition of the carpet and foam pads in the rear seat back and cushions. The section of carpet under the left rear seat cushion and adjacent to the left inner quarter panel showed evidence of heat and fire damage (Fig. 47).

Figure 47. Fire Test F971001. Photograph of the under-side of the carpet from the test vehicle after this fire test. The rear of the carpet is at the top of this photograph.

Material that was adjacent to the left inner quarter panel and left wheelhouse was melted and charred. The section of carpet under the left rear seat cushion and covering the drive train tunnel between the rear seat cushions also had burned and showed signs of thermal degradation.

Estimated isothermal contour plots of floor pan temperatures[10] indicate that the floor pan under these areas of the carpet reached temperatures greater than 500°C by 200 seconds post-ignition (Fig. 48). Heat transfer from the floor pan to the carpet pad and carpet appeared to have caused these materials to undergo thermal decomposition. Airflow into the space between carpet and floor pan was restricted and probably insufficient for well-ventilated combustion of the pyrolysate produced by thermal decomposition of the materials in the carpet pad and carpet. These incomplete combustion products formed the residue of soot particles and an oily liquid film observed on the front and middle floor pan panels after this test (lower photograph, Fig. 43) and carpet pad (Fig. 47).

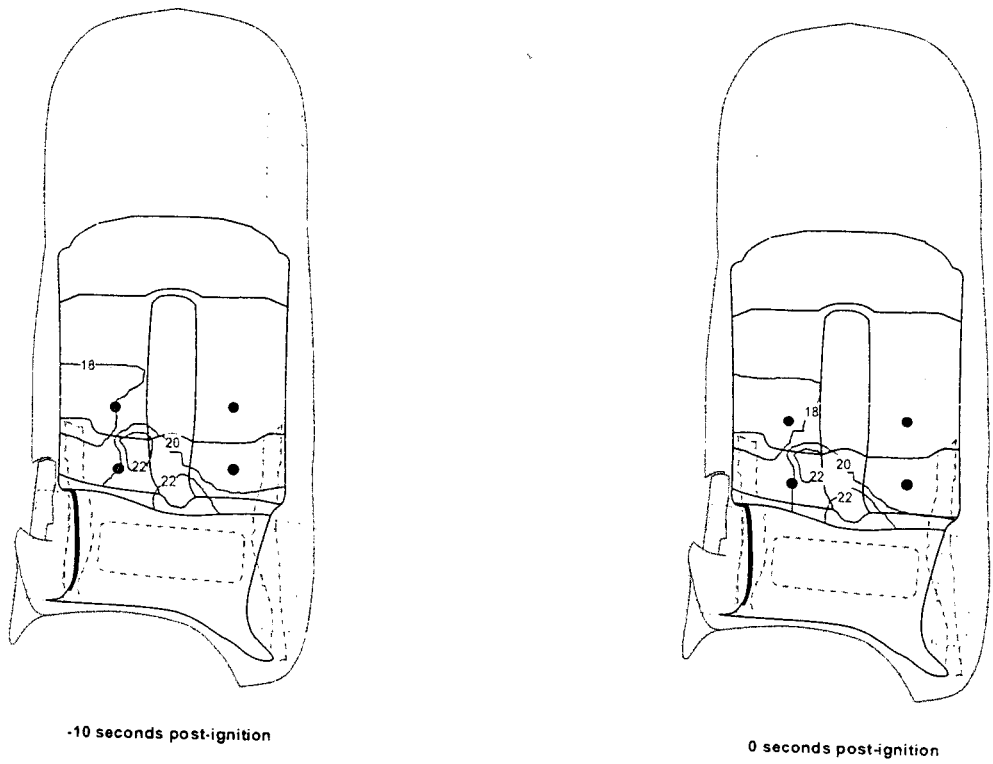

Figure 48. Fire Test F971001. Isothermal contour plots showing estimated temperatures below the floor panel at –10, 0, 25, 50, 75, 100, 125, 150, 175, and 200 seconds post-ignition.

[10]Isothermal contours of the temperature below the floor panel were estimated from the temperature data recorded from the F-Thermocouples located on the upper surface of the floor panel using a three-dimensional interpolation command available in SigmaPlot for Windows Version 4.00 [**5**]. This command used an inverse distance method to generated temperature values for points on a uniformly spaced Cartesian grid from the [x,y,t] triple data from these thermocouples. Refer to **APPENDIX C** for the approximate locations of the F-thermocouples on the floor panel and the data recorded from the F-thermocouples.

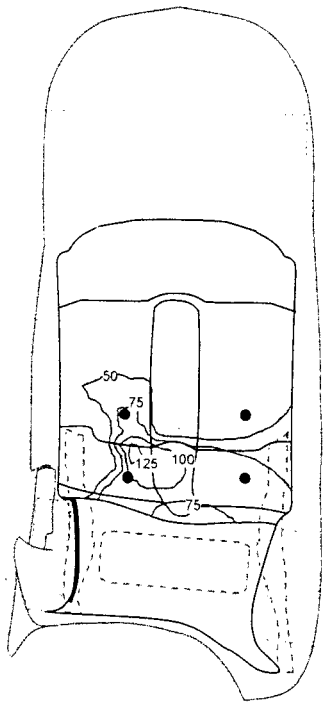

25 seconds post-ignition

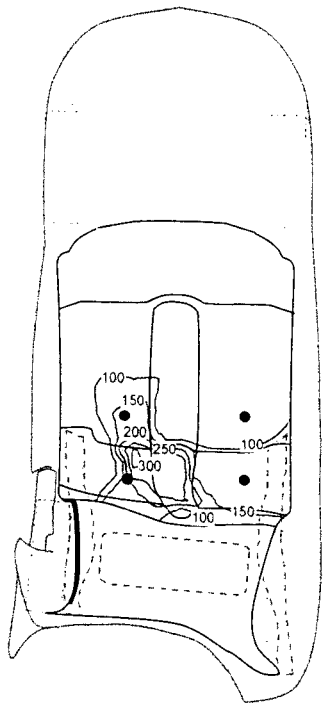

50 seconds post-ignition

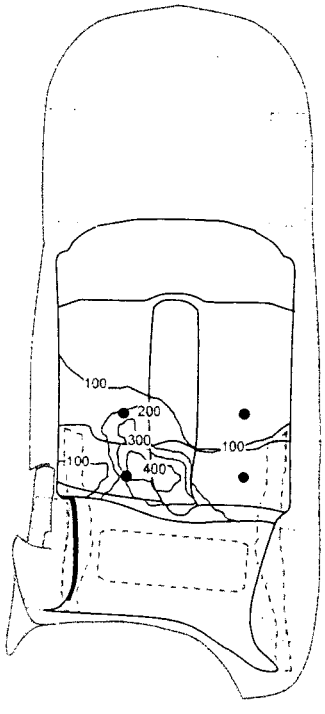

75 seconds post-ignition

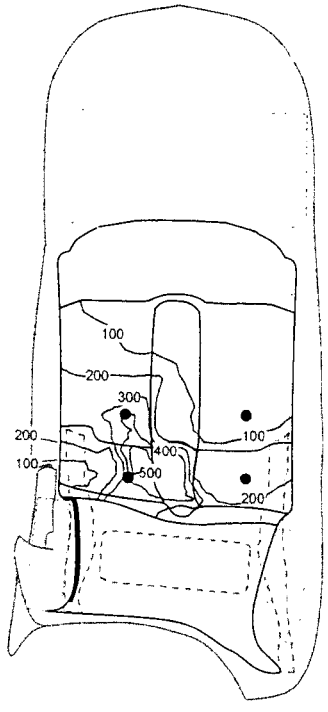

100 seconds post-ignition

Figure 48. Fire Test F971001. Isothermal contour plots showing estimated temperatures below the floor panel at –10, 0, 25, 50, 75, 100, 125, 150, 175, and 200 seconds post-ignition.

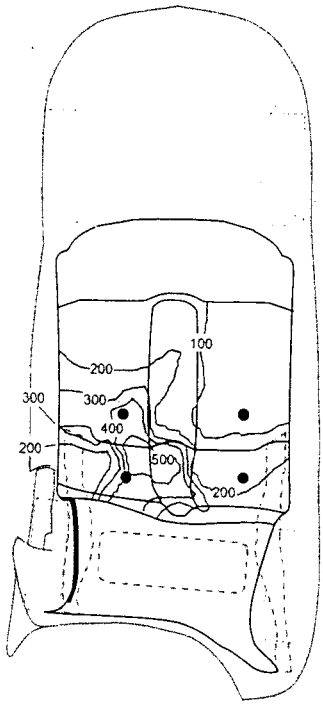

125 seconds post-ignition

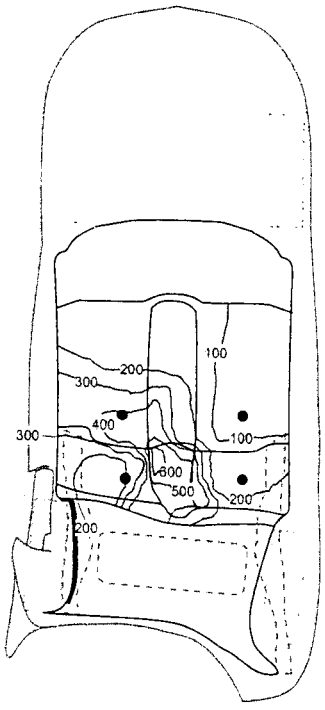

150 seconds post-ignition

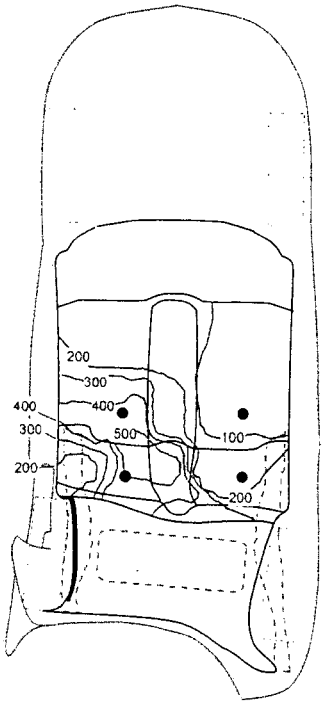

175 seconds post-ignition

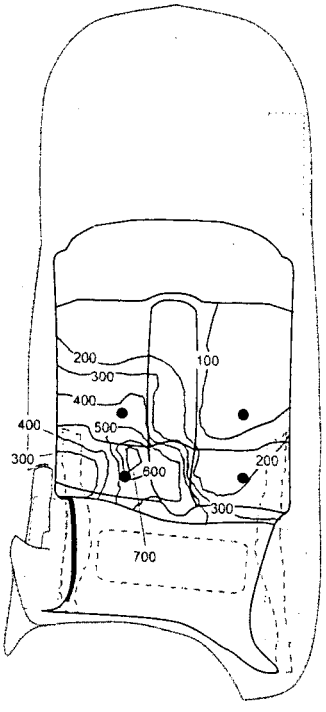

200 seconds post-ignition

Figure 48, continued. Fire Test F971001. Isothermal contour plots showing estimated temperatures below the floor panel at –10, 0, 25, 50, 75, 100, 125, 150, 175, and 200 seconds post-ignition.

6 Combustion Conditions

The output of combustion products from a fire depends on the material burning and on the supply of air to the flame. A well-ventilated fire is one in which the air supplied to the flames is sufficient for complete combustion. In partially enclosed spaces, such as an engine compartment or passenger compartment, airflow to the flames may be inadequate for complete combustion. In this case, called a ventilation-controlled or under-ventilated fire, the supply of air limits both the heat released by the fire and oxidation (combustion) of the gaseous fuel in the fire zone. As ventilation decreases, the output of carbon monoxide, hydrocarbons, smoke, and other products of incomplete combustion increase. The chemical composition of these gases depends on the chemical compositions of the materials burning and on the burning conditions, primarily ventilation. Accumulation of partially oxidized gases and unoxidized thermal decomposition products in an enclosed space can create a hazardous condition. In most cases, these gases are heated relative to the surrounding air and, because of their buoyancy, typically accumulate below the ceiling or roof of the enclosed space, forming what is called the upper layer. The upper layer can be ignited by flames from burning objects (piloted ignition) or can ignite spontaneously (autoignition) when the temperature of the gases exceeds a minimum threshold temperature (autoignition temperature), which depends on the chemical composition and the fuel/oxygen ratio of the upper layer. Once ignited, radiation from the burning upper layer transfers heat downward, and may ignite combustible materials below the burning upper layer. Some of the partially oxidized gases and unburned thermal decomposition products may be toxic (see **SECTION 8**).

The equivalence ratio is a quantitative measure of ventilation:

$$\Phi = \frac{\left[fuel / O_2 \right]_{fire}}{\left[fuel / O_2 \right]_{stoichiometric}}$$

where Φ is the equivalence ratio, $[fuel/O_2]_{fire}$ is the fuel-to-oxygen ratio in the fire, and $[fuel/O_2]_{stoichiometric}$ is the fuel-to-oxygen ratio required for complete combustion. In most instances, the equivalence ratio cannot be measured directly in a large-scale test such as the one described here. Ventilation, and thus the equivalency ratio is not uniform in situations where objects are burning in different physical environments, such as a burning motor vehicle where different materials burne at different times and in different environments. Estimates of the average ventilation was obtained from the data acquired during this test. It was impossible to isolate and

measure the fire products produced by each of the materials burning, and to measure airflow into each of the unique environments that existed during this test.

Heat and combustion gases produced by burning objects in the test vehicle rose into the Fire Products Collector at the test facility. Thus, data from the Fire Products Collector can be used to estimate the average ventilation for the burning vehicle. A similar approach can be used to estimate the average ventilation for the passenger compartment using the gas concentration data from the FTIR gas analyzer and the air temperature data from the aspirated thermocouples. Estimation of ventilation from these data was done by comparison to the results obtained from testing individual materials in small-scale flammability tests,[11] where the equivalence ratio was measured precisely [7].

Five derived parameters were used in this comparison. Values of these parameters for polymeric materials similar to those used in the test vehicle are shown in Table 1.

Table 2

Fire Products for Well-ventilated Fires[1,2]

material	$Y(CO)/Y(CO_2)$ (g/g)	$Y(HC)/Y(CO_2)$ (g/g)	$Y(CO_2)/\Delta H_{CON}$ (g/kJ)	$Y(CO)/\Delta H_{CON}$ (g/kJ)	$Y(HC)/\Delta H_{CON}$ (g/kJ)
gasoline	0.011 – 0.014	0.0032 – 0.0039	0.14 – 0.16	0.0021 – 0.0026	0.00058 – 0.00073
poly(ethylene)	0.0087	0.0025	0.13	0.0011	0.00032
poly(propylene)	0.0086	0.0022	0.12	0.0011	0.00027
poly(styrene)	0.026	0.0060	0.21	0.0054	0.00127
polyester	0.05	0.019	0.15	0.0065	0.00185
Nylon	0.018	0.0078	0.13	0.0035	0.00098
Flexible urethane foams	0.006 - 0.027	0.0013 - 0.0033	0.15 - 0.21	0.0012 - 0.0055	0.00023 - 0.00069
Rigid urethane foams	0.015 - 0.046	0.006 - 0.036	0.17 - 0.23	0.0028 - 0.0081	0.00011 - 0.00070

[1]Values reported in Table 1 were calculated from data reported in Table 3-4.11 in reference 6.

[2]Y(CO) is the mass-yield of carbon monoxide (g). $Y(CO_2)$ is the mass-yield of carbon dioxide (g). Y(HC) is the mass-yield of gaseous hydrocarbons (g). $Y(CO_2)/\Delta H_{con} = (C_{CO_2}/c_p\Delta T)(\rho_{CO_2}/\rho_{air})$, $Y(CO)/\Delta H_{con} = (C_{CO}/c_p\Delta T)(\rho_{CO}/\rho_{air})$, and $Y(HC)/\Delta H_{con} = (C_{HC}/c_p\Delta T)(\rho_{HC}/\rho_{air})$. ΔH_{CON} is the convective heat of combustion per unit fuel vaporized (kJ/g). The C_j are the gas-phase concentrations (volume fraction) of carbon dioxide, carbon monoxide, and total hydrocarbons. The ρ_j are the gas-phase densities (g/m^3) of carbon dioxide, carbon monoxide, total hydrocarbons, and air. c_p is the heat capacity of air (kJ/g-K). ΔT is the difference between the gas temperature and the temperature of the ambient air (K).

[11] Small-scale flammability tests to determine combustion properties of materials were conducted in the Factory Mutual Research Corporation Flammability Apparatus is a small-scale test apparatus (see reference 7).

These parameters include $Y(CO)/Y(CO_2)$, $Y(HC)/Y(CO_2)$, $Y(CO_2)/\Delta H_{CON}$, $Y(CO)/\Delta H_{CON}$, $Y(HC)/\Delta H_{CON}$. The values of these parameters in Table 1 were determined for the well-ventilated combustion of a poly(ethylene), a poly(propylene), a poly(styrene), a polyester, a Nylon, a group of flexible urethane foams, and a group of rigid urethane foams.[12]

Analysis of the data from the Fire Products Collector suggests that initially, the production of carbon monoxide relative to carbon dioxide was greater than expected for well-ventilated combustion of gasoline and of materials similar to those used in the test vehicle. Figure 49 shows a plot of $[G_{CO}]/[G_{CO2}]$ versus time post-ignition, where G_{CO} and G_{CO2} are the carbon monoxide- and carbon dioxide-release rates measured using the Fire Products Collector (**APPENDIX G**).

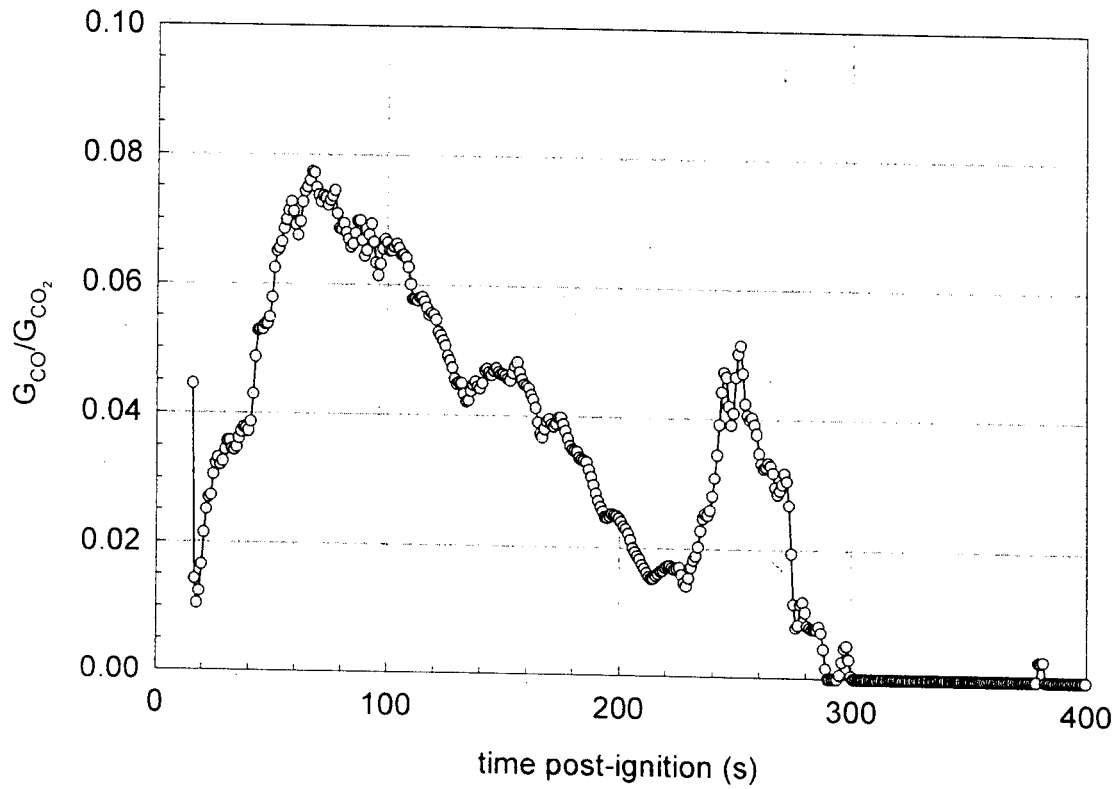

Figure 49. Fire Test F971001. Plot of $[G_{CO}]/[G_{CO2}]$ versus time post-ignition determined from the carbon monoxide- and carbon dioxide-release rates measured by the Fire Products Collector.

[12] The compositions and physical properties such as density, thermal conductivity, and heat capacity of these materials were not specified. As these properties can effect the combustion characteristics of these materials, testing of materials in the current US motor vehicle fleet may yield somewhat different values than those shown in Table 1.

The ratio $[G_{CO}]/[G_{CO2}]$ calculated for this test is equivalent to the ratio $[Y(CO)]/[Y(CO_2)]$ determined for individual materials listed in Table 1. Values of $[G_{CO}]/[G_{CO2}]$ greater than the ranges in Table 1 indicate the fire was under-ventilated. That is, the supply of oxygen to the flames was not sufficient for stoichiometric combustion. Before ignition, $[G_{CO}]/[G_{CO2}]$ was undefined because $G_{CO} = G_{CO2} = 0$.

Values of $[G_{CO}]/[G_{CO2}]$ could not be calculated for the first 17 seconds post-ignition because the concentration of carbon dioxide in the air entering the Fire Products Collector was less than the lower limit of detection of the measurement equipment (Fig. 49).[13] The value of $[G_{CO}]/[G_{CO2}]$ increased from about 0.01 to almost 0.08 between 17 and 65 seconds post-ignition, indicating that the overall combustion efficiency of the fire decreased during this time. Gasoline was the predominant fuel for the fire during at this time. One possible explanation for the increasing values of $[G_{CO}]/[G_{CO2}]$ is that airflow into the restricted space below the test vehicle was insufficient for stoichiometric combustion of the hydrocarbons vaporizing from the gasoline pool. Immediately after ignition, radiation from the burning gasoline vapor transferred heat back to the surface of the gasoline pool, increasing the vaporization rate of hydrocarbons from the liquid gasoline. Oxygen in the air flowing into the space under the vehicle would have been consumed at an increasing rate as the rate of vaporization of the gasoline increased, and the efficiency of combustion would have decreased as the fuel-to-air ratio became greater than stoichiometric.

After about 60 seconds post-ignition, the value of $[G_{CO}]/[G_{CO2}]$ decreased (Fig. 49), approaching the ranges expected for well-ventilated combustion (Table 1) by the end of this test. The heat release rate measured with the Fire Products Collector at the test facility increased exponentially from about 250 to 1200 kW during this time (Plot G1). The flow rate of gasoline from the outlet of the gasoline delivery system remained constant throughout this test and heat release rate from the burning gasoline appeared to have reached a steady-state at this time. The increase in heat release rate measured by the Fire Products Collector starting at about 60 seconds indicated that other combustible materials had started to ignite at this time. One consequence of flame-spread to these other materials was that a significant portion of the growing fire plume extended out from the restricted space below the test vehicle. This may have allowed higher buoyant flow and greater air entrainment into the flames extending away from the vehicle, resulting in an increase in the overall combustion efficiency after 60 seconds post-ignition. A correlation between heat

[13] The 17-second time-delay in the Fire Products Collector data may have been caused by low thermal convection at the beginning of this test. The upward flow of fire products into the collection duct was driven solely by thermal convection of hot gases leaving the flames. Initially the output of heat and products by the fire was low, and the upward flow rate of fire products into the Fire Products Collector was slow.

output and ventilation has been demonstrated in laboratory experiments during combustion for a number of solid materials similar to the materials used in the test vehicle [7].

The value of $[G_{CO}]/[G_{CO2}]$ increased when fire suppression began between 210 and 220 seconds post-ignition, indicating that the overall combustion efficiency decreases as the flames were extinguished. Although flames were visibly suppressed relatively quickly, many materials in the test vehicle continued to produce smoke. Continued thermal decomposition of these materials after the flames were visibly extinguished would have increased the produced of partially oxidized and unoxidized gases relative to carbon dioxide, resulting in increasing values of $[G_{CO}]/[G_{CO2}]$.

A similar analysis was performed using gas concentration data from the passenger compartment (**APPENDIX H**). This data was used to calculate values for $[C_{CO} \times d_{CO}]/[C_{CO2} \times d_{CO2}]$ and $[C_{HC} \times d_{HC}]/[C_{CO2} \times d_{CO2}]$ (Fig.'s 50 and 51).

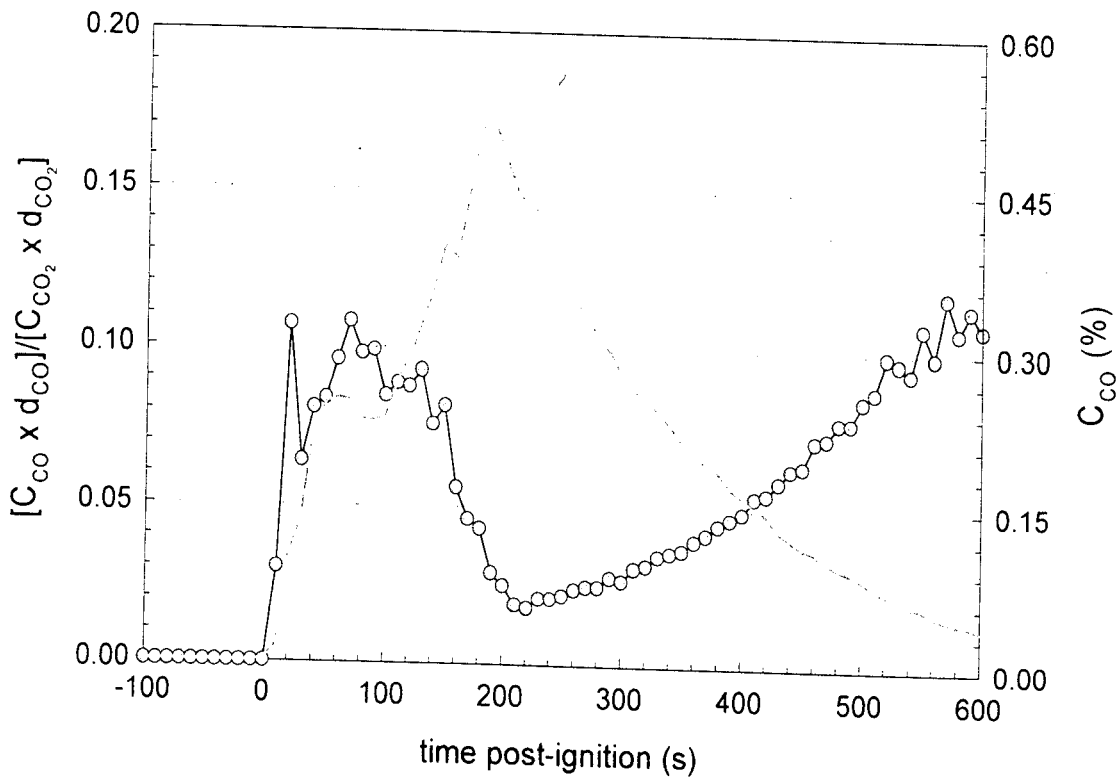

Figure 50. Fire Test F971001. Plots of $[C_{CO} \times d_{CO}]/[C_{CO2} \times d_{CO2}]$ (—●—, left axis) and the concentration of carbon monoxide (—, right axis) in the passenger compartment.

Values for $[C_{CO2} \times d_{CO2}]/[t_{air} \times Cp_{air}]$, $[C_{CO} \times d_{CO}]/[t_{air} \times Cp_{air}]$, and $[C_{CO2} \times d_{CO2}]/[t_{air} \times Cp]$ could not be determined for this test because air temperature data in the passenger compartment was not

available. The terms in these ratios are defined as follows: C_j is the gas-phase concentration of species j; d_j is the vapor density of species j; t_{air} is the air temperature; and Cp_{air} is the heat capacity of air. The product $[C_j \times d_j]$ equals the mass-concentration of species j in passenger compartment; therefore the $[C_{CO} \times d_{CO}]/[C_{CO2} \times d_{CO2}]$ and $[C_{HC} \times d_{HC}]/[C_{CO2} \times d_{CO2}]$ are equivalent to the ratios $[Y(CO)]/[Y(CO_2)]$ and $[Y(HC)]/[Y(CO_2)]$ determined for individual materials listed in Table 1.

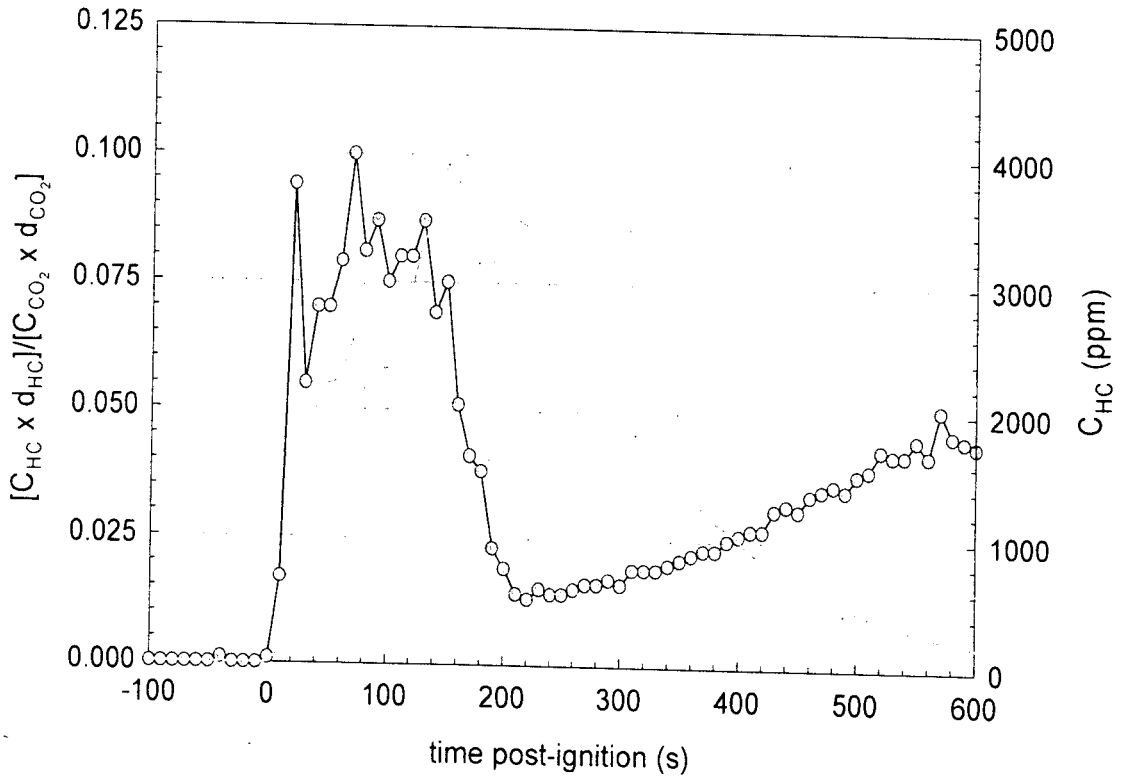

Figure 51. Fire Test F971001. Plots of $[C_{HC} \times d_{HC}]/[C_{CO2} \times d_{CO2}]$ (—◉—, left axis) and the concentration of total hydrocarbons (—, right axis) in the passenger compartment.

The values of $[C_{CO} \times d_{CO}]/[C_{CO2} \times d_{CO2}]$ and $[C_{HC} \times d_{HC}]/[C_{CO2} \times d_{CO2}]$ varied within narrow ranges around 0.090 and 0.080, respectively, from 20 seconds after ignition until 150 seconds post-ignition. These plots do not reflect combustion conditions inside the test vehicle during this time because combustible materials in the passenger compartment had not ignited (**SECTION 5**). There were two potential sources of gases in the passenger compartment at this time: combustion gases from the burning gasoline entering the test vehicle through the seam openings around the left rear wheelhouse and gases produced by pyrolysis of materials in contact with heated metal surfaces such as the floor pan. As discussed above, the Fire Products Collector data indicates that the burning gasoline, which was under the test vehicle, was under-ventilated. The relative concentrations of carbon dioxide, carbon monoxide, partially oxidized, and

unoxidized hydrocarbons in the gas mixture entering the passenger compartment from below the test vehicle would have reflected this condition. Similarly, the mixture of gases produced by thermal decomposition of materials in the test vehicle would have contained relatively higher concentrations of carbon monoxide, partially oxidized, and unoxidized hydrocarbons than cqrbon dioxide.

The plots in Figures 50 and 51 also suggest that combustible material inside the passenger compartment ignited between 140 and 160 seconds post-ignition. This timing is consistent with the timing of flame-spread into the passenger compartment determined in **SECTION 5**, where the first direct evidence of flames inside the passenger compartment was between 160 and 170 seconds post-ignition. The values of $[C_{CO} \times d_{CO}]/[C_{CO2} \times d_{CO2}]$ and $[C_{HC} \times d_{HC}]/[C_{CO2} \times d_{CO2}]$ started to decrease at 150 seconds post-ignition, approaching the ranges expected for well-ventilated combustion at 220 seconds post-ignition. And the values of $[C_{CO} \times d_{CO}]/[C_{CO2} \times d_{CO2}]$ and $[C_{HC} \times d_{HC}]/[C_{CO2} \times d_{CO2}]$ increased when fire suppression began between 210 and 220 seconds post-ignition, indicating that the overall combustion efficiency decreases as the flames were extinguished.

7 Estimation of Skin Temperature Profiles from Measured Heat Flux Data, Fractional Equivalent Dose Parameters from Measured Gas Concentration Data, and Thermal Damage to the Respiratory Tract from Measured Air Temperature Data

The mathematical model "BURNSIM: A Burn Hazard Assessment Model" [8] was used to estimate the time and depth of burns to exposed skin. The inputs to this model were heat fluxes derived from the directional flame thermometer measurements and air temperatures measured using the aspirated thermocouple probe.

Two models were used to estimate the potential for toxicity from exposure to the combustion gases measured in the passenger compartment. The Federal Aviation Administration (FAA) Combined Hazard Survival Model [9] was used to estimate the time to incapacitation and the time to lethality. A model described by Purser [10] also was used to estimate the time to incapacitation. Both models estimate the risk from exposure to hot air, reduced oxygen, carbon monoxide, carbon dioxide, hydrogen cyanide, hydrogen chloride, hydrogen fluoride, hydrogen bromide, acrolein, and nitrogen dioxide. Both models also account for the physiological effect of carbon dioxide-induced hyperventilation, which increases the respiratory uptake.

7.1 The BURNSIM Model

The computer model BURNSIM was the analytical tool chosen to estimate skin temperature depth profiles from the heat flux data in **APPENDIX G**. The BURNSIM model divides the skin into a series of ten layers, with a uniform thickness of 0.2 mm per layer. The top layer was divided into 8 layers each with a uniform thickness of 0.025 mm to better account for the non-instantaneous heat transfer from the epidermal surface into the first layer.

Skin Model of BURNSIM

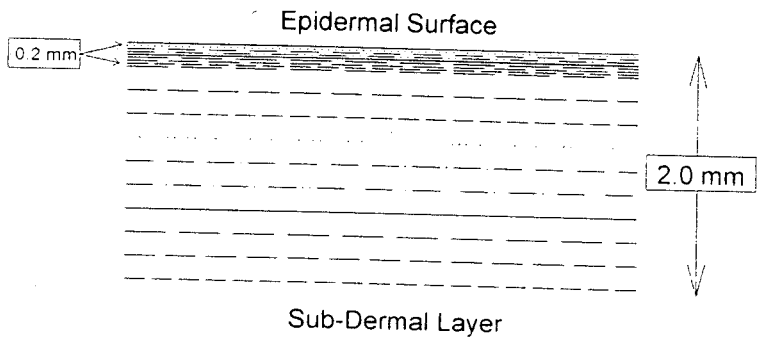

The BURNSIM analysis used here incorporated the following assumptions to estimate skin temperature profiles. The absorbtivity of exposed skin was assumed to be 0.60 (i.e., the skin absorbs 60% of the radiation incident upon the epidermal surface). The absorbtivity of surface

hair was assumed to be 0.05 (i.e., surface hair absorbs 5% of the incident radiation before it reached the skin). Exposed skin was assumed to absorb 100% of the measured convective heat flux to its surface. The temperature of each layer was estimated as a function of the time of exposure to an external heat flux. A portion of the absorbed heat is removed from the skin by the circulatory system. Thermal damage to a layer of skin exceeds the capacity of the physiological repair processes when the temperature of that layer exceeds 45°C.

In estimating skin temperature, the analysis presented in this paper using BURNSIM did not account for the presence of facial or head hair, or clothing covering the skin, all of which may block direct heat transfer to the skin. This analysis also did not account for variations in skin thickness among individuals, or variations in skin thickness at different parts of the body on the same individual. For example, skin thickness can vary from 1 to 5 mm with body location. This analysis also did not account for effect of skin pigmentation on absorbtivity. In using the radiative and convective heat flux estimates shown in **APPENDIX G** to estimate skin temperature profiles, this analysis assumed that the location and orientation of the skin was identical to that of the HFT/RAD transducer assemblies used to measure heat flux. Small changes in position or angle of the surface can result in large differences between in the incident heat flux to the surface (see below). Based on the currently available information and data, the accuracy of the estimated skin temperature depth profiles in humans exposed to heat flux levels from fire such as measured in this test obtained using BURNSIM has not been determined.

7.1.1 Estimation of Skin Temperature Profiles using BURNSIM

The absorbed heat flux at each of the HFT/RAD assembly locations was estimated from the data recorded from HFT/RAD 6 through HFT/RAD 10. These estimates of absorbed heat flux were input into the BURNSIM model to estimate skin temperature profiles for exposed skin at these locations. The BURNSIM calculations were performed using data recorded between 0 and 241 seconds post-ignition. The resulting estimated temperature profiles are shown in Figures 52 through 57.

These estimated skin temperature profiles contain two peaks. The first peak occurred during the first 50 seconds post-ignition, which corresponded to the time when flames appeared briefly in the left rear corner of the passenger compartment. For example, HFT/RAD Assembly 5 was located above the head-rest of the driver's seat back and facing upward. The total and radiative heat fluxes recorded from this transducer increased as flames appeared behind the displaced left inter quarter trim finishing panel, reaching maximum values of 9.8 kW/m^2 (total) and 9.3 kW/m^2 (radiative) at 29 seconds post-ignition (**Appendix E**, Plots E9 and E10). The total and radiative

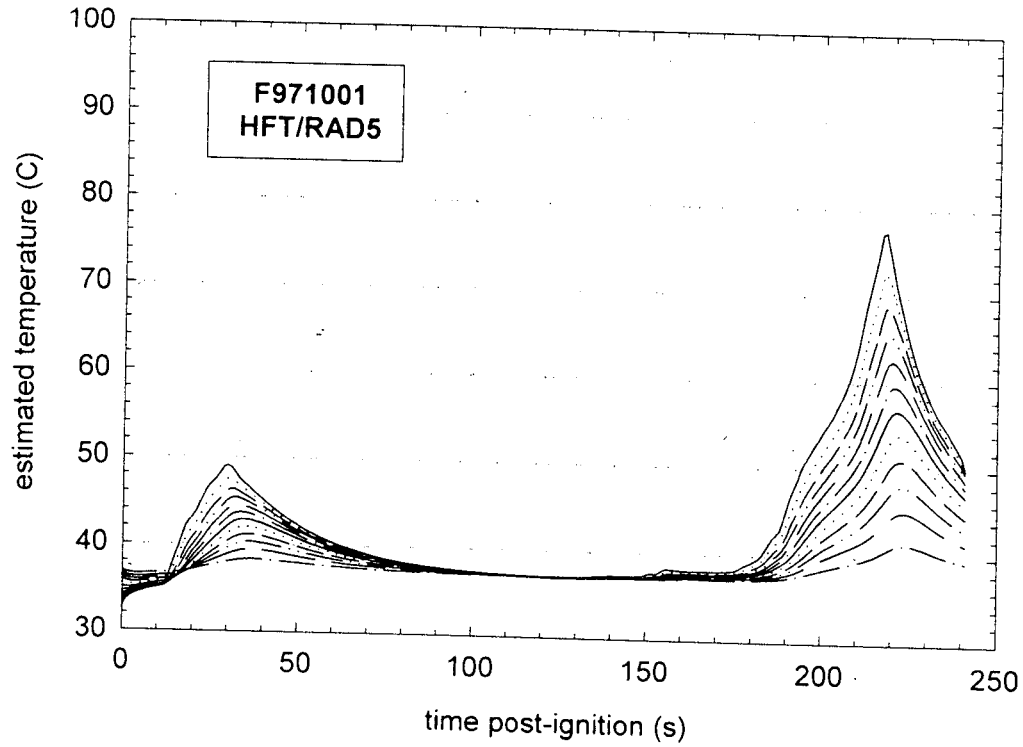

Figure 52. Fire Test F971001. Skin temperature profiles estimated from heat flux data recorded from HFT/RAD Assembly 5 (**APPENDIX E**, Plots E9 and E10).

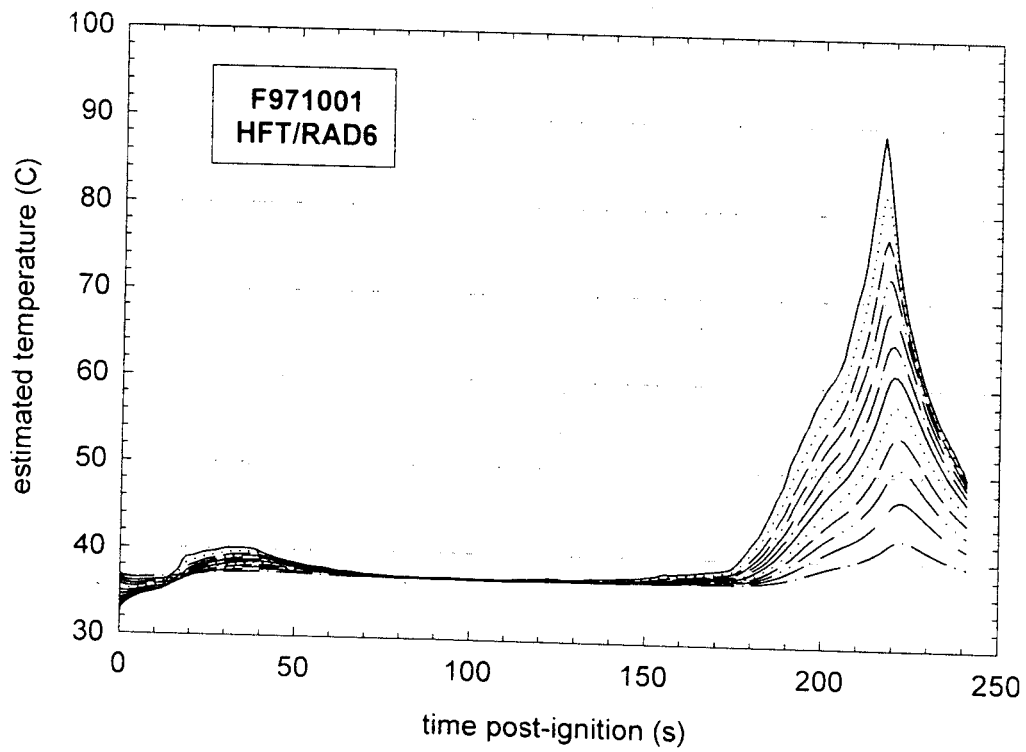

Figure 53. Fire Test F971001. Skin temperature profiles estimated from data recorded from HFT/RAD Assembly 6 (**APPENDIX E**, Plots E11 and E12).

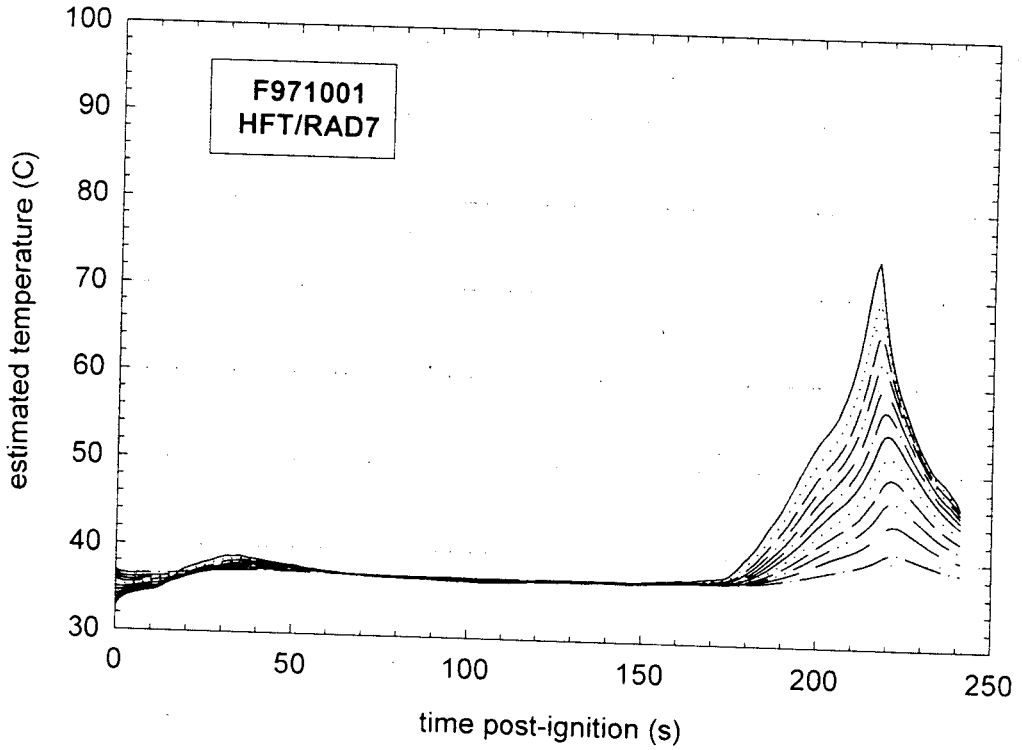

Figure 54. Fire Test F971001. Skin temperature profiles estimated from data recorded from HFT/RAD Assembly 7 (**APPENDIX E**, Plots E13 and E14).

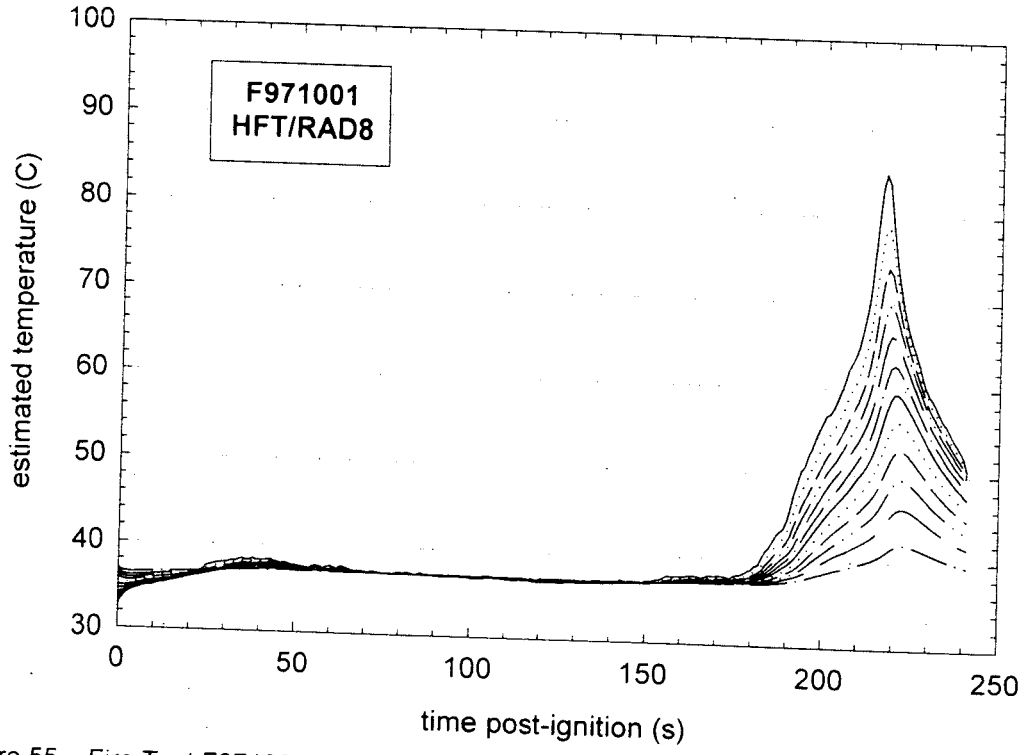

Figure 55. Fire Test F971001. Skin temperature profiles estimated from data recorded from HFT/RAD Assembly 8 (**APPENDIX E**, Plots E15 and E16).

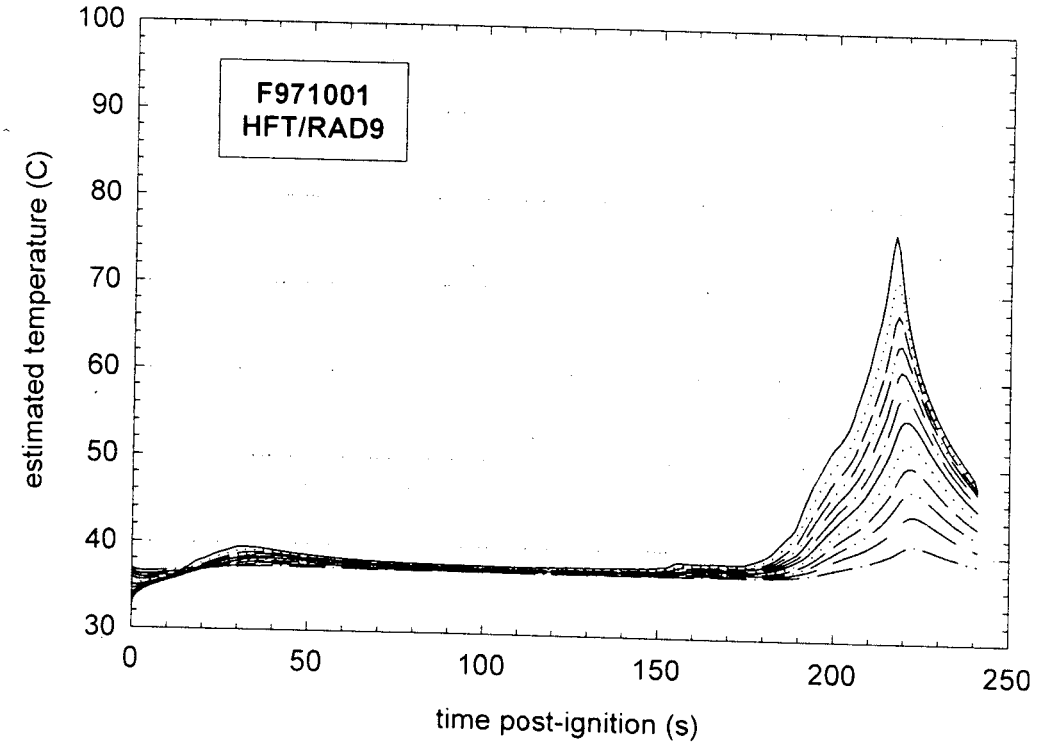

Figure 56. Fire Test F971001. Skin temperature profiles estimated from data recorded from HFT/RAD Assembly 9 (**APPENDIX E**, Plots E17 and E18).

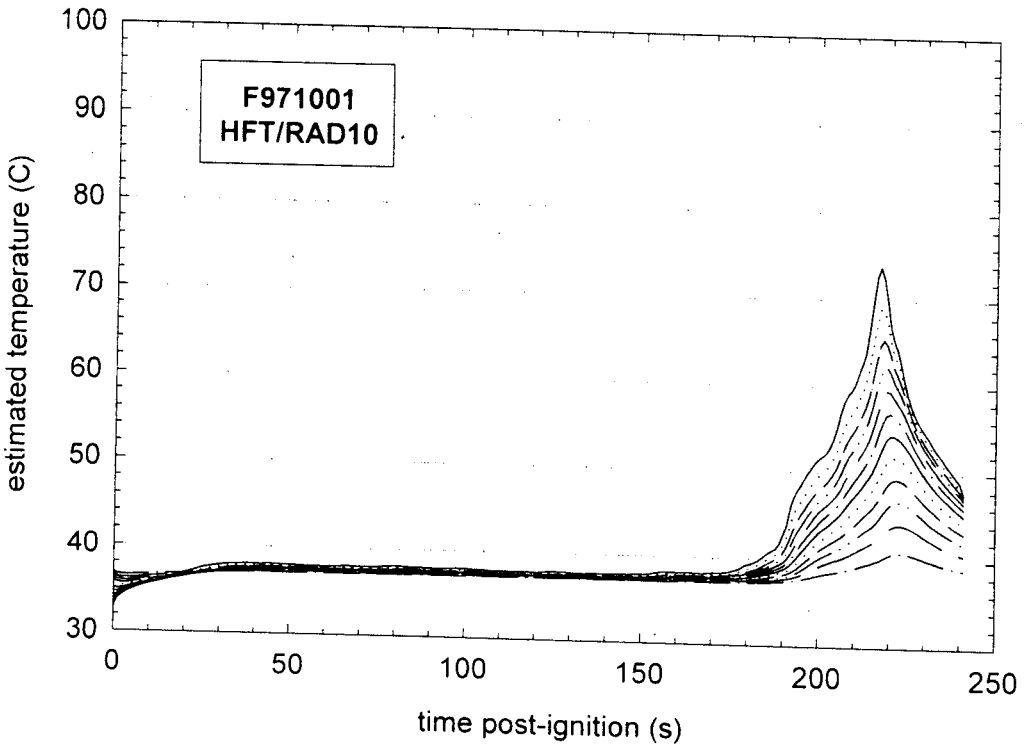

Figure 57. Fire Test F971001. Skin temperature profiles estimated from data recorded from HFT/RAD Assembly 6 (**APPENDIX E**, Plots E19 and E20)

heat fluxes recorded from this transducer decreased as flames disappeared from this area (see **SECTION 5.1**). These trends in the total and radiative heat flux data indicate that radiation from the flames along left inner quarter panel and left rear corner of the roof of the test vehicle accounted for 95% of the measured heat transfer to this transducer at this time. The skin temperatures at the epidermal surface and sub-dermal interface estimated from this heat flux data were approximately 48 and 39°C, respectively, at 29 seconds post-ignition (Fig. 52).

The second peak in the estimated skin temperature profiles occurred at 218 seconds post-ignition, which corresponded the end of the test and the beginning of flame suppression. For example, the total and radiative heat fluxes recorded from HFT/RAD Assembly 6 started to increase from background levels between 150 and 160 seconds post-ignition. A total heat flux of 30.4 kW/m^2 and a radiative heat flux of 30.9 kW/m^2 (radiative) were recorded from HFT/RAD Assembly 6 at 217 seconds post-ignition (**Appendix E**, Plots E9 and E10). These values suggest that radiation accounted for essentially all of the heat transferred to the transducer at this time. The slightly lower value of the measured total heat flux may have been the result of convection from the transducer body to the surrounding air – cooling. The skin temperatures at the epidermal surface and sub-dermal interface estimated from this heat flux data were approximately 77 and 41°C, respectively, at 217 seconds post-ignition (Fig. 52).

7.2 The FAA Combined Hazard Survival Model and Purser's Model of Combustion Gas Toxicity

The FAA Combined Hazard Survival Model and Purser's model utilize the concept of a Fractional Effective Dose [FED] to estimate the cumulative effects of exposure to a mixture of gases produced by burning materials. For exposure to a single gas with an unchanging concentration in air, the Fractional Effective Dose for Incapacitation [FED(I)] is defined as the product of the gas-phase concentration and the time of exposure ($C \times t$) normalized to the concentration-time product that results in incapacitation of 50% of an exposed population [8, 9]. Similarly, the Fractional Effective Dose for lethality [FED(L)] is defined as the product of the gas-phase concentration and the time of exposure normalized to the concentration-time product that results in the death of 50% of an exposed population [see references in 8 and 9]. The estimates of FED(I) and FED(L) obtained using the FAA Combined Hazard Survival Model or Purser's model of combustion gas toxicity and presented in this report cannot be used to predict precisely when the gas concentrations measured in this test would have resulted in incapacitating narcosis or death for a vehicle occupant. Whether exposure to these gases results in toxicity depends on a number of complex physical and physiological variables.

Some of the physical variables include the exact chemical composition of the gaseous mixture, the concentration of each component of the gaseous mixture, and the time of exposure. Exposure to these gases in a burning vehicle can be highly variable, and depend on factors such as elevation in the passenger compartment and airflow through the passenger compartment. As mentioned in the previous section, combustion gases are hotter than the ambient air and form an upper-layer. As both heat and mass are conserved in a fire, the existence of a steep vertical air-temperature gradient implies the existence of similarly steep vertical concentration gradients for gaseous combustion products accumulating in the passenger compartment. The location of the head and nose in the passenger compartment will effect the exposure concentration. An occupant whose head was located below the level where gases were measured, such as an occupant bent over in the seat, would have been exposed to lower concentrations of combustion gases than those shown in **APPENDIX H**. Airflow through the passenger compartment will dilute or remove these gases.

Uncertainties in the responses of humans exposed to these gases also complicated the determination of when and whether toxicity occurs. The mathematical equations for the calculation of FED(I) and FED(L) were derived by analysis of data from controlled experiments in which different species of laboratory animals were exposed to a range of concentrations of each gas. In using data from these laboratory animal experiments to define FED(I) and FED(L), both models implicitly assume that humans respond the same as laboratory animals to exposure to these gases – an assumption that is largely untested and may not be accurate. For example, except for incapacitation from exposure to carbon dioxide, none of the model predictions using either the FAA Combined Hazard Survival Model or Purser's model have been validated for humans. That is, the accuracy of FED(I) and FED(L) in predicting human responses to exposure to the combustion gases measured in this test has not been determined. Consequently, there is a high degree of uncertainty as to the effect exposure to these levels of combustion gases would actually have on a human vehicle occupant. In addition, neither of these models accounts for variation in individual responses to these gases nor the effect of trauma suffered during the crash on an occupant's response to these gases.

The equations presented in both the FAA Combined Hazard Survival Model and in Purser's model divide the exposure into one-minute intervals when the concentration of the gaseous species changes with time. In this test, Fourier Transform Infrared spectra were obtained at seven-second intervals to characterize the changing gas concentrations observed in the passenger compartment. The equations presented in the FAA Combined Hazard Survival Model and in Purser's model were modified to account for the faster sampling times used in this test.

These modified equations are shown below and were used to derive the estimated of FED(I) and FED(L) shown in **SECTION 7.2.1.**

Carbon dioxide-induced hyperventilation can increase the respiratory uptake of airborn combustion products. The FAA Combined Hazard Survival Model uses a multiplication factor to account for the increased respiratory uptake of gaseous combustion products because of exposure to elevated levels of carbon dioxide [V_{CO2}]:

$$V_{CO_2} = \frac{\exp(1.9086 + 0.2496 \times C_{CO_2})}{6.8} \quad (1)$$

where the units of C_{CO2} are %. This equation was not modified for the analysis presented in **SECTION 7.2.1**.

The Fractional Effective Doses for Incapacitation from exposure to carbon dioxide, carbon monoxide, hydrogen chloride, hydrogen cyanide and decreased oxygen were calculated using the following equations modified to account for sampling intervals of less than 1 minute:

$$FED(I)_{CO_2} = \left(\frac{t}{60}\right) \times \sum \left\{ \frac{1}{2193.8 - (311.6 \times C_{CO_2})} \right\} \quad (2)$$

when $5.5 \leq C_{CO2} \leq 7.0\%$,

$$FED(I)_{CO_2} = \left(\frac{t}{60}\right) \times \sum \left\{ \frac{1}{\exp(6.1623 - (0.5189 \times C_{CO_2}))} \right\} \quad (3)$$

when $C_{CO2} > 7.0\%$,

$$FED(I)_{CO} = \left(\frac{t}{60}\right) \times \left(\frac{1}{3.4250}\right) \times \sum \{V_{CO_2} \times C_{CO}\} \quad (4).$$

when $V_{CO2} \times C_{CO} > 0.01\%$,

$$FED(I)_{HCl} = \left(\frac{t}{60}\right) \times \sum \left\{ \frac{1}{3 + \frac{336{,}000}{(V_{CO_2} \times C_{HCl}) - 300}} \right\} \quad (5)$$

when $V_{CO2} \times C_{HCl} > 300$ ppm;

$$FED(I)_{HCN} = \left(\frac{t}{60}\right) \times \left(\frac{1}{564}\right) \times \sum \left\{\left(V_{CO_2} \times C_{HCN}\right) - 63\right\} \quad (6)$$

when $V_{CO2} \times C_{HCN} > 63$ ppm; and

$$FED(I)_{O_2} = \left(\frac{t}{60}\right) \times \sum \left\{\frac{1}{\exp\left(8.55 - \left(0.511 \times \left(20.9 - C_{O_2}\right)\right)\right)}\right\} \quad (7)$$

when $C_{O2} < 11\%$. The value of t in these equations was the time in seconds between acquisition of FTIR spectra. The overall Fractional Effective Dose for Incapacitation was calculated by summing the terms in equations 2 through 7:

$$FED(I)_{TOTAL} = FED(I)_{CO_2} + FED(I)_{CO} + FED(I)_{HCl} + FED(I)_{HCN} + FED(I)_{O_2} \quad (8)$$

The Fractional Effective Doses for Lethality from exposure to carbon monoxide and hydrogen cyanide were calculated using the following equations modified to account for sampling intervals of less than 1 minute:

$$FED(L)_{CO} = \left(\frac{t}{60}\right) \times \sum \left\{\frac{1}{\exp\left(5.85 - \left(0.00037 \times V_{CO_2} \times C_{CO}\right)\right)}\right\} \quad (9)$$

when $2000 \leq V_{CO2} \times C_{CO} \leq 9000$ ppm,

$$FED(L)_{CO} = \left(\frac{t}{60}\right) \times \sum \left\{\frac{1}{0.4 + \left(\frac{58{,}000}{V_{CO_2} \times C_{CO}}\right)}\right\} \quad (10)$$

when $V_{CO2} \times C_{CO} > 9000$ ppm, and

$$FED(L)_{HCN} = \left(\frac{t}{60}\right) \times \left(\frac{1}{2586}\right) \times \sum \left\{\left(V_{CO_2} \times C_{HCN}\right) - 43.2\right\} \quad (11)$$

when $V_{CO2} \times C_{HCN} > 43.2$ ppm;

The overall Fractional Effective Dose for Lethality was calculated by summing the terms in equations 8 through 10:

$$FED(L)_{TOTAL} = FED(L)_{CO} + FED(L)_{HCN} \tag{12}$$

The model described by Purser also uses a multiplication factor to account for the enhanced respiratory uptake of toxic gases because of exposure to elevated levels of carbon dioxide:

$$V_{CO_2} = \frac{\exp(1.9086 + (0.2496 \times C_{CO_2}))}{6.8} \tag{13}$$

The Fractional Effective Doses for Incapacitation from exposure to carbon monoxide and hydrogen cyanide were calculated using the following equations modified to account for sampling intervals of less than 1 minute:

$$FED(I)_{CO_2} = \left(\frac{t}{60}\right) \times \sum \left\{ \frac{1}{\exp(6.1623 - (0.5189 \times C_{CO_2}))} \right\} \tag{14}$$

when $C_{CO2} > 5\%$,

$$FED(I)_{CO} = \left(\frac{t}{60}\right) \times V_{CO_2} \times \sum \left\{ \frac{0.00082925 \times C_{CO}}{30} \right\} \tag{15}$$

where the units of C_{CO} are ppm,

$$FED(I)_{HCN} = \left(\frac{t}{60}\right) \times V_{CO_2} \times \sum \left\{ \frac{4.4}{185 - C_{HCN}} \right\} \tag{16}$$

when $80 \leq C_{HCN} \leq 180$ ppm,

$$FED(I)_{HCN} = \left(\frac{t}{60}\right) \times V_{CO_2} \times \sum \left\{ \frac{1}{\exp(5.396 - (0.023 \times C_{HCN}))} \right\} \tag{17}$$

when $C_{HCN} > 180$ ppm; and

$$FED(I)_{O_2} = \left(\frac{t}{60}\right) \times \sum \left\{ \frac{1}{\exp(8.13 - (0.54 \times (20.9 - C_{O_2})))} \right\} \tag{18}$$

when $C_{O2} < 11.3\%$.

As in the FAA model, the value of t in these equations was the time in seconds between acquisition of FTIR spectra. The overall Fractional Effective Dose for Incapacitation was calculated by summing the terms in equations 14 through 18:

$$FED(I)_{TOTAL} = FED(I)_{CO_2} + FED(I)_{CO} + FED(I)_{HCN} + FED(I)_{O_2} \qquad (19)$$

Both the FAA Combined Hazard Survival model and Purser's model predict that 50% of an exposed population would experience incapacitating narcosis (*i.e.*, an occupant loses consciousness and would be unable to exit a vehicle without assistance) when $FED(I)_{TOTAL} = 1.0$. Similarly, both of these models predict that 50% of an exposed population would die when $FED(L)_{TOTAL} \geq 1.0$.

7.2.1 Estimation of Fractional Equivalent Dose Parameters

The analysis presented in this report included estimates of FED(I) and FED(L) for carbon dioxide, carbon monoxide, hydrogen cyanide, hydrogen chloride and oxygen using the FAA Combined Hazard Survival Model and Purser's model for assessment of the toxicity of combustion products. The other gaseous species included in the FAA Combined Hazard Model and Purser's model were not measured during this test; therefore, values of FED(I) or FED(L) were not estimated for these gases. Figures 58 through 62 show plots of $FED(I)_{co2}$, $FED(I)_{co}$, $FED(I)_{HCN}$, $FED(I)_{HCL}$, and $FED(I)_{O2}$ computed using the FAA Combined Hazard Survival Model and Purser's model for assessment of the toxicity of combustion products.

Plots of the $FED(I)_{co2}$ parameters estimated using the FAA Combined Hazard Model and Purser's model are shown in Figure 58. Both models yielded estimates of $FED(I)_{TOTAL} > 0$ starting at about 170 seconds post-ignition, when the concentration of carbon dioxide was about 5%. And both models yielded estimates of $FED(I)_{co2} > 1$ starting at about 220 seconds post-ignition. The estimates of $FED(I)_{co2}$ reached values of about 3 by 350 seconds post-ignition (Fig. 58).

Plots of the $FED(I)_{co}$ parameters estimated using both models are shown in Figure 59. The equations presented in the Purser model for computation of $FED(I)_{co}$ include a term for respiratory minute volume. Minute volumes corresponding to respiration during rest (8.5 L/min) and light activity (25 L/min) were used in these calculations [9]. Purser's model also accounts for the effect of exposure to carbon dioxide on respiratory rate.

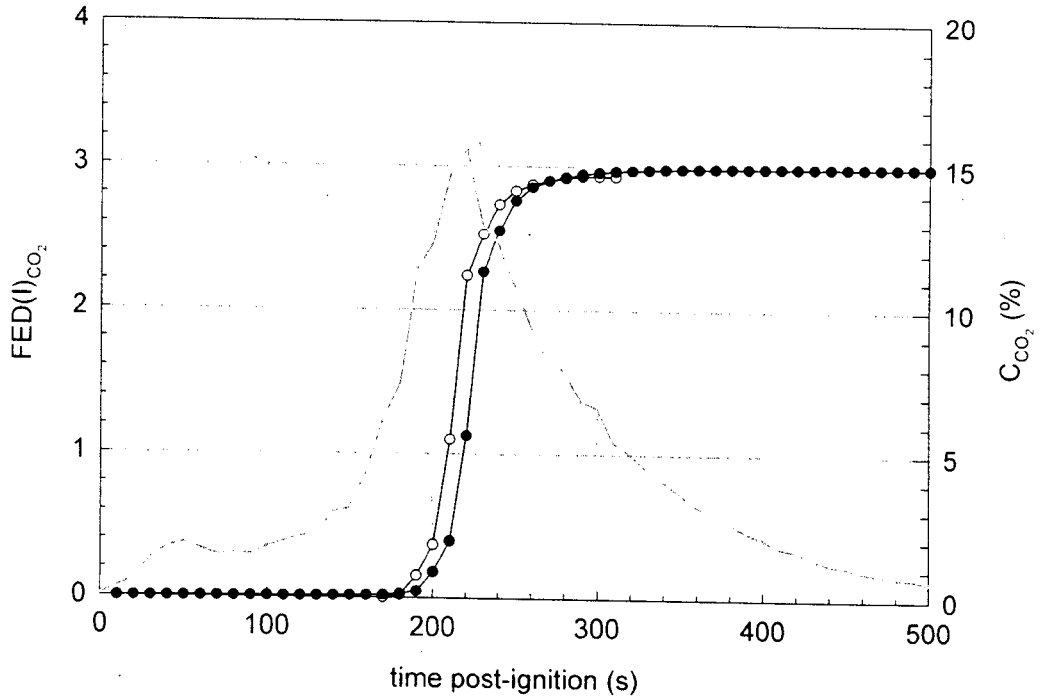

Figure 58. Fire Test F971001. Plots of $FED(I)_{CO2}$ versus time post-ignition: FAA Combined Hazard Survival Model (—○—); and Purser's model (—●—). A plot of C_{CO2} (——) is included for reference.

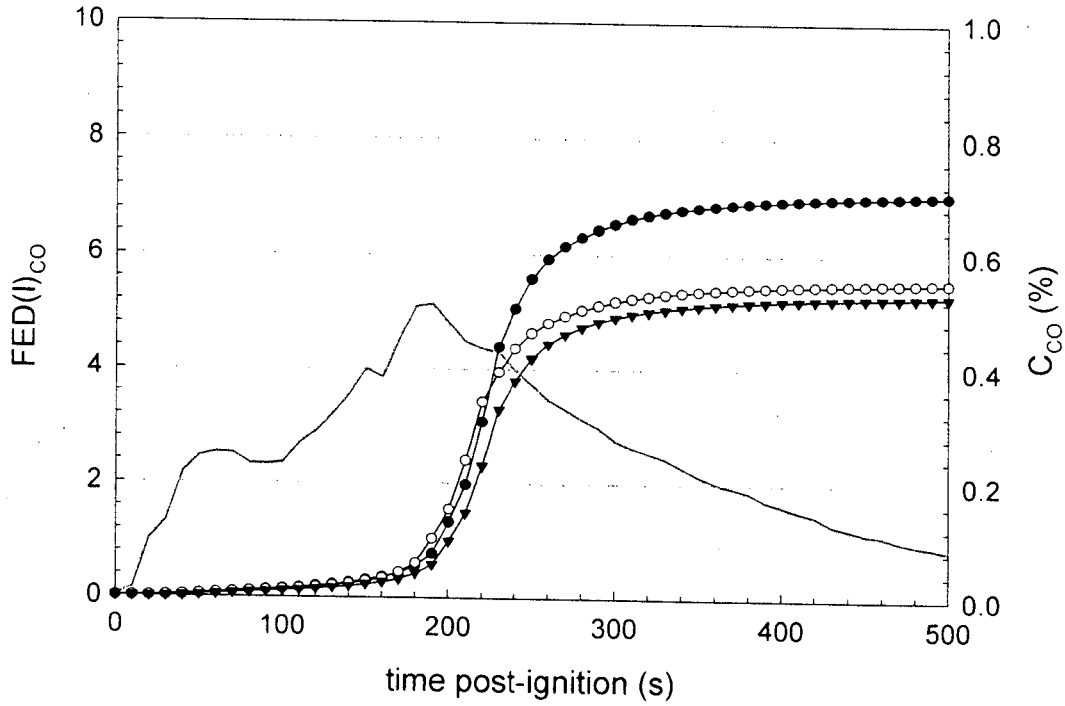

Figure 59. Fire Test F971001. Plots of estimates of $FED(I)_{CO}$ versus time post-ignition computed using the FAA Combined Hazard Survival Model (—○—), the Purser model with a respiratory minute volume of 8.5 L/min (—▼—), and the Purser model with a respiratory minute volume of 25 L/min (—●—). A plot of C_{CO} (——) is included for reference.

The FAA Combined Survival Hazard Model computes only one estimate of $FED(I)_{co}$, which accounts for the effect of exposure to carbon dioxide on respiratory rate [8]. These three estimates of $FED(I)_{co}$ became greater than zero between 10 and 30 seconds post-ignition. The estimates of $FED(I)_{co}$ derived using the FAA model and Purser's model with a respiratory minute volume of 25 L/min became greater than unity between 190 and 200 seconds post-ignition, and reached values of about 5.5 and 7.0, respectively, at 500 seconds post-ignition. The estimate of $FED(I)_{co}$ derived using Purser's model with a respiratory minute volume of 8.5 L/min became greater than unity between 200 and 210 seconds post-ignition, and reached a value of approximately 5.3 at 500 seconds post-ignition.

Plots of the $FED(I)_{HCN}$ parameters estimated using both models are shown in Figure 60. Both the FAA Combined Survival Hazard Model and Purser's model employ a threshold concentrations to determine when to start computing $FED(I)_{HCN}$ (refer to equations 6 and 14, respectively). The estimates of $FED(I)_{HCN}$ using the FAA model start at 160, became greater than unity between 200 and 210 seconds post-ignition, and reached a maximum value of about 6.8 by 360 seconds post-ignition. The estimates of $FED(I)_{HCN}$ started at 210 seconds post-ignition, became greater than unity between 220 and 230 seconds post-ignition, and reached a maximum value of about 2.2 by 310 seconds post-ignition.

Plots of the $FED(I)_{HCL}$ parameters estimated using both models are shown in Figure 61. Both estimates were zero from the time of ignition through 500 seconds post-ignition. The concentration of oxygen in the passenger compartment was greater that 11% throughout this test, which was the threshold for calculating $FED(I)_{O2}$ in Purser's model. Therefore, a plot of $FED(I)_{O2}$ is not shown here.

Plots of the $FED(I)_{TOTAL}$ parameters estimated using both models are shown in Figure 62. The FAA Combined Survival Hazard Model yielded $FED(I)_{TOTAL} > 1$ starting at 190 seconds post-ignition, where $FED(I)_{CO}$ accounted for 67% of $FED(I)_{TOTAL}$, $FED(I)_{HCN}$ accounted for 23.3% of $FED(I)_{TOTAL}$, and $FED(I)_{CO2}$ accounted for 9.7% of $FED(I)_{TOTAL}$. $FED(I)_{O2}$ did not contribute to $FED(I)_{TOTAL}$. The estimated $FED(I)_{TOTAL}$ reached a value of 14.8 at 300 seconds post-ignition. Purser's model yielded $FED(I)_{TOTAL} > 1$ starting at 200 seconds post-ignition using a respiratory minute volumes of 8.5 L/min and 25 L/min in the calculations. With a respiratory minute volume of 8.5 L/min, $FED(I)_{CO}$ accounted for 85..9% of $FED(I)_{TOTAL}$ and $FED(I)_{CO2}$ accounted for 14.1% of $FED(I)_{TOTAL}$. Neither $FED(I)_{HCN}$ or $FED(I)_{O2}$ did not contribute to $FED(I)_{TOTAL}$. With a respiratory minute volume of 8.5 L/min, $FED(I)_{CO}$ accounted for 89.1% of $FED(I)_{TOTAL}$ and $FED(I)_{CO2}$ accounted for 10.9% of $FED(I)_{TOTAL}$.

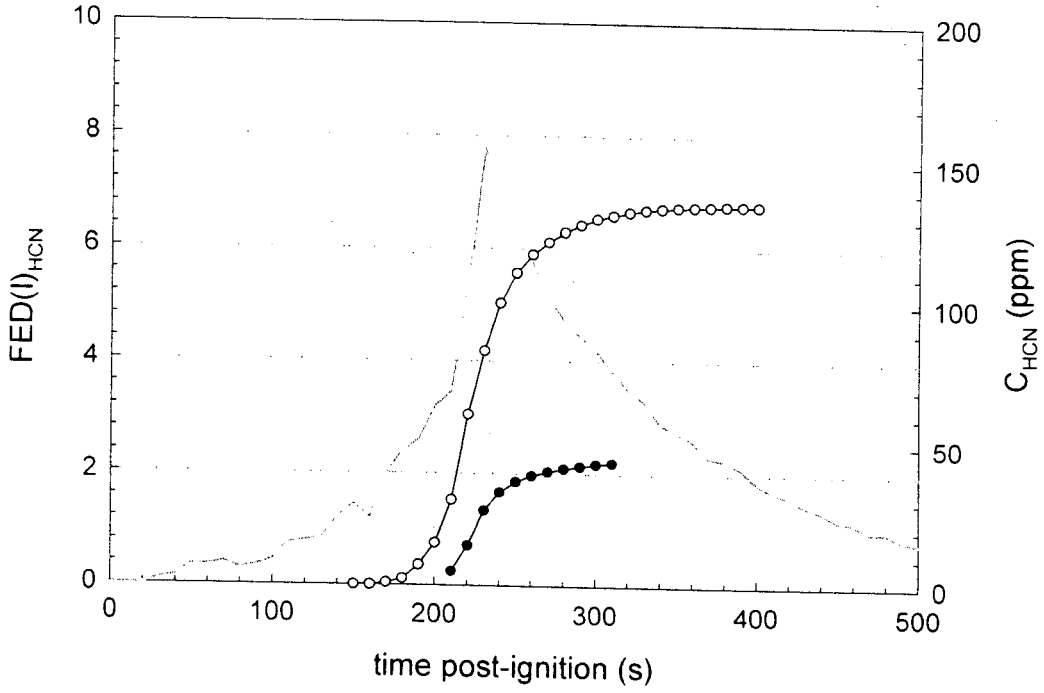

Figure 60. Fire Test F971001. Plots of $FED(I)_{HCN}$ versus time post-ignition: FAA Combined Hazard Survival Model (—○—); and Purser's model (—●—). A plot of C_{HCN} (——) is included for reference.

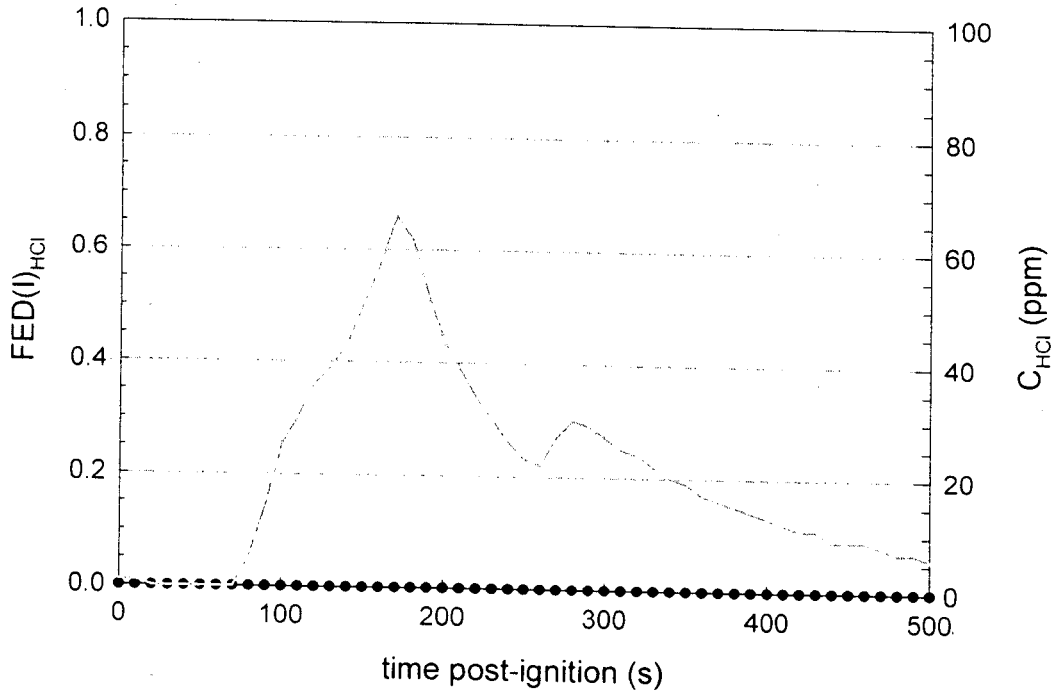

Figure 61. Fire Test F971001. Plots of $FED(I)_{HCL}$ versus time post-ignition: FAA Combined Hazard Survival Model (—○—); and Purser's model (—●—). A plot of C_{HCL} (——) is included for reference.

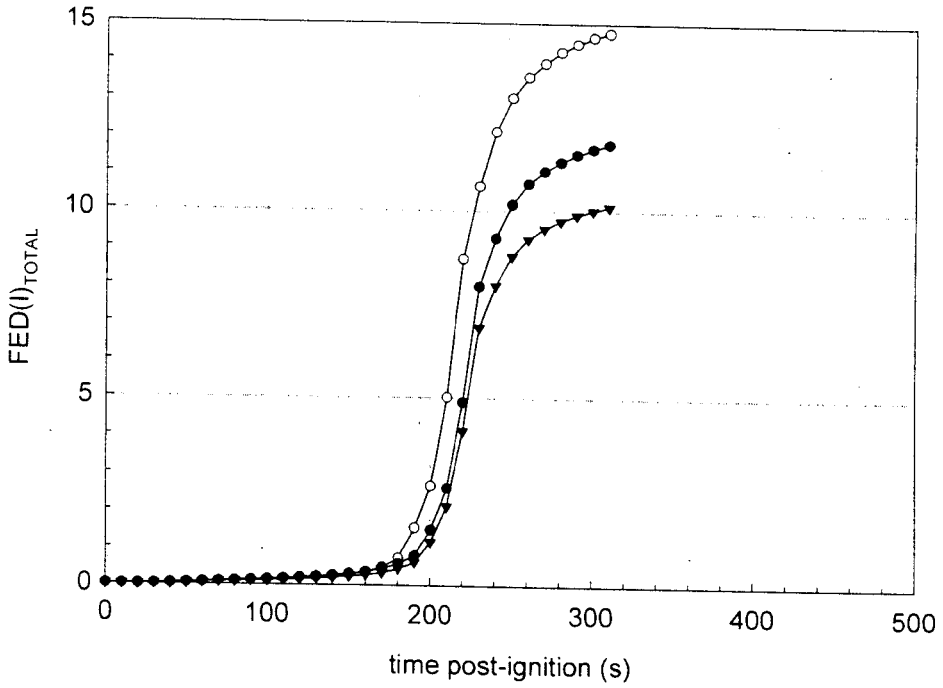

Figure 62. Fire Test F971001. Plots of $FED(I)_{TOTAL}$ versus time post-ignition: FAA Combined Hazard Survival Model (—○—); Purser's model with RMV = 8.5 L/min (—▼—); and Purser's model with RMV = 25 L/min (—●—).

Neither $FED(I)_{HCN}$ nor $FED(I)_{O2}$ contributeed to $FED(I)_{TOTAL}$. The estimated $FED(I)_{TOTAL}$ reached values of about 10.1 and 11.7 at 300 seconds post-ignition.

Figure 63 shows plots of $FED(L)_{CO}$, $FED(L)_{HCN}$, and $FED(L)_{TOTAL}$ computed using the FAA Combined Survival Hazard Model. These calculations yielded $FED(L)_{CO} > 1$ starting at 230 seconds post-ignition, $FED(L)_{HCN} > 1$ starting at 240 seconds post-ignition, and $FED(L)_{TOTAL} > 1$ starting at 210 seconds post-ignition. The estimates of $FED(L)_{CO}$, $FED(L)_{HCN}$, and $FED(L)_{TOTAL}$ were 1.7, 1.5, and 3.2 at 430 seconds post-ignition.

As stated previously, the estimates of FED(I) and FED(L) obtained using the FAA Combined Hazard Survival Model and Purser's model of combustion gas toxicity can not predict precisely when the gas concentrations measured in this test would have resulted in incapacitating narcosis or death. This is especially true for prediction of lethality, where the mathematical relationships in these models were derived from experiments using laboratory animals or accidental, uncontrolled human exposures [8, 9]. Variation in the susceptibility to these hazards among the human population also will contribute to the uncertainty in these predictions. In addition, the effect of

trauma caused by the crash on an occupant's tolerance to these toxic gases is impossible to quantify.

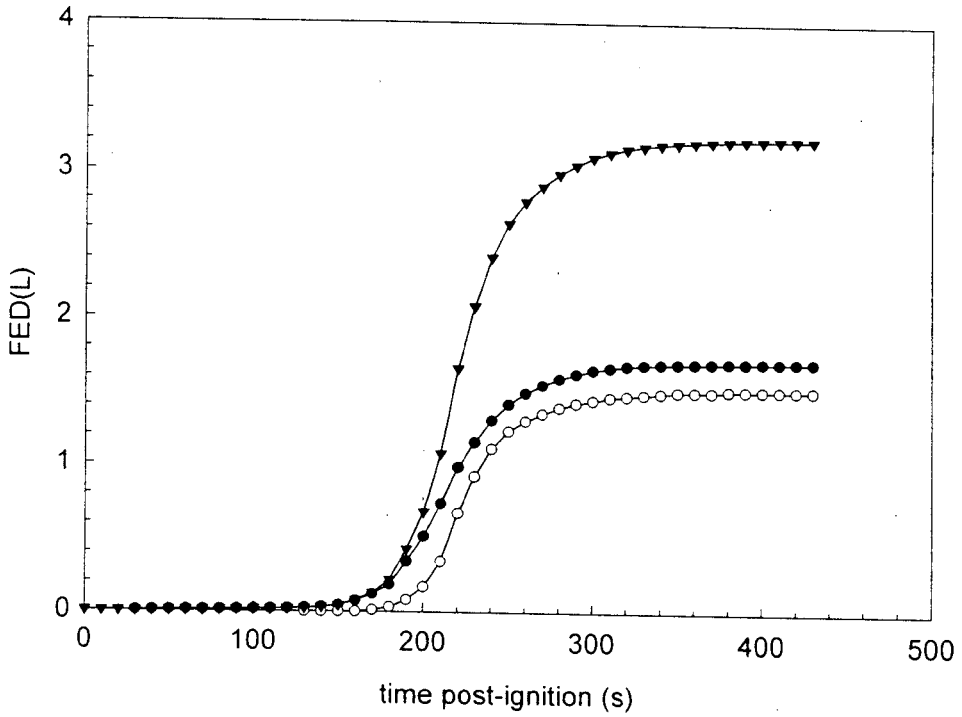

Figure 63. Fire Test F971001. Plots of $FED(L)_{CO}$ (—●—), $FED(L)_{HCN}$ (—○—), and $FED(L)_{TOTAL}$ (—▼—) versus time post-ignition computed using the FAA Combined Hazard Survival Model Fire.

Another variable that may affect an occupant's susceptibility to the combustion products is the location of the head. The data from the aspirated thermocouples indicated that a steep air-temperature gradient developed in the front of the passenger compartment during this test. Since both heat and mass are conserved in a fire, the existence of a steep vertical air-temperature gradient implies the existence of a similarly steep vertical concentration gradient for combustion products accumulating in the passenger compartment. The inlet to the gas sampling tube in the passenger compartment was in the breathing zone of that of a six-foot tall adult male sitting upright in either the driver's or front passenger's seat. An occupant whose head was located below the level where gases were sampled would have been exposed to lower concentrations of combustion gases that those shown in **APPENDIX H**. And the estimated values of FED(I) and FED(L) for this occupant would have been lower than those shown in Figures 58 through 63.

7.3 Estimation of Burn-Injury to the Respiratory Tract

Valid air temperature data was not obtained during this test (see **APPENDIX D**).

ACKNOWLEDGEMENTS

Dr. Thomas Ohlemiller and Thomas Cleary of the Building and Fire Research Laboratory, National Institute of Standards and Technology were responsible for video taping this fire test, and provided an initial analysis of the test data for fire propagation. Dr. Archibald Tewarson of Factory Mutual Research Corporation provided the data from the Fire Products Collector at the test facility that was collected during this test.

REFERENCES

1. Jack L. Jensen and Jeffrey Santrock. Evaluation of Motor Vehicle Fire Initiation and Propagation. Part 1: Vehicle Crash Test and Fire Propagation Test Program. Submitted to the National Highway Transportation Safety Administration pursuant to the Settlement Agreement between General Motors and the Department of Transportation. Submitted July 31, 1997.

2. Jack L. Jensen and Jeffrey Santrock. Evaluation of Motor Vehicle Fire Initiation and Propagation. Part 5: Crash Tests on a Rear Wheel Drive Passenger Car. To be submitted to the National Highway Transportation Safety Administration pursuant to the Settlement Agreement between General Motors and the Department of Transportation.

3. Federal Safety Standards. Motor Vehicle Safety Standard No. 214 Side Impact Protection - Passenger Cars, Trucks, Buses & Multipurpose Passenger Vehicles with GVWR of 10,000 Pounds or Less. 60FR57838-39 (November 22, 1995).

4. Federal Safety Standards. Motor Vehicle Safety Standard No. 301 Fuel System Integrity - Passenger Cars; MPV's, Trucks and Busses with GVWR of 10,000 Pounds or Less; and School Buses with GVWR Greater than 10,000 Pounds. 61FR19201-02 (May 1, 1996)

5. SigmaPlot® 4.0 for Windows®, SPSS Inc., 444 North Michigan Avenue, Chicago, IL 60611. Copyright © 1997 by SPSS Inc..

6. Thomas J. Ohlemiller and John R. Shields. Aspects of the Motor Vehicle Fire Threat from Flammable Liquid Spills on a Road Surface. National Institute of Standards and Technology Internal Report NISTIR 6147. March 1998. Submitted to the National Highway Transportation Safety Administration pursuant to the Settlement Agreement between General Motors and the Department of Transportation. Date Submitted on September 9, 1998.

7. Archibald Tewarson. "Generation of Heat and Chemical Compounds in Fires" Section 3/Chapter 4, SFPE Handbook of Fire Protection Engineering, 2nd Edition, 1995, pp. 3:53-124.

8. F. S. Knox III, Dena Bonetti, and Chris Perry. User's Manual for BRNSIM/BURNSIM: A Burn Hazard Assessment Model. United States Army Aeromedical Research Laboratory Report No. 93-13. Fort Rucker, Alabama 36362-5292. February 1993.

9. L. C. Speitel. Toxicity Assessment of Combined Gases and Development of a Survival Model. DOT/FAA/AR-95-5. July 1995.

10. David A. Purser. "Toxicity Assessment of Combustion Products" Section 2/Chapter 8, SFPE Handbook of Fire Protection Engineering, 2nd Edition, 1995, pp. 2:85-146

APPENDIX A
VIDEO CAMERA SET-UP

Scientific and technical personnel from the Building and Fire Research Laboratory, National Institute of Standards and Technology were primarily responsible for obtaining a video record of this test. Seven video cameras were used in this test. Figure A1 shows the approximate locations of the video cameras relative to the test vehicle during this test.

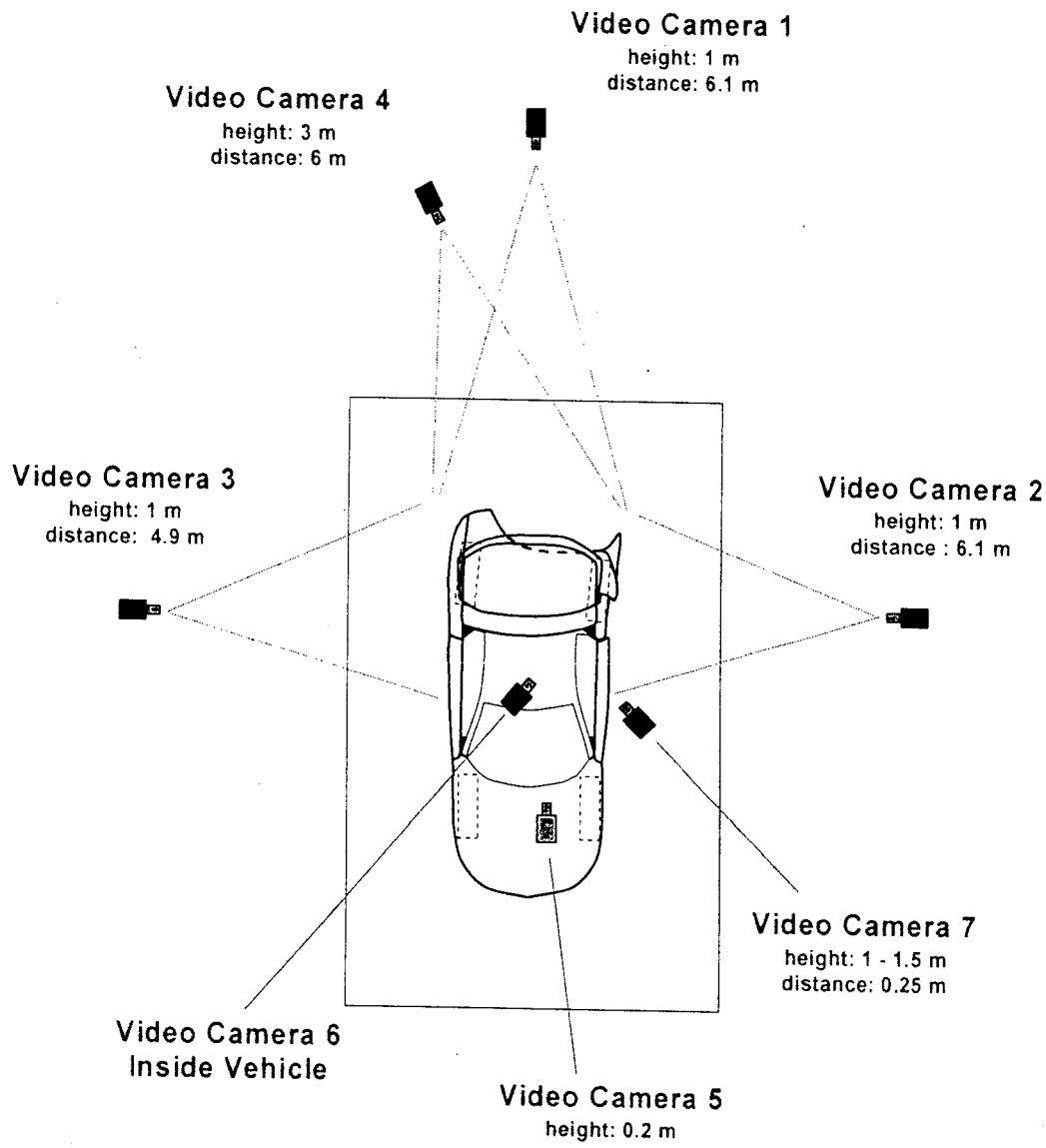

Figure A1. Fire Test F971001. Diagram showing the approximate locations of the video cameras during this test. Distances in this figure are not to scale in this diagram.

Cameras 1, 2, 3, and 4 were Hi-8 camcorders mounted on tripods. Camera 1 had a field-of-view that included the full height and width of the rear of the test vehicle. Camera 2 had a field-of-view

that included the full height of the test vehicle from the rear bumper fascia to the middle of the left door. Camera 3 had a field-of-view that included the full height of the test vehicle from the rear bumper fascia to the middle of the right door. Camera 4 was on a tower between 8 and 10 m above the test vehicle. Its field-of-view included the full width and length of the test vehicle. Water pipes for the extinguishing system on the fire products collector were visible in the Cameras 2 and 3, and partially obscured sections of the test vehicle.

Cameras 5 through 7 were black-and-white CCD cameras with fixed focal lengths. The outputs from the CCD cameras were sent to standard VHS video recorders. Camera 5 was located under the test vehicle facing rearward. Its field-of-view included the full height and width of the area under the rear of the test vehicle, defined by the floor pan and simulated road surface, and the rear wheels, respectively. Camera 6 was located inside the passenger compartment above the front passengers seat and was focused on the rear left passengers seat and left B-pillar trim panel. Camera 7 was located a tripod adjacent to the left door. Its field-of-view included the full height and width of the liftgate opening.

All video cameras were started before the test. A microphone on each camera recorded the air horn, which signaled removal of the plug from the hole in filler neck, ignition of the gasoline, and the end of the test.

Quartz-halogen floodlights were used to illuminate the exterior of the vehicle. The level of illumination provided by these lamps was insufficient to balance the intensity of light reflecting from the vehicle surfaces with the brightness of the flames. To compensate for this imbalance, the light sensitivity adjustments on the Hi-8 camcorders were set to the manual position so that the apparent brightness of the vehicle surfaces did not change as the fire developed. As a result, the flames were overexposed, causing them to appear more opaque than they actually were.

APPENDIX B
INFRARED THERMOGRAPHY

Infrared thermal imaging radiometers were used to help determine fire propagation, flame, and surface temperatures during this test. These imaging systems measure thermal radiation within a definite waveband, over a variable field of view. The data obtained from these measurements can be analyzed to produce a two-dimensional map of apparent temperature called a thermogram.

Thermal imaging systems produce a spatially resolved map of surface temperatures from the radiant energy emitted in the field of view. The response time of these systems is nanoseconds, giving them the capability to acquire over 1 million discrete measurements per second. The capability of high-speed data acquisition is advantageous in that it can provide a tremendous amount of thermal data during a vehicle fire test, which can be over in only a few minutes. Thermal imaging radiometers can be used concurrently as a vision system and a measurement system. However, the thermal sensitivity, scan speed, and spatial resolution must be optimized for a particular application.

B.1 Infrared Camera Location

Figure B1 shows the approximate locations of the infrared cameras relative to the test vehicle during this test. IR1 through IR5 were mounted outside the test vehicle. IR1 was an Inframetrics 740 thermal imaging system (Inframetrics Inc, Billerica, MA) with an optical window of 3 to 14 μm. Its was focused on the interior of the test vehicle through the left side window. The glass was broken during the crash test. IR2 was an Inframetrics Model 760 thermal imaging system with an optical window of 3 to 14 μm. Its field-of-view included the rear left quarter of the test vehicle. IR3 was an Inframetrics Model 760 thermal imaging system with an optical window of 3 to 14 μm. Its field-of-view included the rear of the test vehicle. IR4 was an Agema Model 900 thermal imaging system with an optical window of 3 to 14 μm. It was mounted on a tower behind the test vehicle. It was focused on the interior of the test vehicle through the broken rear lift glass. IR5 was an Agema Model 900 thermal imaging system with an optical window of 3 to 14 μm. Its field-of-view included the rear right quarter of the test vehicle.

IR6 was located inside the test vehicle. IR6 was a Flir Model 7300 thermal imaging radiometer (Flir Systems, Inc., Portland, OR) with an optical window of 3 to 5 μm. This system was placed in an insulated metal box mounted to the top of the instrument panel. Its field-of-view included the upper portion of the driver's seat back, the left section of the rear seat back, a portion of the left quarter interior finishing panel, and the rear left section of the headlining.

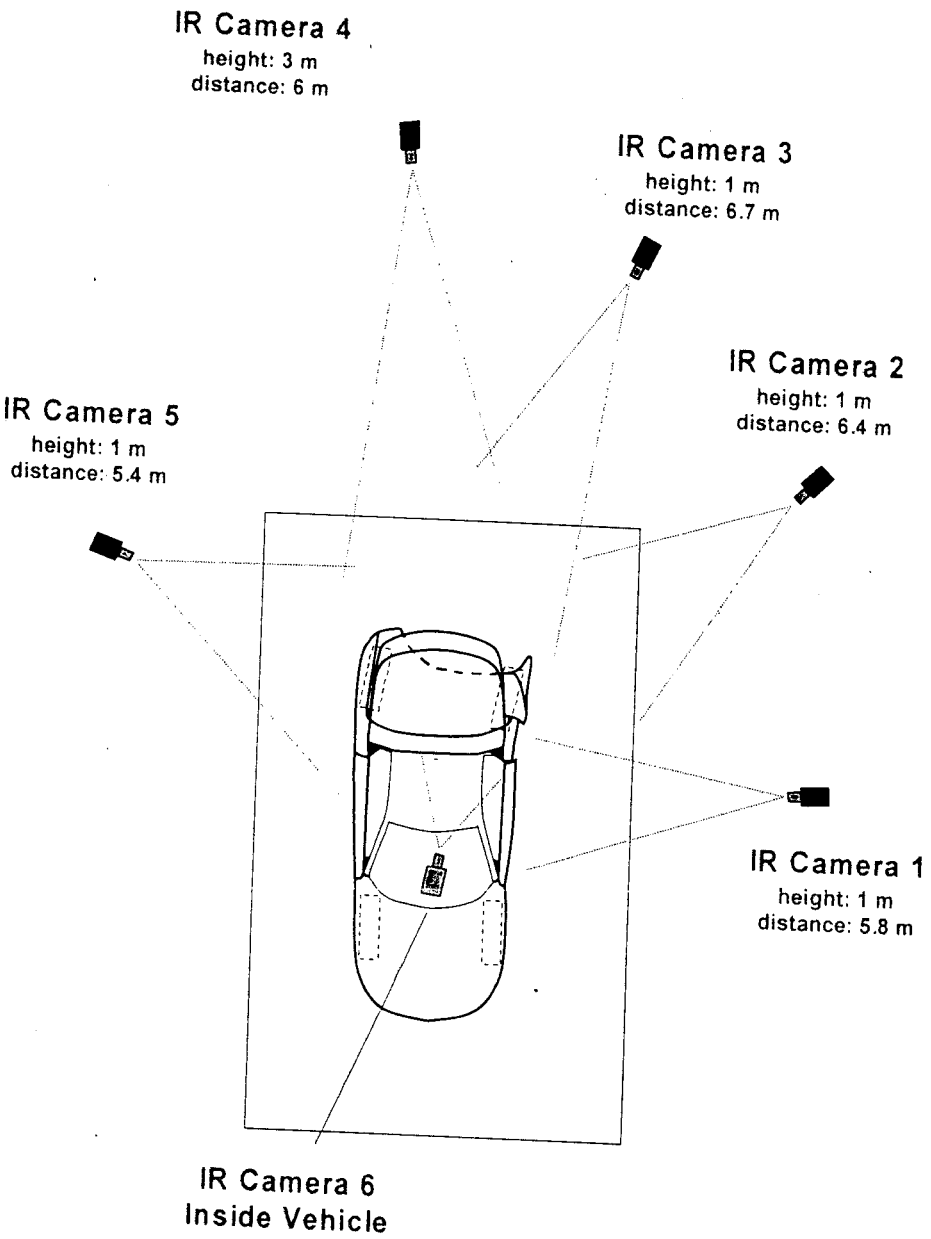

Figure B1. Fire Test F971001. Placement of infrared thermal imaging systems around the test vehicle during this test. Distances and heights are approximate and not to scale in this diagram.

B.2 Data Analysis

Thermal imaging systems measure infrared radiation within a certain spectral band and must be calibrated to convert radiant intensity in that spectral band to temperature. Due to variations in system response, every system has to be calibrated. Calibration curves for the basic thermal imaging radiometers are measured at the factory and stored in read-only memory or in analysis

software programs. Additional calibrations are needed for the optical filters. These calibrations are stored in the analysis software programs. Since thermal imaging radiometers are AC coupled devices, they measure differences in thermal radiation. To get absolute temperatures, there must be a reference to provide DC restoration. In these instruments, the reference is an internal blackbody reference source that is viewed periodically by the detector.

The general radiometric equation was used to convert radiant energy to temperature:

$$I = [E_t \times F(T_t)] + [(1 - E_t) \times F(T_b)] - [E_r \times F(T_r)] - [(1 - E_r) \times F(T_b)] \qquad \text{(B1)}$$

Where I is the difference in radiance between the target and a reference surface; E_t is the emittance of the target surface, generally unknown; E_r is the emittance of the reference surface, T_t is the temperature of the target surface; T_b is the temperature of background surfaces (i.e., ambient temperature), or other emitters such as flames reflected from the target; T_r is the temperature of the reference surface; $F(T_t)$ is the radiance from an ideal emitting surface (i.e., black body) at the temperature of the target surface (T_t); $F(T_r)$ is the radiance from an ideal emitting surface at the temperature of the reference (T_r); and $F(T_b)$ is the radiance from the background relative to the radiance value from the reference surface when $E_r = 1$. Factors other than temperature determine the emittance of an object. These factors include the type of material, the texture of the surface, the wavelength of the detector, and the view-angle. In determining temperatures from the radiant energy from an object, the operator can set the emittance of an unknown target surface to a value of between .01 and 1.0.

Radiant intensity measured by the thermal imaging system is converted to a gray-scale value. An 8 bit system provides gray scale values from 0 to 255 for the radiant energy at each pixel in the instantaneous field of view. A 12 bit system provides gray scale values from 0 to 4095. As the radiometer scans the image, each pixel is assigned a gray scale value, and the gray scale image is stored either in a computer memory or onto videotape. When stored in computer memory, a single frame (1 thermogram) can contain up to 68,000 pixels (discrete measurements) with an assigned 8 bit or 12 bit value. Videotape provides a temporal resolution of 30 frames per second. Depending on the thermal range of the thermal imaging radiometer, a temperature value was assigned to each pixel using either the factory calibration curves accompanying each instrument, or calibration curves stored in IR analysis software.

Separation of the apparent temperatures of various surfaces on and inside a burning vehicle from the captured data is not a trivial task. The data represent a complex combination of emitted infrared energy from those surfaces as well as reflected infrared energy from the flames, and

reflected infrared energy from high intensity lights used to illuminate the vehicle for visual data capture. In addition, the flames themselves were emitting infrared radiation due to their sooty content, some part of which was captured by the infrared thermal imaging systems. Also, some of the infrared radiation being emitted by the vehicle surfaces had to pass through flames containing soot from incomplete combustion of synthetic polymers or through clear (clean) flames where more complete combustion was occurring, and/or a combination of both types of flames. In all of these cases, gases in the flame absorbed some of the infrared radiation emitted by objects behind the flame.

The following steps were taken to minimize the impact of unwanted infrared radiation being captured by the thermal imaging systems.

- Anti-reflection tapes, paint, and glazes were applied to highly reflective surfaces on the test vehicle to minimize interference from reflections of the video floor and spot lights on the test vehicle.
- The thermal imaging systems were located in the shadows of the vehicle to block the video lights from shining directly into the radiometer.
- In some cases, flame filters (3.9 μm) were used in an attempt to screen out a portion of the infrared radiation from flames.

Despite these precautions, accurate surface temperatures could not be determined for areas of the vehicle blocked by intense flame. As a result, only surface temperatures determined to be reliable by the IR analysts are reported here. In some cases, specialized data analysis techniques were used to obtain reliable surface temperatures from areas in close proximity to, but not shielded by flame. Where possible, temperature data were reported from areas that lie in the shadow of the flames, which comes from highly emissive surfaces not affected by the flame radiation, and/or is deemed reliable based on the experience of the analysts. Data from nearby thermocouples were compared to IR temperature readings for a more comprehensive analysis.

During the data analysis, the videotapes were reviewed frame-by-frame to observe the burn sequence. The analyst captured images from selected frames on a video board. The image was processed to produce a digitized gray scale value for each element in the pixel matrix utilizing the camera settings automatically documented between video frames on the videotape during data acquisition. Thermograms were produced from the digitized image matrix using a commercial software package (Thermogram Pro V1.3, sold by Inframetrics, Inc., Billerica, MA). This software utilized the NIST traceable calibration tables supplied by the manufacturer with each thermal imaging system.

APPENDIX C
THERMOCOUPLE DATA

The thermocouples used in this test were type-N thermocouples fabricated by Medtherm Corporation (Huntsville, AL). Each thermocouple consisted of an ungrounded thermocouple junction (30 AWG thermocouple wire) enclosed in an Inconel 600 sheath insulated with magnesium oxide (o.d. = 0.040 in. (1 mm), length = 50 ft. (15.2 m)). A transition was made through a stress-relief bushing to a duplex thermocouple extension cable (24 AWG) with fiberglass insulation and a stainless steel over-braid (length = 1 ft. (0.28 m)). Each thermocouple wire terminated in a grounded, compensated Type-N thermocouple plug. The thermocouples were connected to the data acquisition system using Type-N thermocouple extension cables (length = 50 ft. (15.2 m)).

The data acquisition system consisted of a PC (75 MHz Pentium Processor, 16 MB RAM, an 814 MB hard disk, and a 16-bit, Model BG45-AP5CP, ACER Inc., Taiwan R. O. C.) with a 100 kHz I/O board with 16 analog input channels (DaqBoard 200A; IOTech, Inc., Cleveland, OH). Thermocouple multiplex expansion cards (DBK-19, IOTech, Inc., Cleveland, OH) were used for data acquisition from the thermocouples. The expansion cards were mounted in an electronics cabinet and hard-wired to a panel containing compensated Type-N thermocouple jacks.

To reduce electronic noise on the thermocouples, the ground leads from each thermocouple jack was connected to the electronic chassis ground of the thermocouple mutliplex extension cards. The vehicle chassis was connected to the electronic chassis ground by a large-gauge cable. The electronic chassis ground was connected to an isolated earth ground.

The data acquisition software (DASYLab, Daten System Technik GmbH, Mönchengladbach, Germany) was configured to sample each channel at a rate of 10 Hz and store the data in 10-point block averages.

Figures C1 through C7 show the approximate locations of thermocouples in the test vehicle. Plots C1 through C105 show plots of the temperature data recorded from these thermocouples during this test.

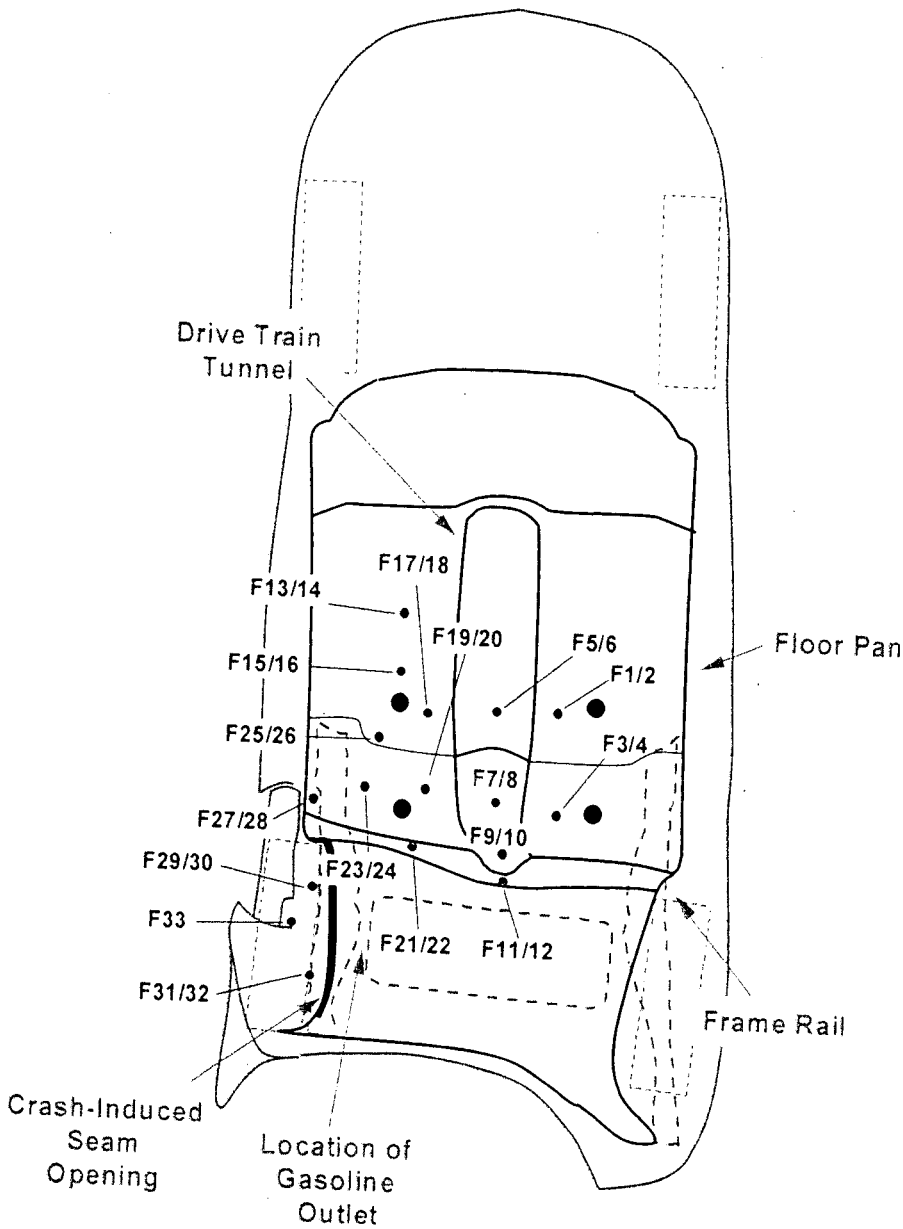

Figure C1. Fire Test F971001. Diagram showing the approximate locations of thermocouples on the floorpan of the test vehicle. Thermocouples F1 through F32 were installed on the floor pan in pairs. The odd-numbered thermocouple of each pair was located approximately 1 cm below the lower surface of the floor pan. The even-numbered thermocouple of each pair was attached to the upper surface of the floor pan with thermally conducting ceramic cement. Thermocouple F33 was located on the rear left wheelhouse panel liner approximately above the center of the rear left tire.

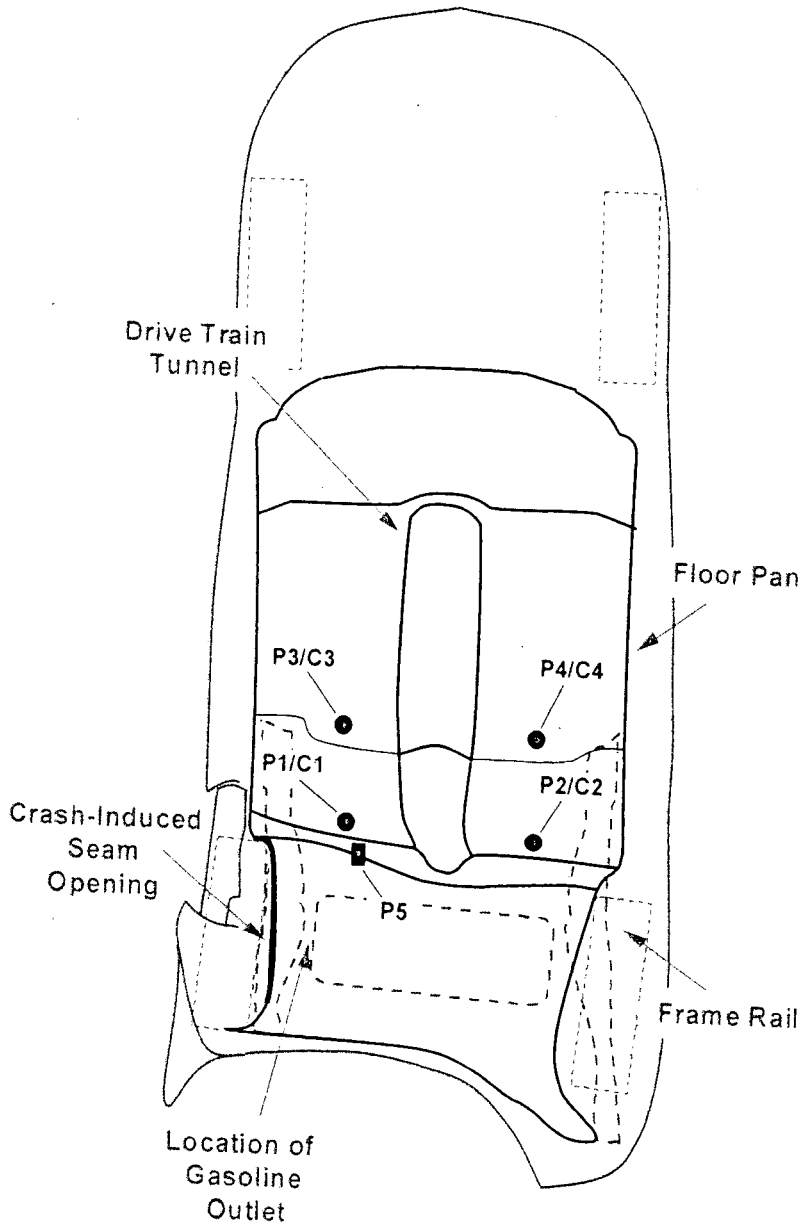

Figure C2. Fire Test F971001. Diagram showing the approximate locations of thermocouples on the floorpan drain hole plugs and carpet of the test vehicle. Thermocouples P1 through P4 were located on the upper surfaces of drain plugs in the floor pan. Thermocouple P5 was located on an electrical pass-through in the panel behind the rear seatback. Thermocouples C1 through C4 were located on the upper surfaces of the carpet above the drain plugs in the floor pan.

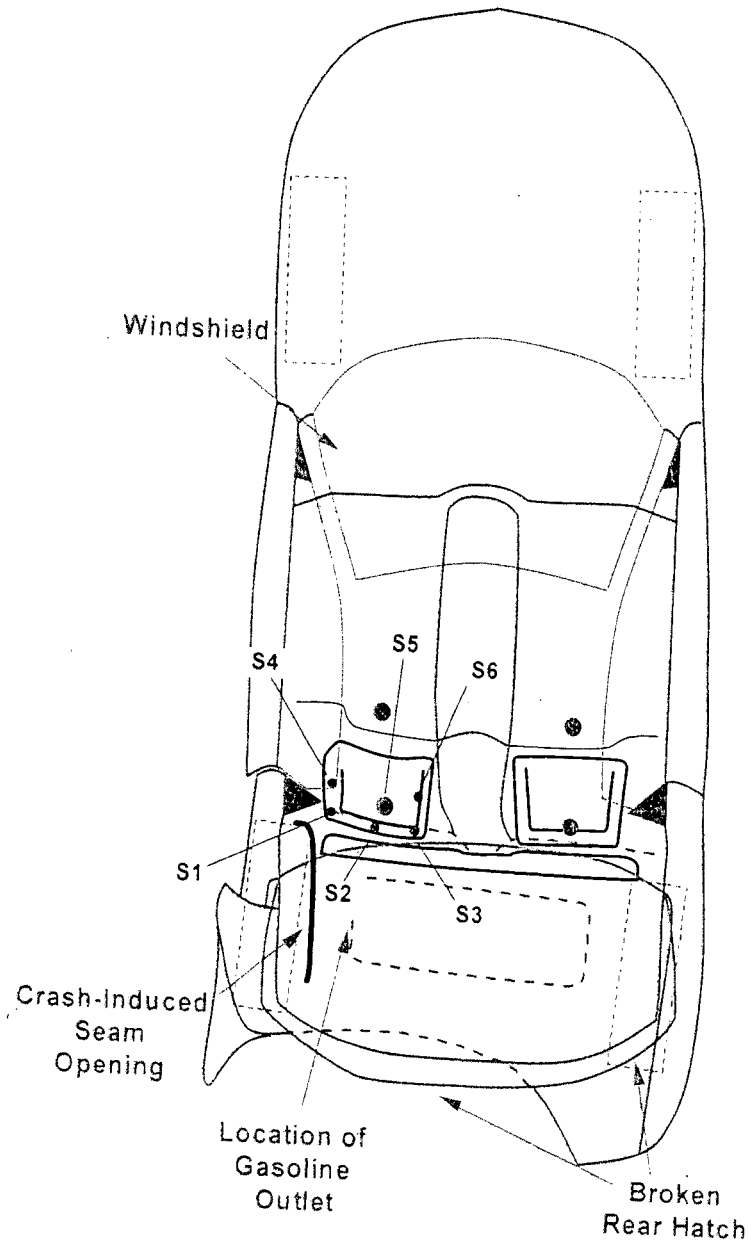

Figure C3. Fire Test F971001. Diagram showing the approximate locations of thermocouples on the rear left seat cushion of the test vehicle. Thermocouples S1 through S6 were located approximately 1 cm below the lower surface of the foam pad in the rear left seat cushion.

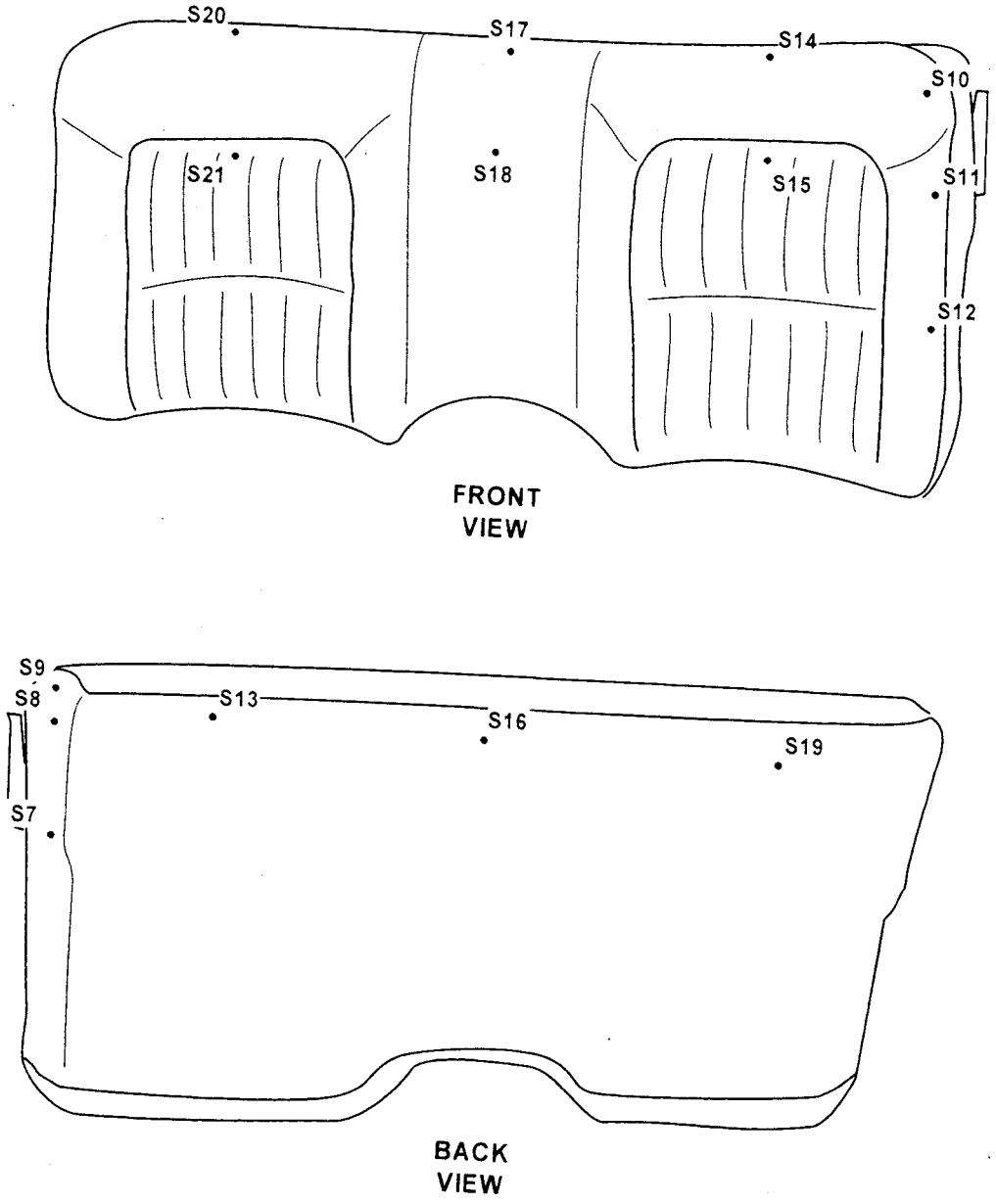

Figure C4. Fire Test F971001. Diagram showing the approximate locations of thermocouples on the seat back in the test vehicle. Thermocouples S9 through S11 were located on the outer surface of the left side panel of the seat cover. Thermocouples S10, S11, S12, S14, S15, S17, S18, S20, and S21 were located on the outer surface of the front panel of the seat cover. Thermocouples S13, S16, and S19 were located on the outer surface of the back panel of the seat cover.

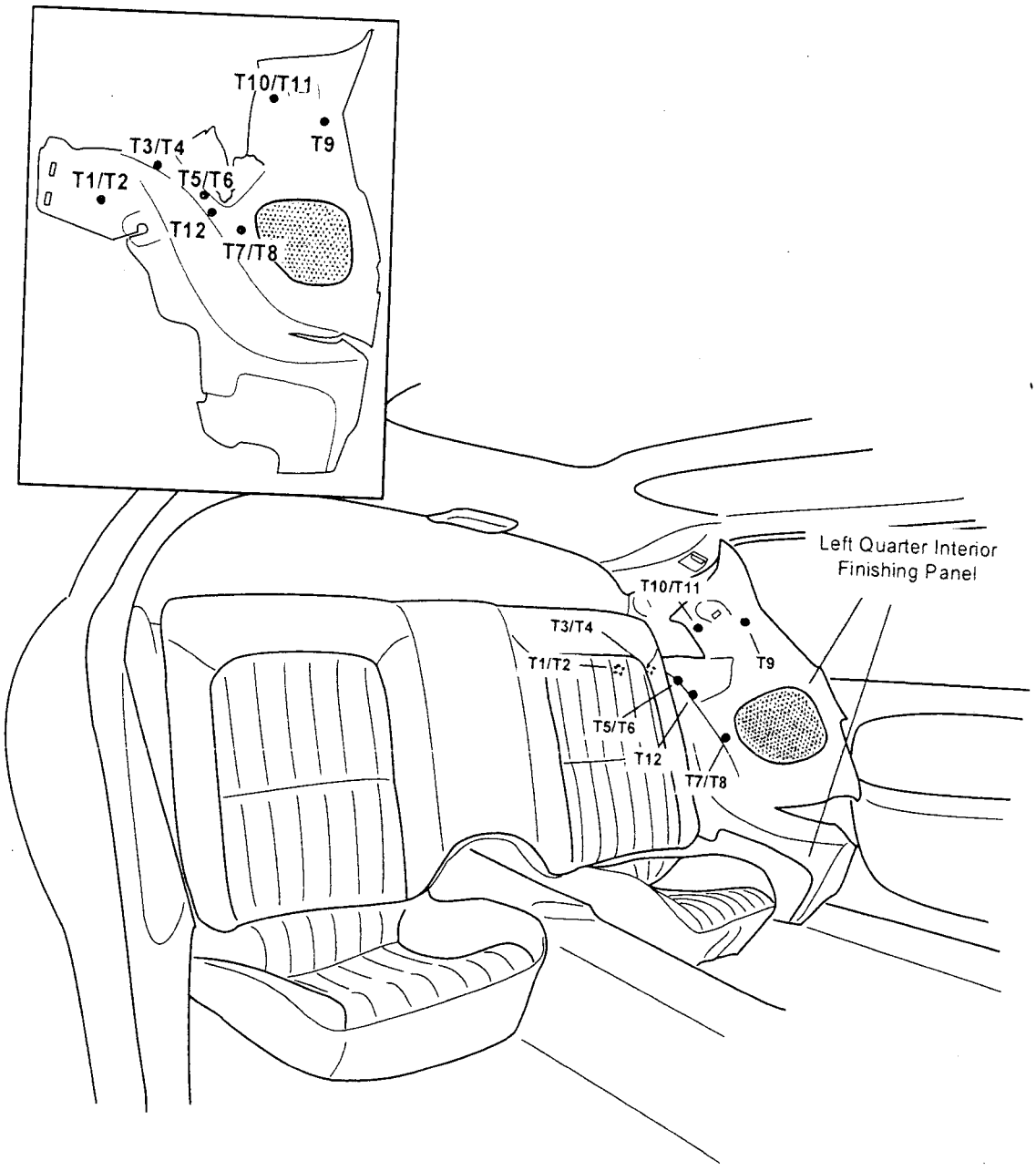

Figure C5. Fire Test F971001. Diagrams showing the approximate locations of on the left quarter interior finishing panel in the test vehicle. Thermocouples T1, T3, T5, T7, T9, and T10 were located behind the left quarter interior finishing panel, approximately 10 cm from the interior surface (back-side). Thermocouples T2, T4, T6, T8, and T11 were located on the exterior surface (front-side) of the left quarter interior finishing panel. Thermocouple T12 was located on HFT 3.

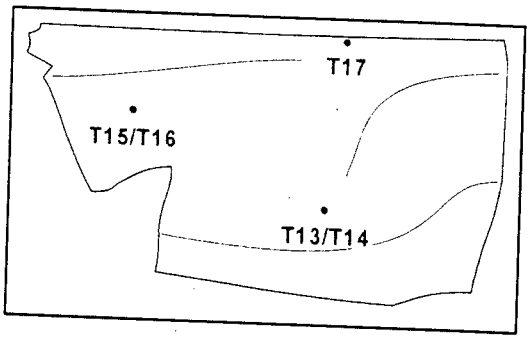

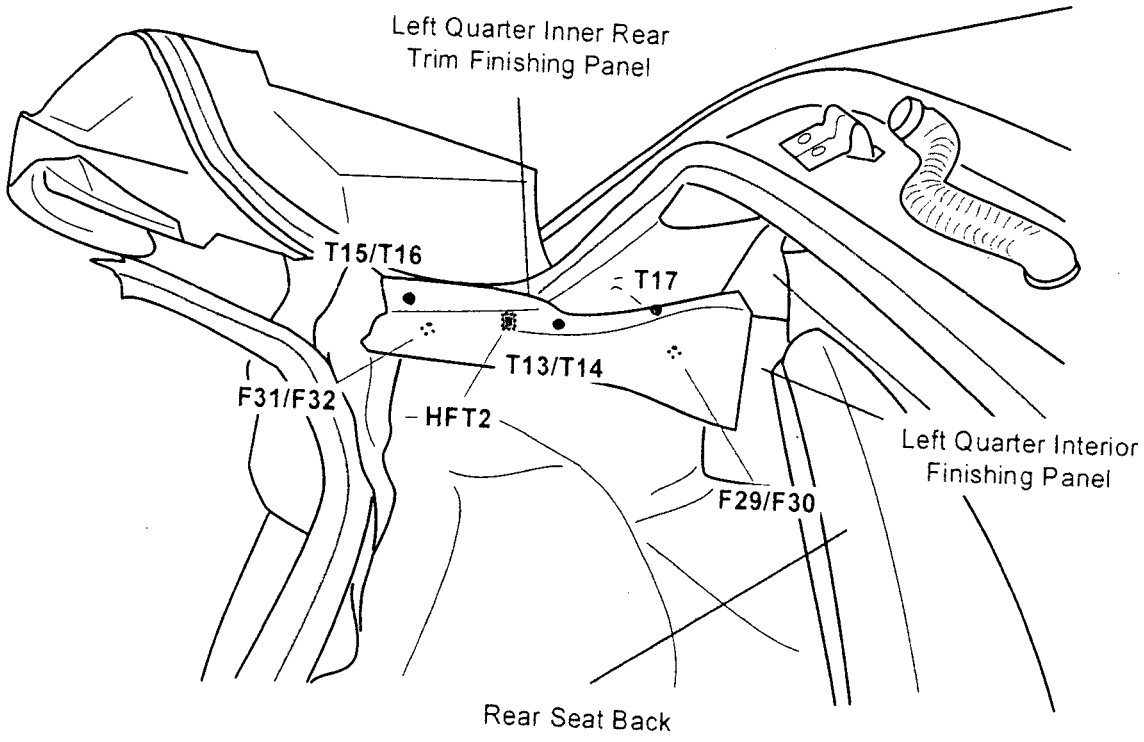

Figure C6. Fire Test F971001. Diagrams showing the approximate locations of thermocouples on a section of the left quarter inner rear trim finishing panel in the test vehicle. Thermocouples T13 and T15 were located behind the left quarter inner rear trim finishing panel, approximately 10 cm from the interior surface (back-side). Thermocouples T14, T16, and T17 were located on the exterior surface (front-side) of the left quarter inner rear trim finishing panel. The approximate locations of Thermocouples F29 through F32 and of HFT2 are shown for reference.

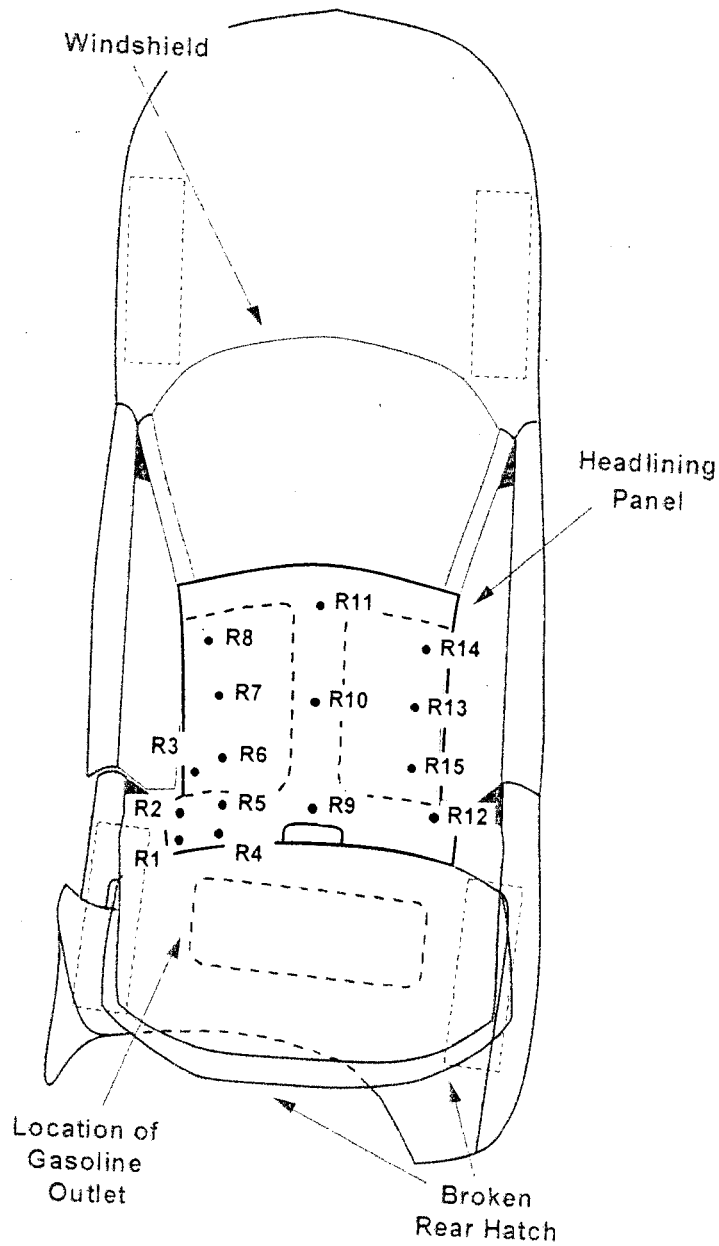

Figure C7. Fire Test F971001. Diagram showing the approximate locations of thermocouples on the headliner in the test vehicle. Thermocouples R1 through R15 were locates approximately 10 cm below the lower surface of the headliner.

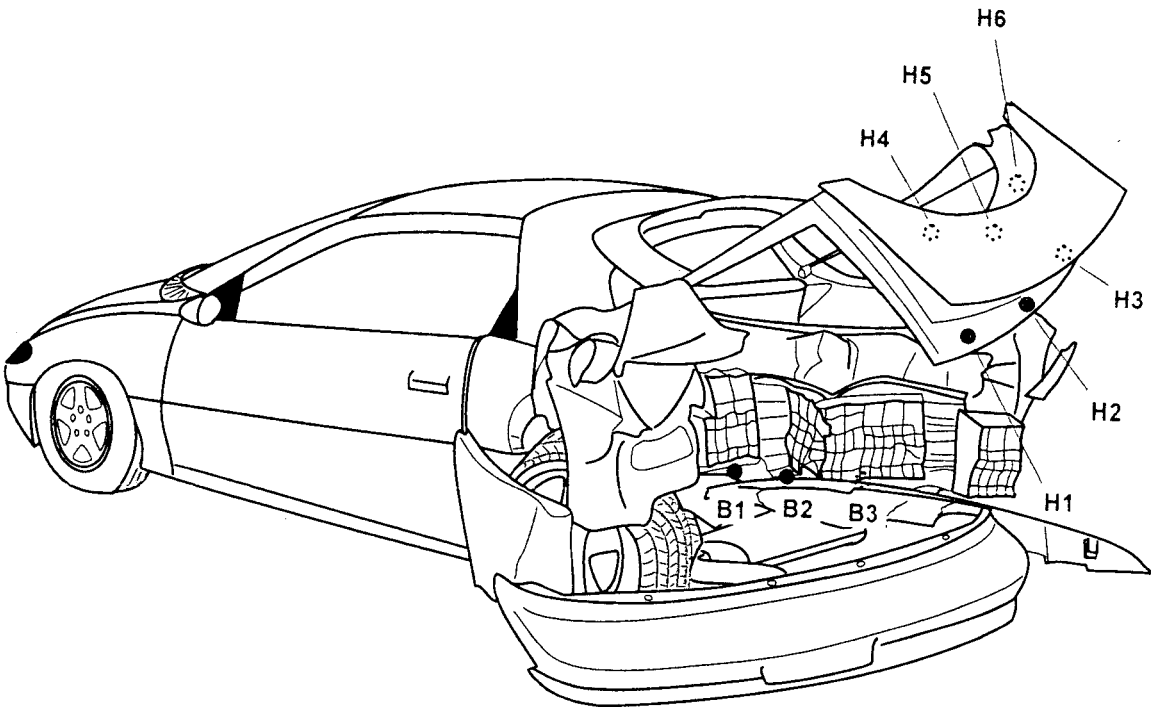

Figure C8. Fire Test F071001. Diagram showing the approximate locations of thermocouples on the rear bumper energy absorber and the rear liftgate of the test vehicle. Thermocouples B1, B2, and B3 were located below the lower surface of the rear bumper energy absorber. Thermocouples H1, H2, and H3 were located on the lower outside edge of the rear liftglass outer panel. Thermocouples H4, H5, and H6 were located inside surface of the rear liftglass inner panel. The filled circles indicate that the thermocouples were visible in this view of the test vehicle. The unfilled, dashed circles indicate that the thermocouples were hidden from view.

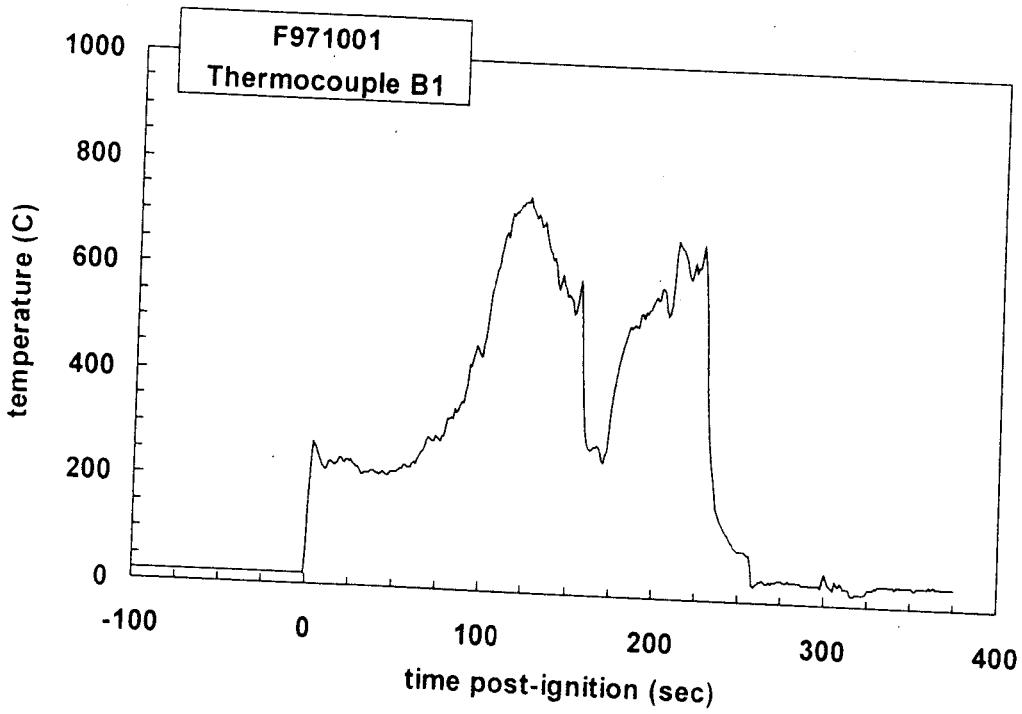

Plot C1. Fire Test F971001. Data plot from thermocouple B1.

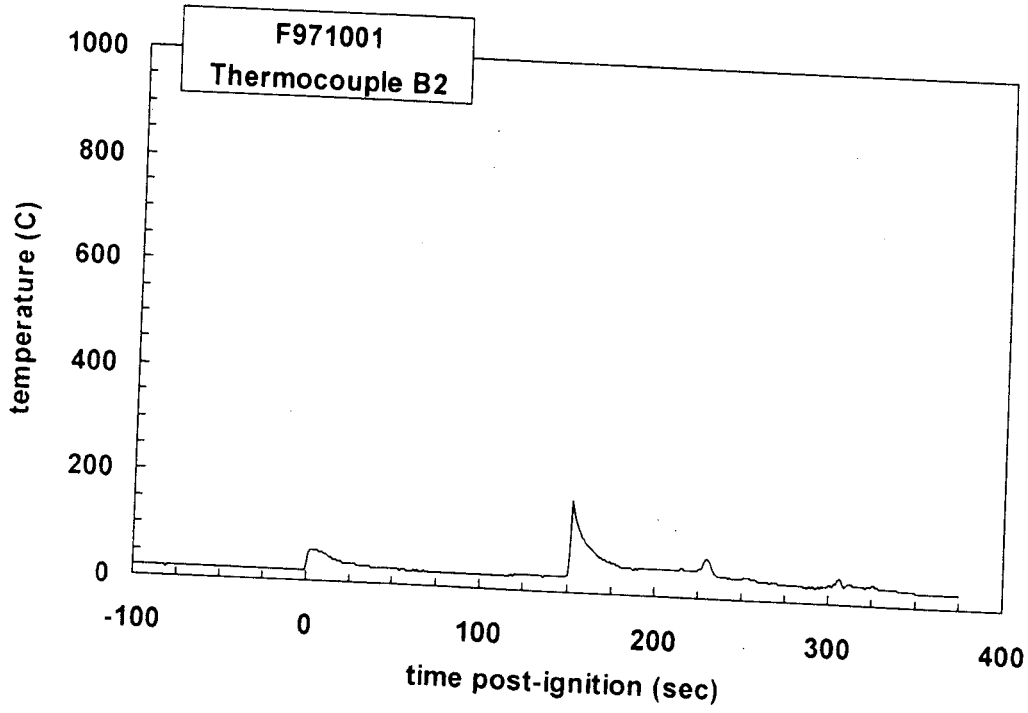

Plot C2. Fire Test F971001. Data plot from thermocouple B2.

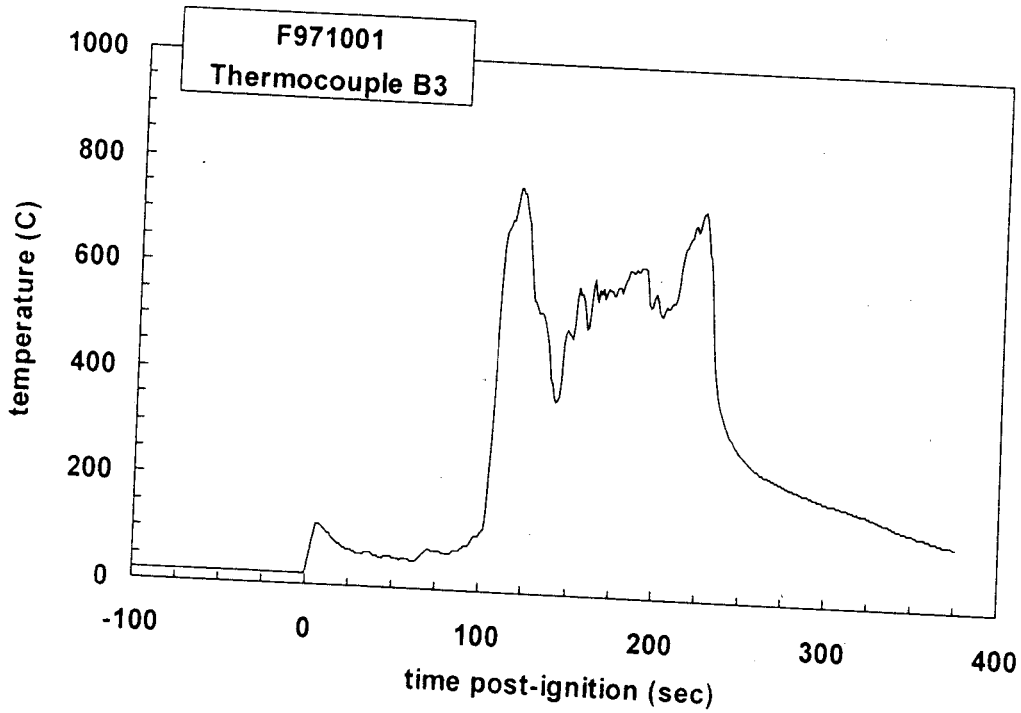

Plot C3. Fire Test F971001. Data plot from thermocouple B3.

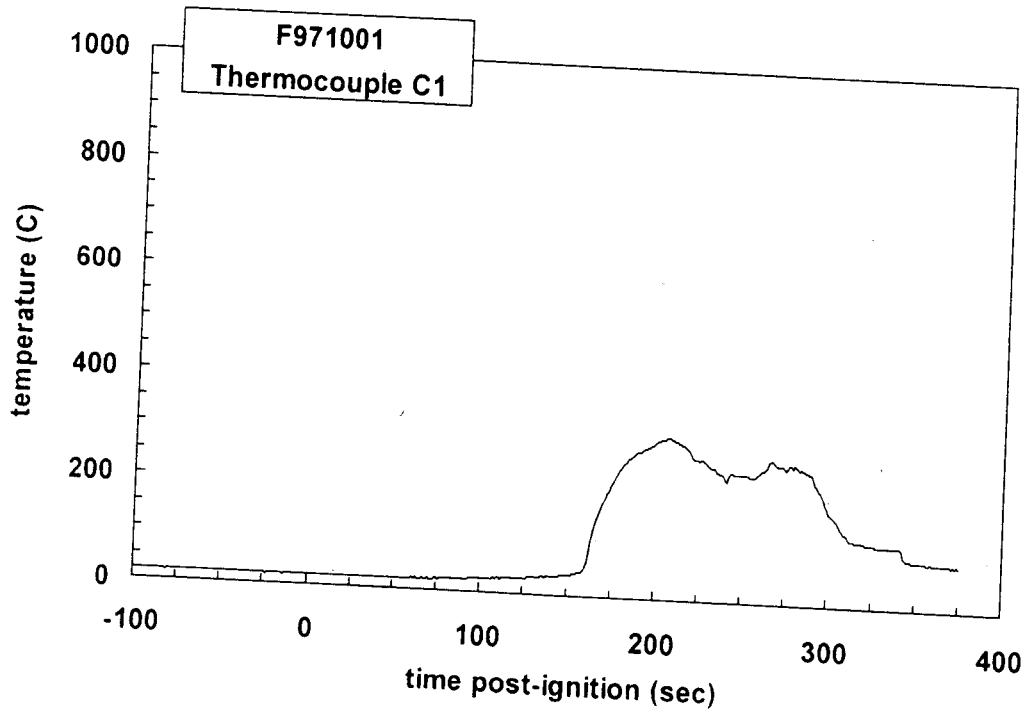

Plot C4. Fire Test F971001. Data plot from thermocouple C1.

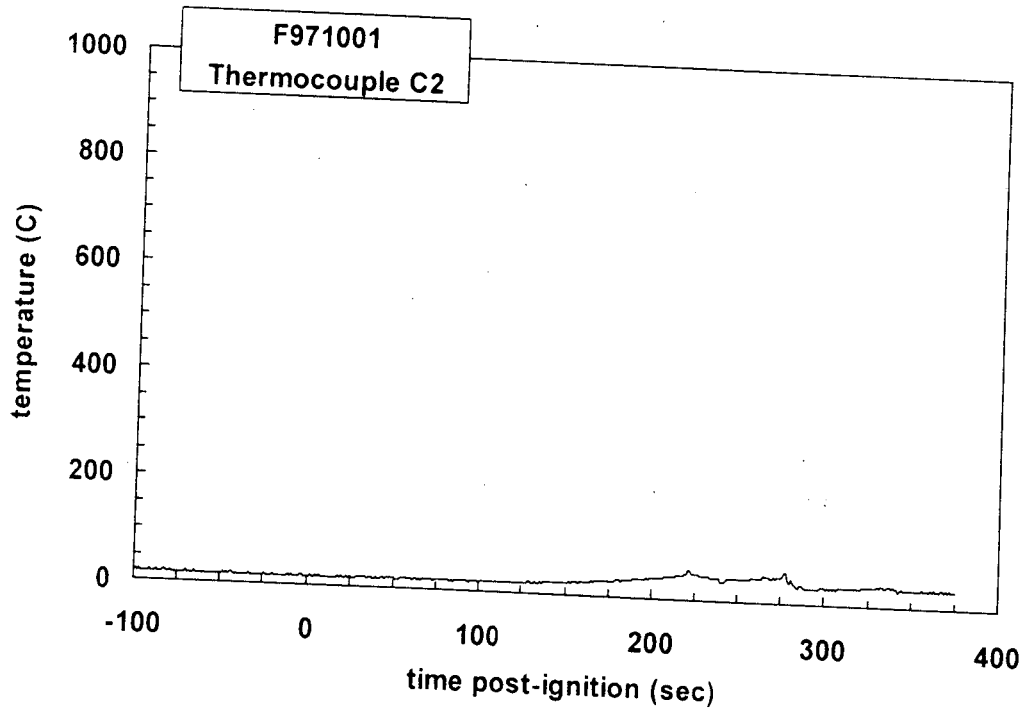

Plot C5. Fire Test F971001. Data plot from thermocouple C2.

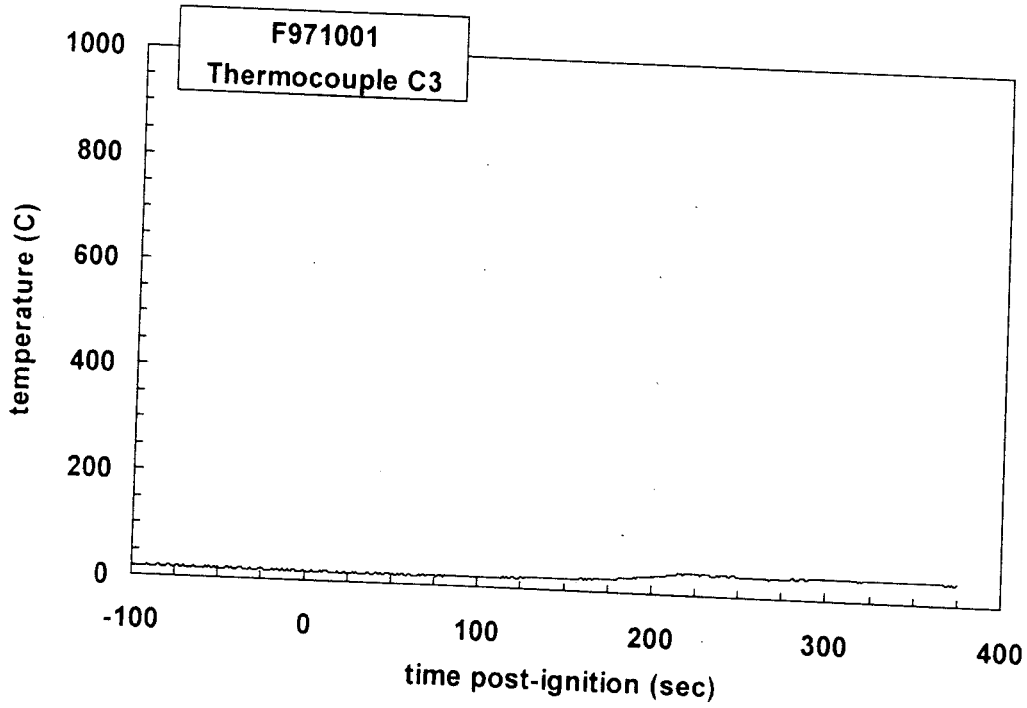

Plot C6. Fire Test F971001. Data plot from thermocouple C3.

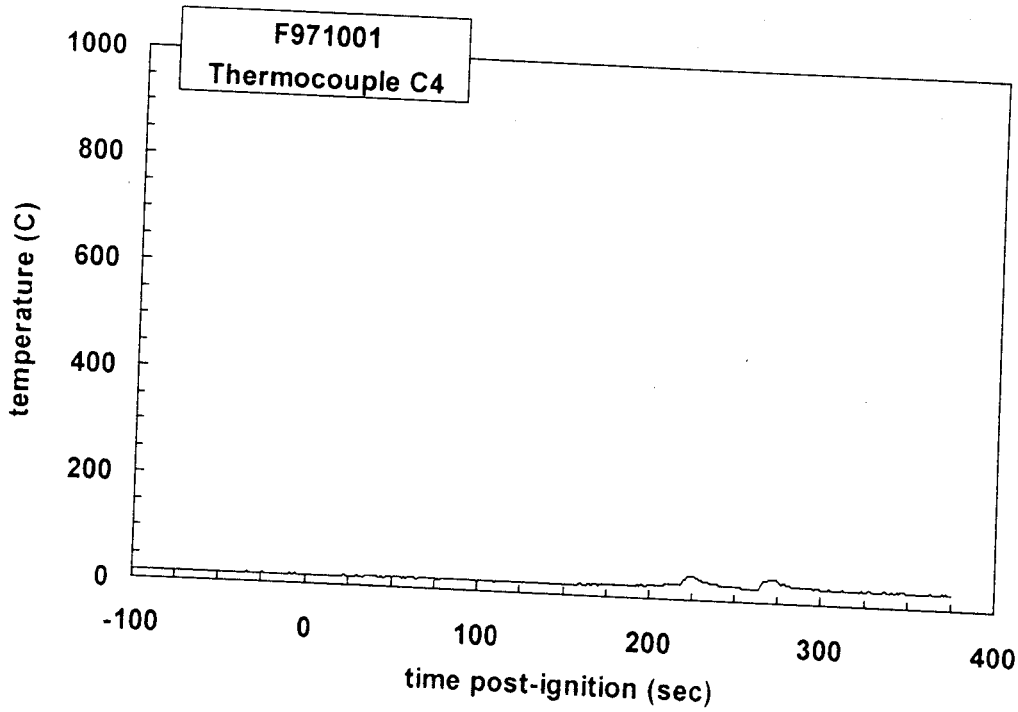

Plot C7. Fire Test F971001. Data plot from thermocouple C4.

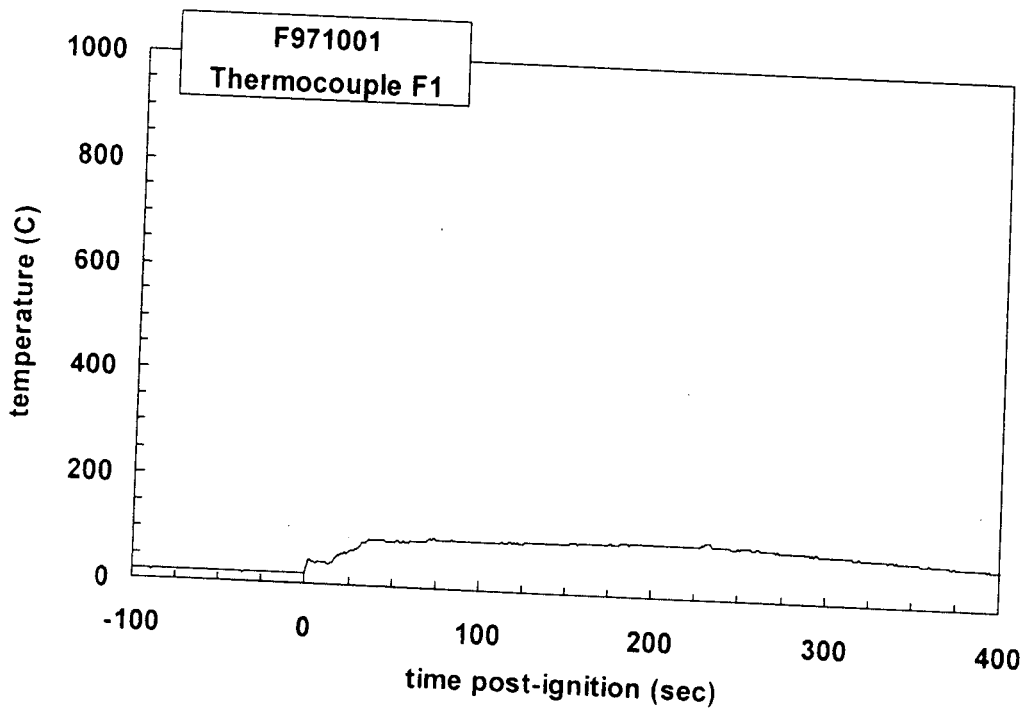

Plot C8. Fire Test F971001. Data plot from thermocouple F1.

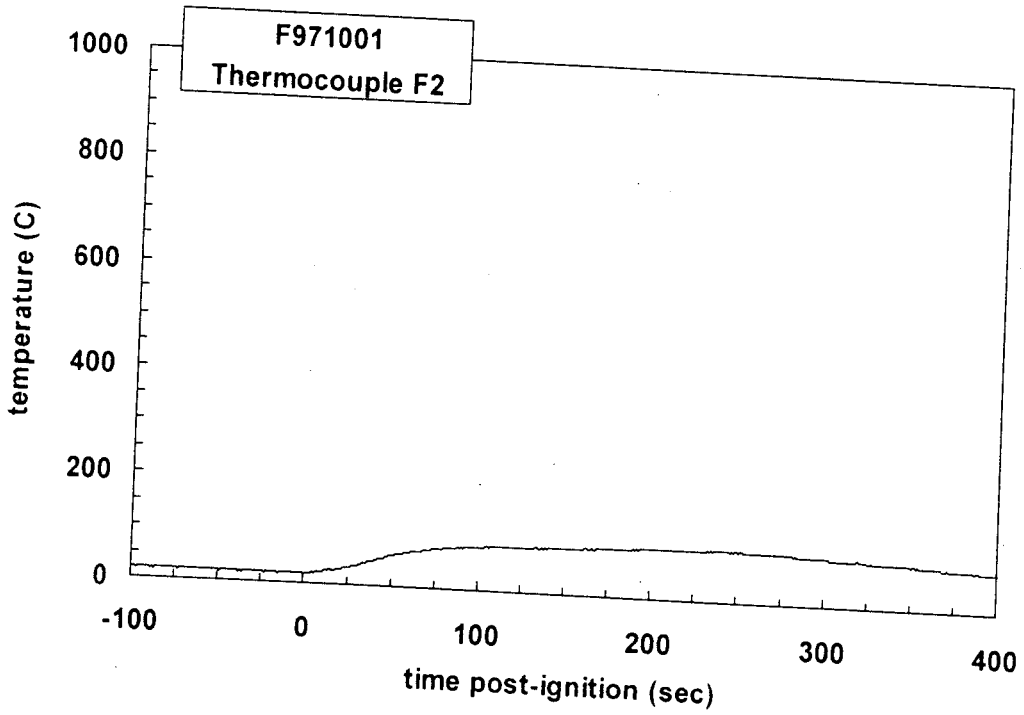

Plot C9. Fire Test F971001. Data plot from thermocouple F2.

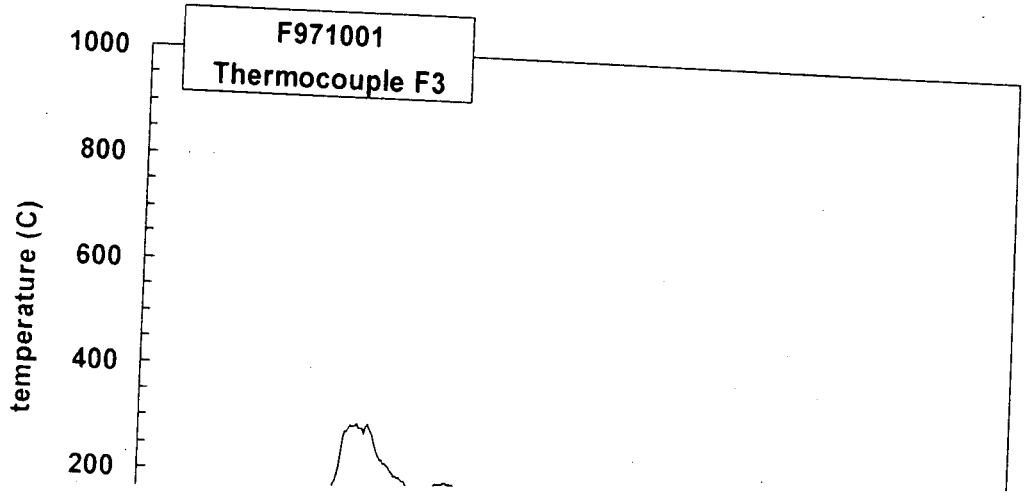

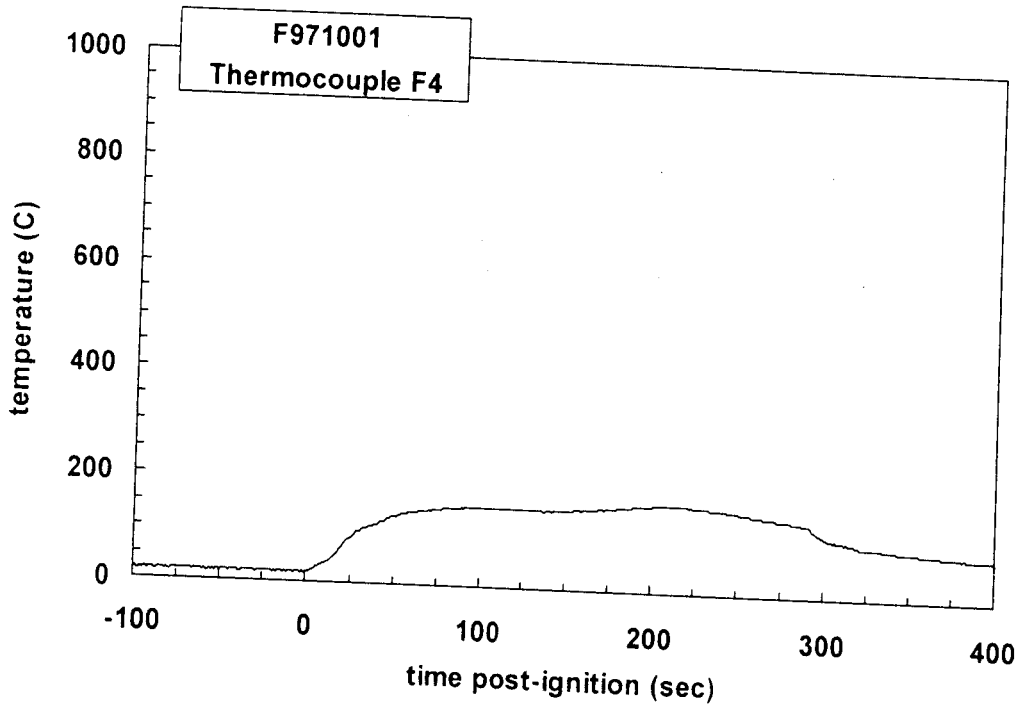

Plot C11. Fire Test F971001. Data plot from thermocouple F4.

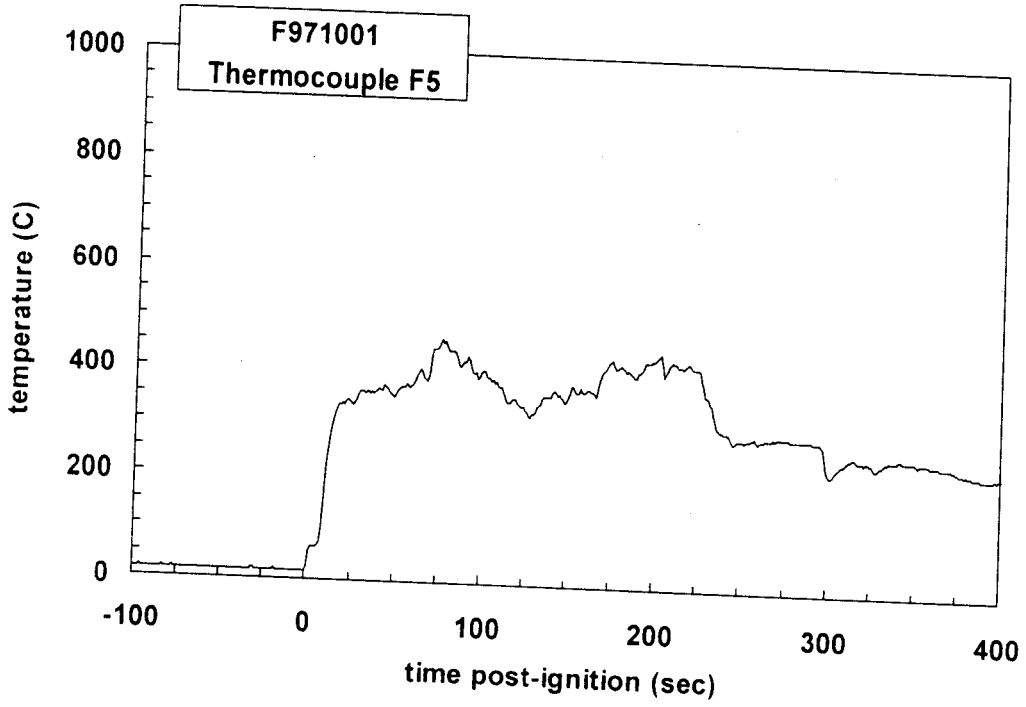

Plot C12. Fire Test F971001. Data plot from thermocouple F5.

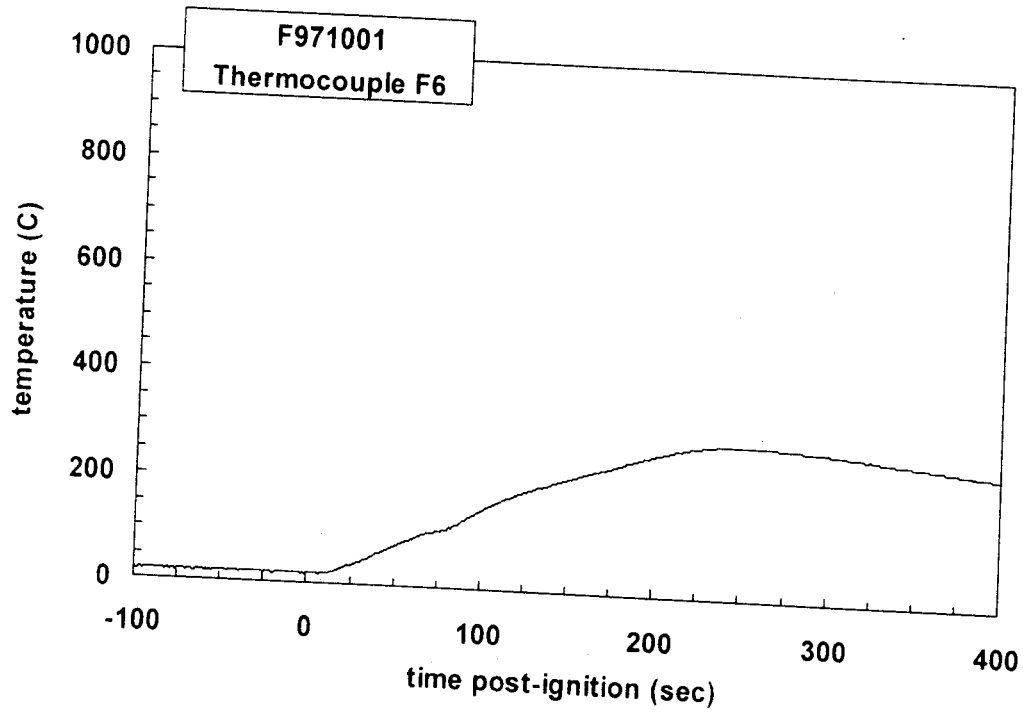

Plot C13. Fire Test F971001. Data plot from thermocouple F6.

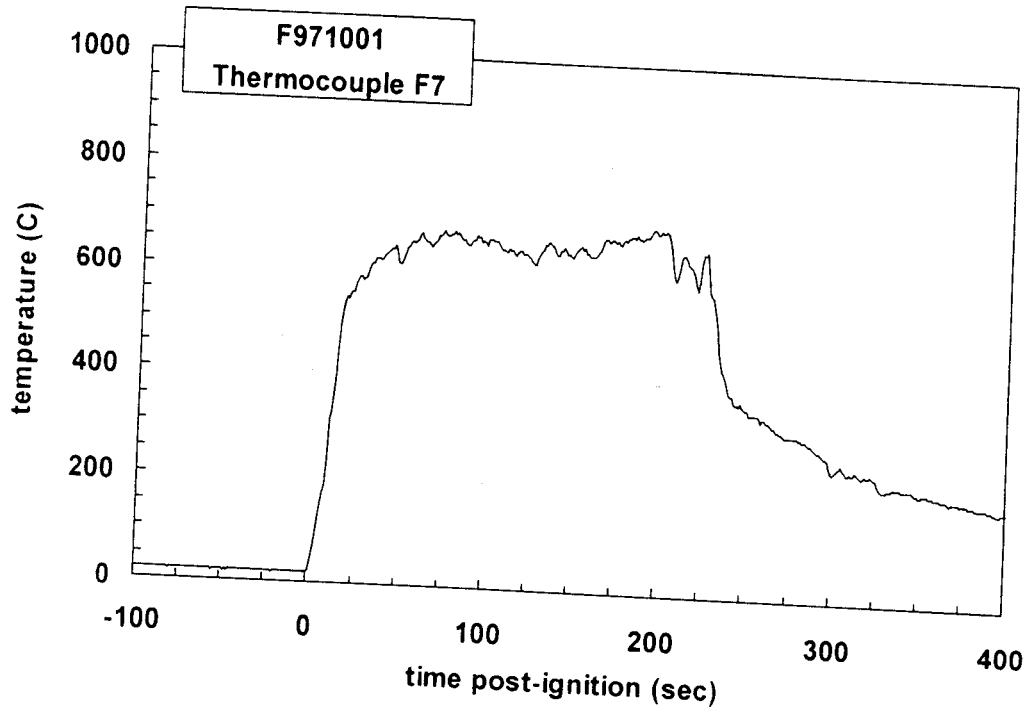

Plot C14. Fire Test F971001. Data plot from thermocouple F7.

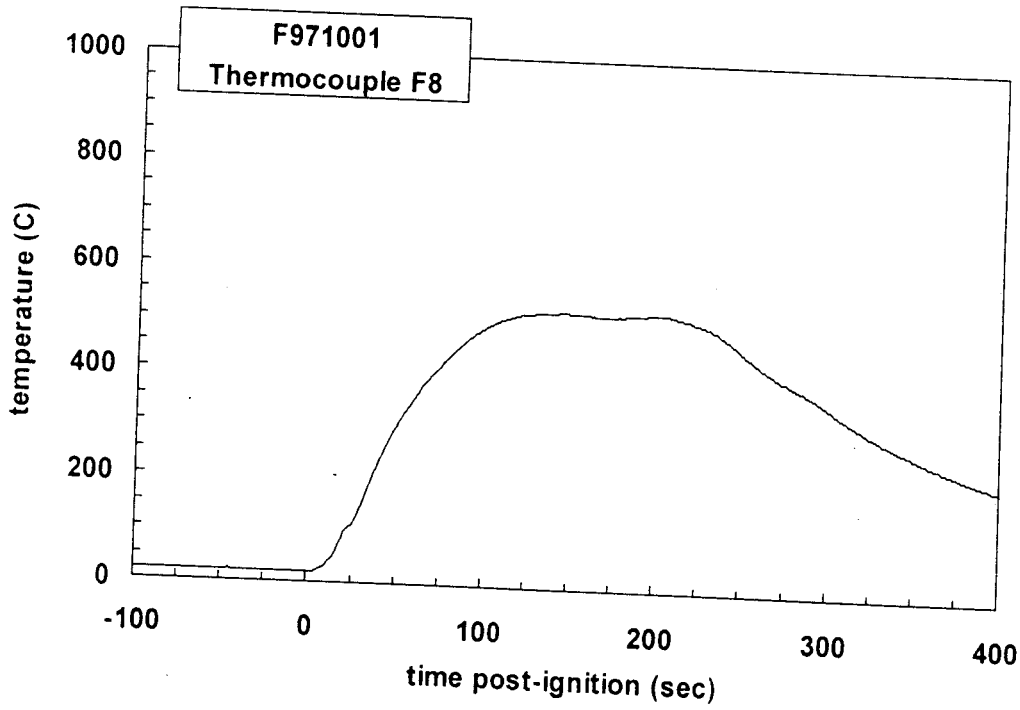

Plot C15. Fire Test F971001. Data plot from thermocouple F8.

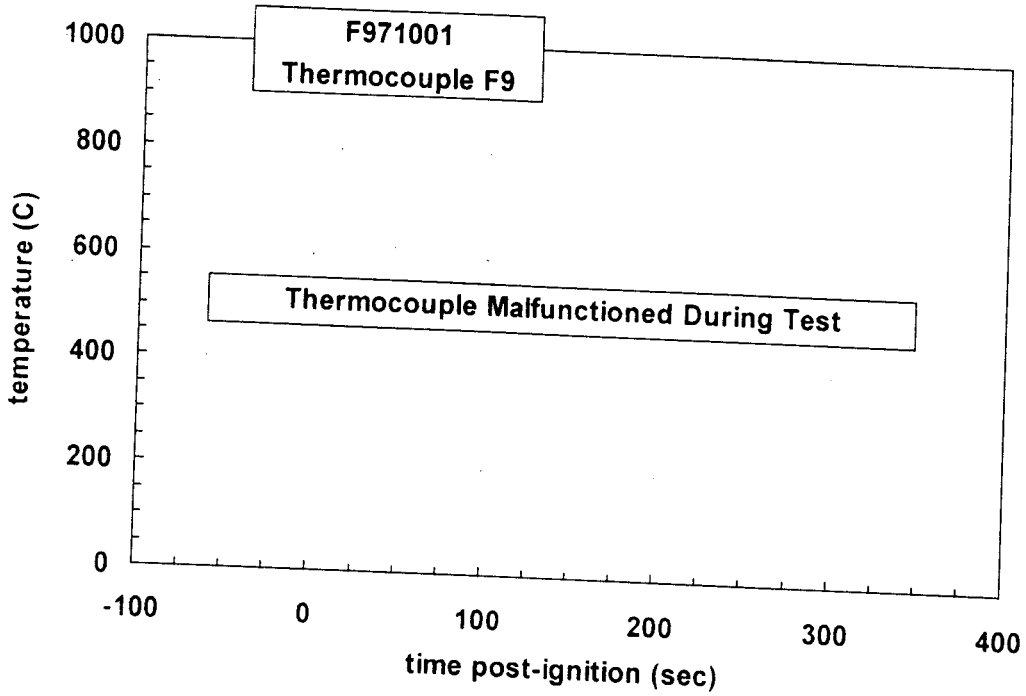

Plot C16. Fire Test F971001. Data plot from thermocouple F9.

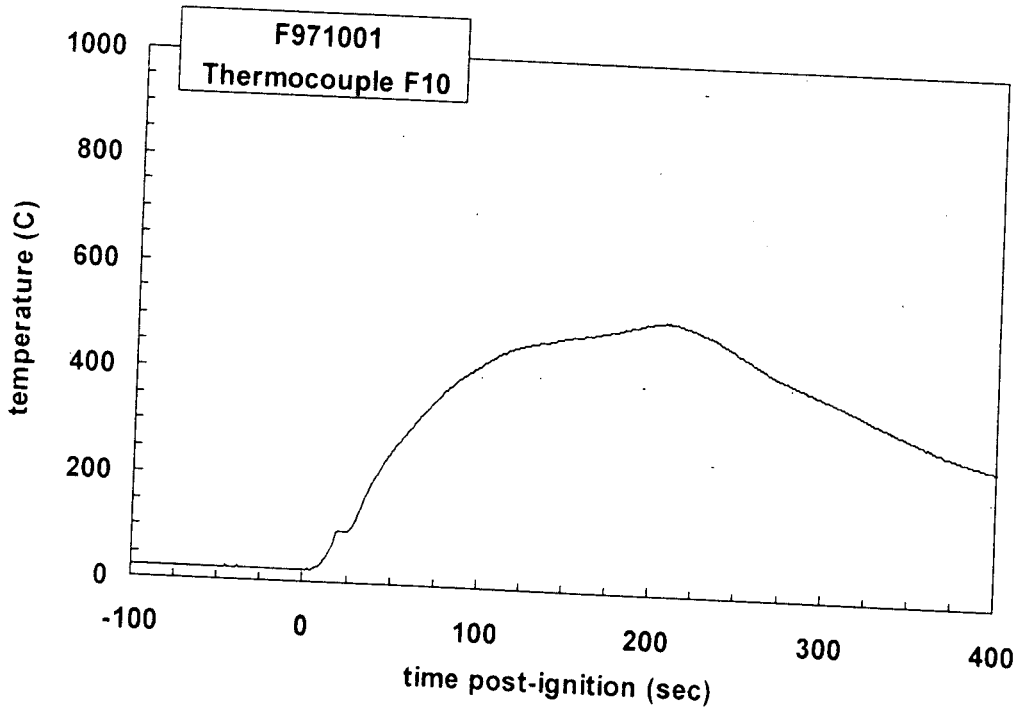

Plot C17. Fire Test F971001. Data plot from thermocouple F10.

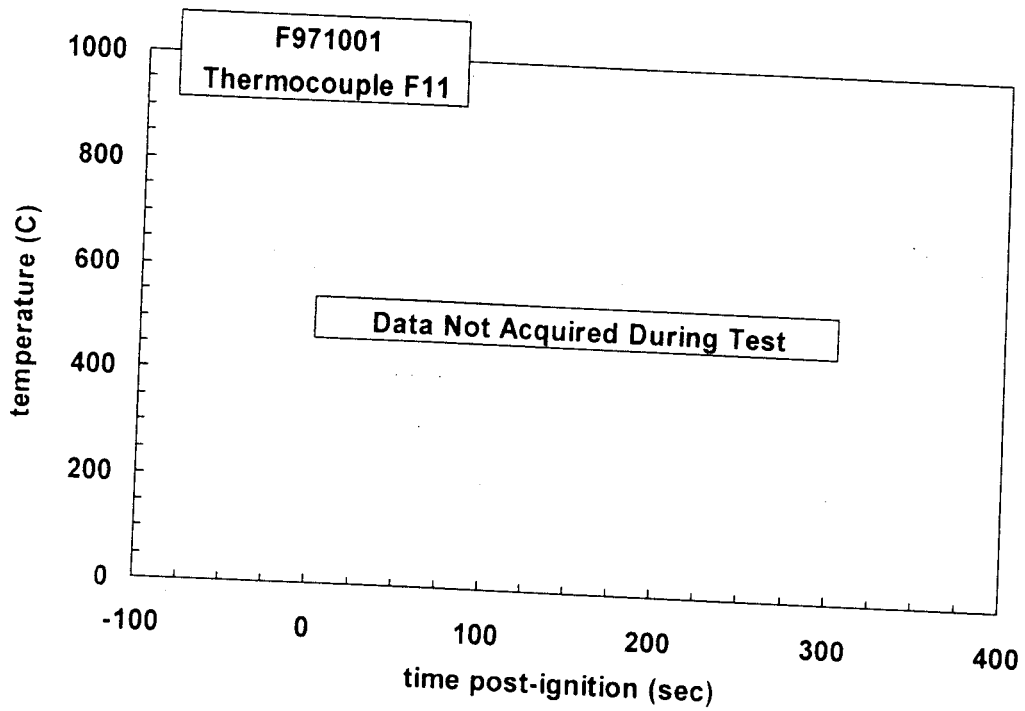

Plot C18. Fire Test F971001. Data plot from thermocouple F11.

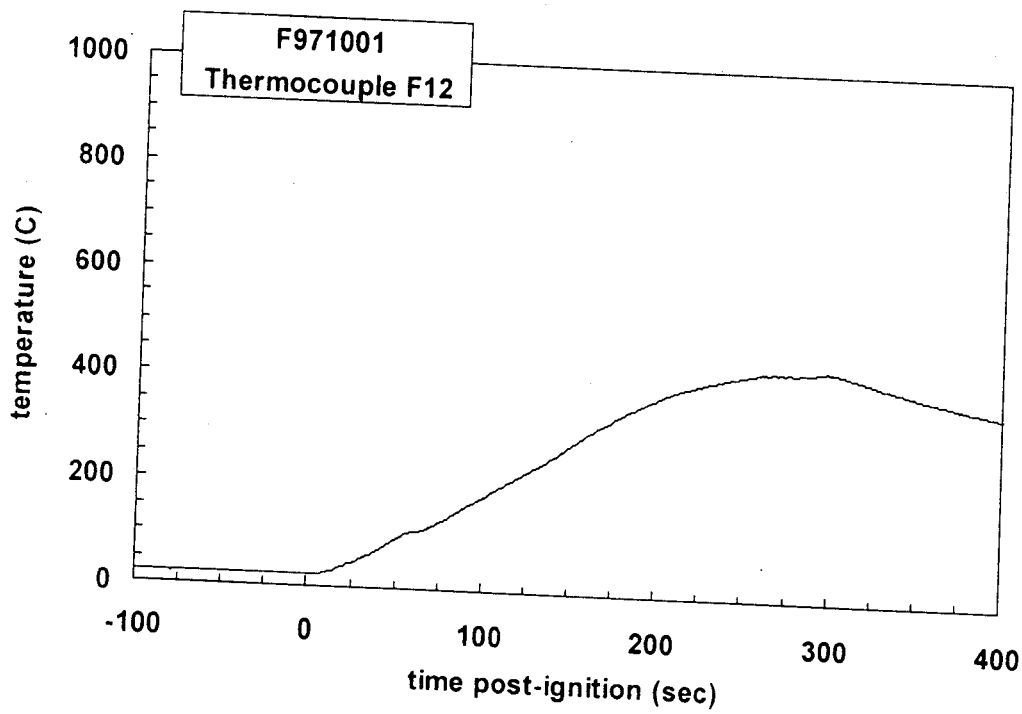

Plot C19. Fire Test F971001. Data plot from thermocouple F12.

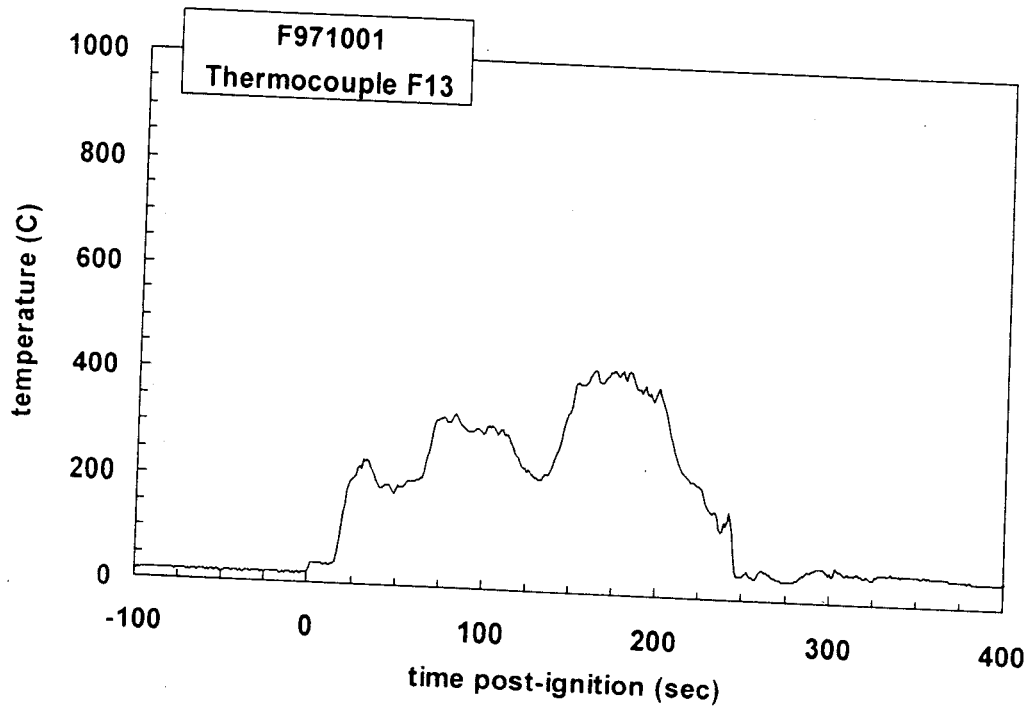

Plot C20. Fire Test F971001. Data plot from thermocouple F13.

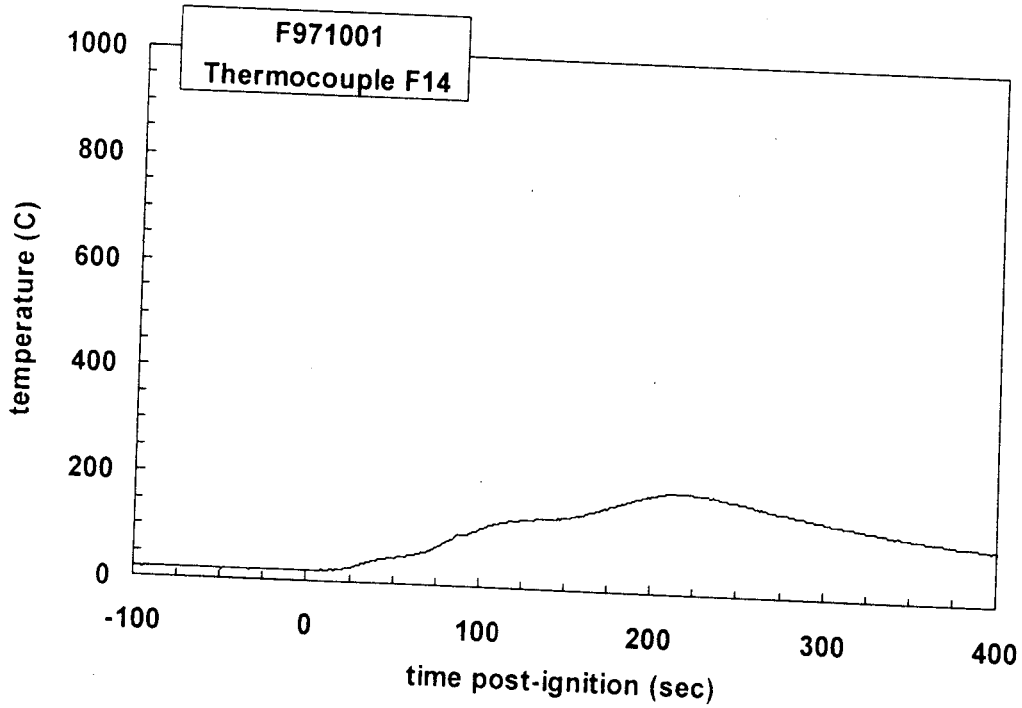

Plot C21. Fire Test F971001. Data plot from thermocouple F14.

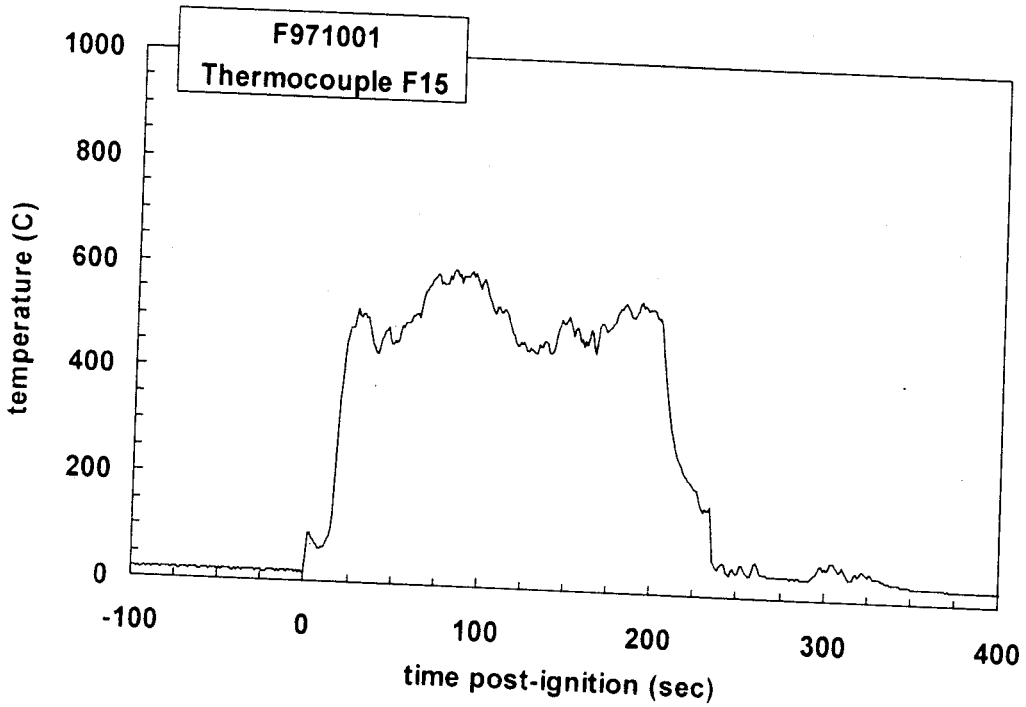

Plot C22. Fire Test F971001. Data plot from thermocouple F15.

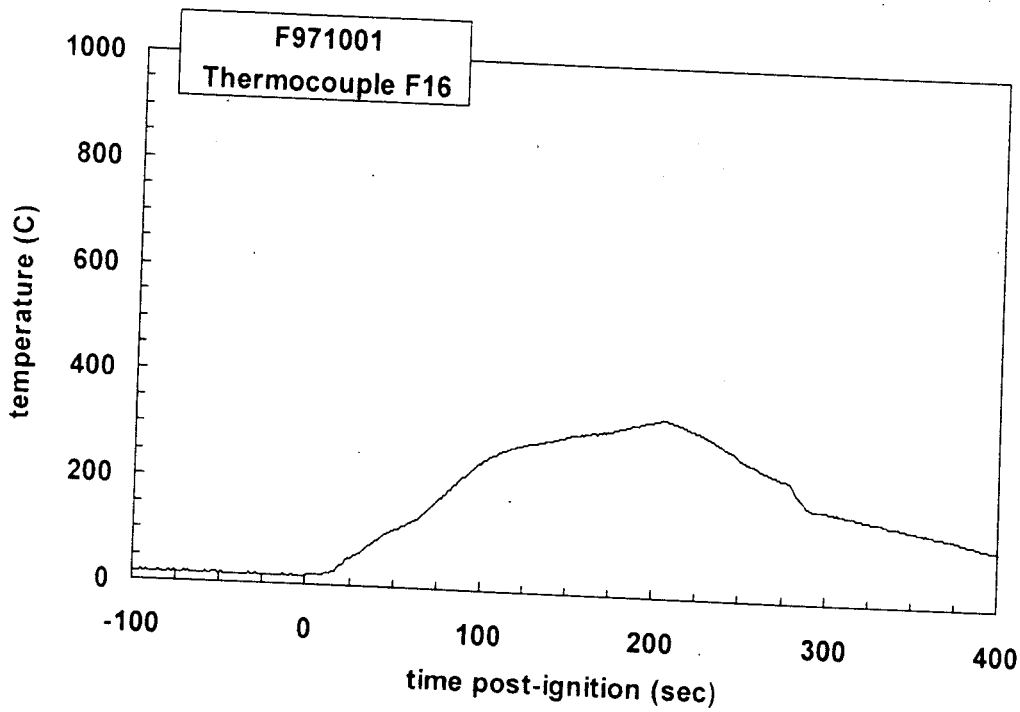

Plot C23. Fire Test F971001. Data plot from thermocouple F16.

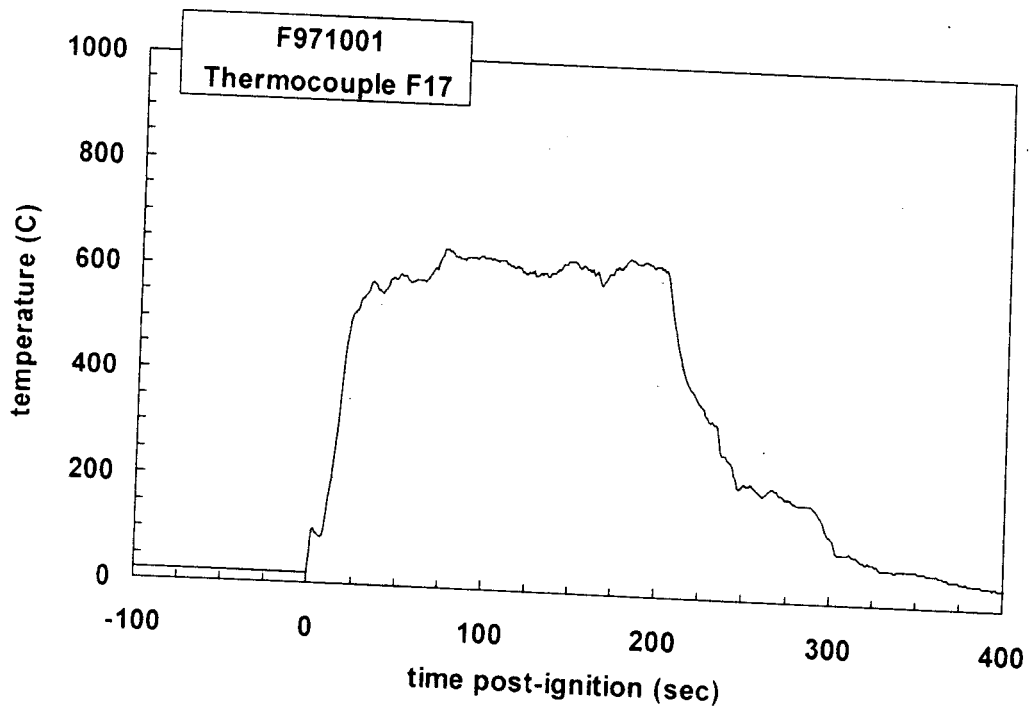

Plot C24. Fire Test F971001. Data plot from thermocouple F17.

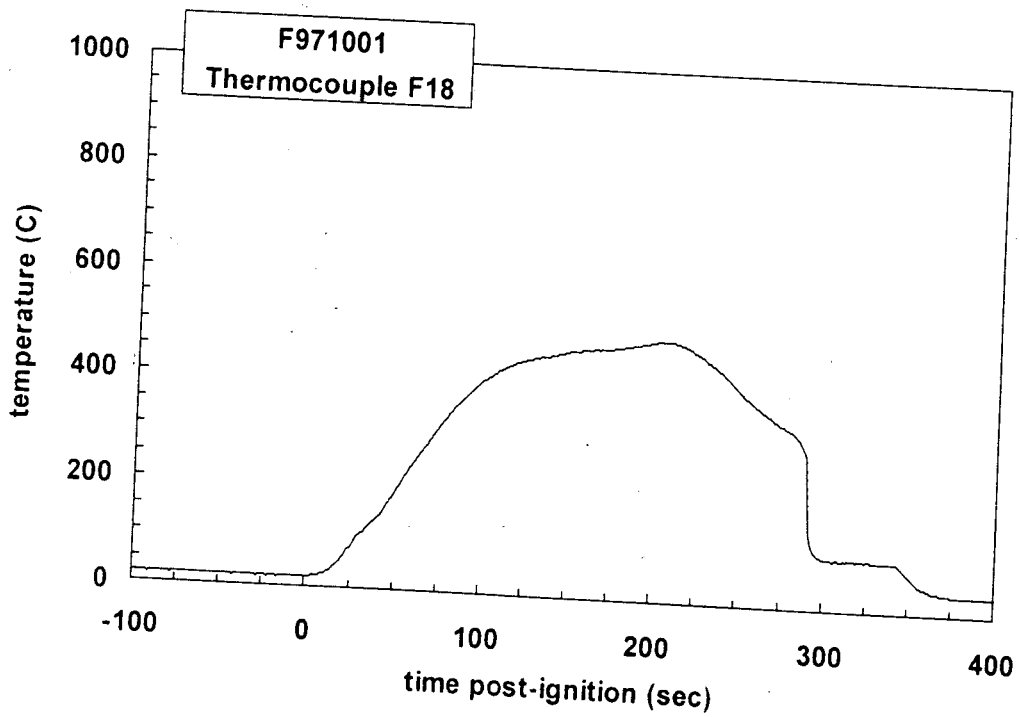

Plot C25. Fire Test F971001. Data plot from thermocouple F18.

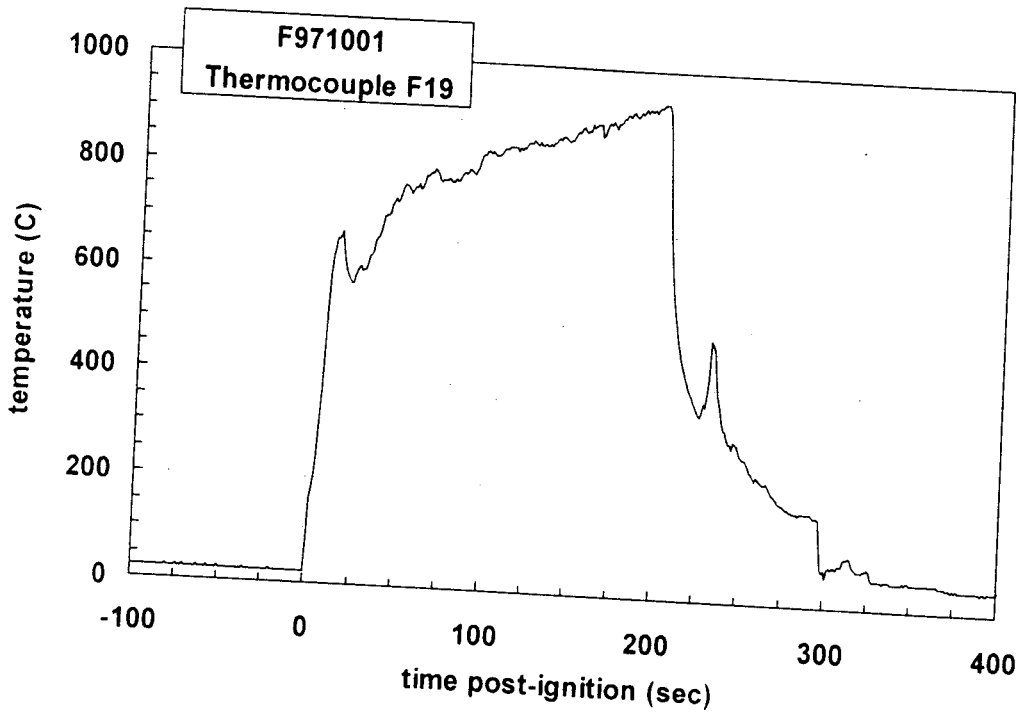

Plot C26. Fire Test F971001. Data plot from thermocouple F19.

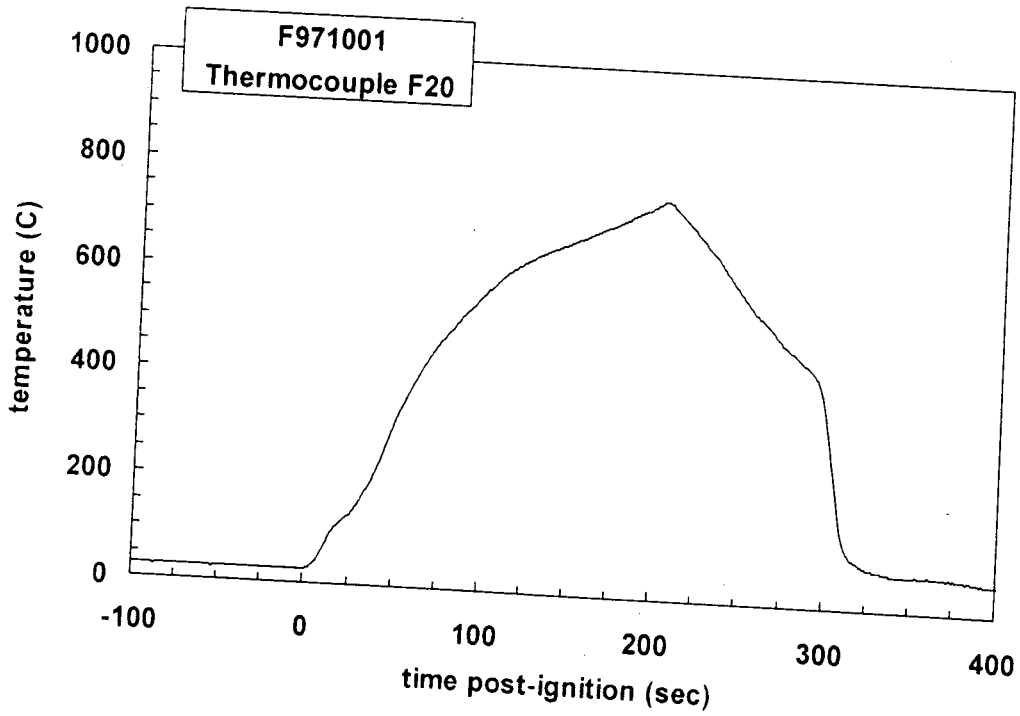

Plot C27. Fire Test F971001. Data plot from thermocouple F20.

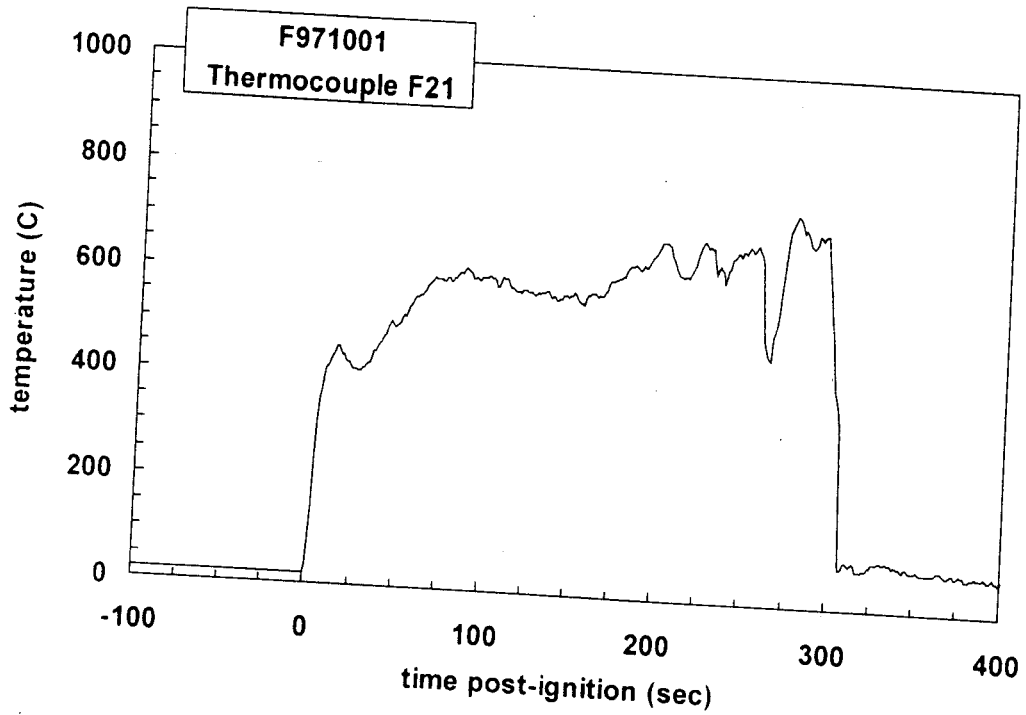

Plot C28. Fire Test F971001. Data plot from thermocouple F21.

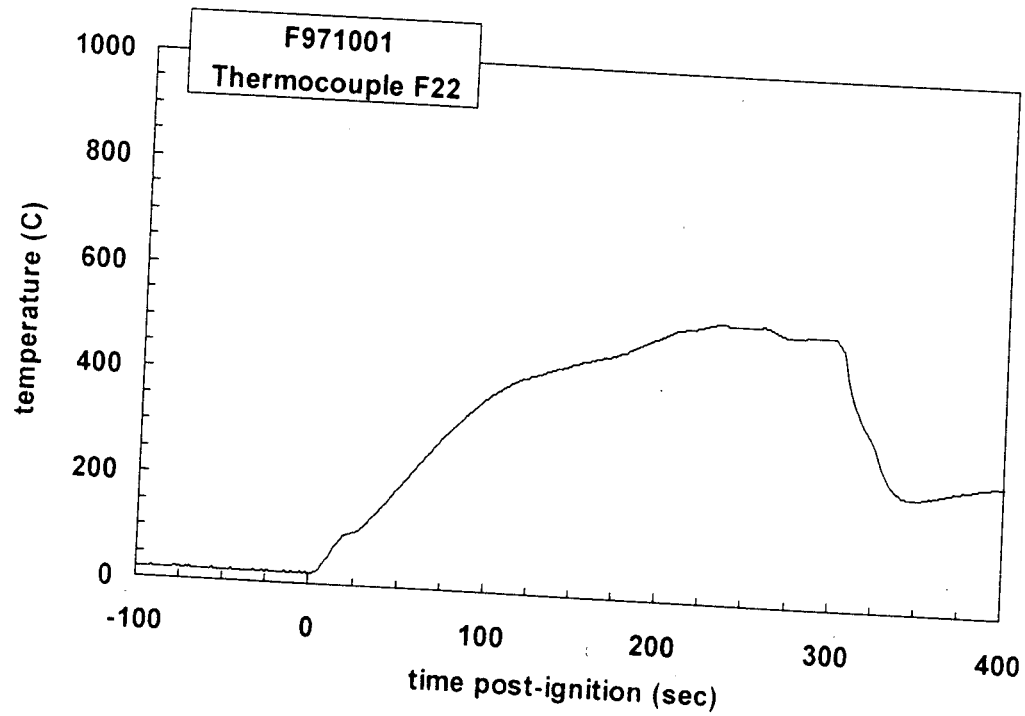

Plot C29. Fire Test F971001. Data plot from thermocouple F22.

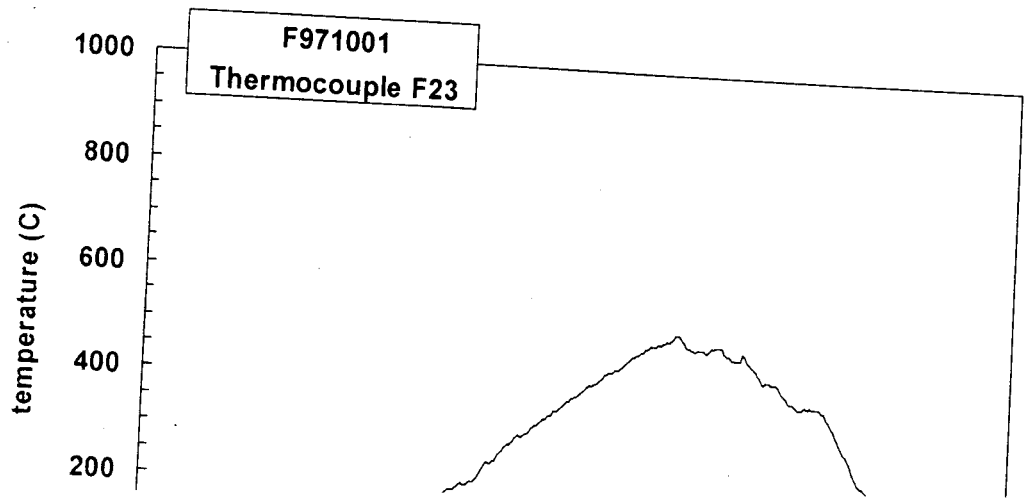

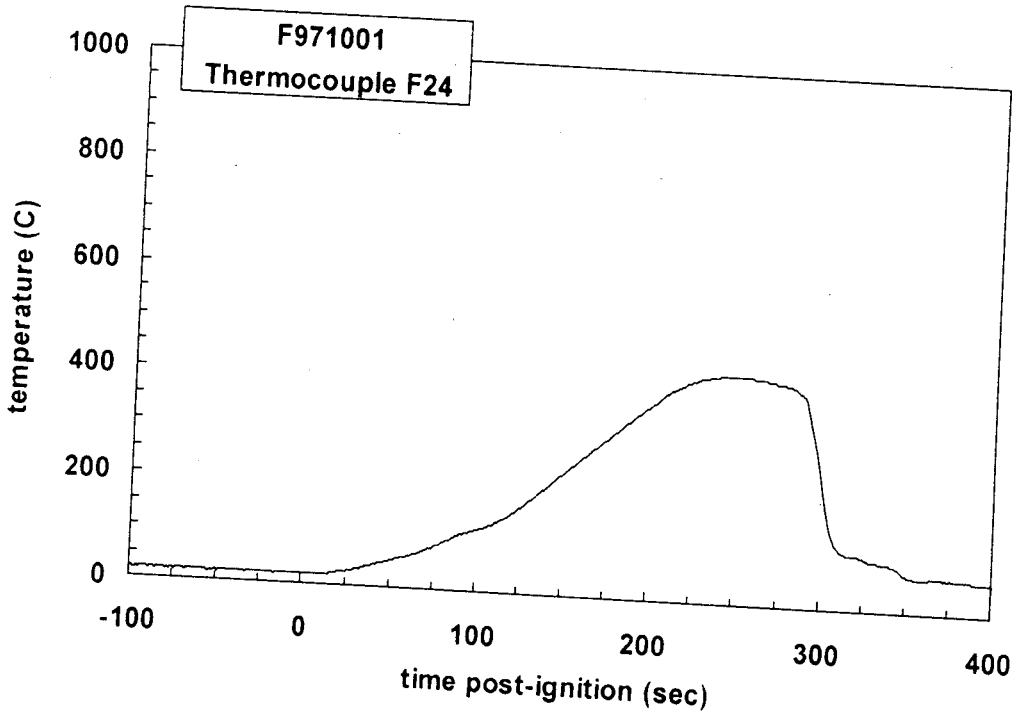

Plot C31. Fire Test F971001. Data plot from thermocouple F24.

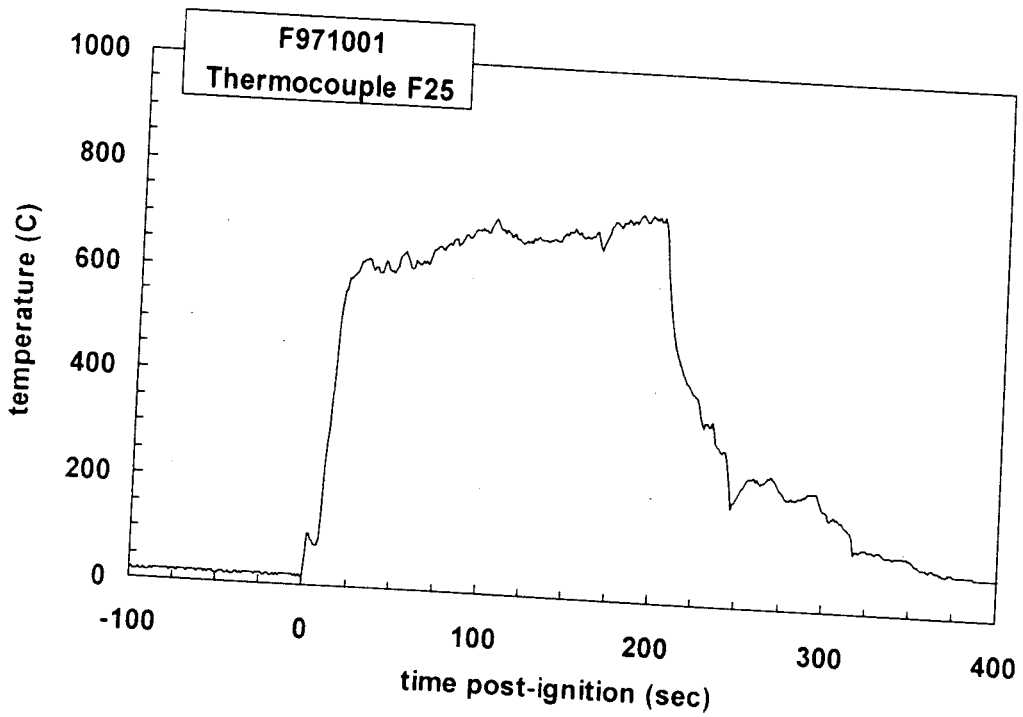

Plot C32. Fire Test F971001. Data plot from thermocouple F25.

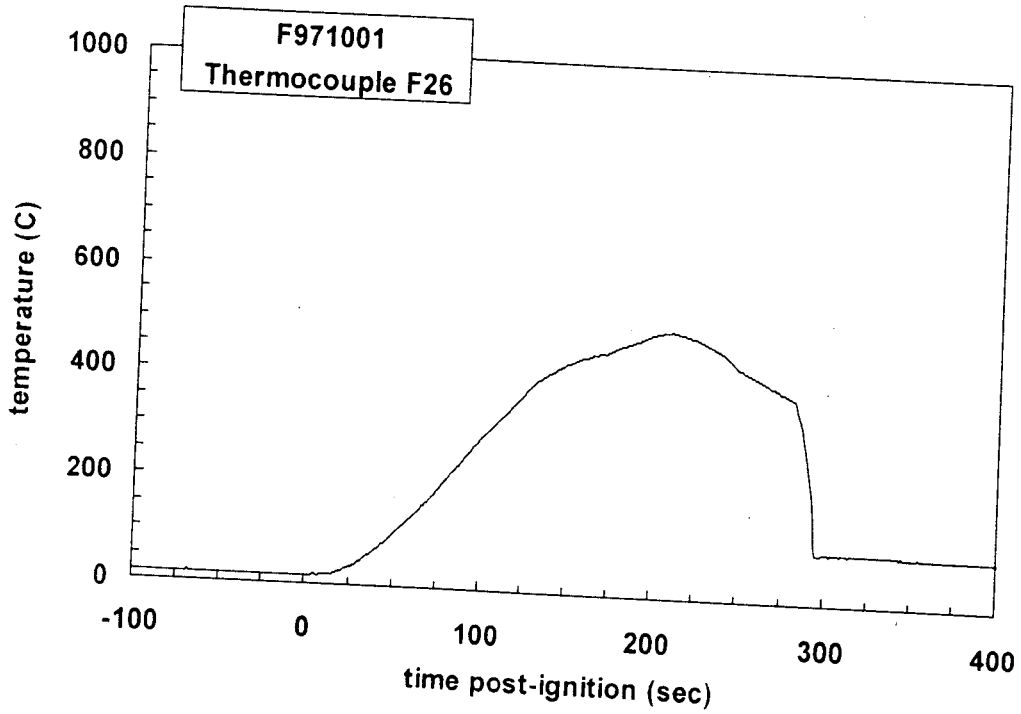

Plot C33. Fire Test F971001. Data plot from thermocouple F26.

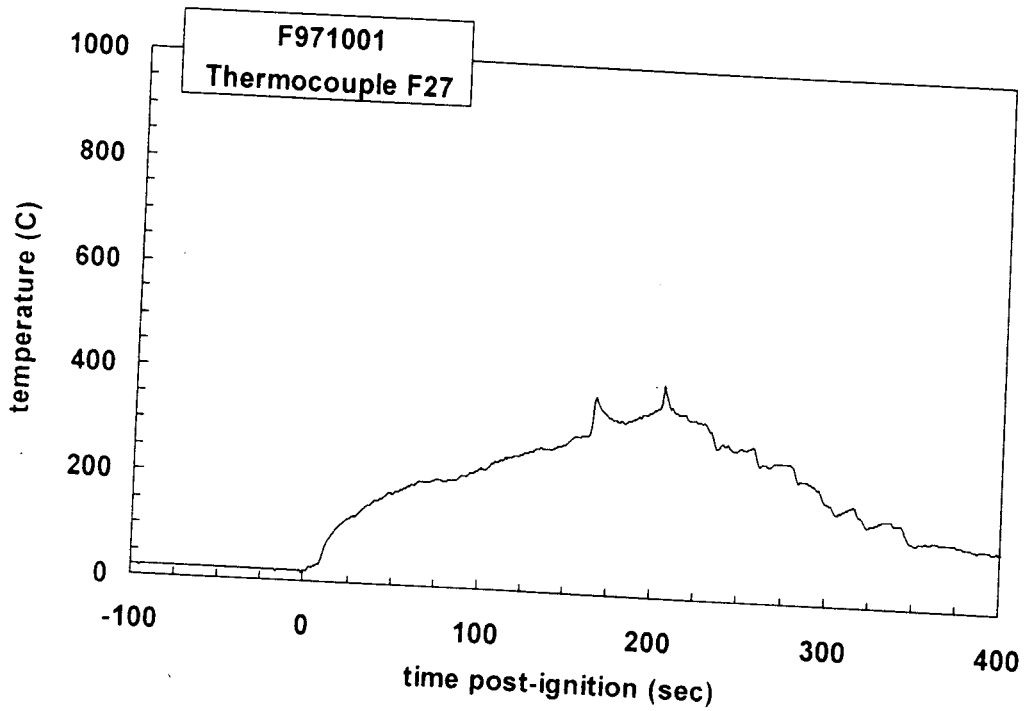

Plot C34. Fire Test F971001. Data plot from thermocouple F27.

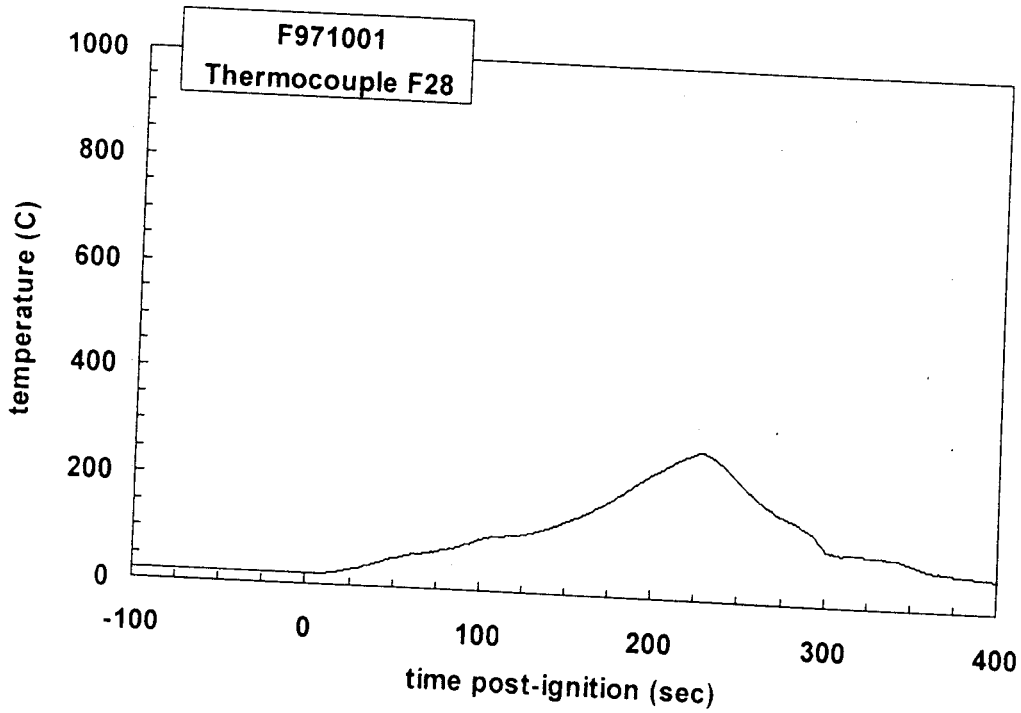

Plot C35. Fire Test F971001. Data plot from thermocouple F28.

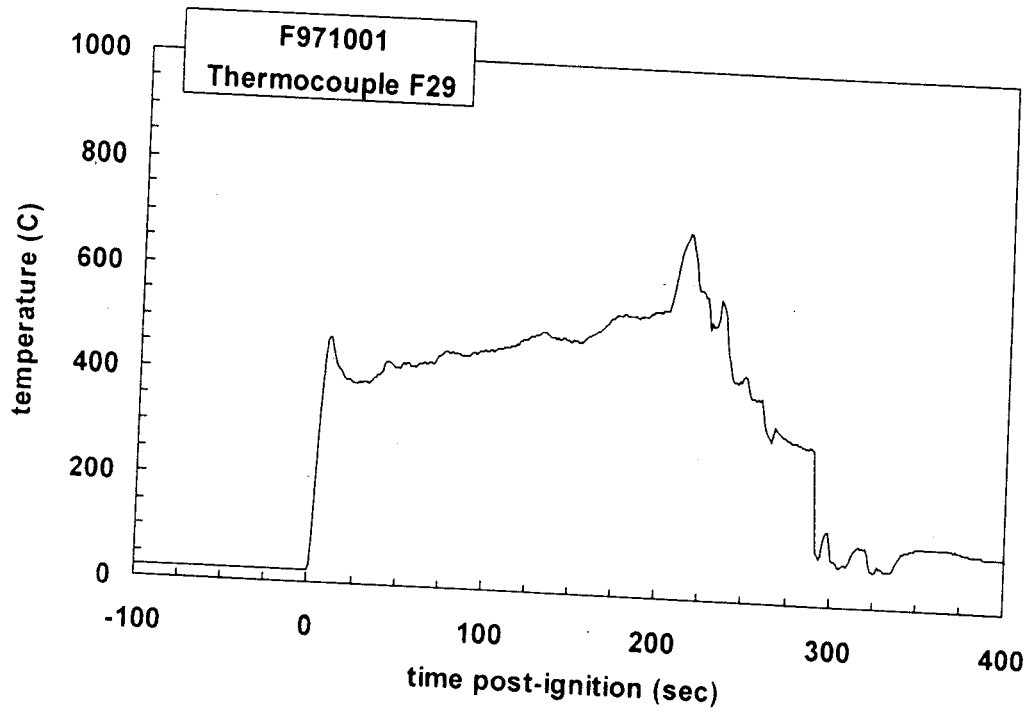

Plot C36. Fire Test F971001. Data plot from thermocouple F29.

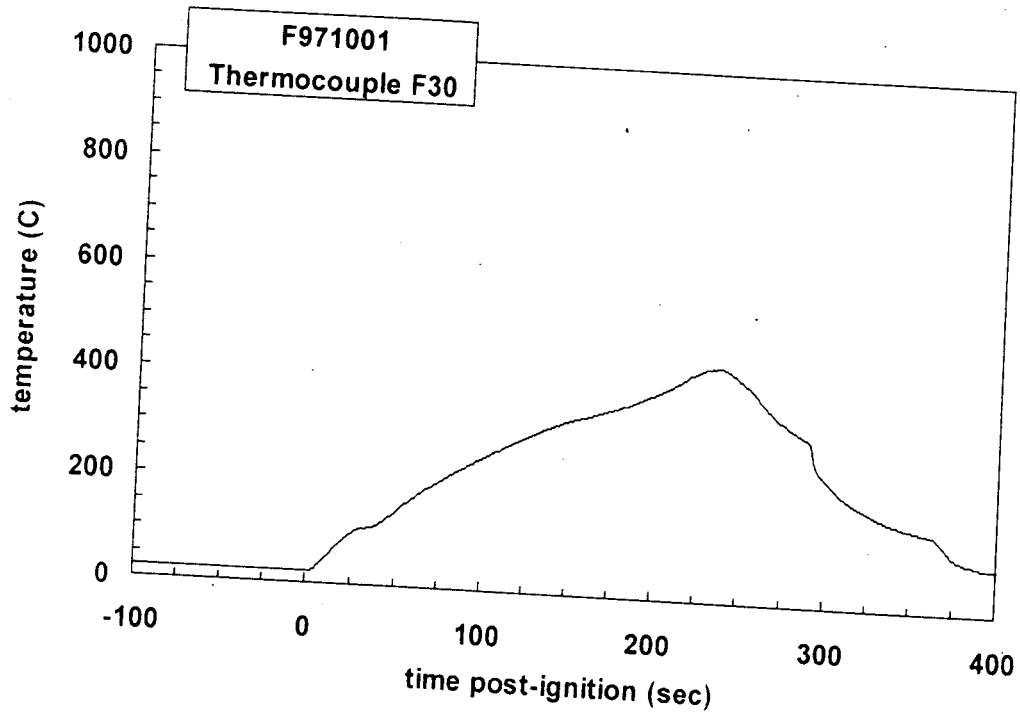

Plot C37. Fire Test F971001. Data plot from thermocouple F30.

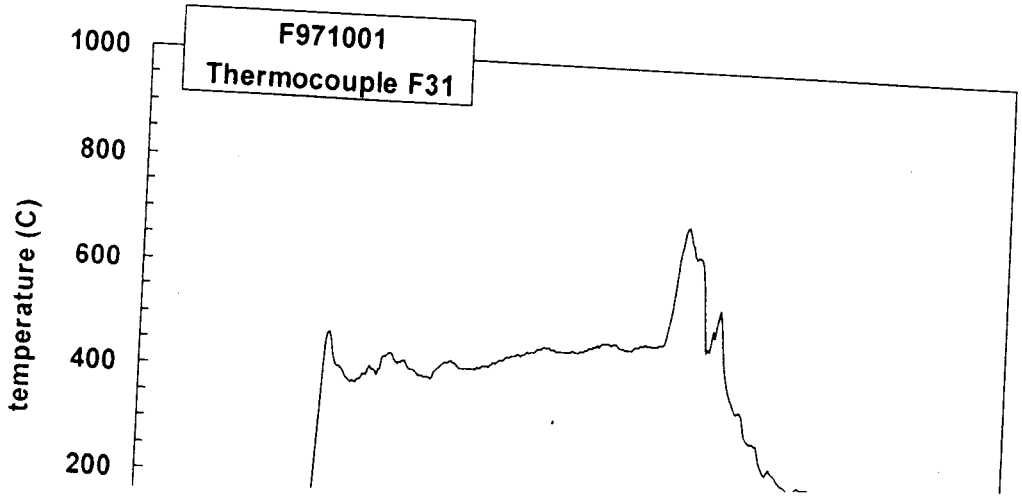

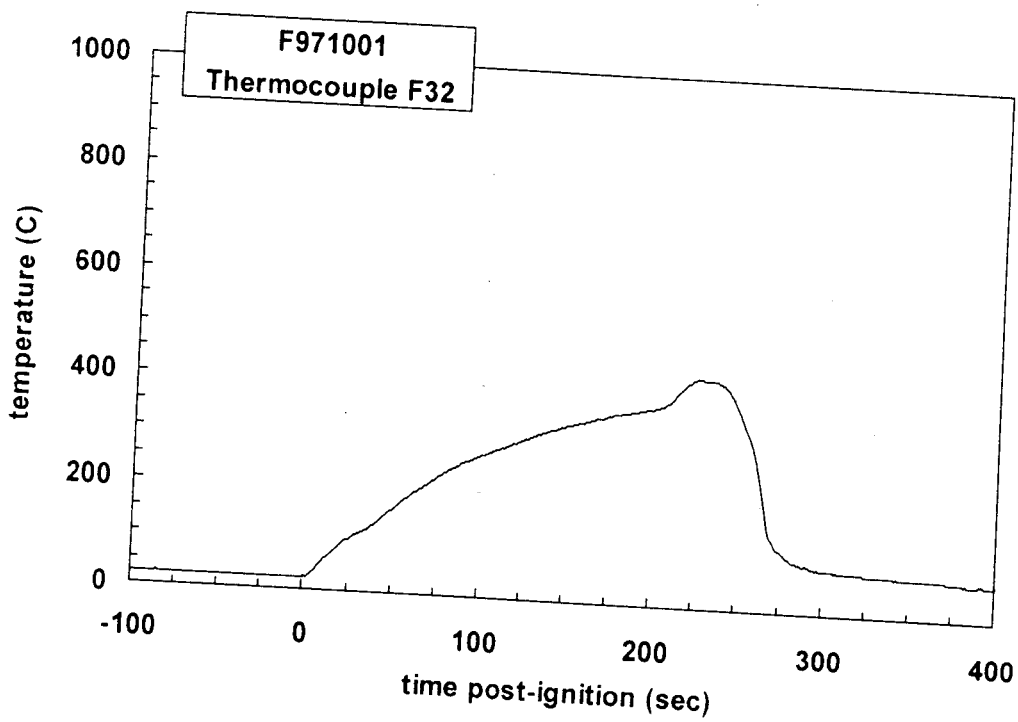

Plot C39. Fire Test F971001. Data plot from thermocouple F32.

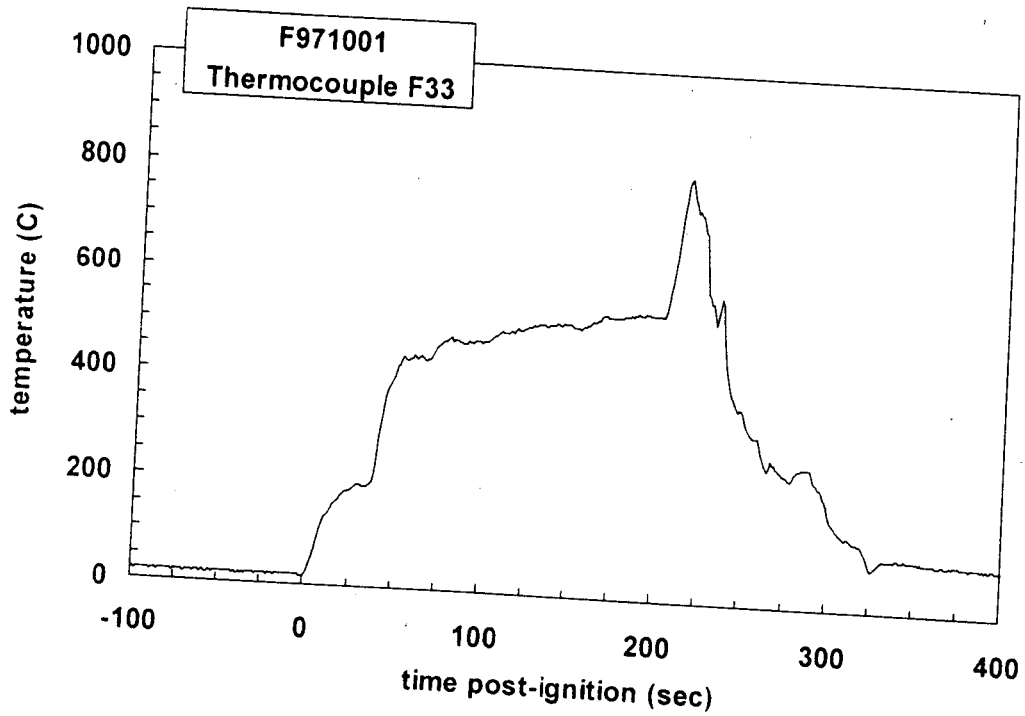

Plot C40. Fire Test F971001. Data plot from thermocouple F33.

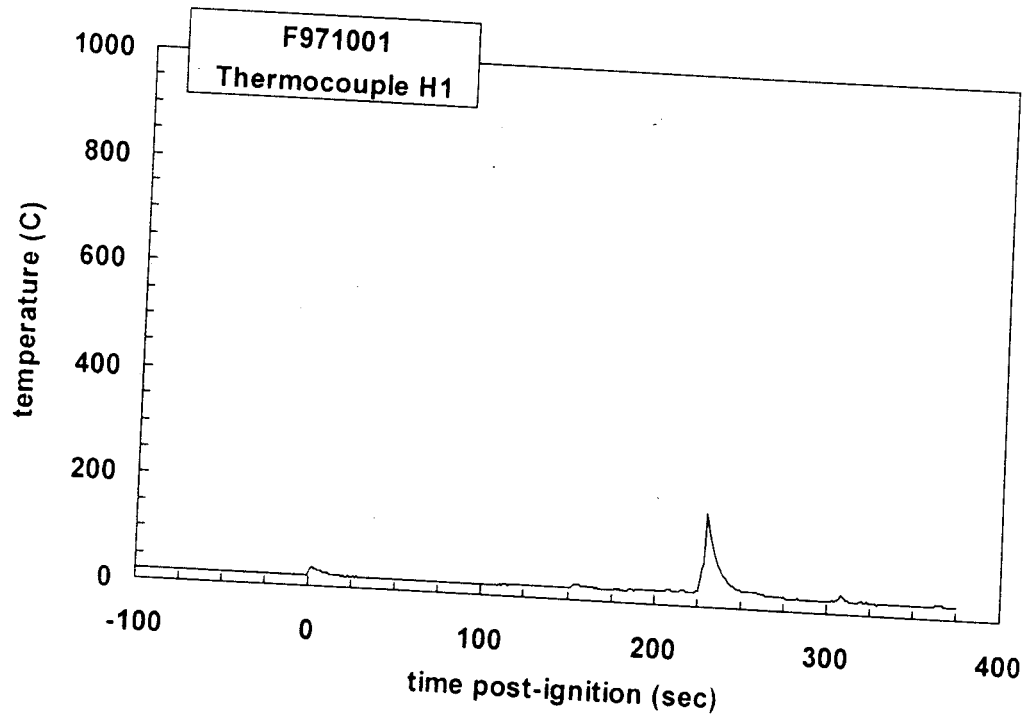

Plot C41. Fire Test F971001. Data plot from thermocouple H1.

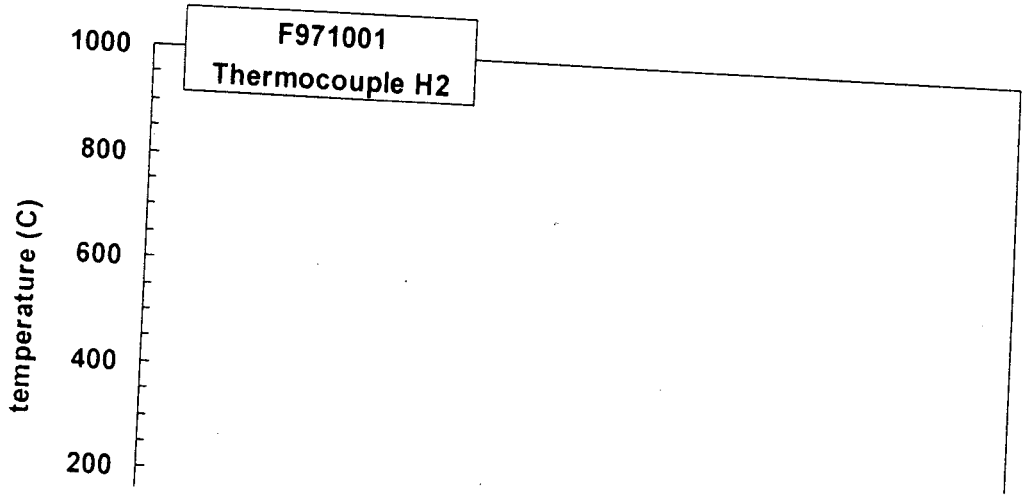

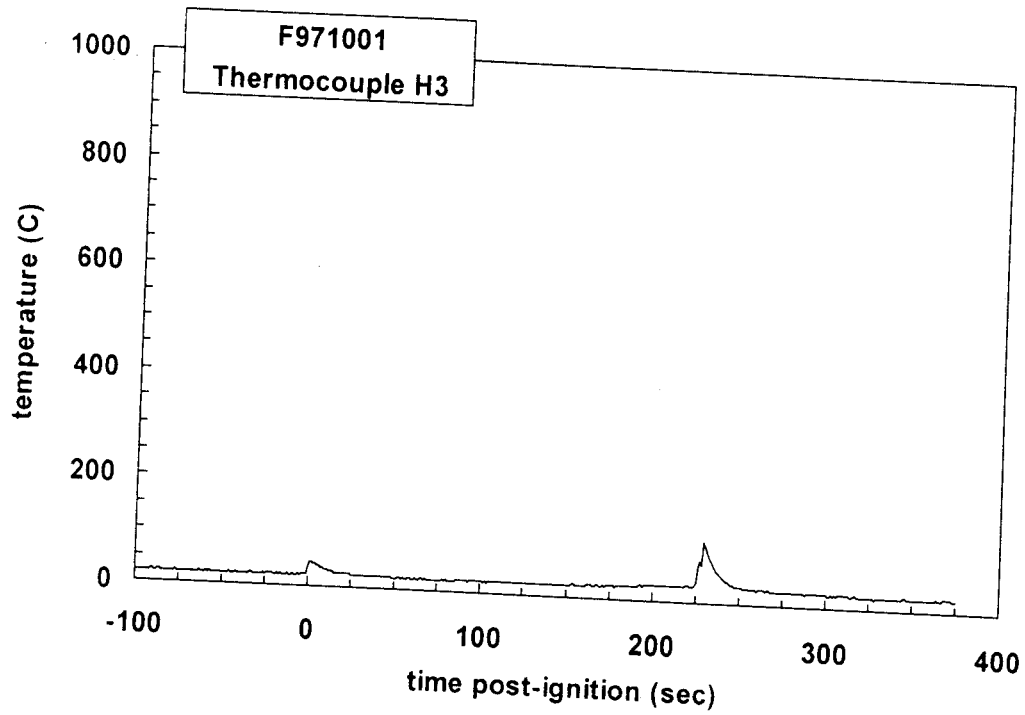

Plot C43. Fire Test F971001. Data plot from thermocouple H3.

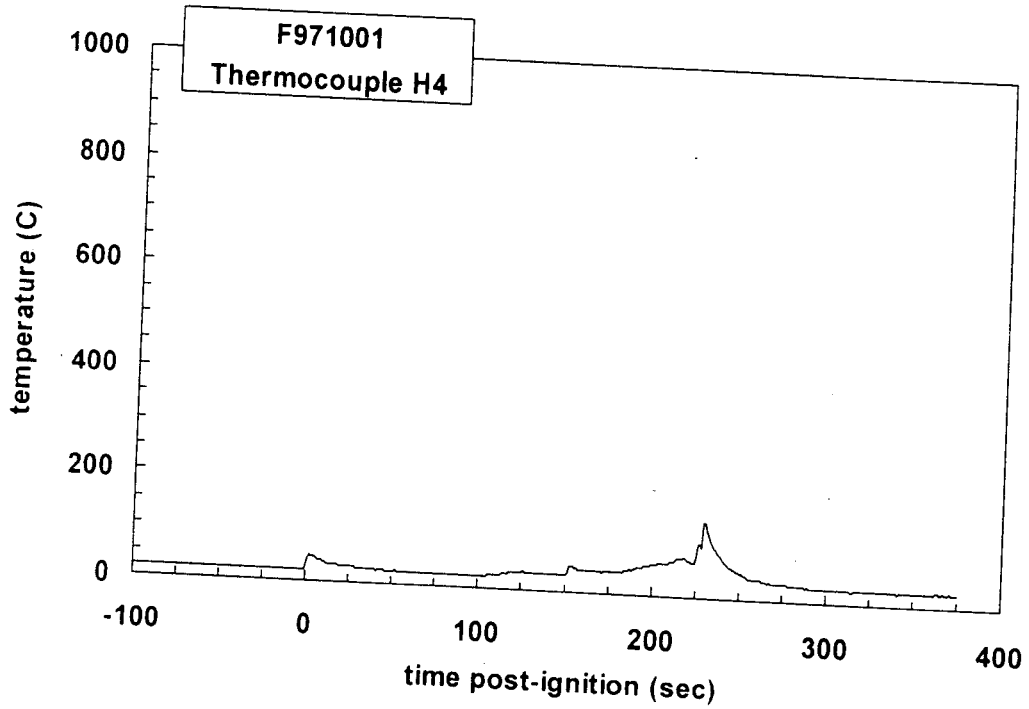

Plot C44. Fire Test F971001. Data plot from thermocouple H4.

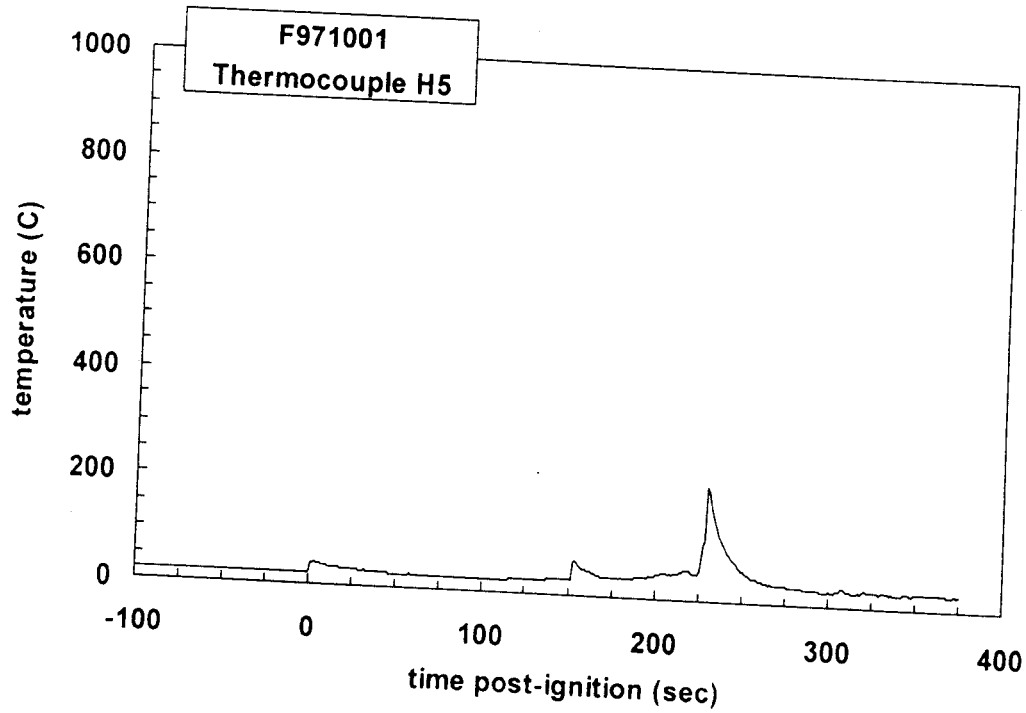

Plot C45. Fire Test F971001. Data plot from thermocouple H5.

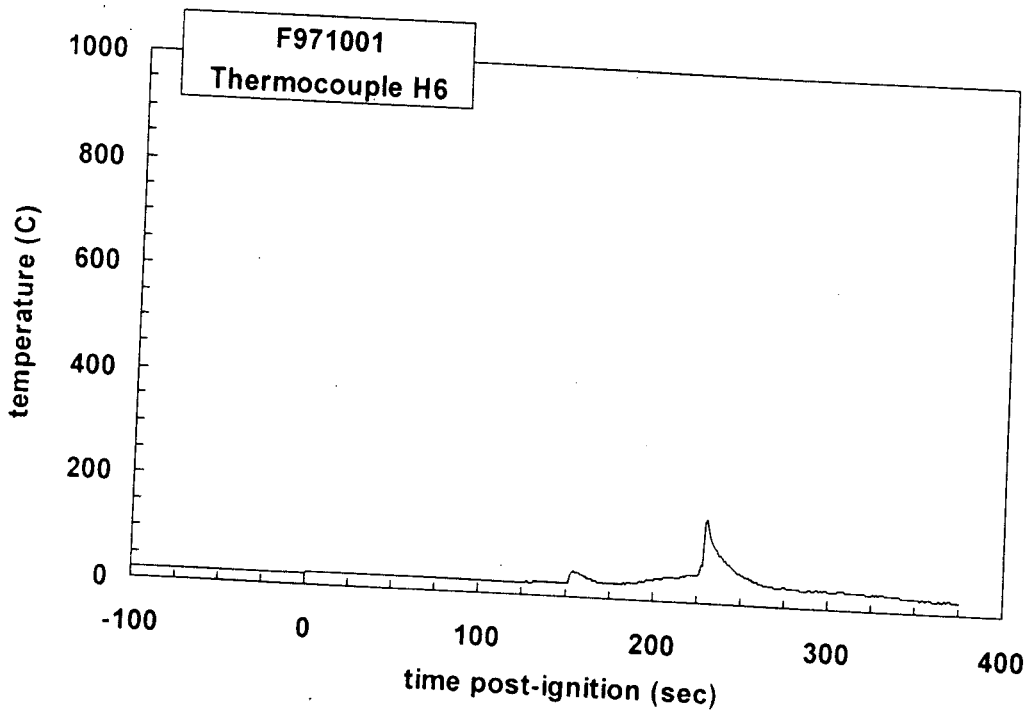

Plot C46. Fire Test F971001. Data plot from thermocouple H6.

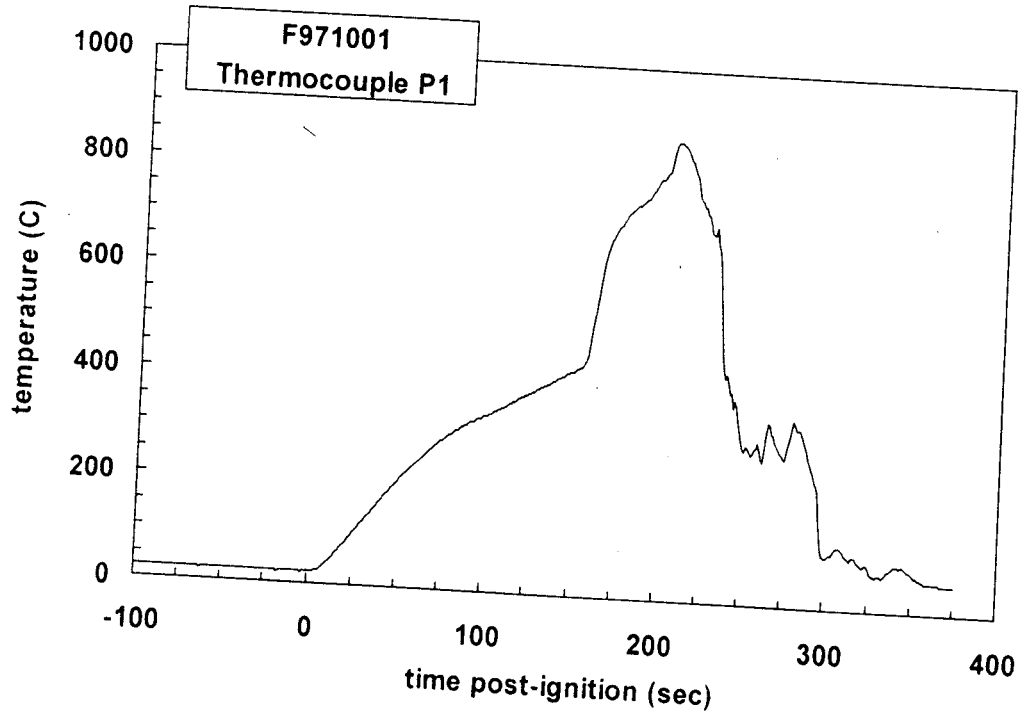

Plot C47. Fire Test F971001. Data plot from thermocouple P1.

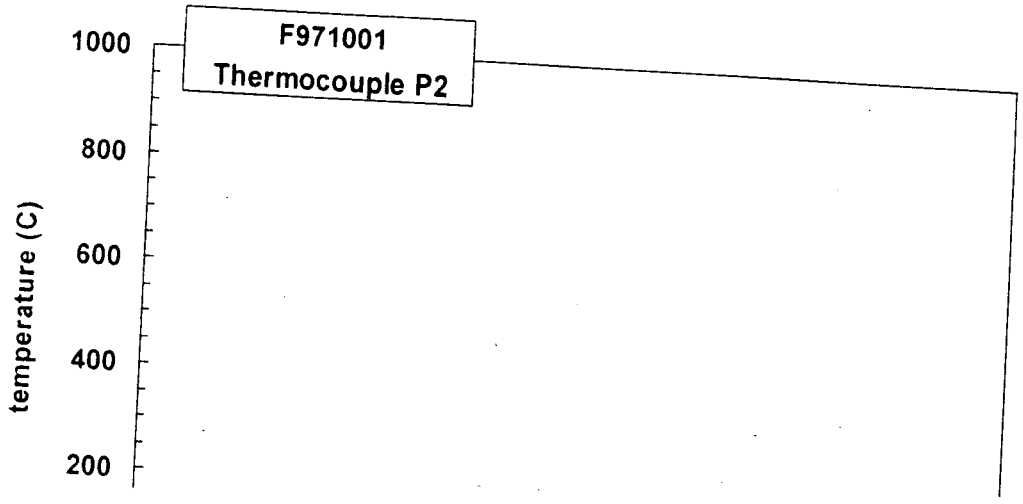

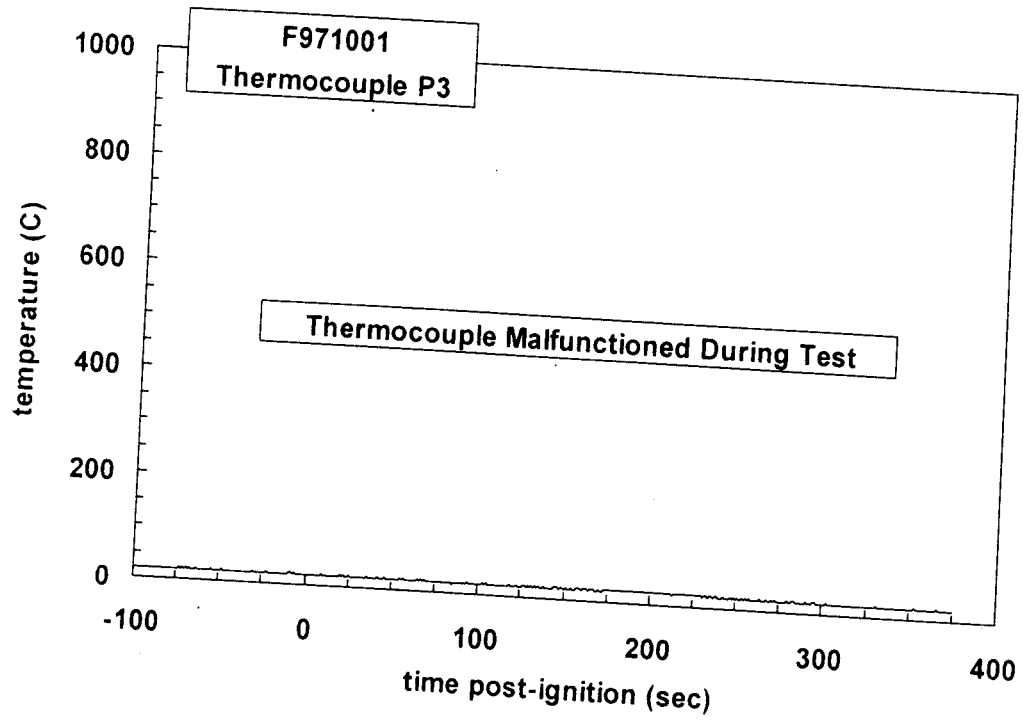

Plot C49. Fire Test F971001. Data plot from thermocouple P3.

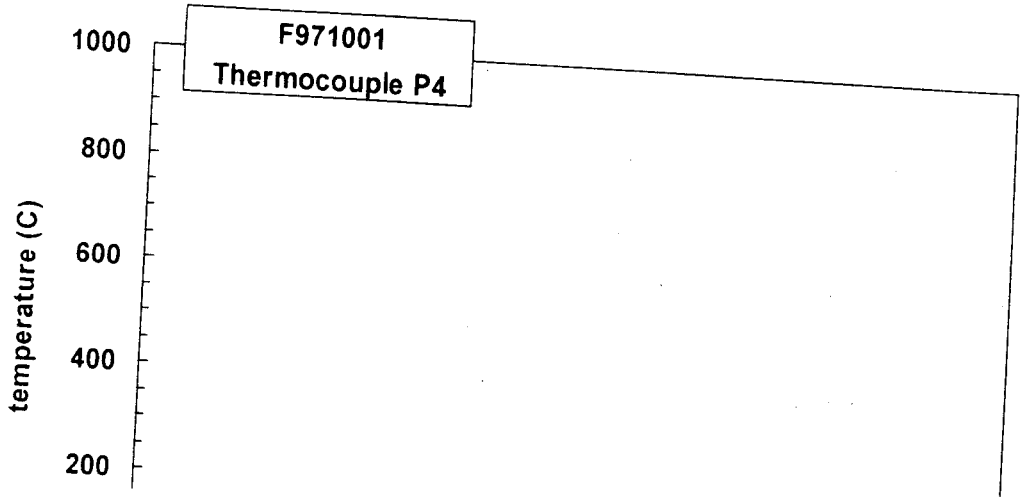

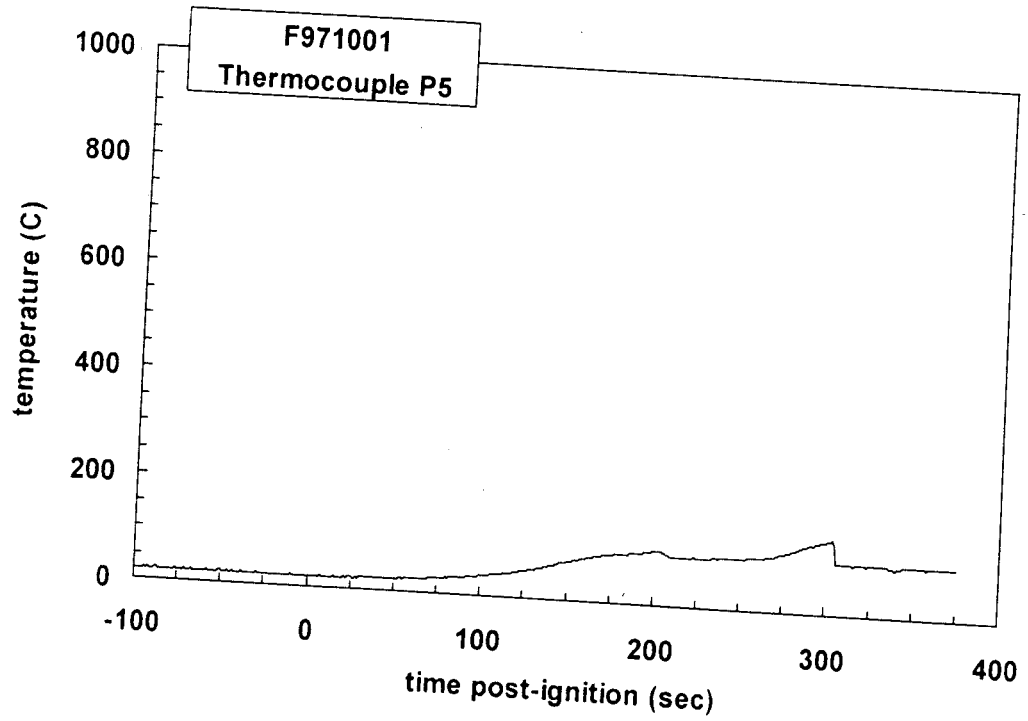

Plot C51. Fire Test F971001. Data plot from thermocouple P5.

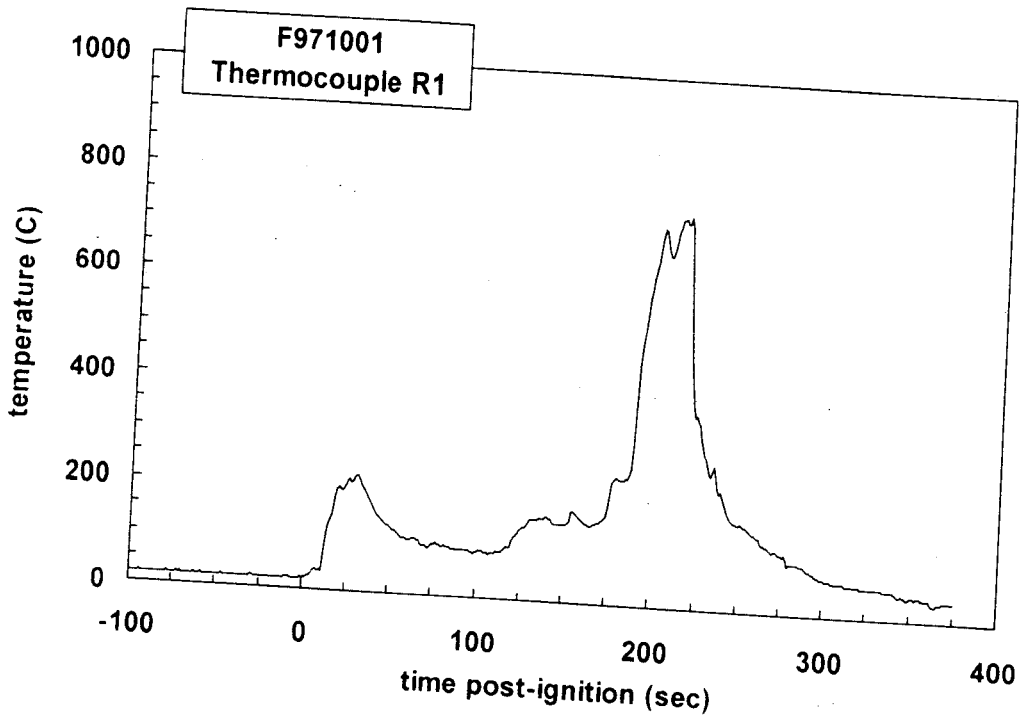

Plot C52. Fire Test F971001. Data plot from thermocouple R1.

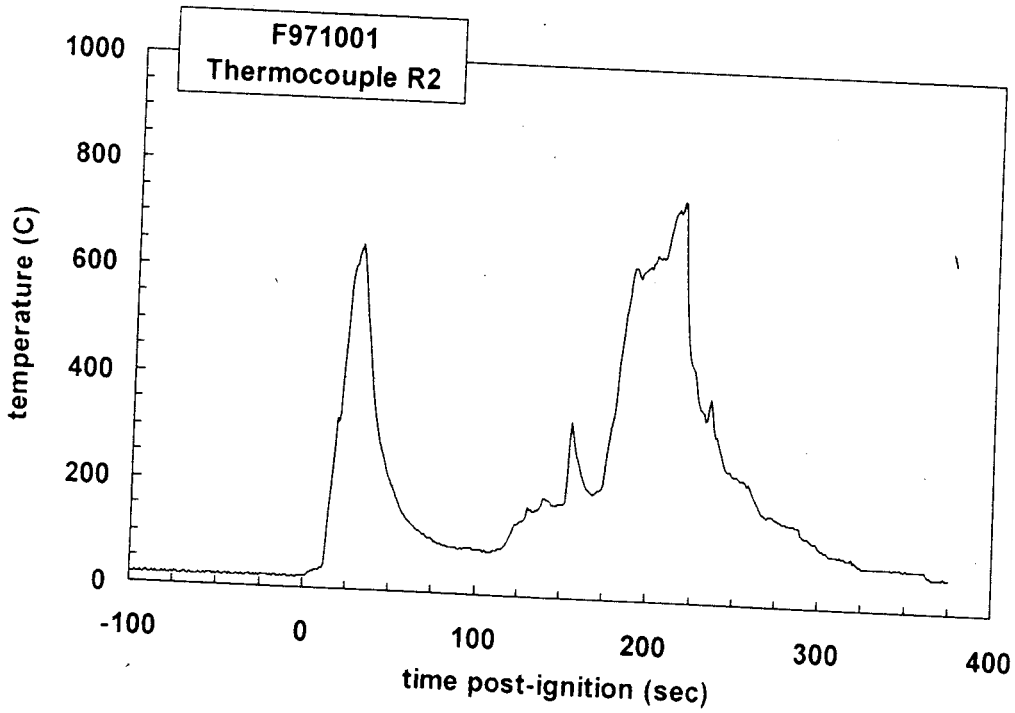

Plot C53. Fire Test F971001. Data plot from thermocouple R2.

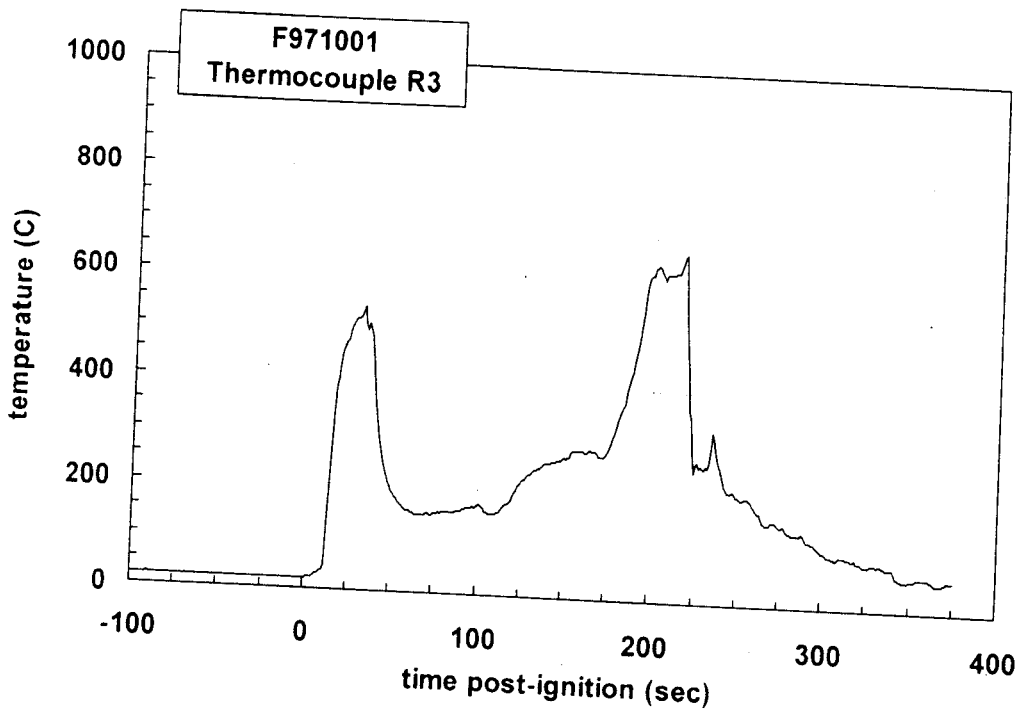

Plot C54. Fire Test F971001. Data plot from thermocouple R3.

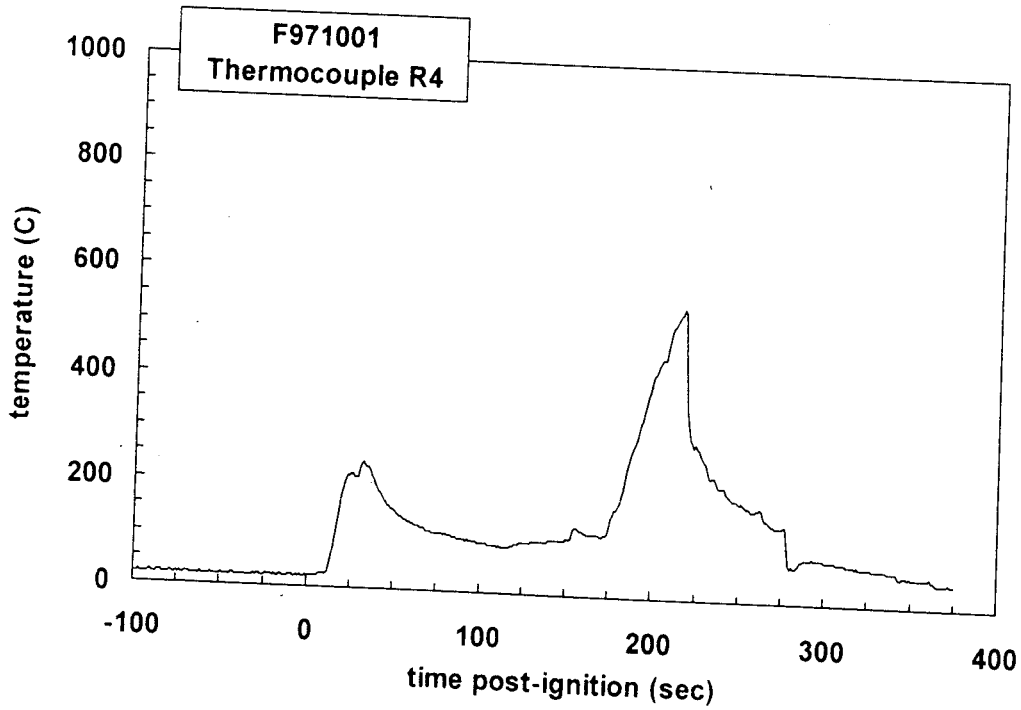

Plot C55. Fire Test F971001. Data plot from thermocouple R4.

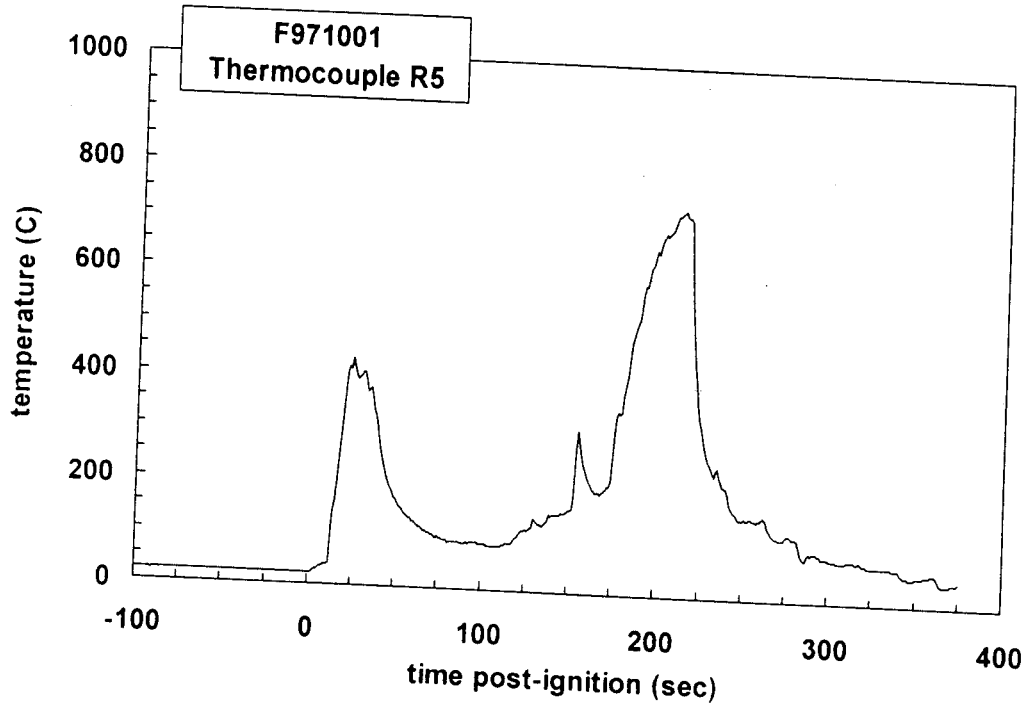

Plot C56. Fire Test F971001. Data plot from thermocouple R5.

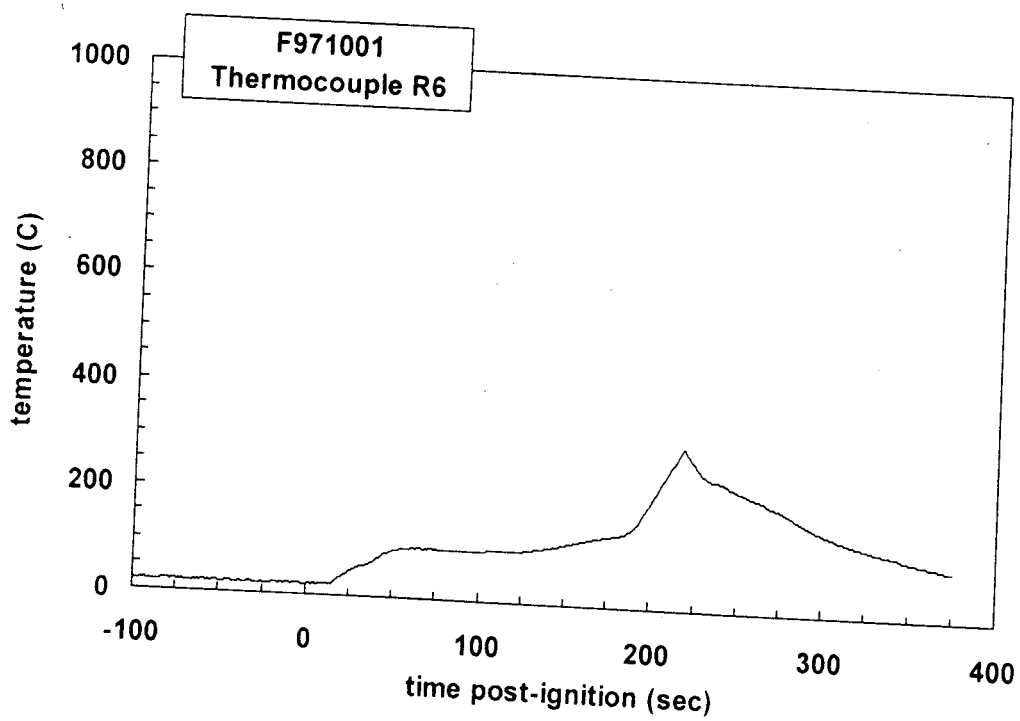

Plot C57. Fire Test F971001. Data plot from thermocouple R6.

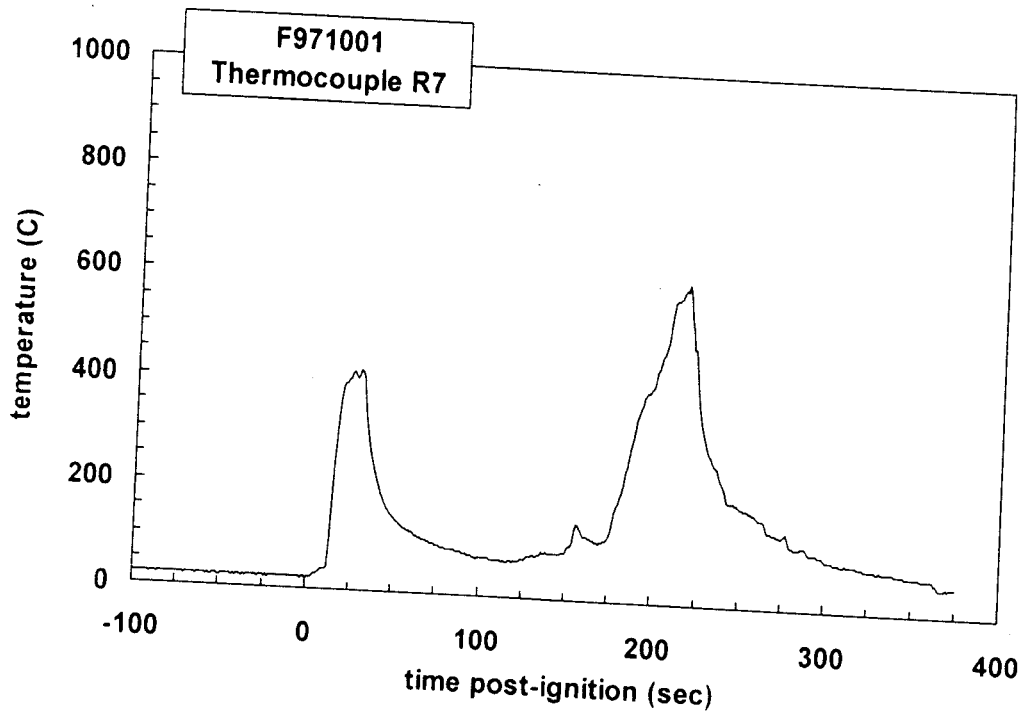

Plot C58. Fire Test F971001. Data plot from thermocouple R7.

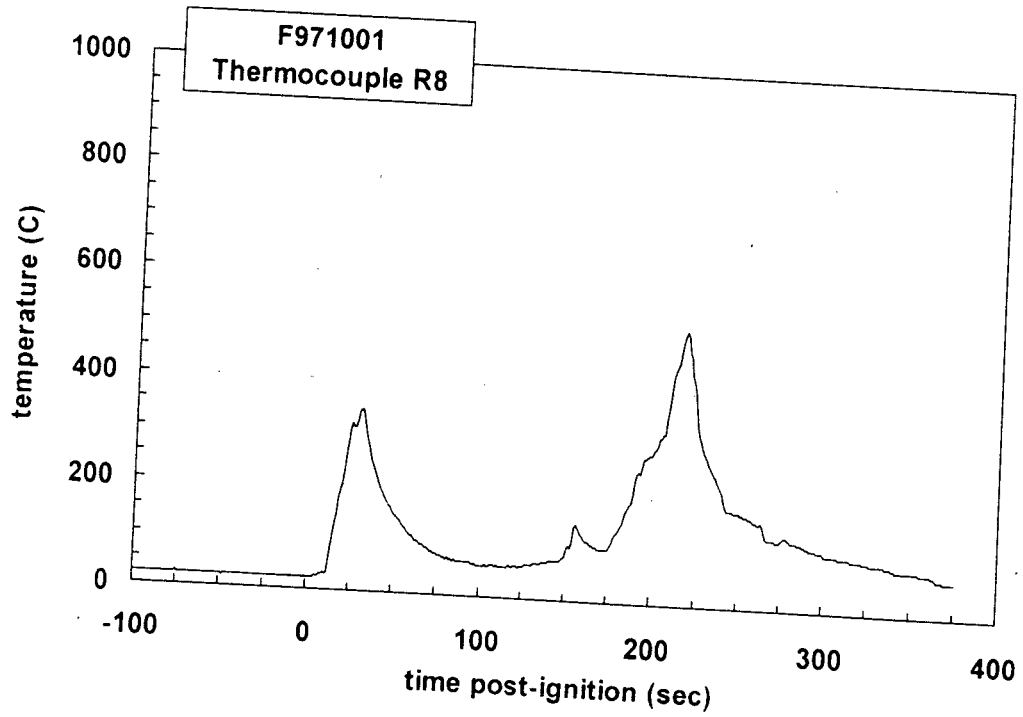

Plot C59. Fire Test F971001. Data plot from thermocouple R8.

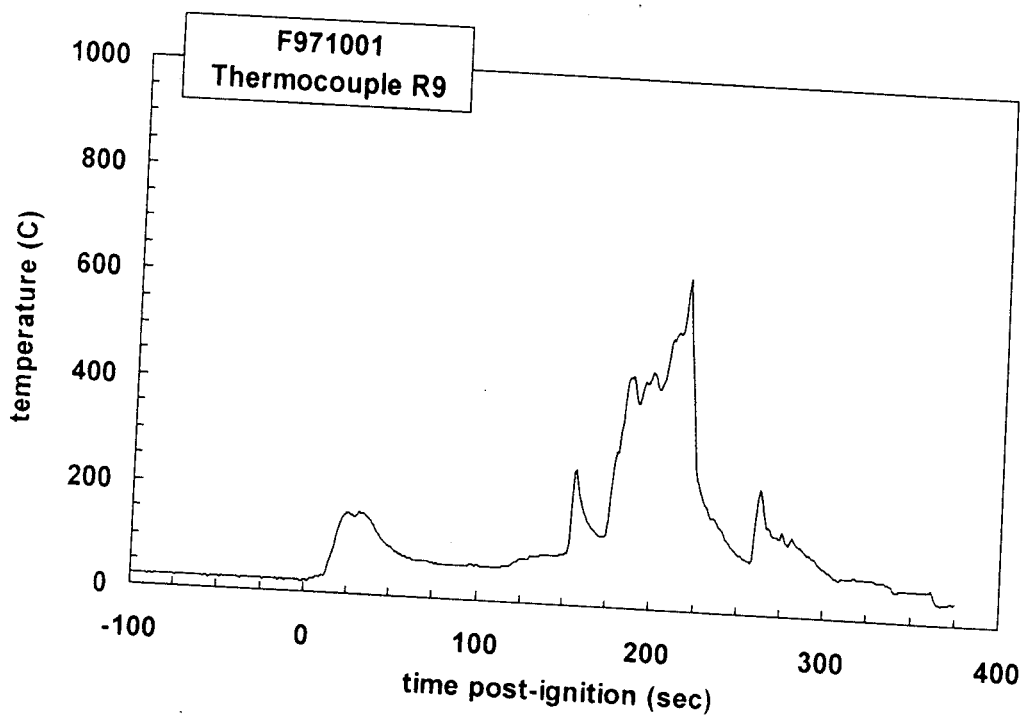

Plot C60. Fire Test F971001. Data plot from thermocouple R9.

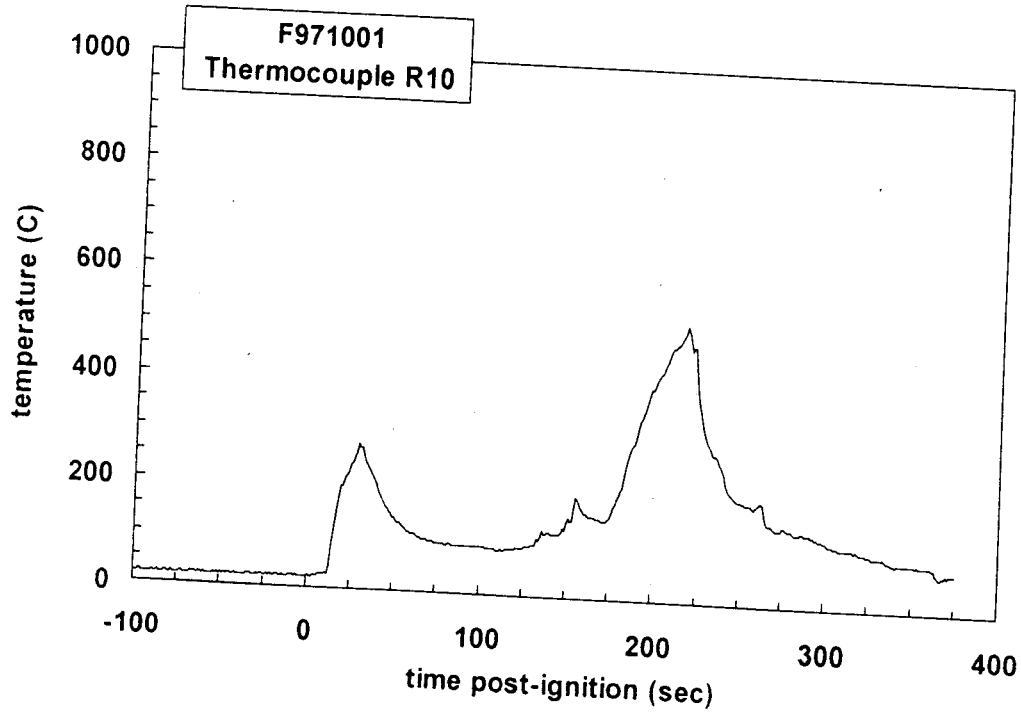

Plot C61. Fire Test F971001. Data plot from thermocouple R10.

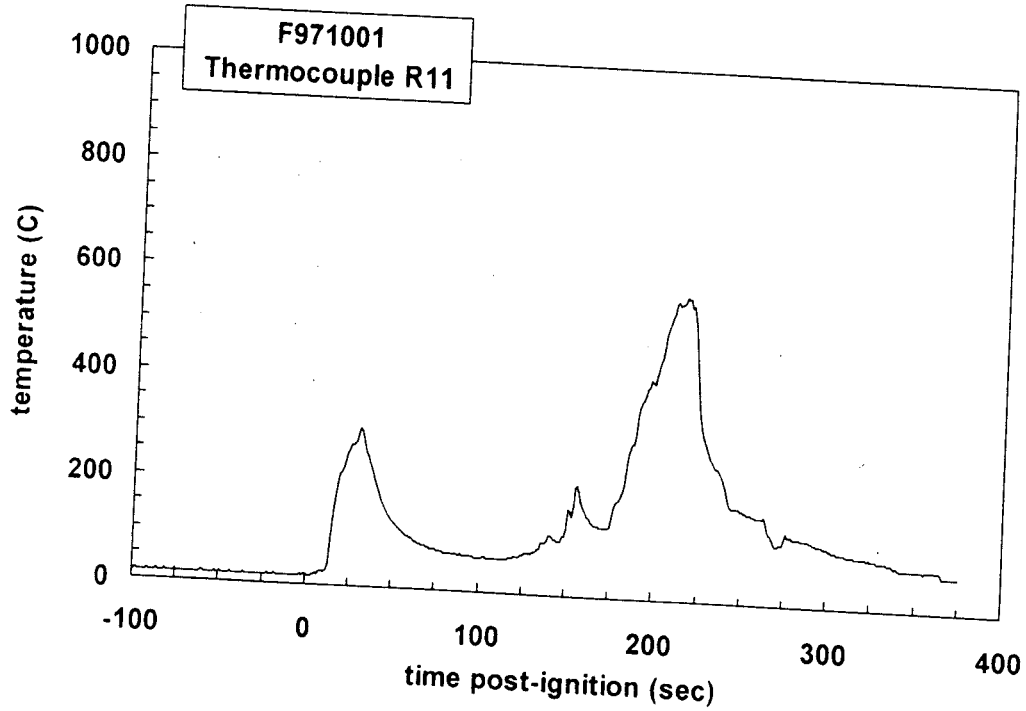

Plot C62. Fire Test F971001. Data plot from thermocouple R11.

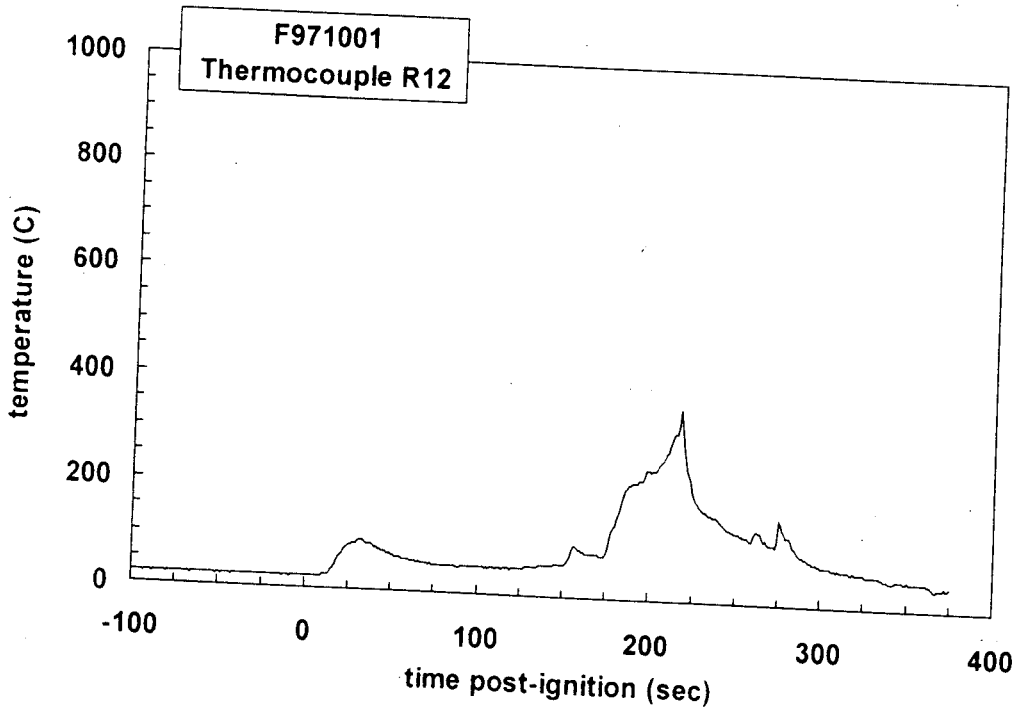

Plot C63. Fire Test F971001. Data plot from thermocouple R12.

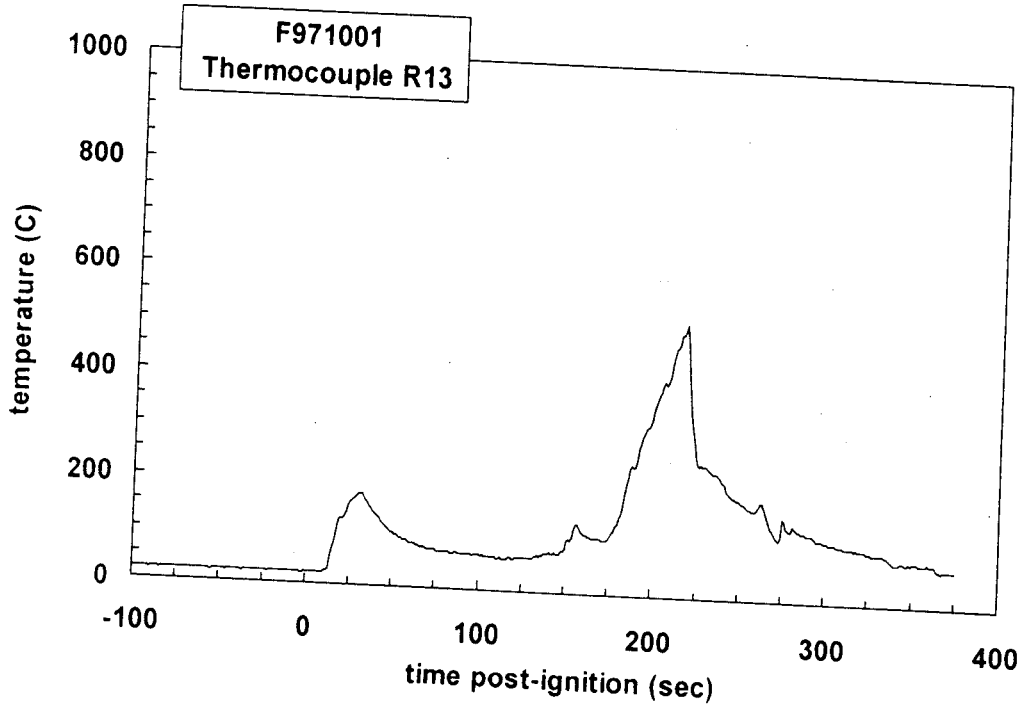

Plot C64. Fire Test F971001. Data plot from thermocouple R13.

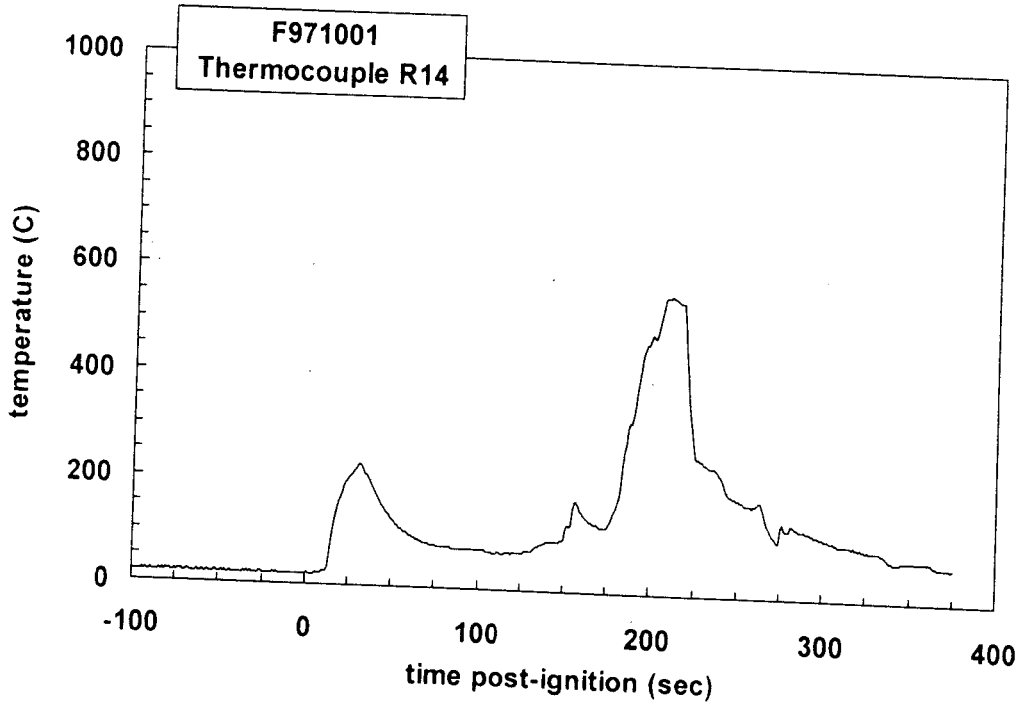

Plot C65. Fire Test F971001. Data plot from thermocouple R14.

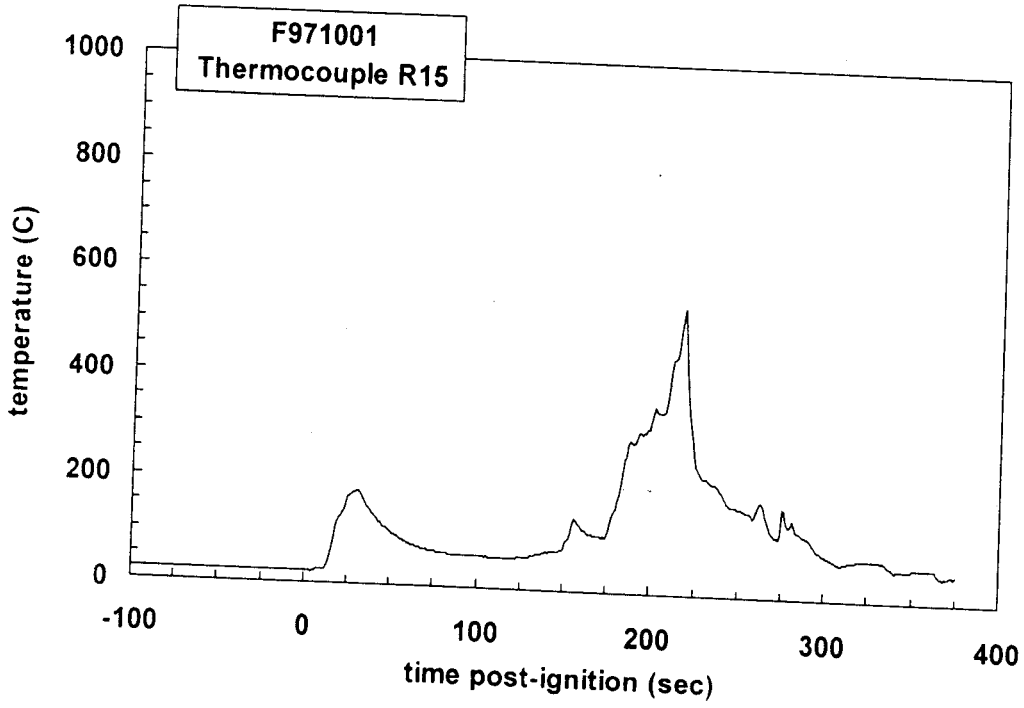

Plot C66. Fire Test F971001. Data plot from thermocouple R15.

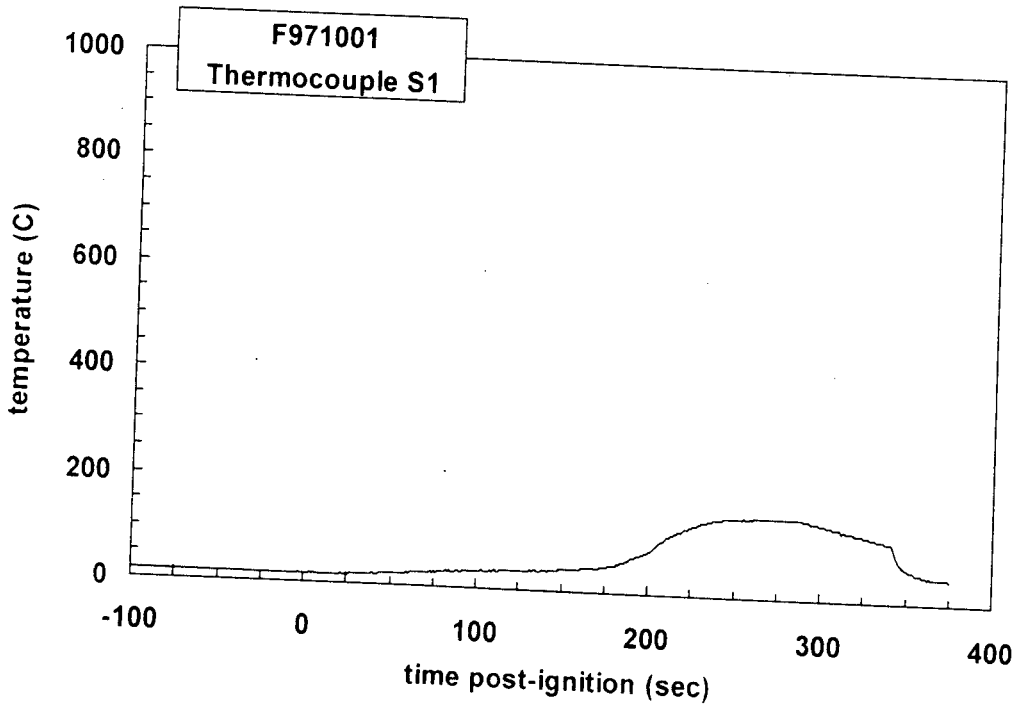

Plot C67. Fire Test F971001. Data plot from thermocouple S1.

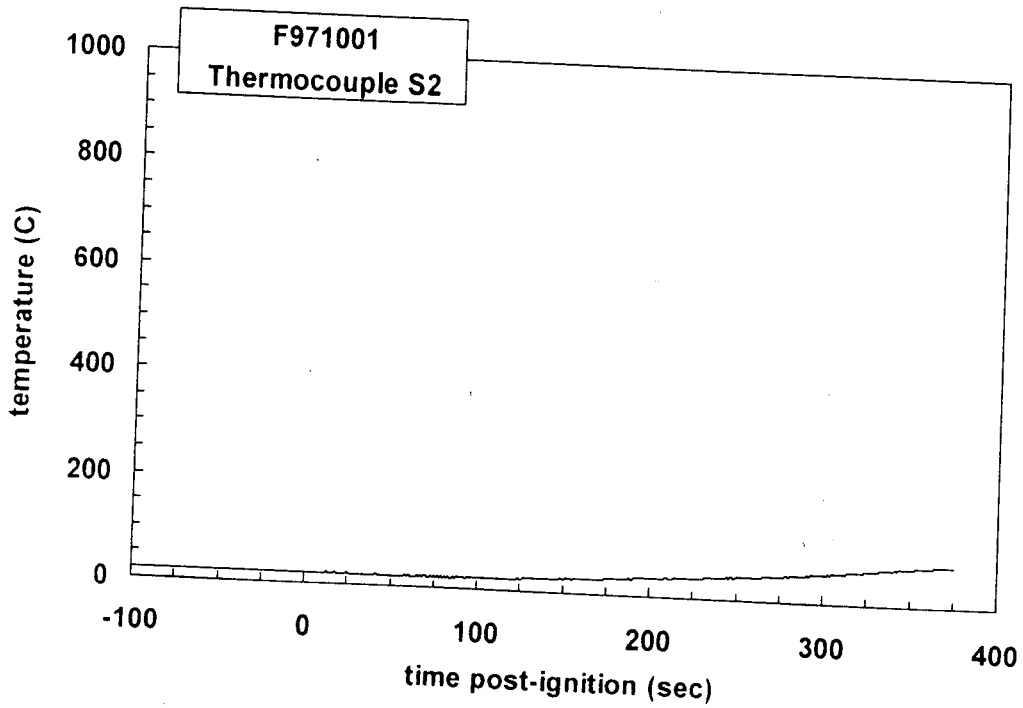

Plot C68. Fire Test F971001. Data plot from thermocouple S2.

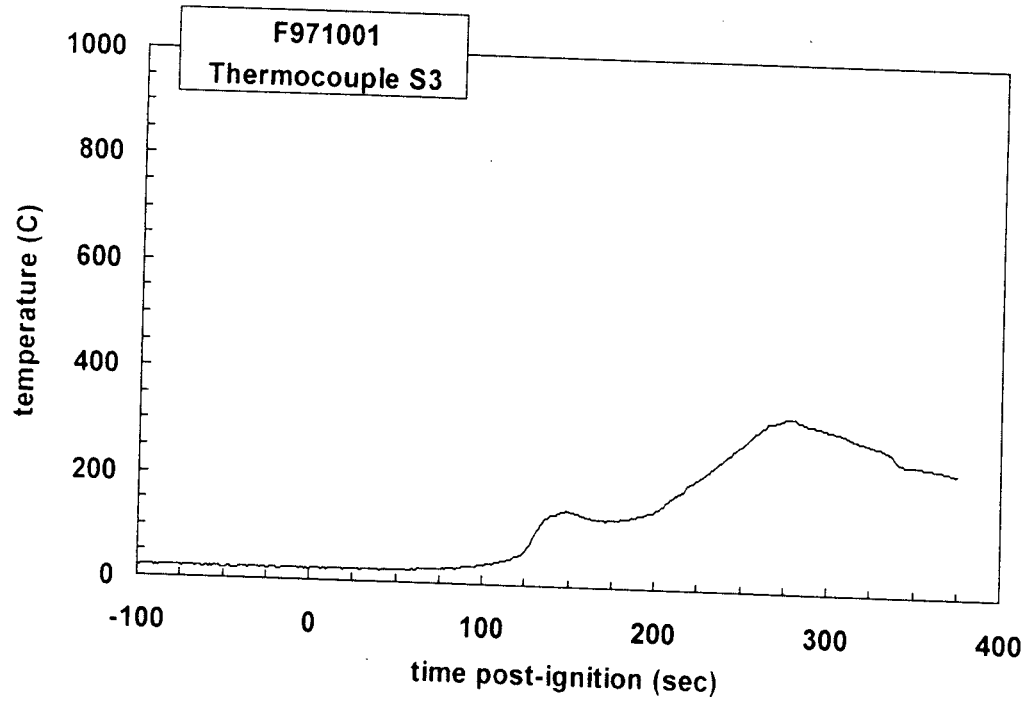

Plot C69. Fire Test F971001. Data plot from thermocouple S3.

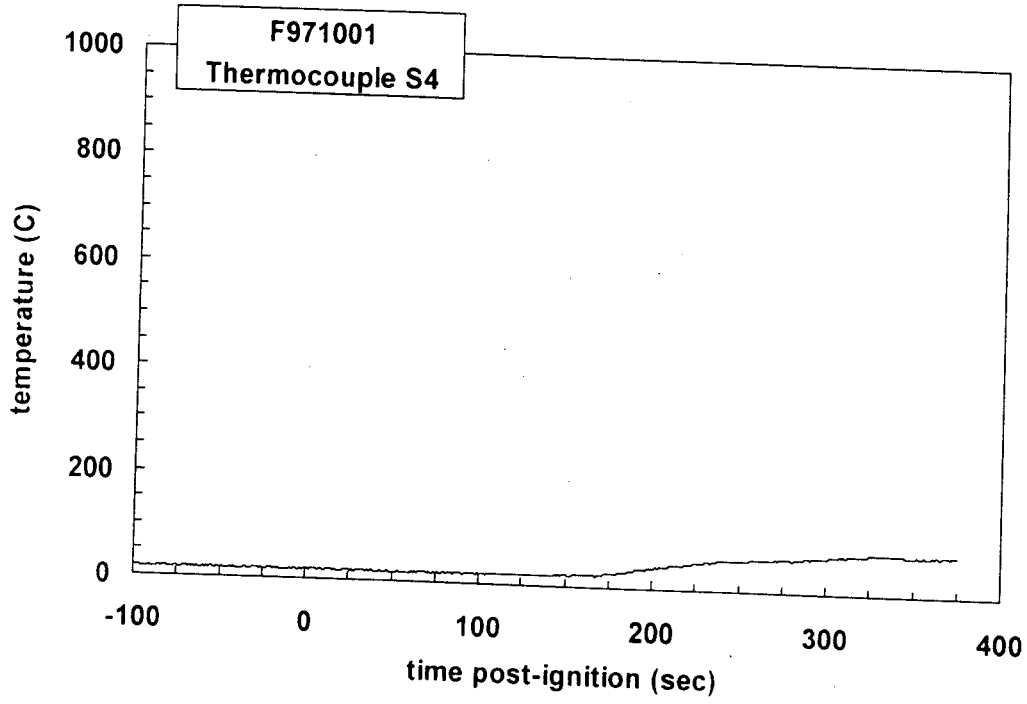

Plot C70. Fire Test F971001. Data plot from thermocouple S4.

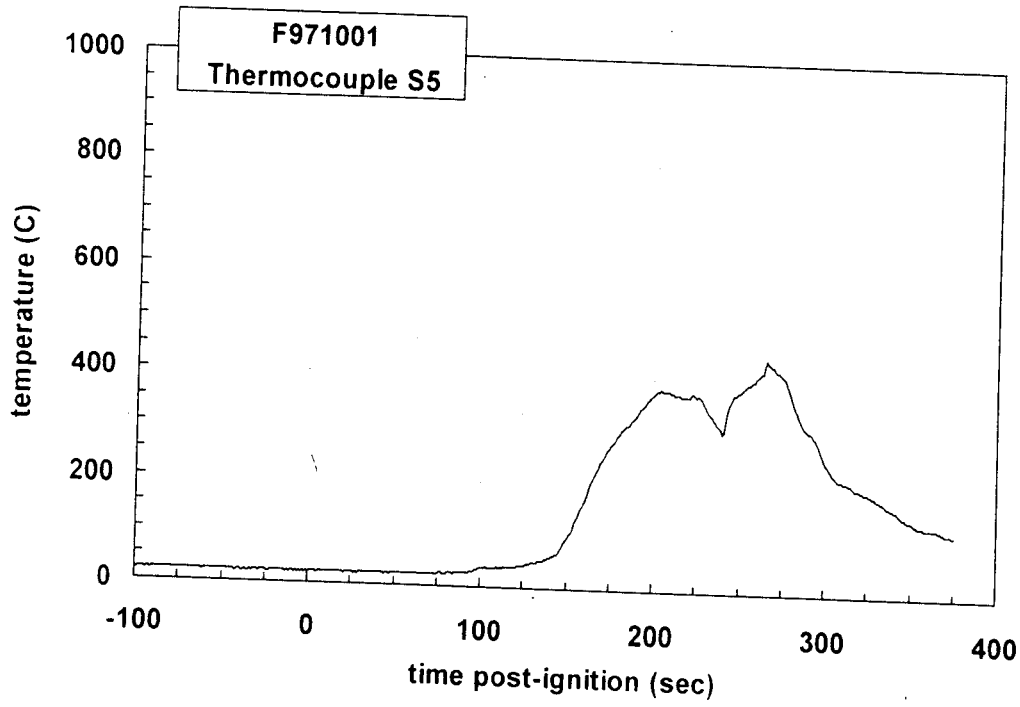

Plot C71. Fire Test F971001. Data plot from thermocouple S5.

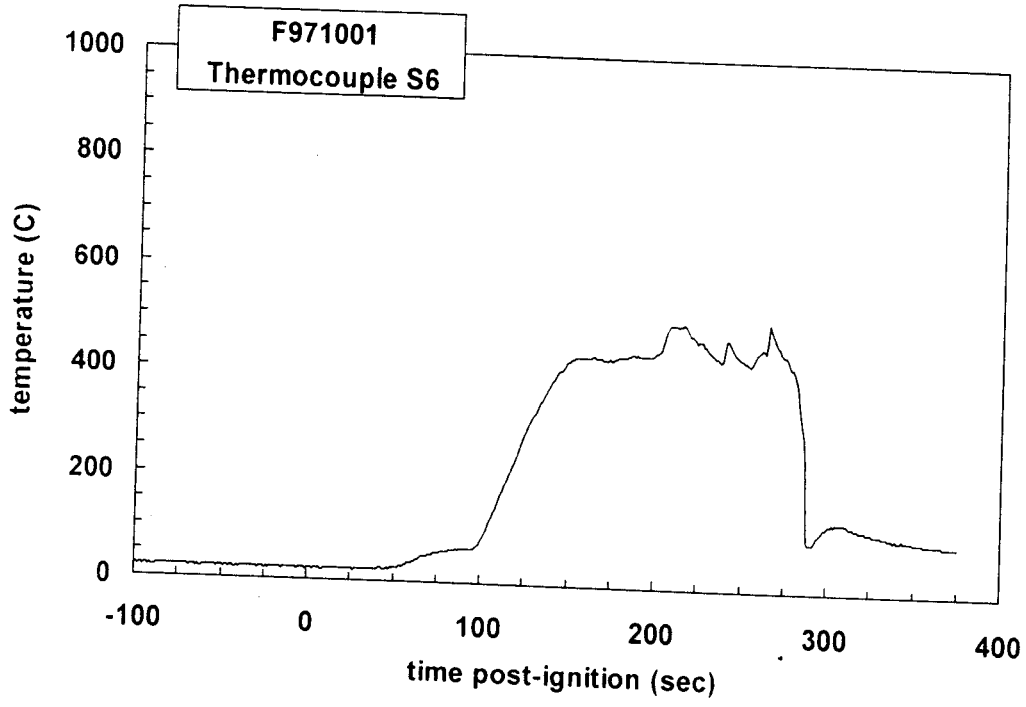

Plot C72. Fire Test F971001. Data plot from thermocouple S6.

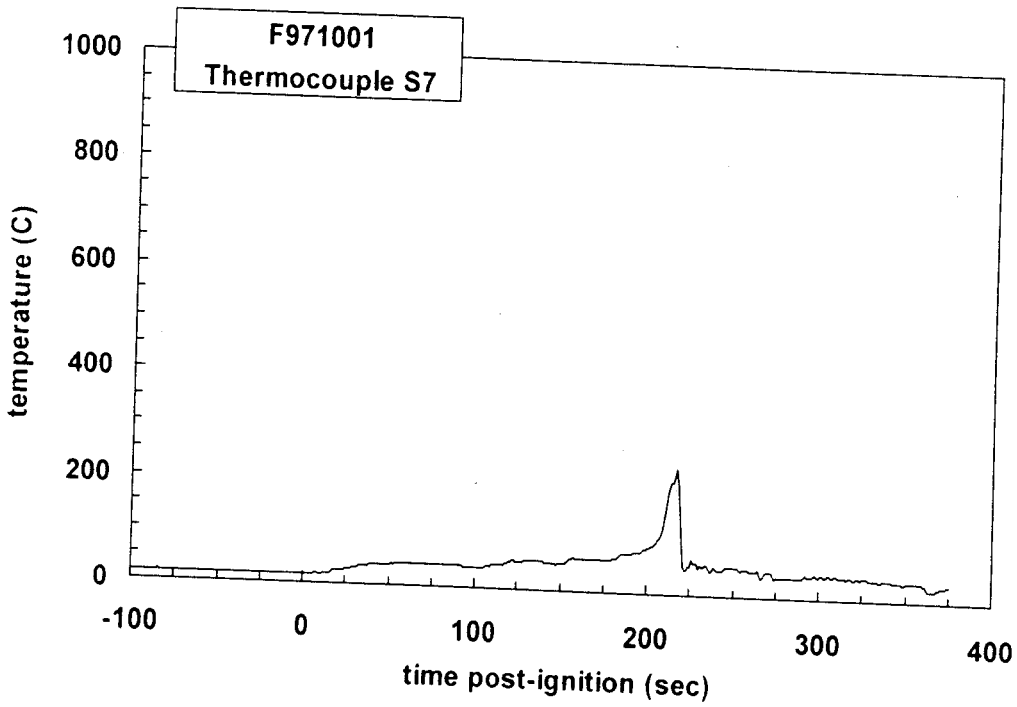

Plot C73. Fire Test F971001. Data plot from thermocouple S7.

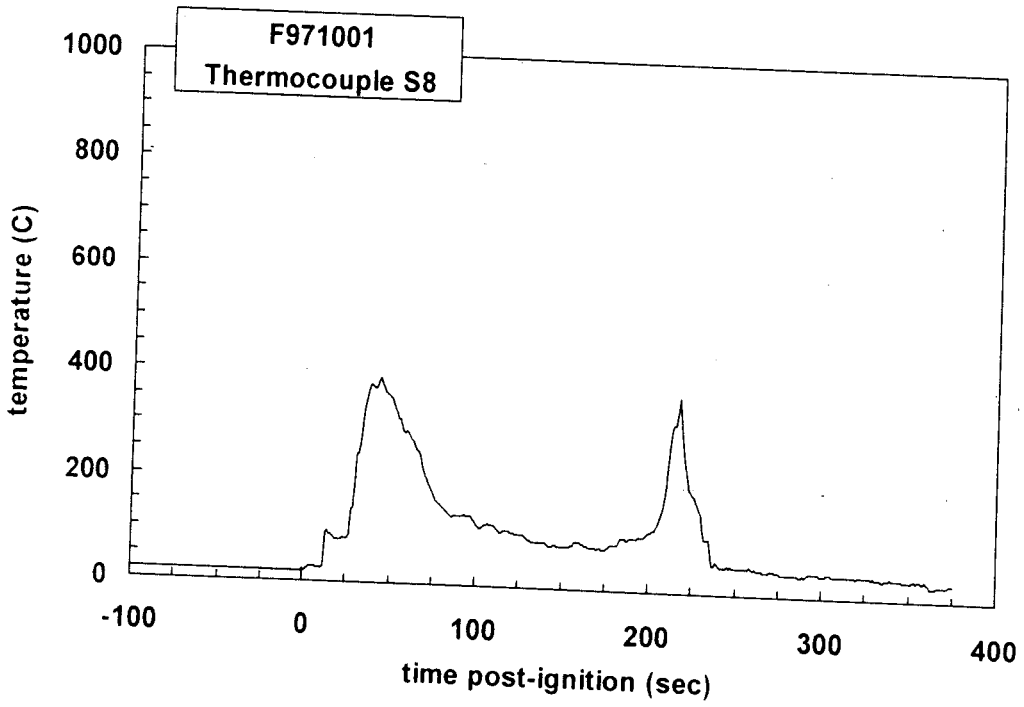

Plot C74. Fire Test F971001. Data plot from thermocouple S8.

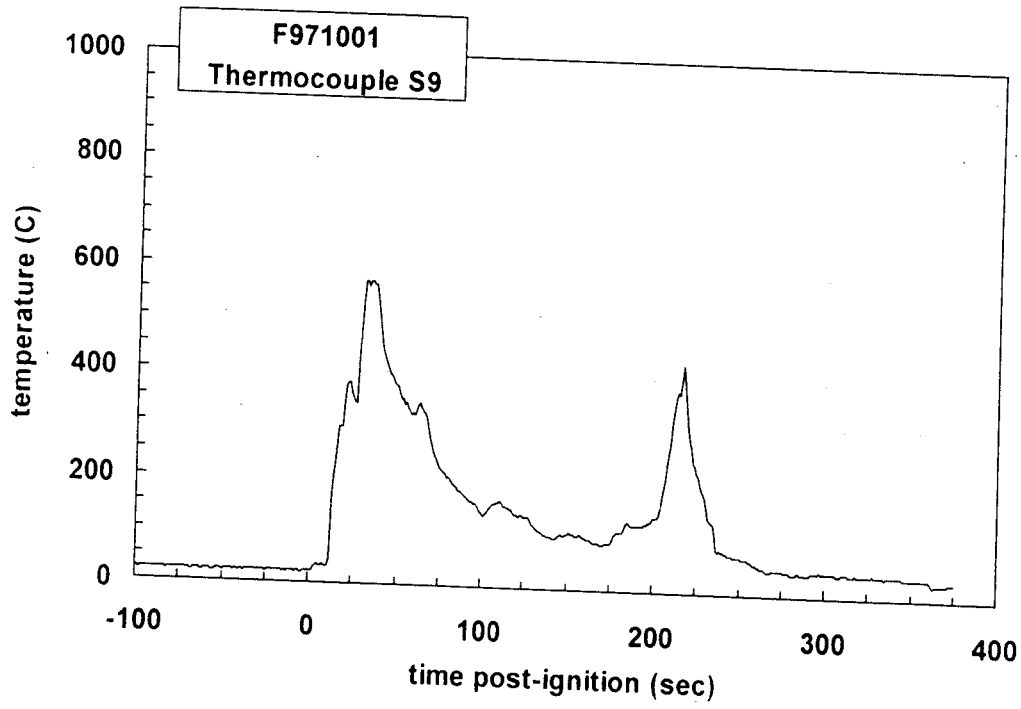

Plot C75. Fire Test F971001. Data plot from thermocouple S9.

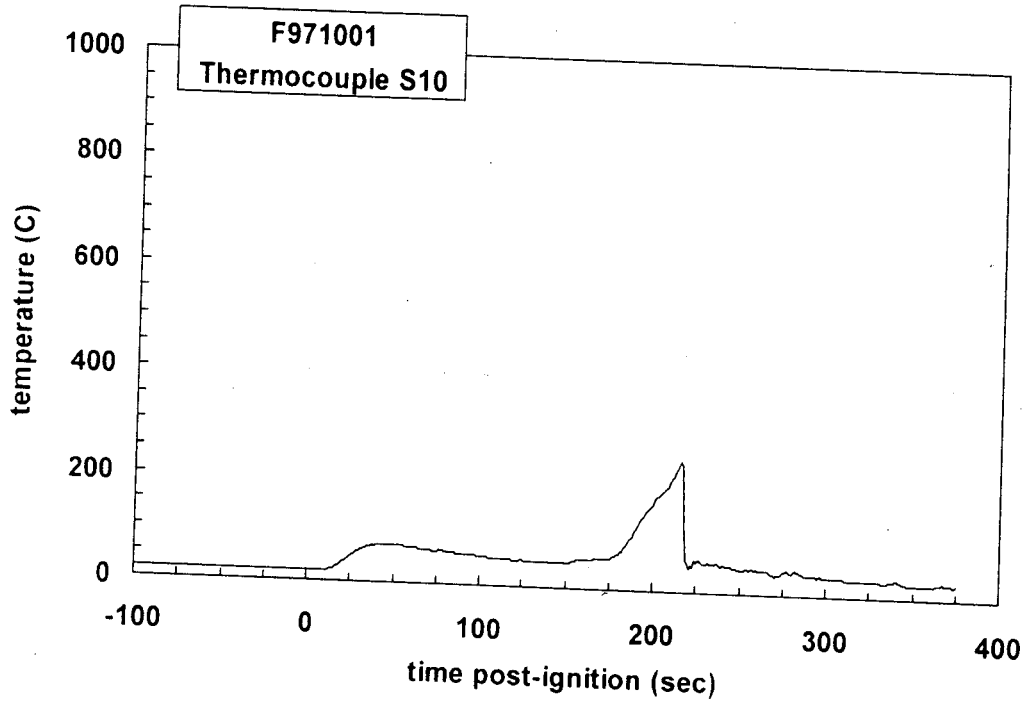

Plot C76. Fire Test F971001. Data plot from thermocouple S10.

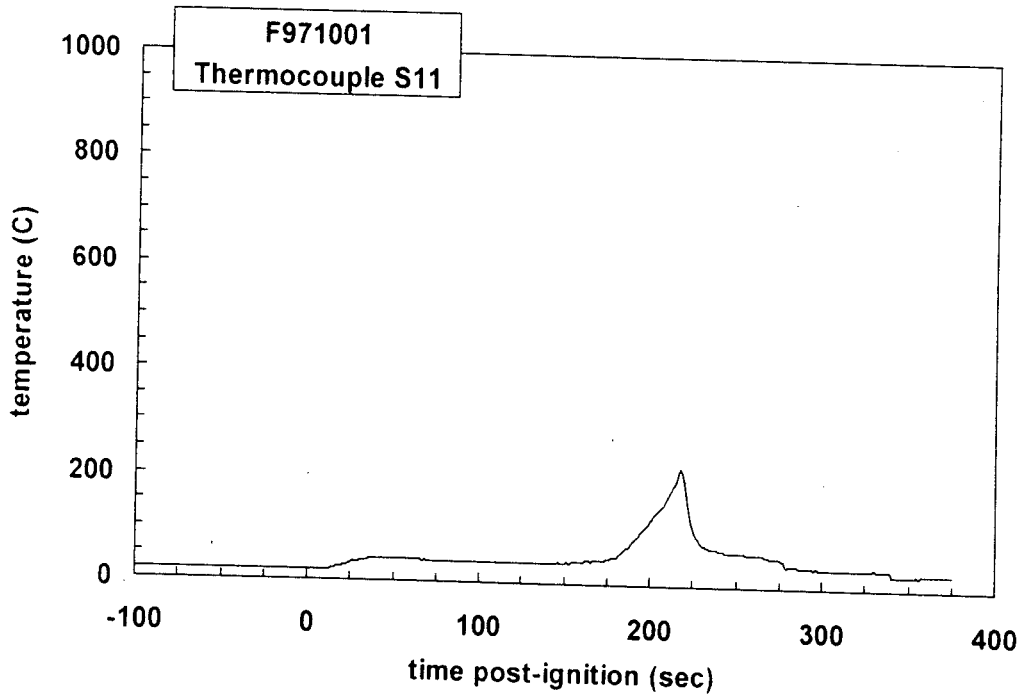

Plot C77. Fire Test F971001. Data plot from thermocouple S11.

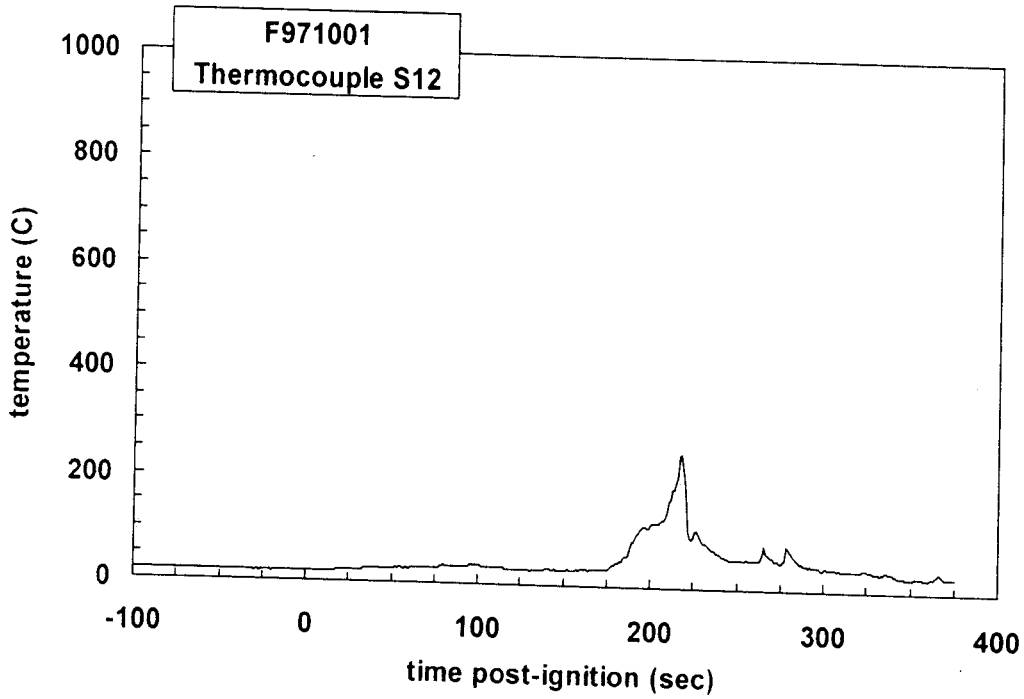

Plot C78. Fire Test F971001. Data plot from thermocouple S12.

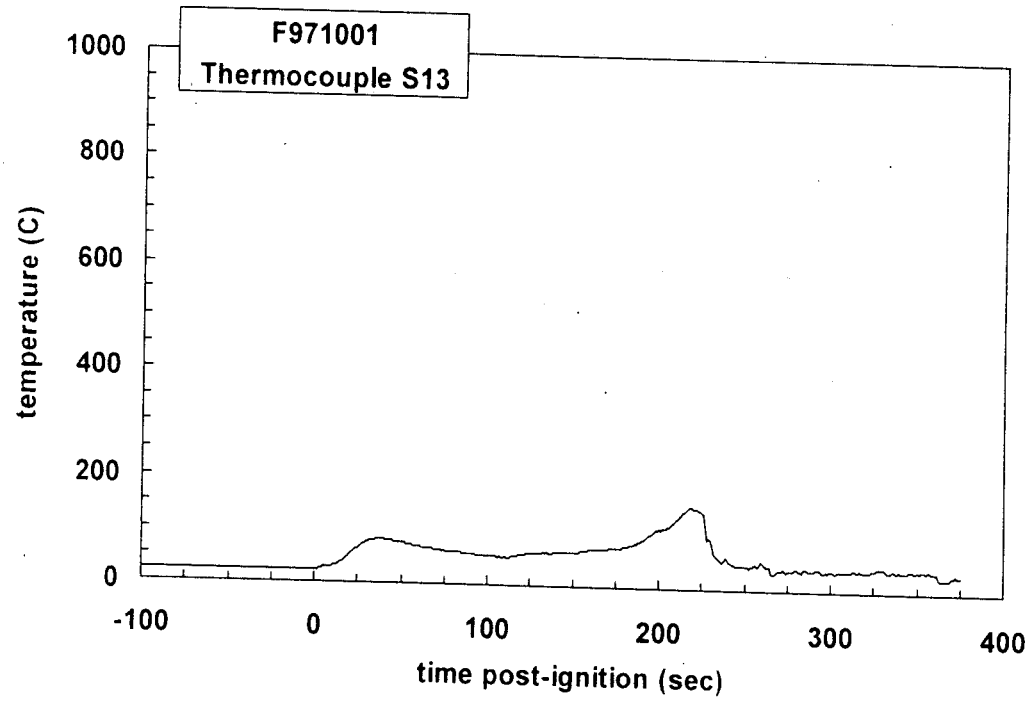

Plot C79. Fire Test F971001. Data plot from thermocouple S13.

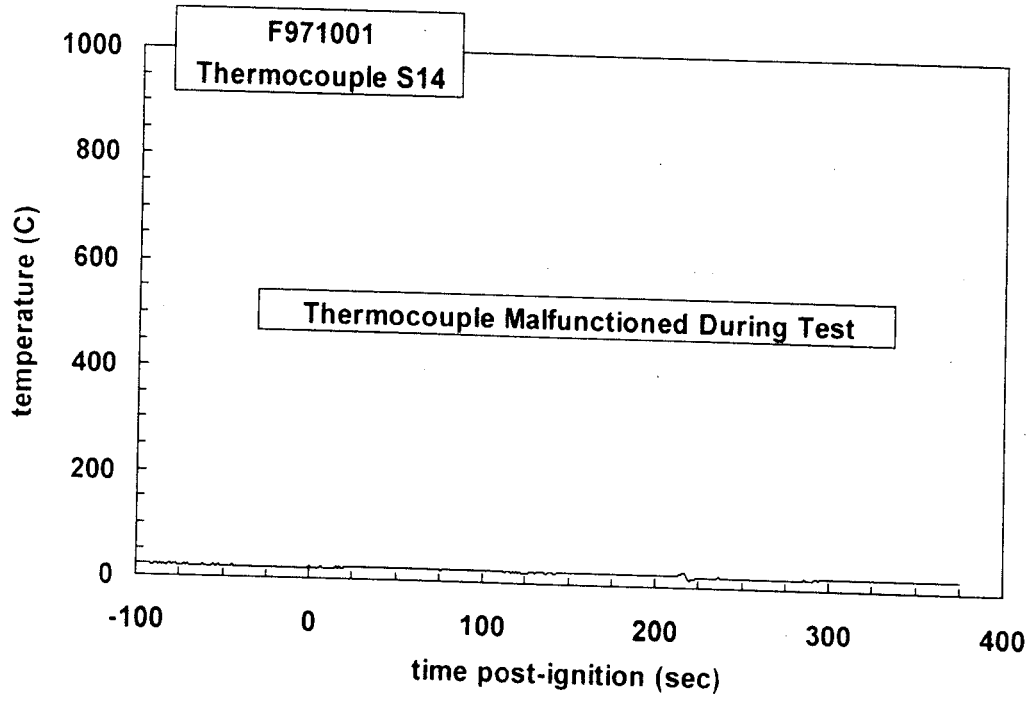

Plot C80. Fire Test F971001. Data plot from thermocouple S14.

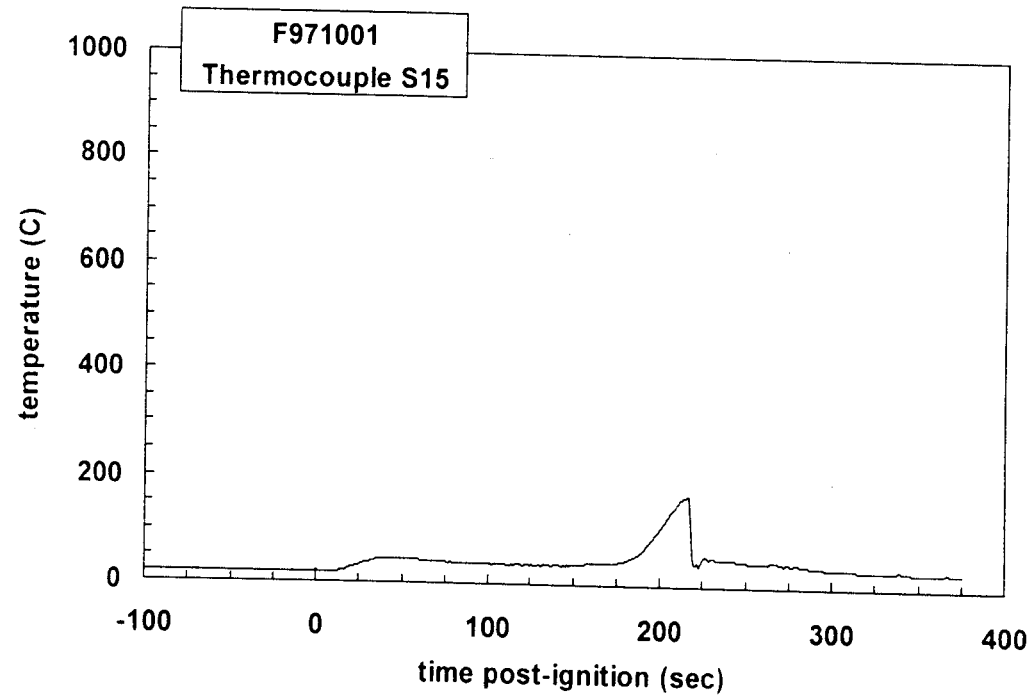

Plot C81. Fire Test F971001. Data plot from thermocouple S15.

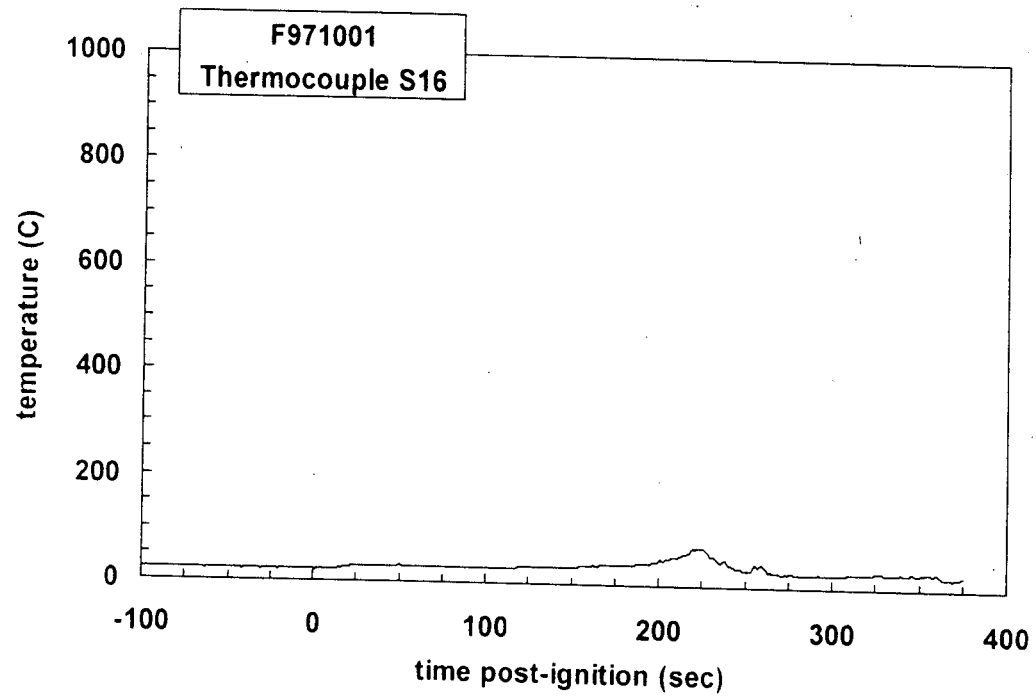

Plot C82. Fire Test F971001. Data plot from thermocouple S16.

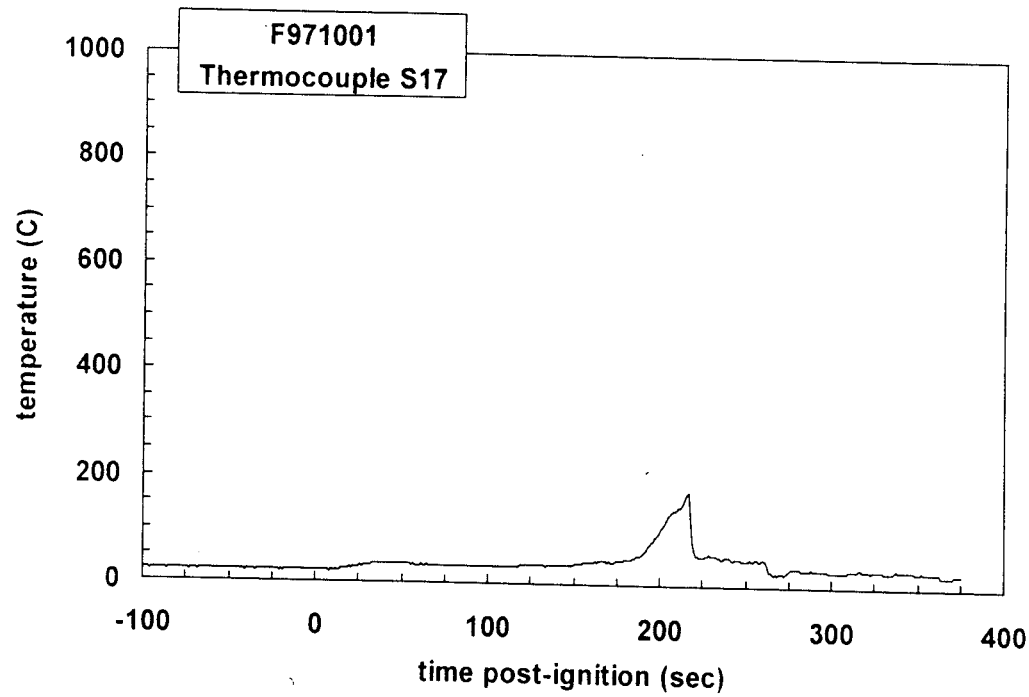

Plot C83. Fire Test F971001. Data plot from thermocouple S17.

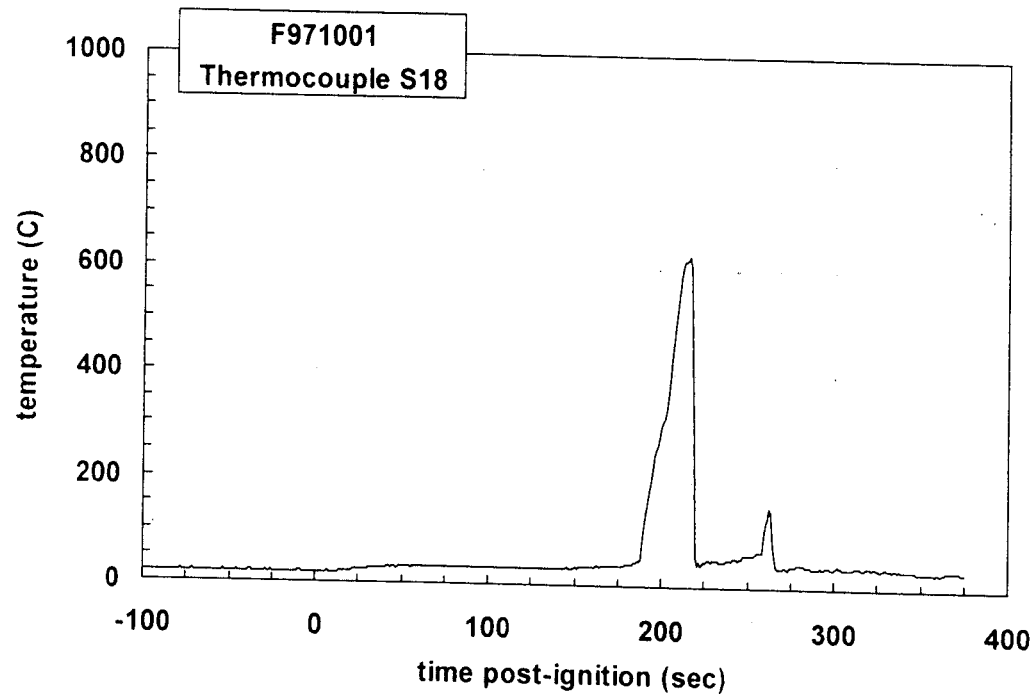

Plot C84. Fire Test F971001. Data plot from thermocouple S18.

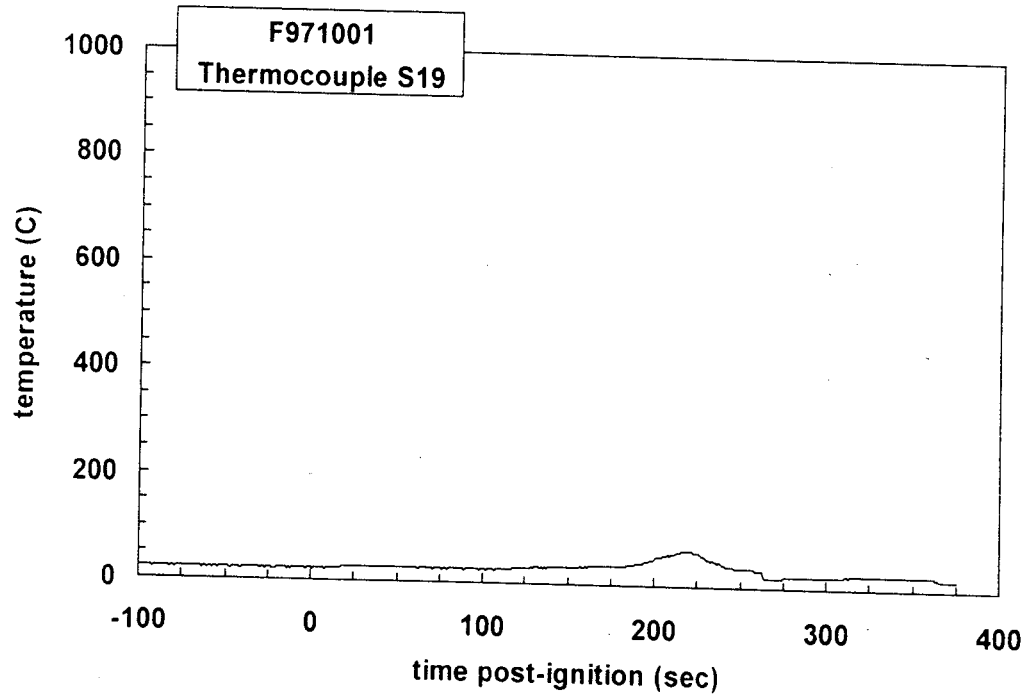

Plot C85. Fire Test F971001. Data plot from thermocouple S19.

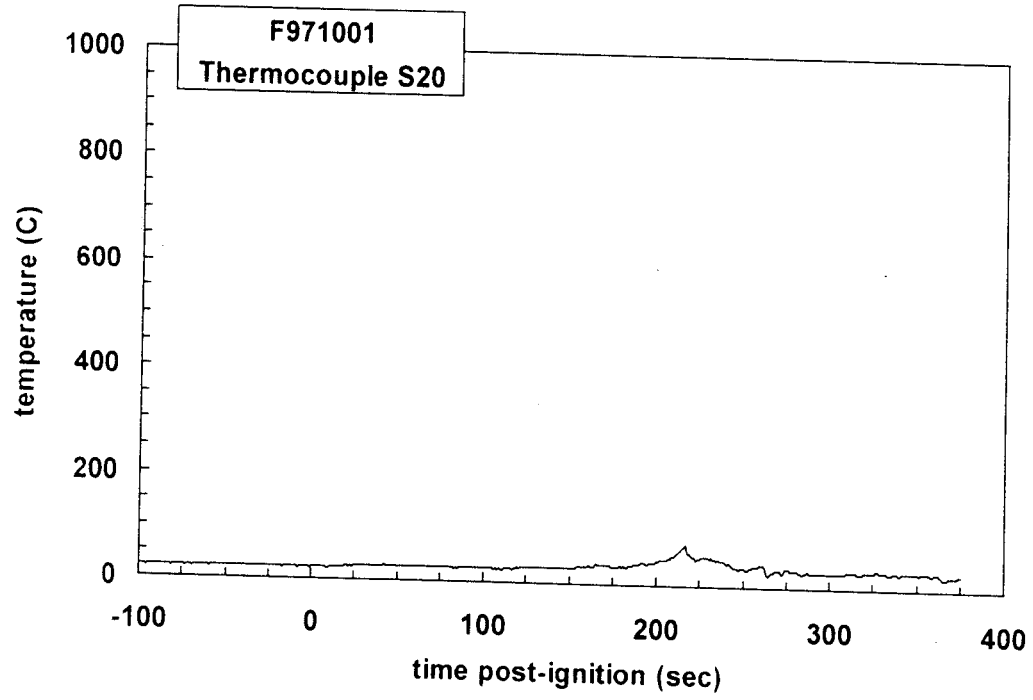

Plot C86. Fire Test F971001. Data plot from thermocouple S20.

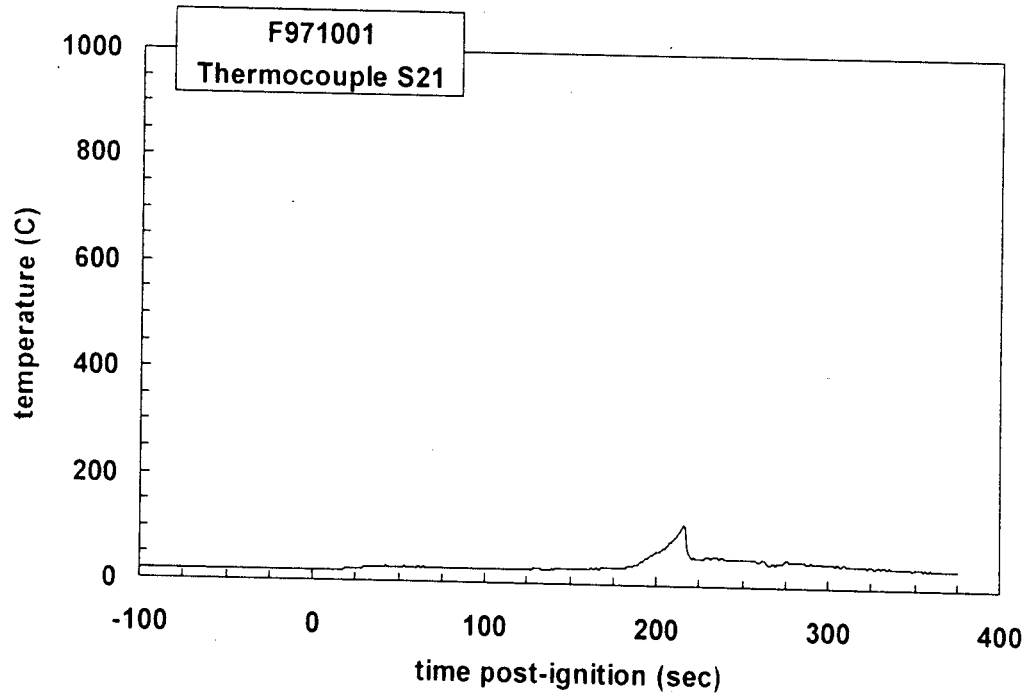

Plot C87. Fire Test F971001. Data plot from thermocouple S21.

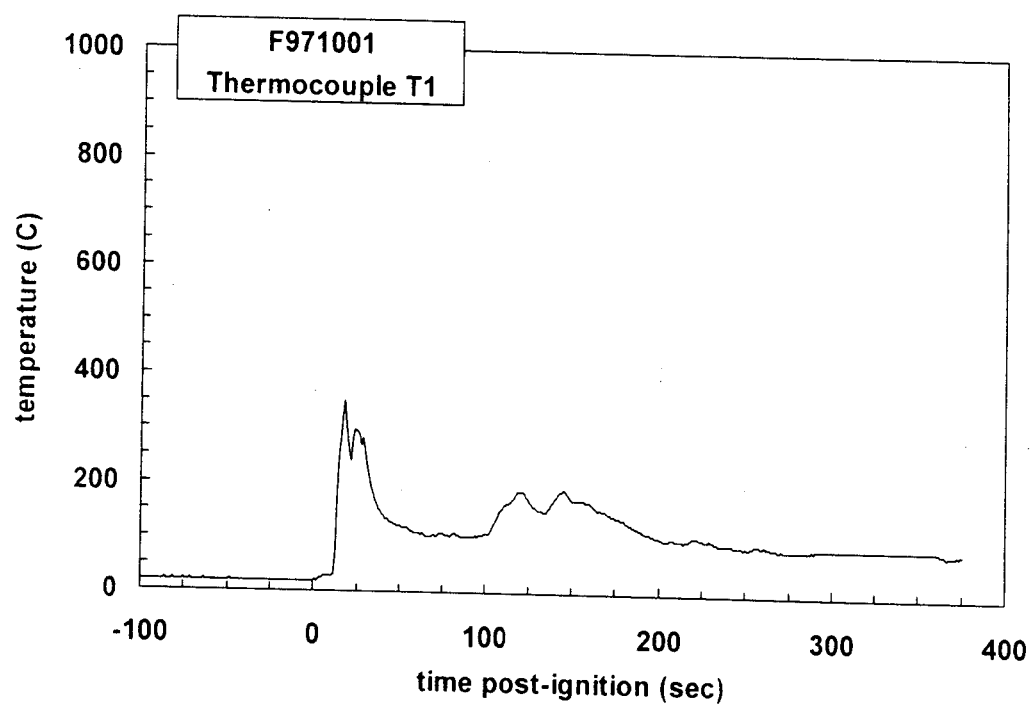

Plot C88. Fire Test F971001. Data plot from thermocouple T1.

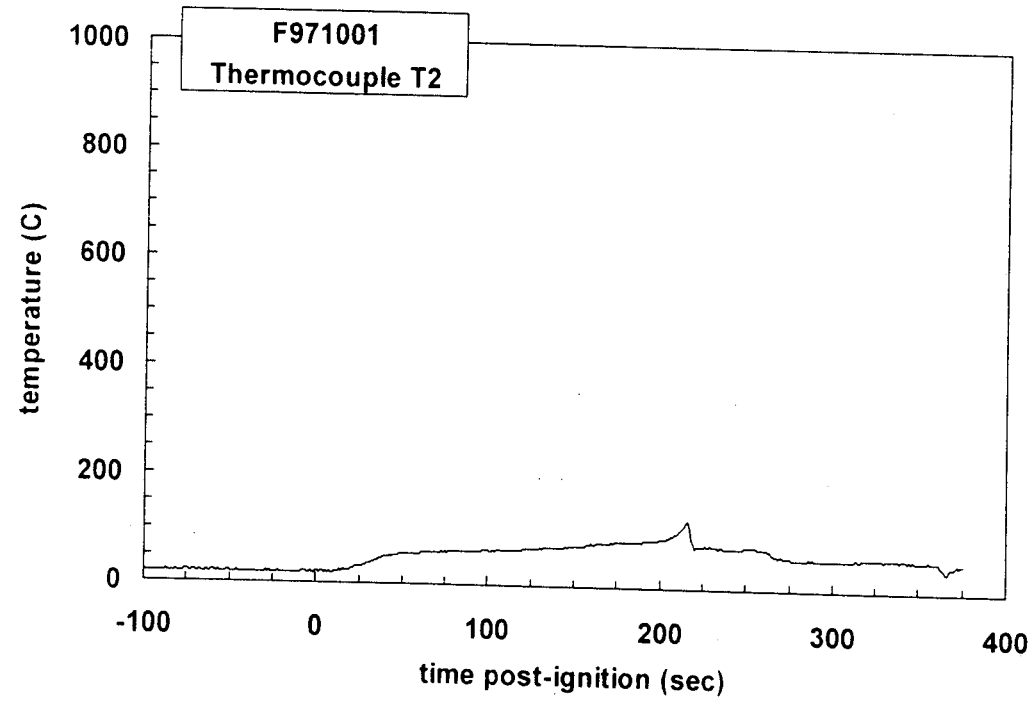

Plot C89. Fire Test F971001. Data plot from thermocouple T2.

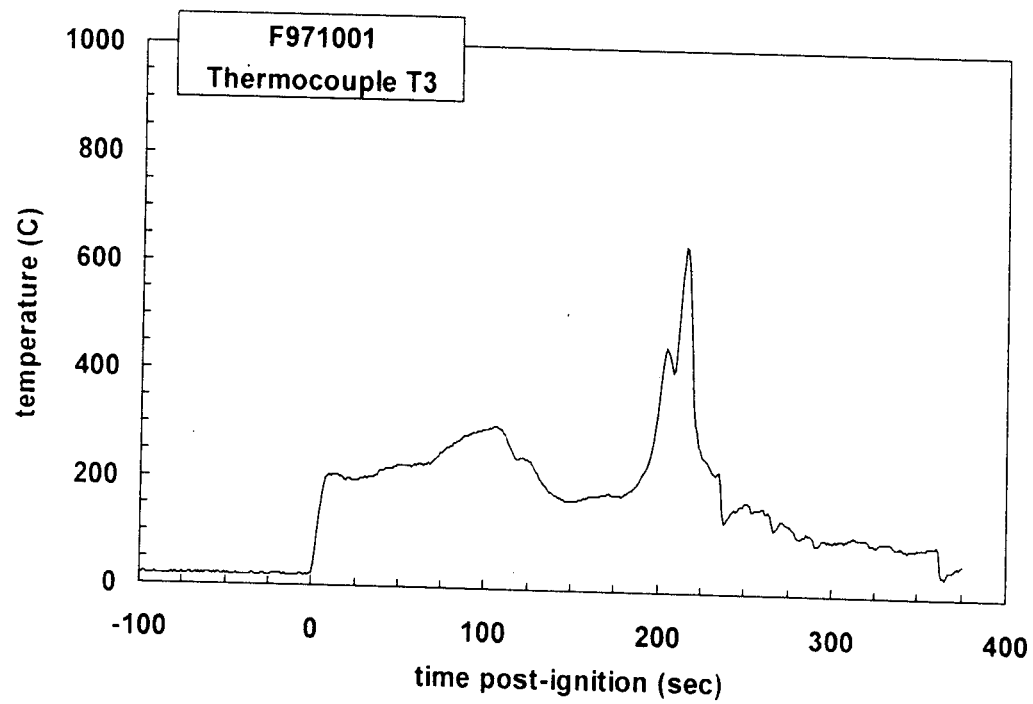

Plot C90. Fire Test F971001. Data plot from thermocouple T3.

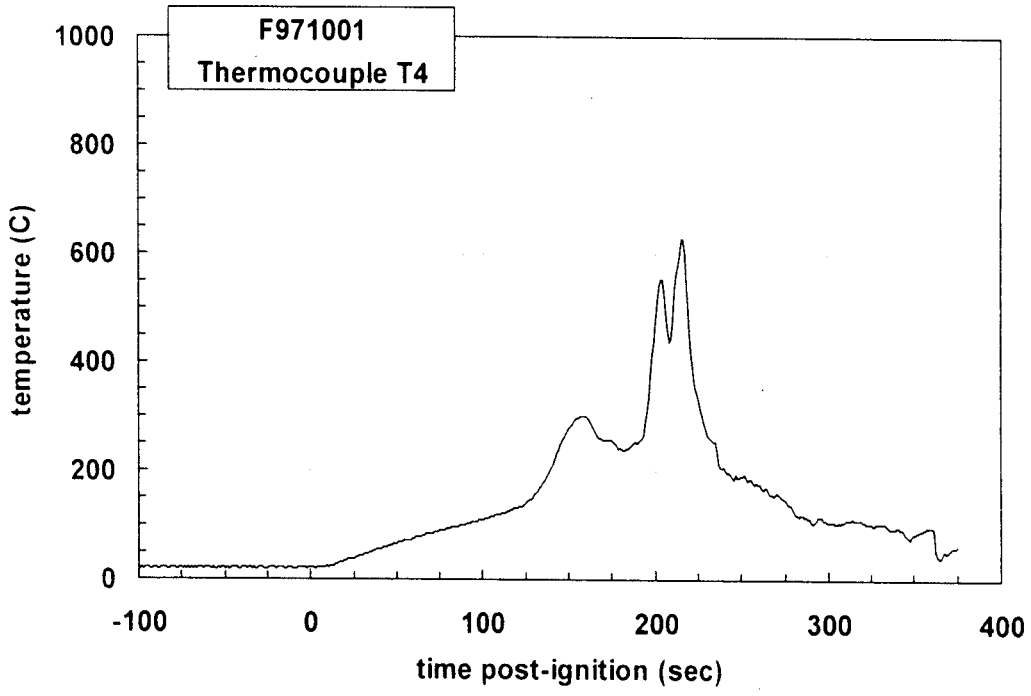

Plot C91. Fire Test F971001. Data plot from thermocouple T4.

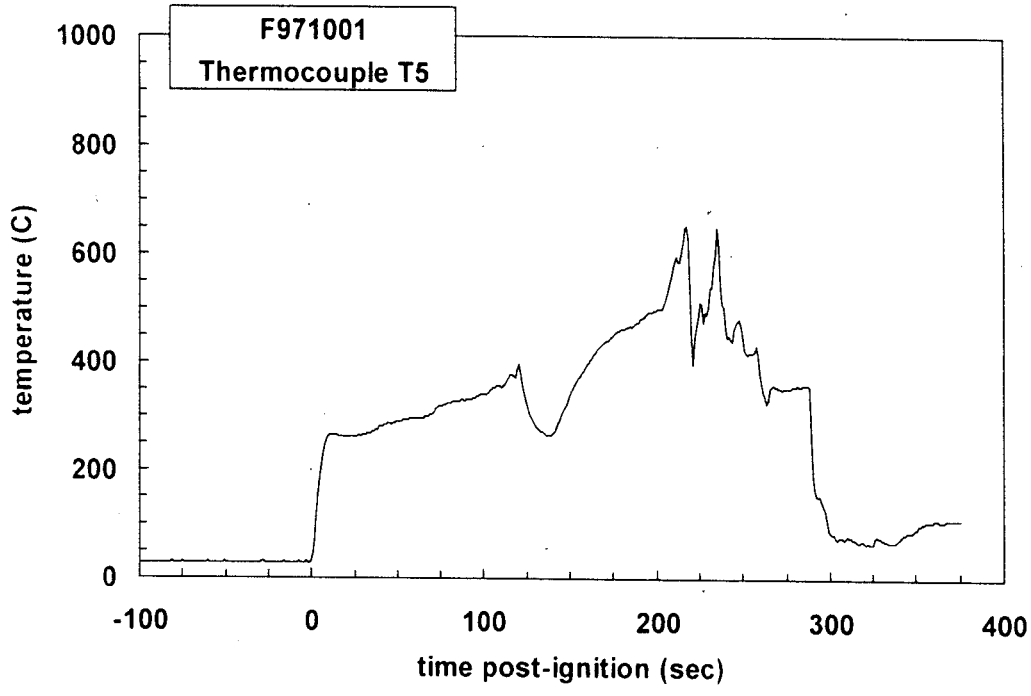

Plot C92. Fire Test F971001. Data plot from thermocouple T5.

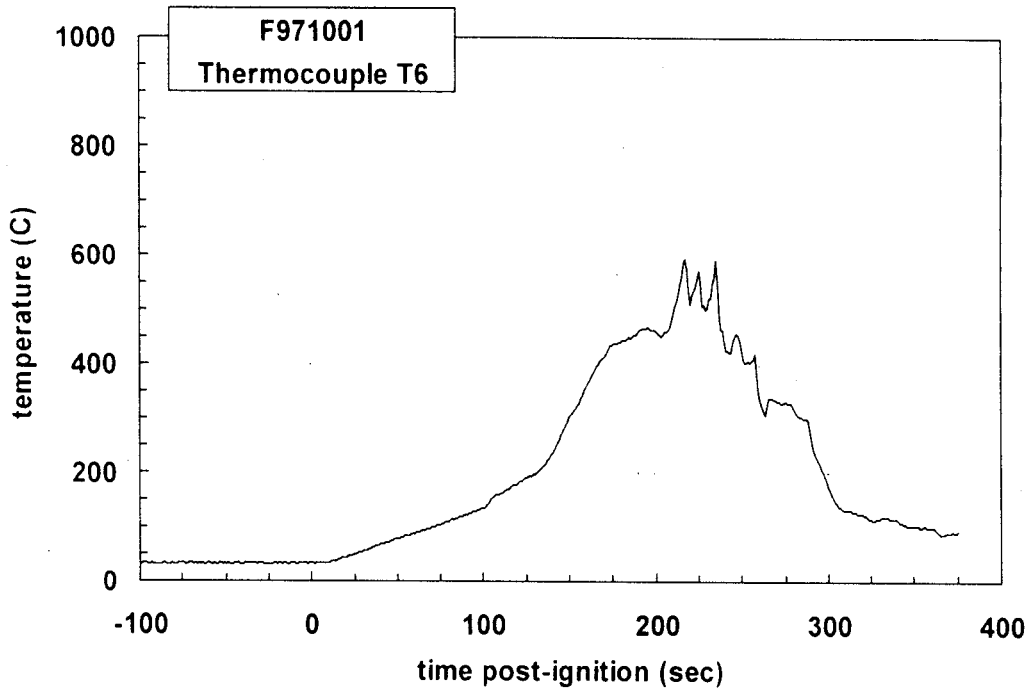

Plot C93. Fire Test F971001. Data plot from thermocouple T6.

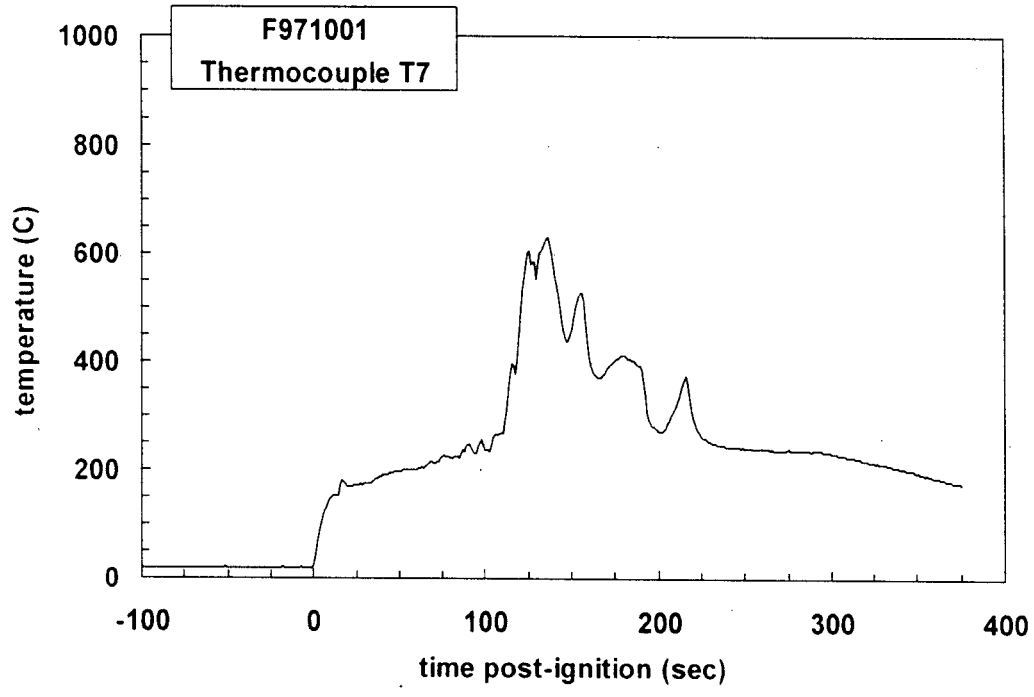

Plot C94. Fire Test F971001. Data plot from thermocouple T7.

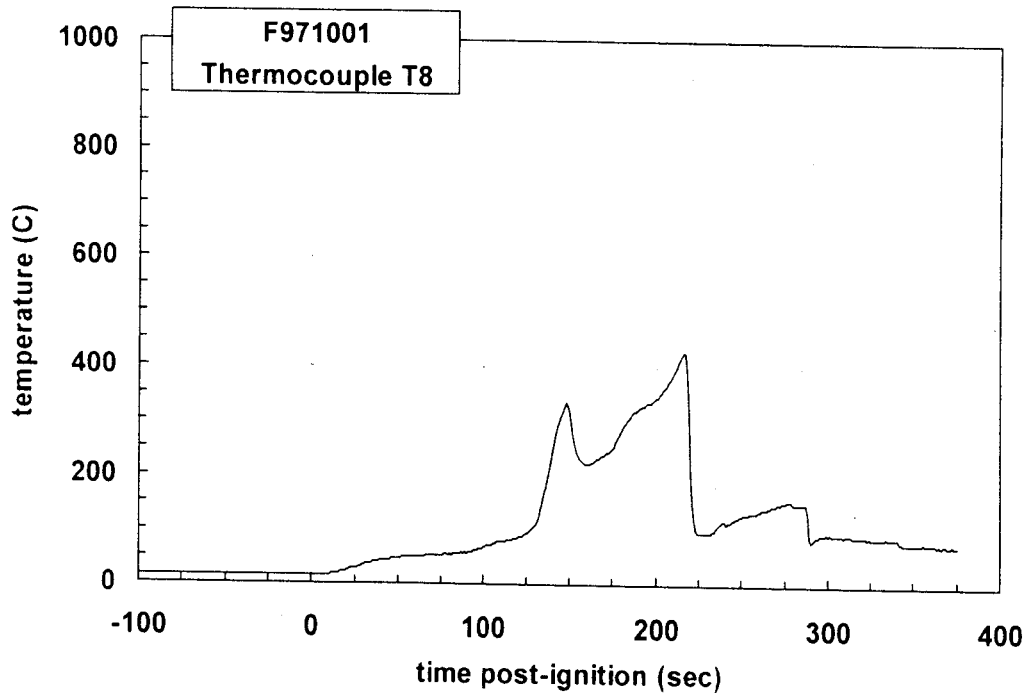

Plot C95. Fire Test F971001. Data plot from thermocouple T8.

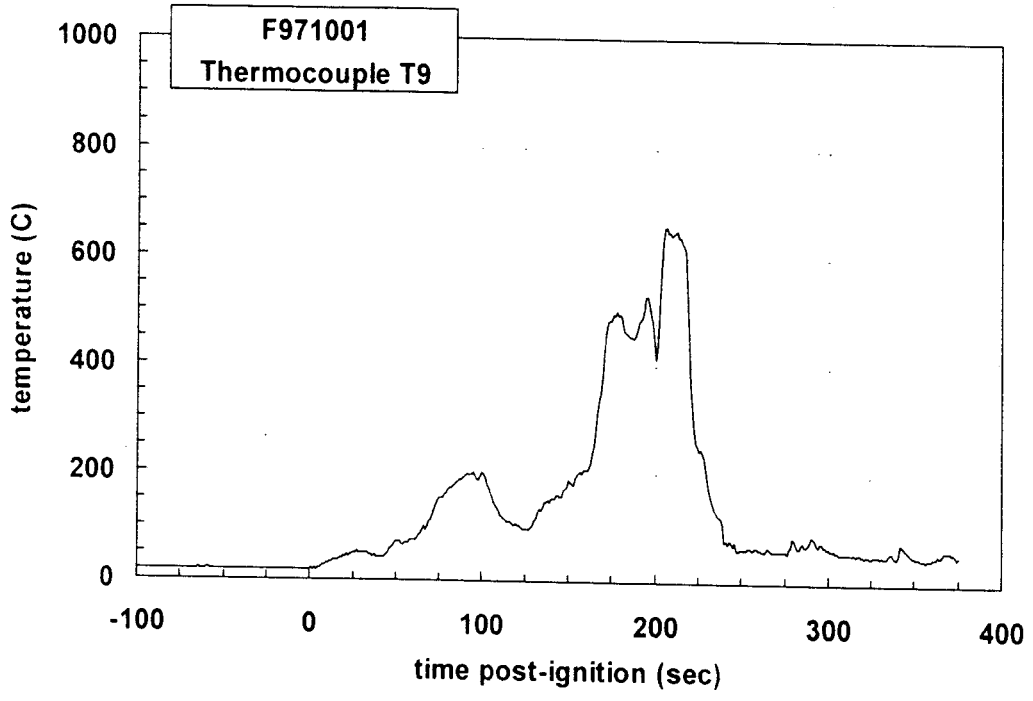

Plot C96. Fire Test F971001. Data plot from thermocouple T9.

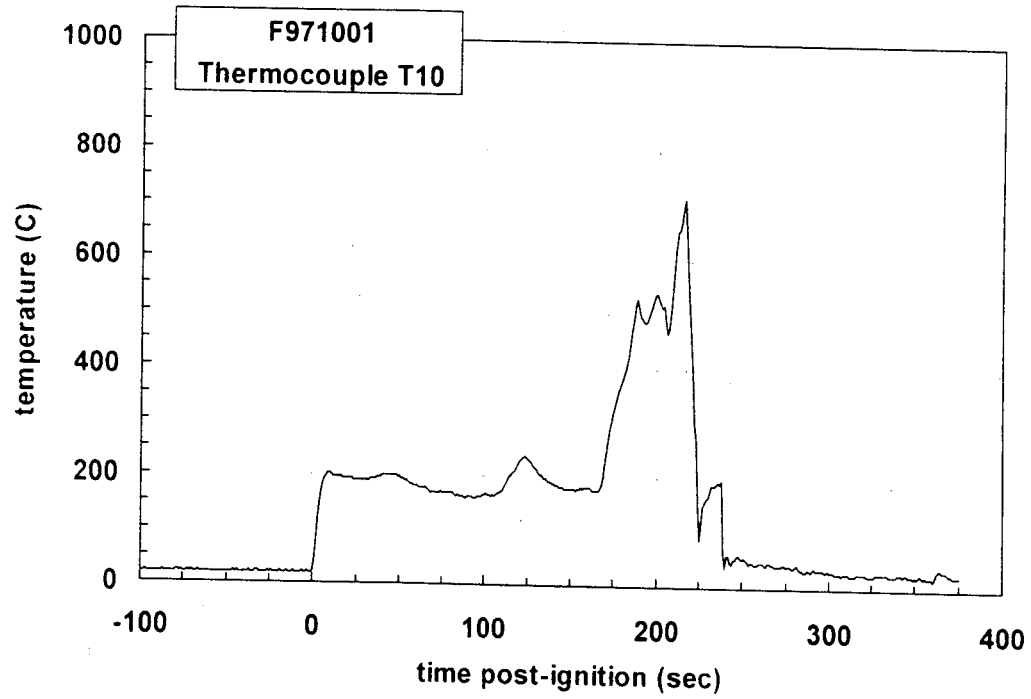

Plot C97. Fire Test F971001. Data plot from thermocouple T10.

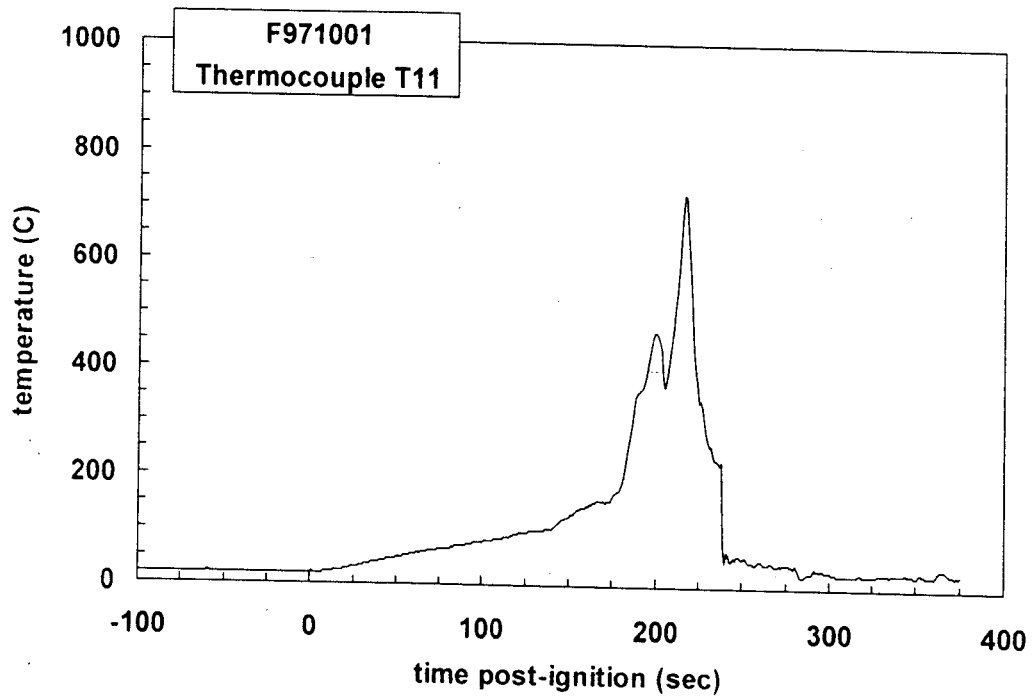

Plot C98. Fire Test F971001. Data plot from thermocouple T11.

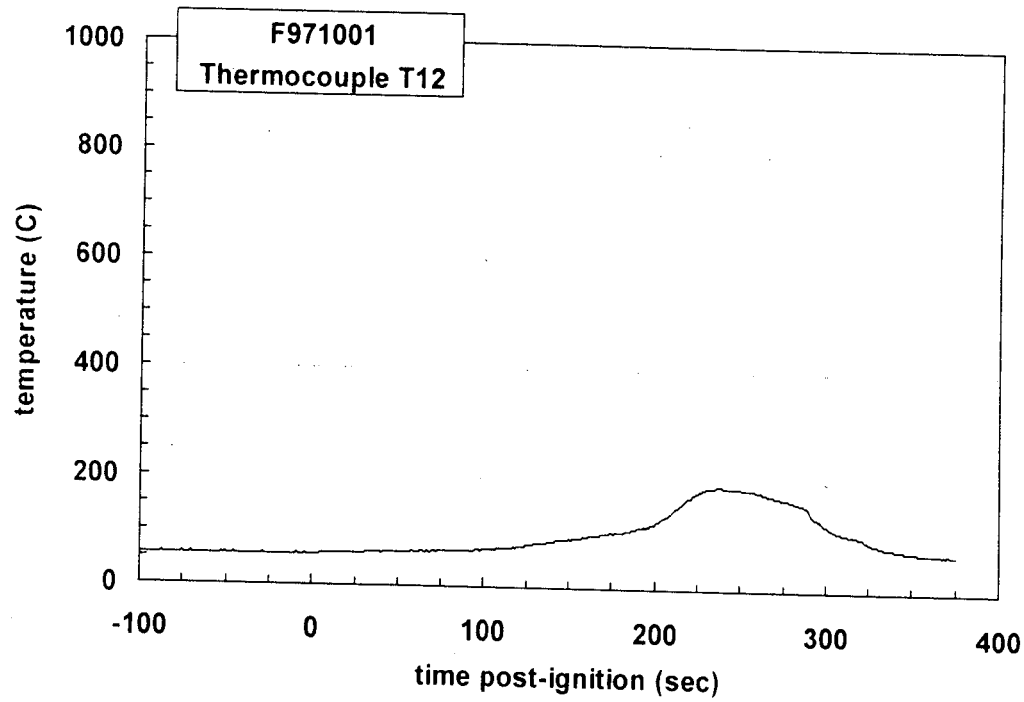

Plot C99. Fire Test F971001. Data plot from thermocouple T12.

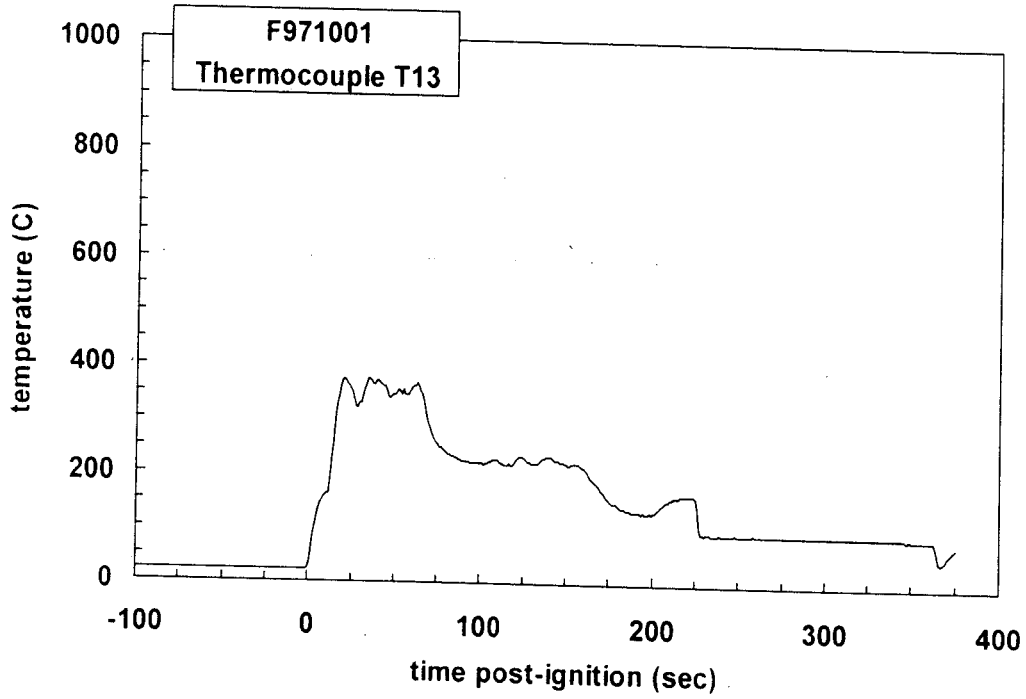

Plot C100. Fire Test F971001. Data plot from thermocouple T13.

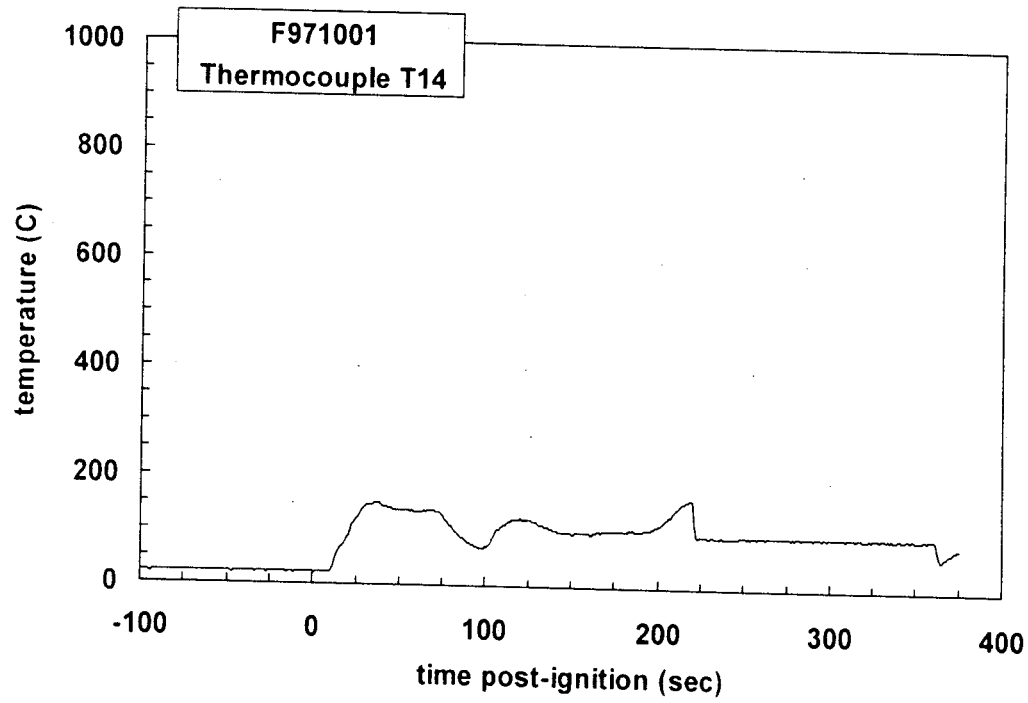

Plot C101. Fire Test F971001. Data plot from thermocouple T14.

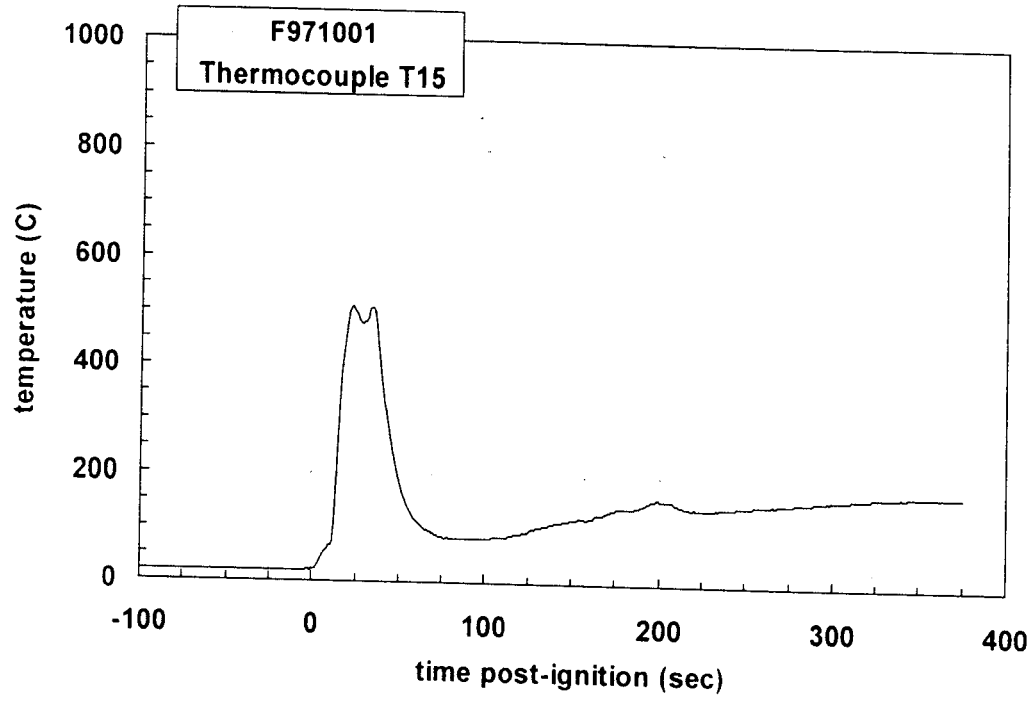

Plot C102. Fire Test F971001. Data plot from thermocouple T15.

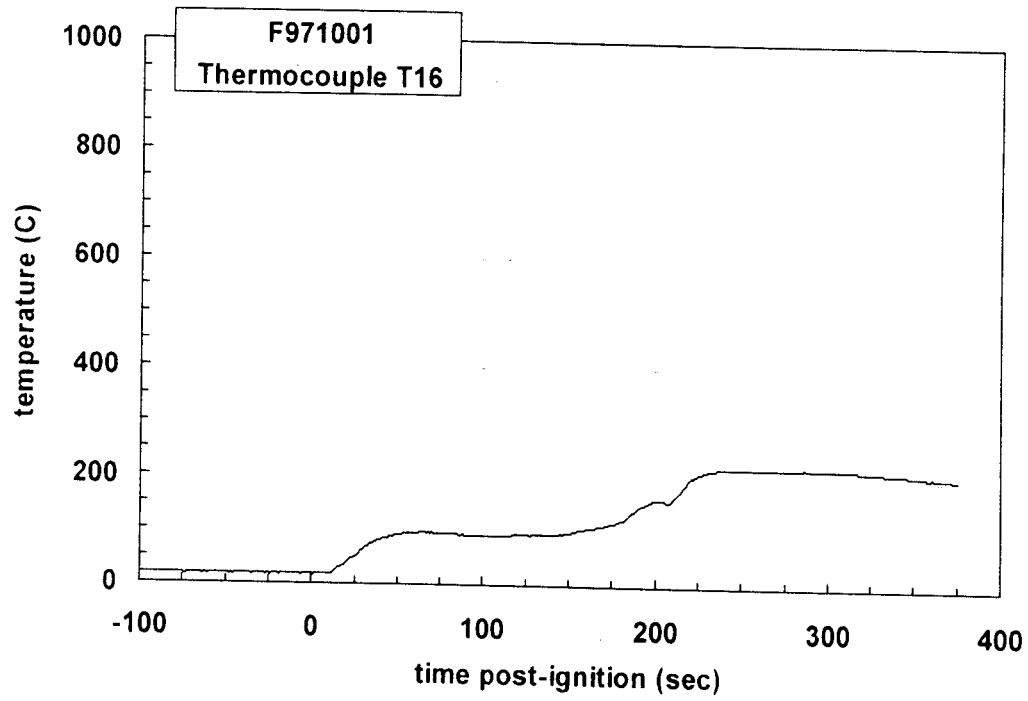

Plot C103. Fire Test F971001. Data plot from thermocouple T16.

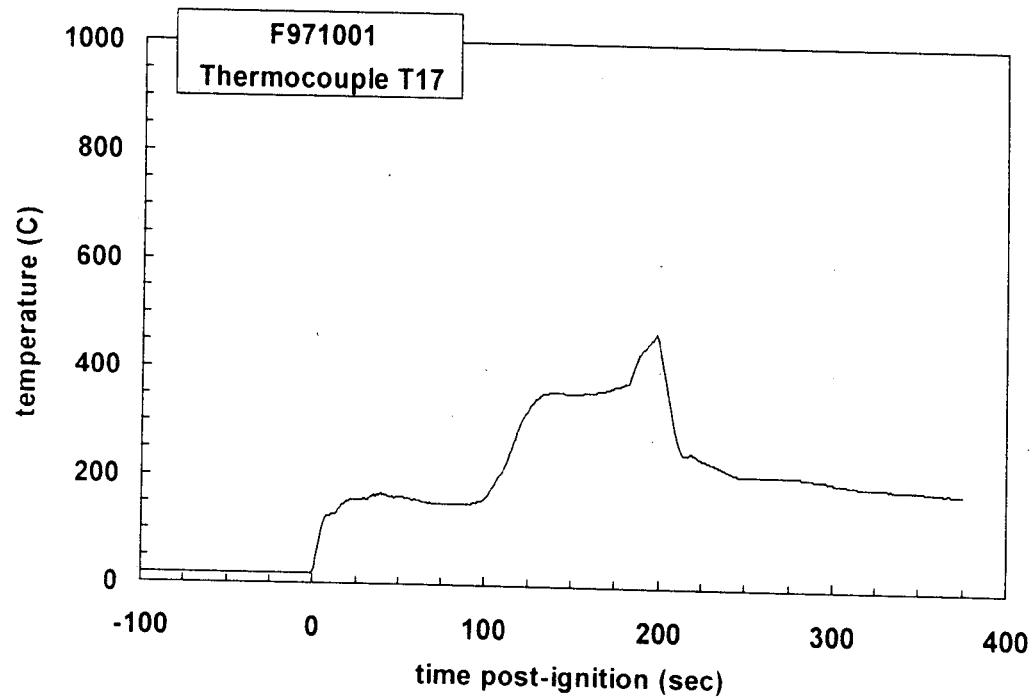

Plot C104. Fire Test F971001. Data plot from thermocouple T17.

APPENDIX D
ASPIRATED THERMOCOUPLE DATA

An aspirated thermocouple assembly (Medtherm Corporation) was installed in the test vehicle and used to measure air temperature at six elevations in the passenger compartment of the test vehicle during this test (Fig. D1). The aspirated thermocouple assembly was fabricated from Inconel 600 tubing. Each assembly consisted of a vertical manifold (o.d. = 0.375 in. (9.5 mm), i.d. = 0.25 in. (6.4 mm), length = 16 in. (406 mm)) with six horizontal radiation shields (o.d. = 0.25 in. (6.4 mm), i.d. = 0.19 in. (4.8 mm), length = 1.00 in. (25.4 mm)). The vertical spacing between the radiation shields along the manifold was 3 in. (75 mm). Three radial holes were drilled near the tip of each radiation shield. The holes were sized to approximately balance the airflow-rates over each thermocouple. A Type-N thermocouple inserted into each radiation shield so that the thermocouple junction was positioned approximately 0.2 in. (5.1 mm) down-stream from the inlet holes.

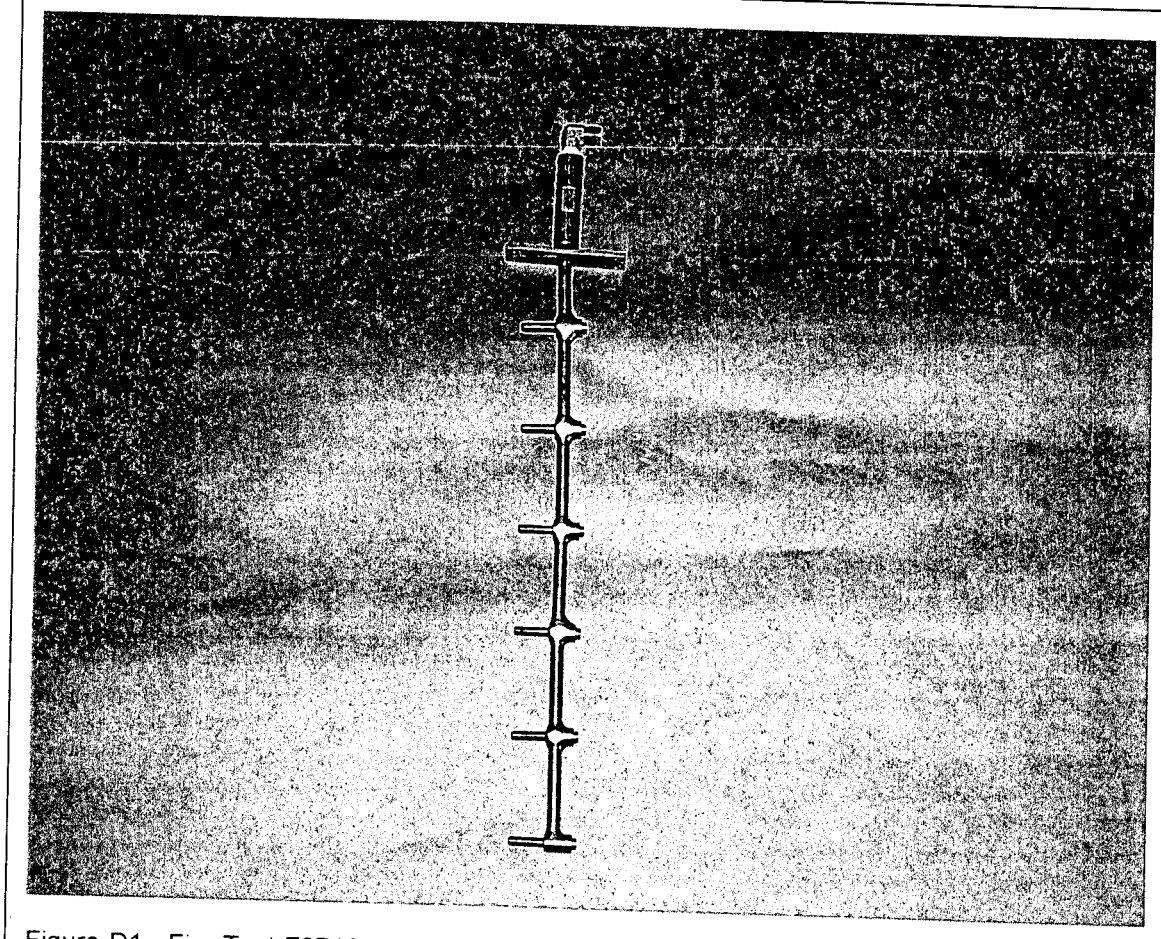

Figure D1. Fire Test F971001. Photograph of the aspirated thermocouple assembly used in the passenger compartment of the test vehicle.

The mounting flange of the aspirated thermocouple probe assembly was attached to the roof of the vehicle. The probe extended into the passenger compartment through a hole in the roof so that all 6 thermocouples were located below the headliner. The probe was vertical and located along the longitudinal mid-line of the vehicle approximately equidistant from the driver and passenger seats. The upper-most aspirated thermocouple was approximately 0.5 in. (12 mm) below the lower surface of the headliner. The manifold was connected to a rotary-vane pump with flexible copper tubing (o.d. = 0.5 in. (12 mm), length = 15 ft. (4.6 m)). The capacity of the pump was 50 L/min at atmospheric pressure. The pump was mistakenly not turned on during the test, and there was no forced airflow into the radiation shields and over the thermocouples. Therefore, all data acquired from Thermocouples ASP1 through ASP6 is invalid [C1 and C2] and was not used in the discussion of this test.

Figures D2 and D3 show the approximate location of the aspirated thermocouple probe assembly in the test vehicle for this test.

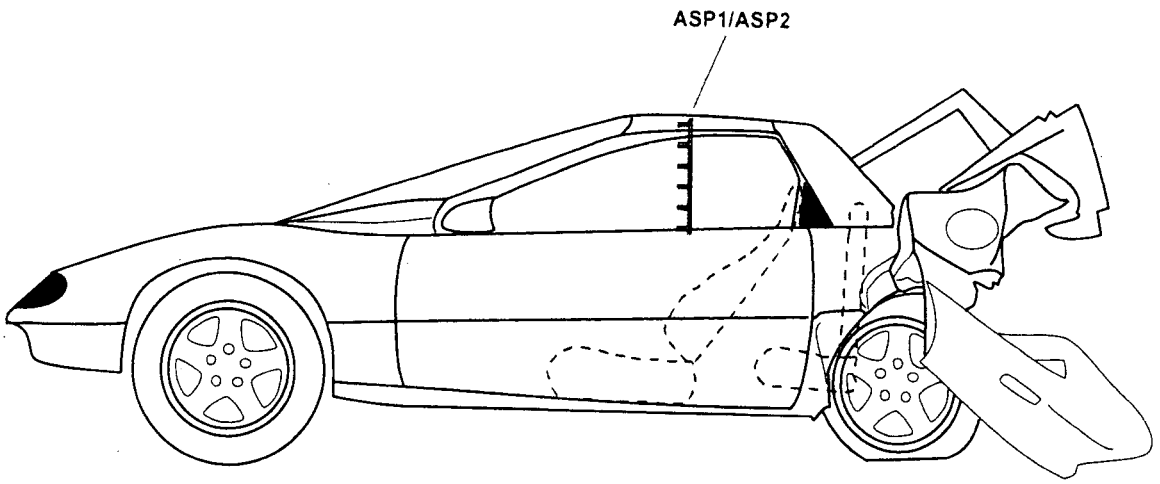

Figure D2. Fire Test F971001. Side view of the test vehicle showing the approximate location of the aspirated thermocouple probe assembly in the passenger compartment.

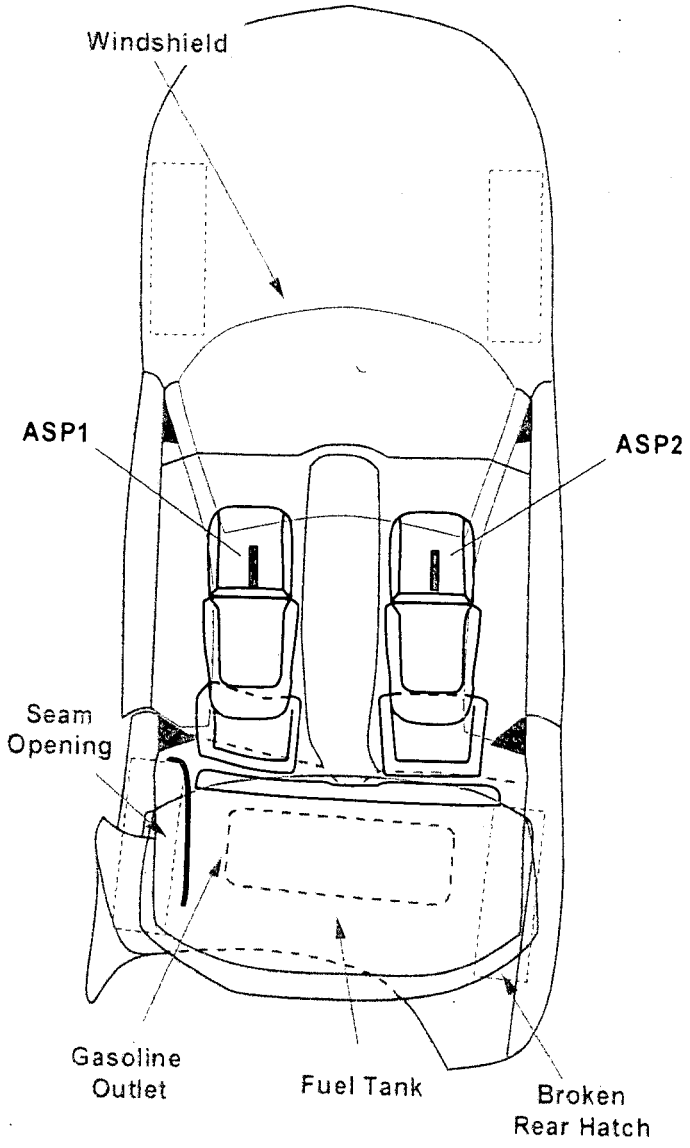

Figure D3. Fire Test F971001. Top view of the test vehicle showing the approximate location of the aspirated thermocouple probe assembly in the passenger compartment.

REFERENCES

D1. J. S. Newman and P. A. Croce. A simple aspirated thermocouple for use in fires. *J. Fire Flamm.* **10**:326-336 (1979).

D2. N. R. Keltner and K. A. Strom. Thermal Measurement Uncertainty and Compensation. Paper in preparation.

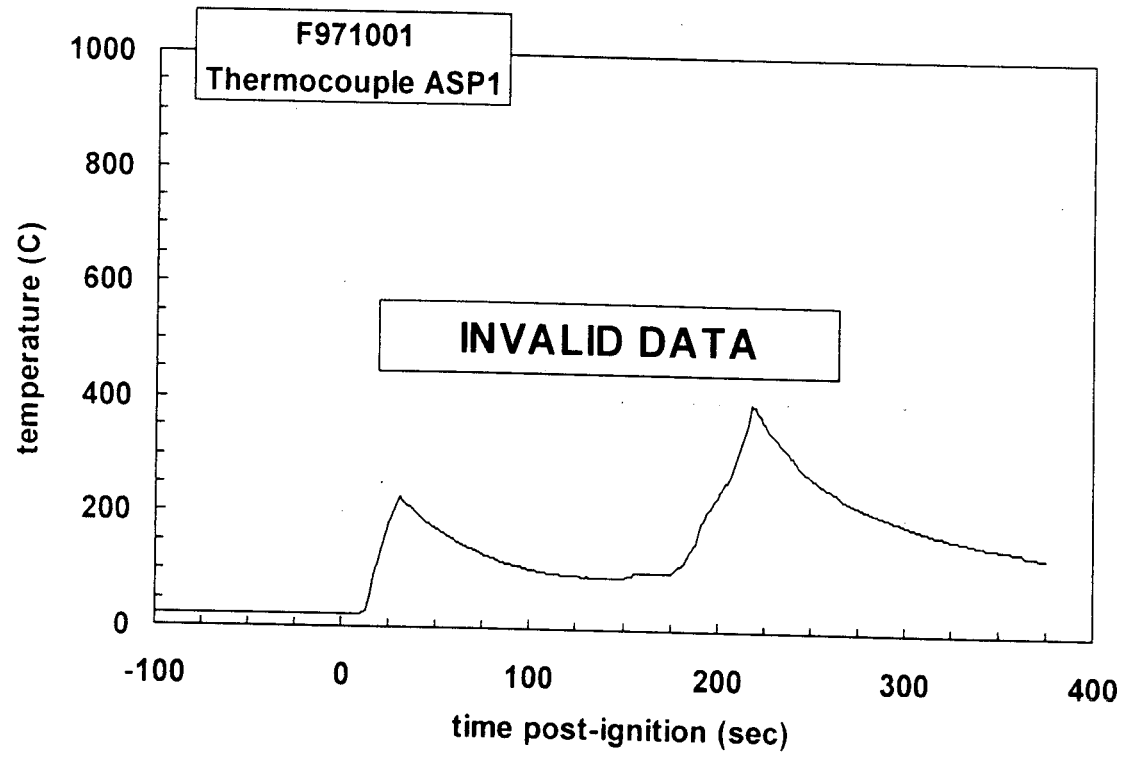

Plot D1. Fire Test F971001. Data plot from thermocouple ASP1.

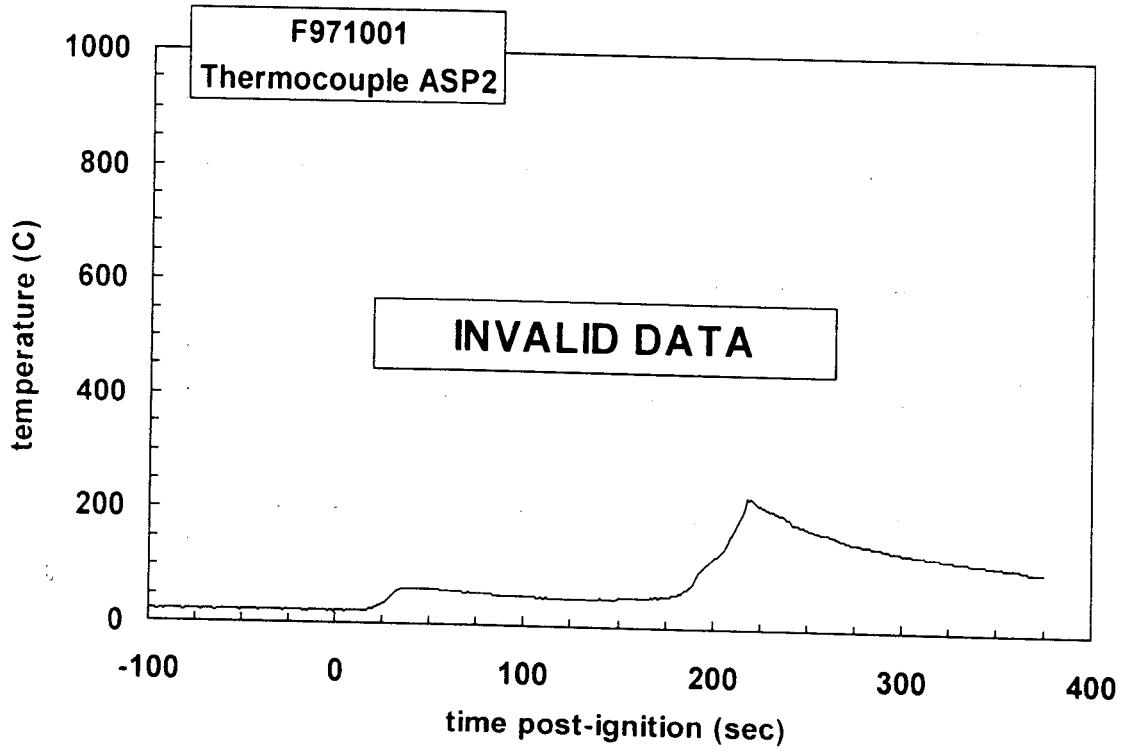

Plot D2. Fire Test F971001. Data plot from thermocouple ASP2.

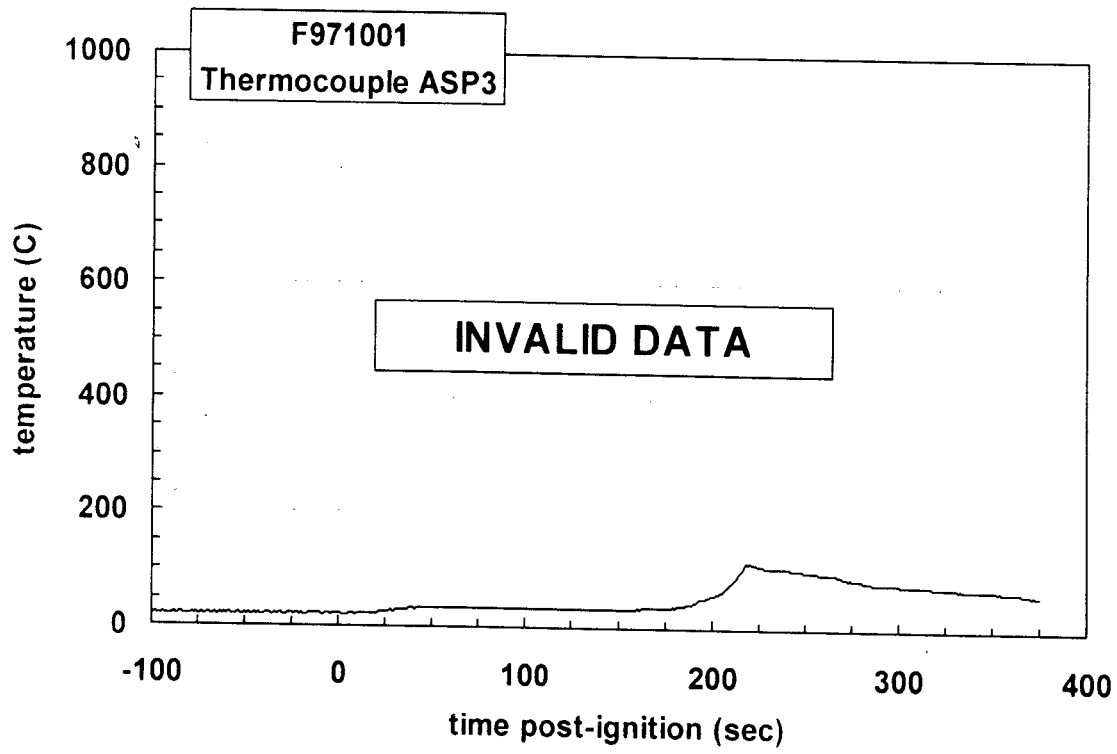

Plot D3. Fire Test F971001. Data plot from thermocouple ASP3.

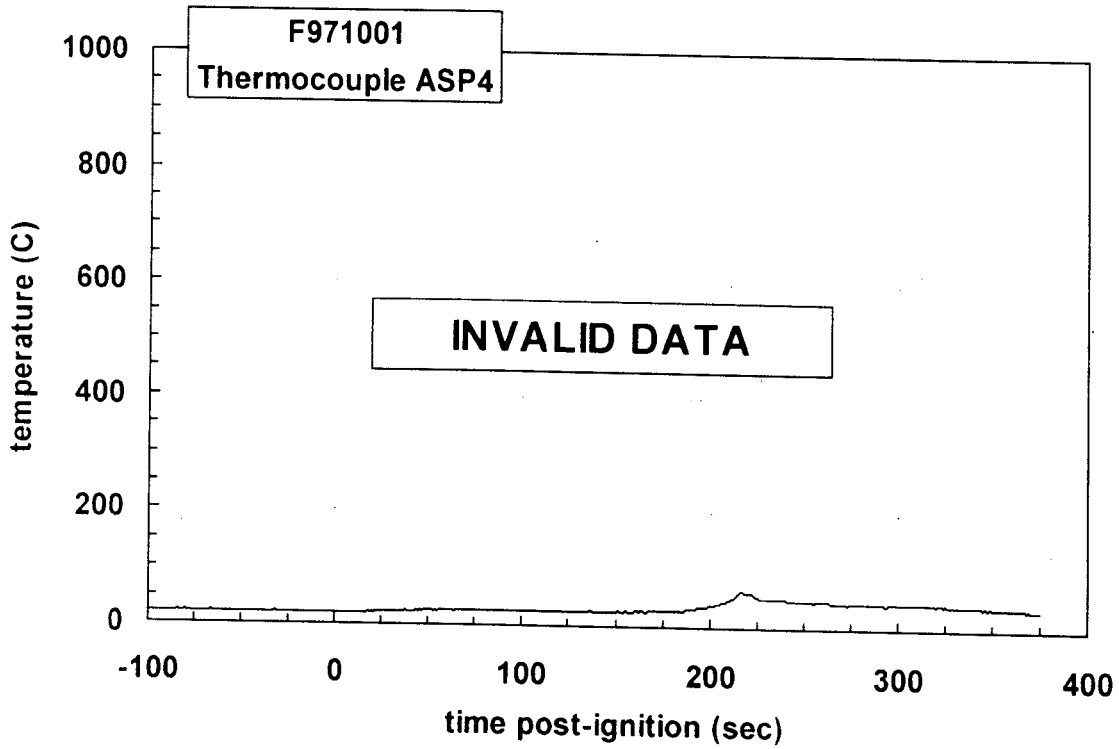

Plot D4. Fire Test F971001. Data plot from thermocouple ASP4.

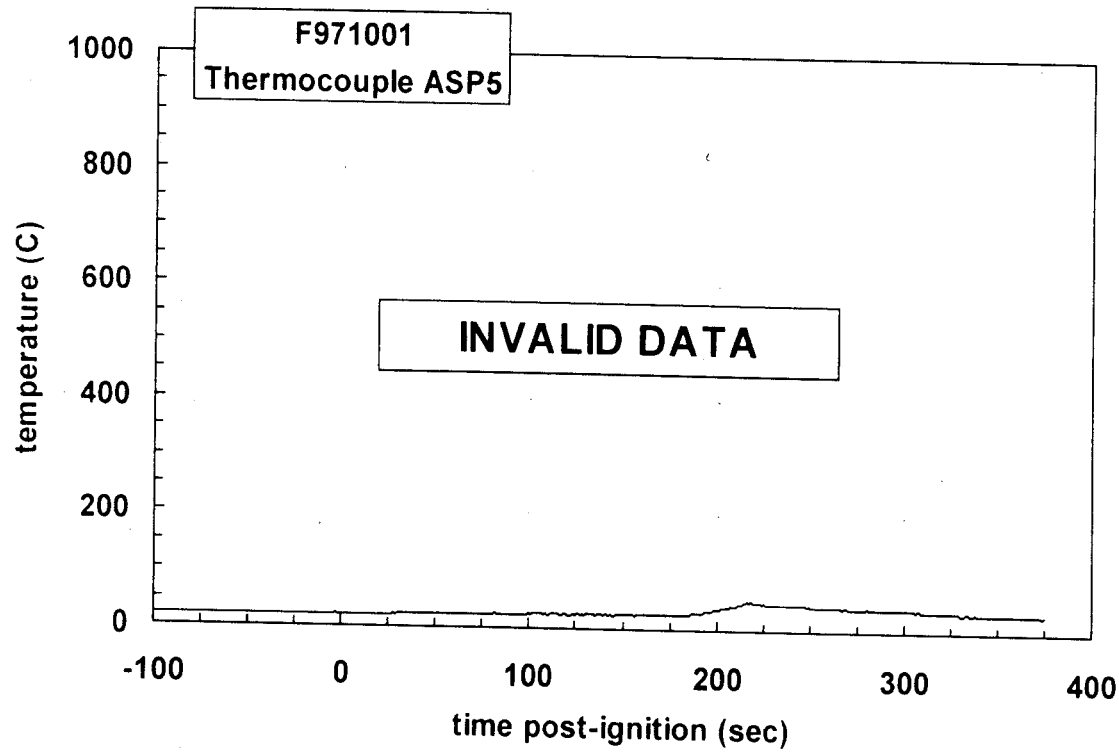

Plot D5. Fire Test F971001. Data plot from thermocouple ASP5.

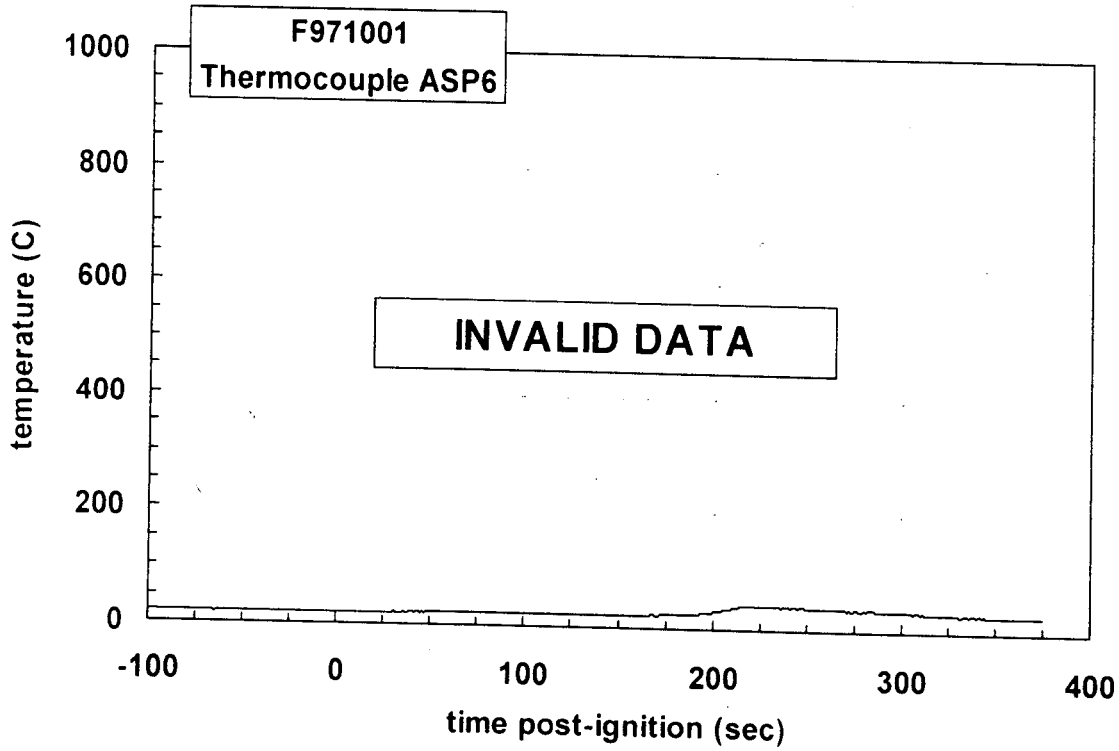

Plot D6. Fire Test F971001. Data plot from thermocouple ASP6.

APPENDIX E
HEAT FLUX TRANSDUCER/RADIOMETER DATA

Heat-flux transducer/radiometer assemblies (64 Series, Medtherm Corporation) were used to measure convective and radiative heat transfer to selected objects in the vehicle. Each assembly contained two Schmidt-Boelter thermopiles in a water-cooled copper body (diameter = 1 in. (25.4 mm), length = 1 in. (25.4 mm)). The faces of the heat flux transducers were coated with high-temperature optical black paint. The radiometers had permanent sapphire windows (view-angle = 150°; optical transmittance range 0.4 to 4.2 μm). Both transducers were calibrated to 100 kW/m^2 at a reference temperature of 25°C.

The PC-based data system used to acquire data from the thermocouples (**APPENDIX C**) also was used to acquire data from the heat flux transducers and radiometers. The electrical signal wires from these transducers terminated in a 5-pin circular connector (165 Series, Amphenol). Each connector was plugged into a panel-mounted jack, which was hard wired to an analog-input multiplex expansion card (DBK-12, IOTech, Inc., Cleveland, OH). As with the thermocouples, the electrical shields on the signal cables were connected to the electronic chassis grounds on the analog-input expansion cards. The data acquisition software (DASYLab) was configured to sample each channel at a rate of 10 Hz and store the data in 10-point block averages.

Figures E1 through E4 show the approximate locations of heat flux transducer/radiometer assemblies in the test vehicle. For HFT/RAD assemblies mounted through the floor pan, a clearance-hole was drilled in the metal bulkhead and the transducer was mounted on stand-offs so that the face of the transducer was flush with the exterior metal surface. HFT/RAD assemblies located above the front seats were mounted to threaded rods (diameter = ½ in.) inserted through holes in the roof. The lower end of each rod was wired to the seat cushion to stabilize the transducers during the test. Copper tubing (o.d. = 0.25 in. (6.4 mm)) was used for the cooling water supply and waste lines. The temperature of the water supplied to the HFT/RAD assemblies was approximately 80°C, and the flow rate of water through each body was approximately 100 mL/min.

Data recorded from these transducers is shown in Plots E1 through E12.

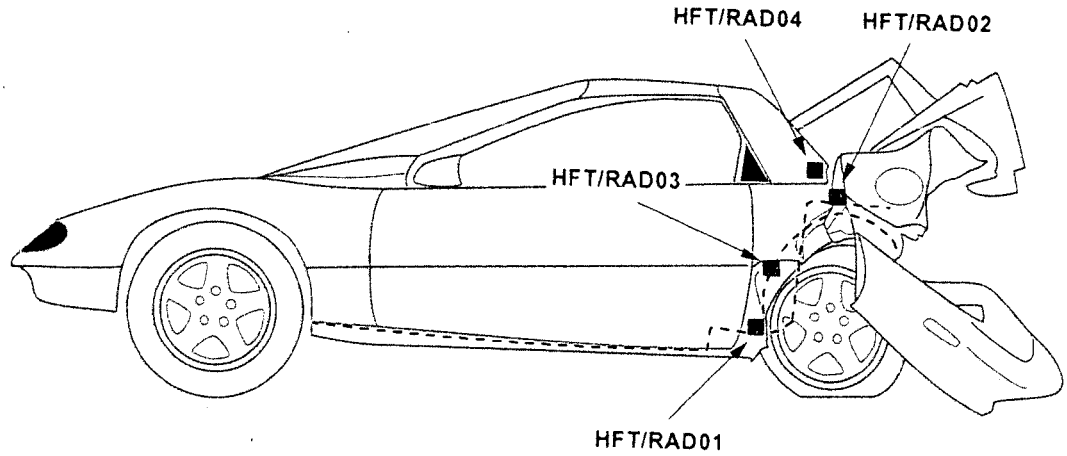

Figure E1. Fire Test F971001. Side view of the test vehicle showing the approximate locations of heat flux transducer/radiometer (HFT/RAD) assemblies mounted to the body of the test vehicle. HFT/RAD01 was mounted to the floorpan under the rear left seat cushion and facing downward. HFT/RAD02 was mounted to the floorpan above the rear left wheel and facing downward. HFT/RAD03 was mounted in the seam opening between the floorpan and rear left wheelhouse panel and facing rearward. HFT/RAF04 was located just behind the rear seat back and facing rearward. It was mounted on a bracket on the section of the rear floorpan panel behind the rear seat back along the longitudinal centerline of the test vehicle.

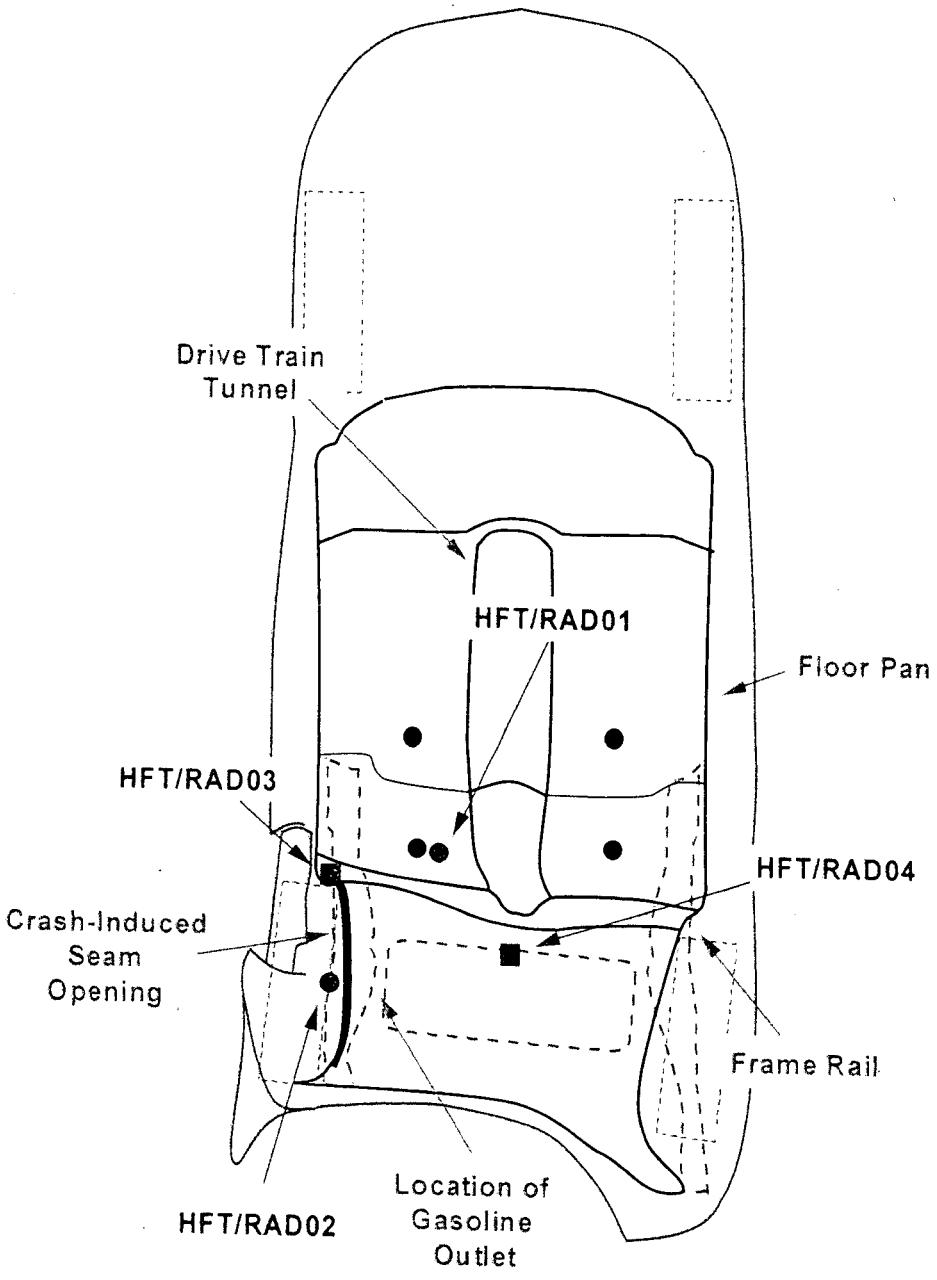

Figure E2. Fire Test F971001. Top view of the test vehicle showing the approximate locations of heat flux transducer/radiometer (HFT/RAD) assemblies mounted to the body of the test vehicle. See the caption to Figure E1 for more detailed description of the location of each transducer.

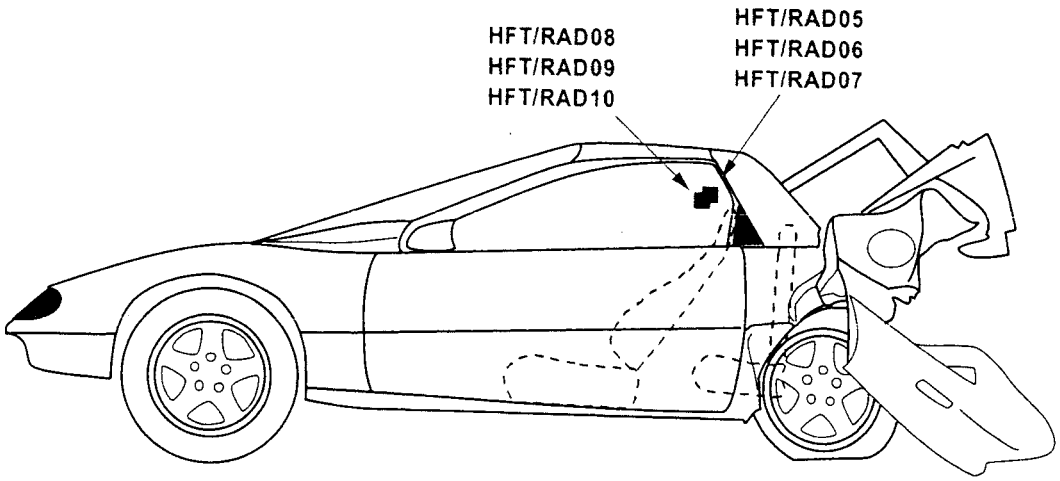

Figure E3. Fire Test F971001. Side view of the test vehicle showing the approximate locations of heat flux transducer/radiometer (HFT/RAD) assemblies located above the front seats of the test vehicle. HFT/RAD05 was located above the left front seat approximately 30 inches above the seat cushion and facing upward. HFT/RAD06 was located above the left front seat approximately 30 inches above the seat cushion and facing rearward. HFT/RAD07 was located above the left front seat approximately 30 inches above the seat cushion and facing toeard the rear left corner of the test vehicle. HFT/RAD08 was located above the right front seat approximately 30 inches above the seat cushion and facing upward. HFT/RAD09 was located above the lright front seat approximately 30 inches above the seat cushion and facing rearward. HFT/RAD10 was located above the right front seat approximately 30 inches above the seat cushion and facing toward the rear left corner of the test vehicle.

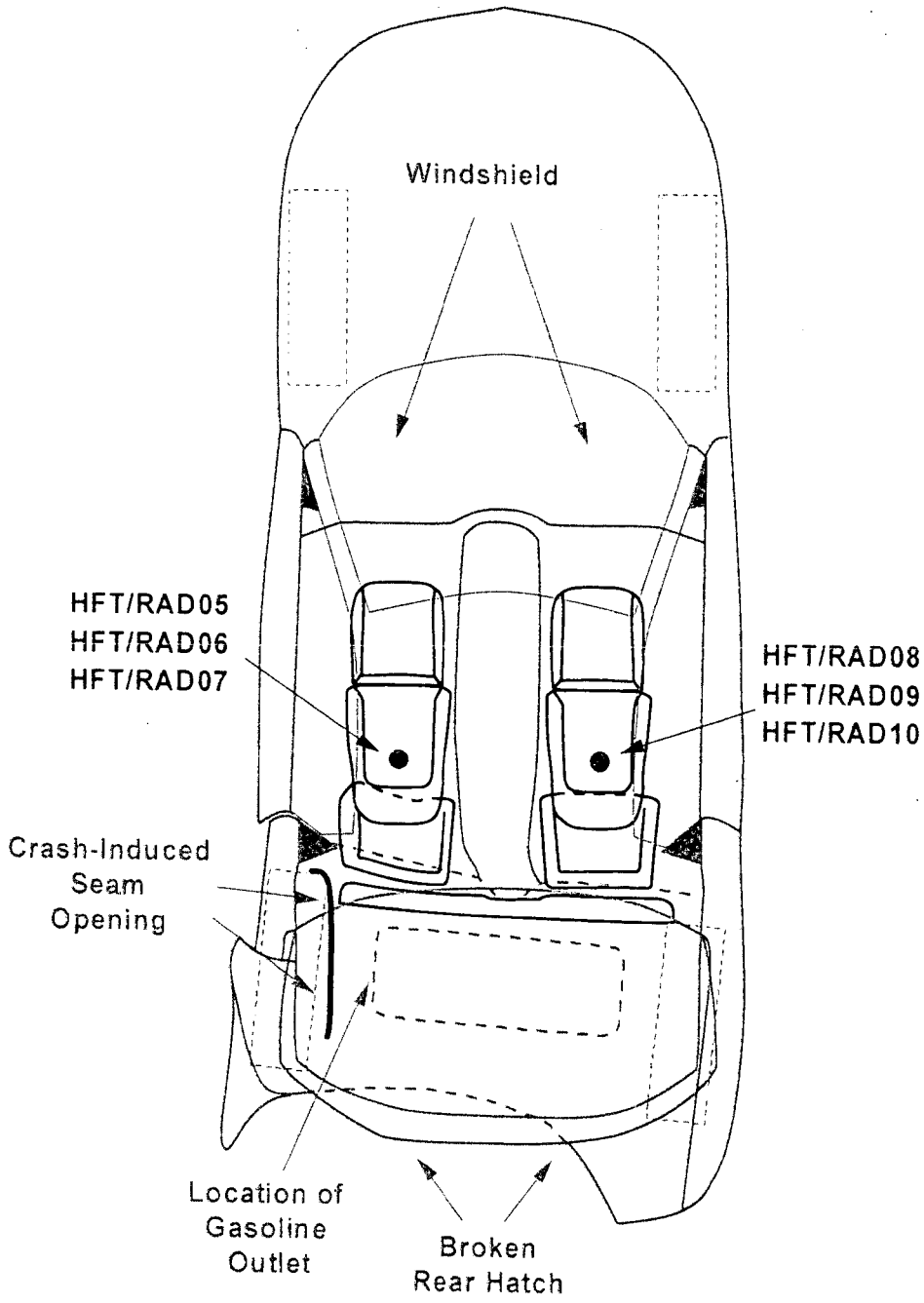

Figure E4. Fire Test F971001. Top view of the test vehicle showing the approximate locations of heat flux transducer/radiometer (HFT/RAD) assemblies located above the front seats of the test vehicle. See the caption to Figure E2 for more detailed description of the location of each transducer.

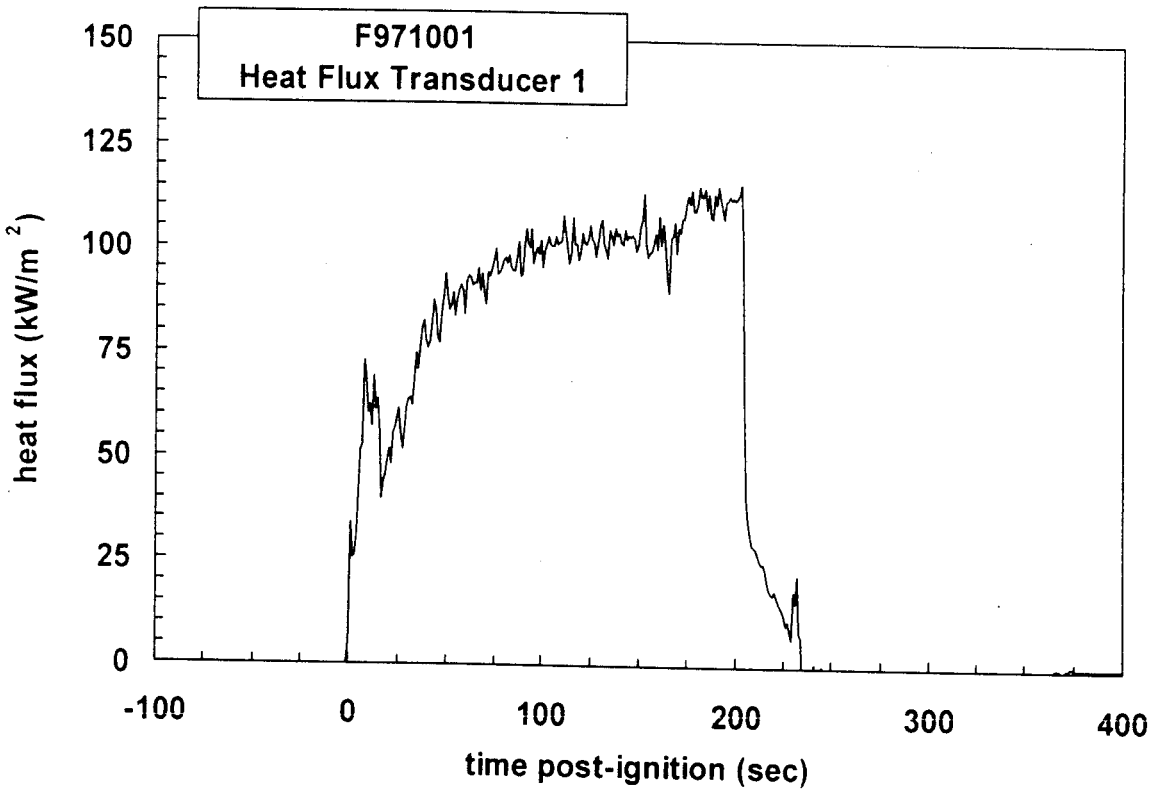

Plot E1. Fire Test F971001. Data plot from Heat Flux Transducer 1.

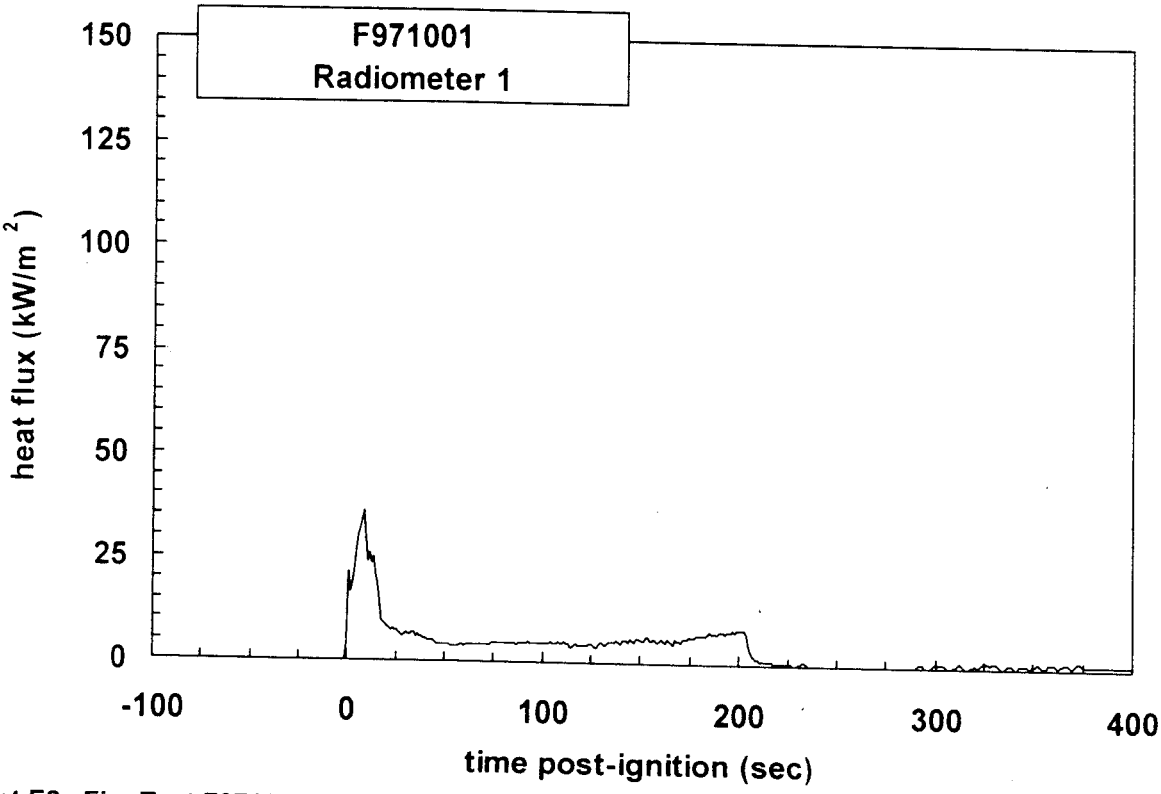

Plot E2. Fire Test F971001. Data plot from Radiometer 1.

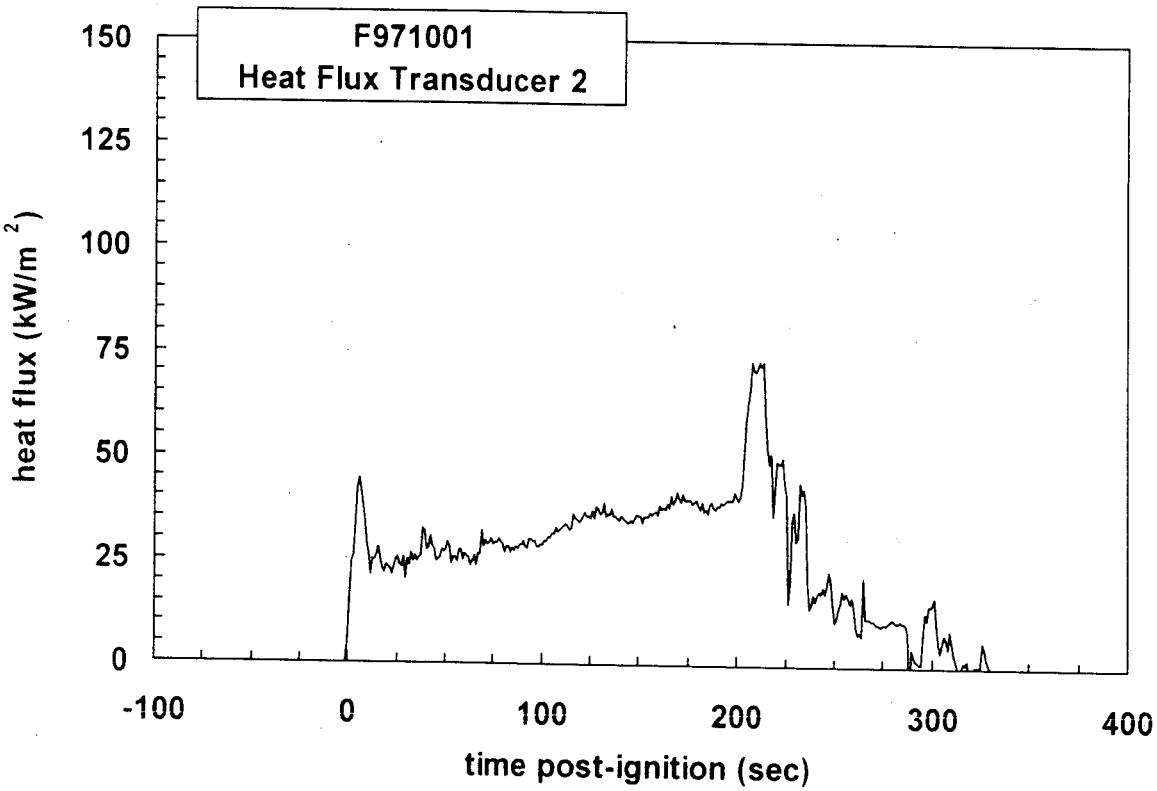

Plot E3. Fire Test F971001. Data plot from Heat Flux Transducer 2.

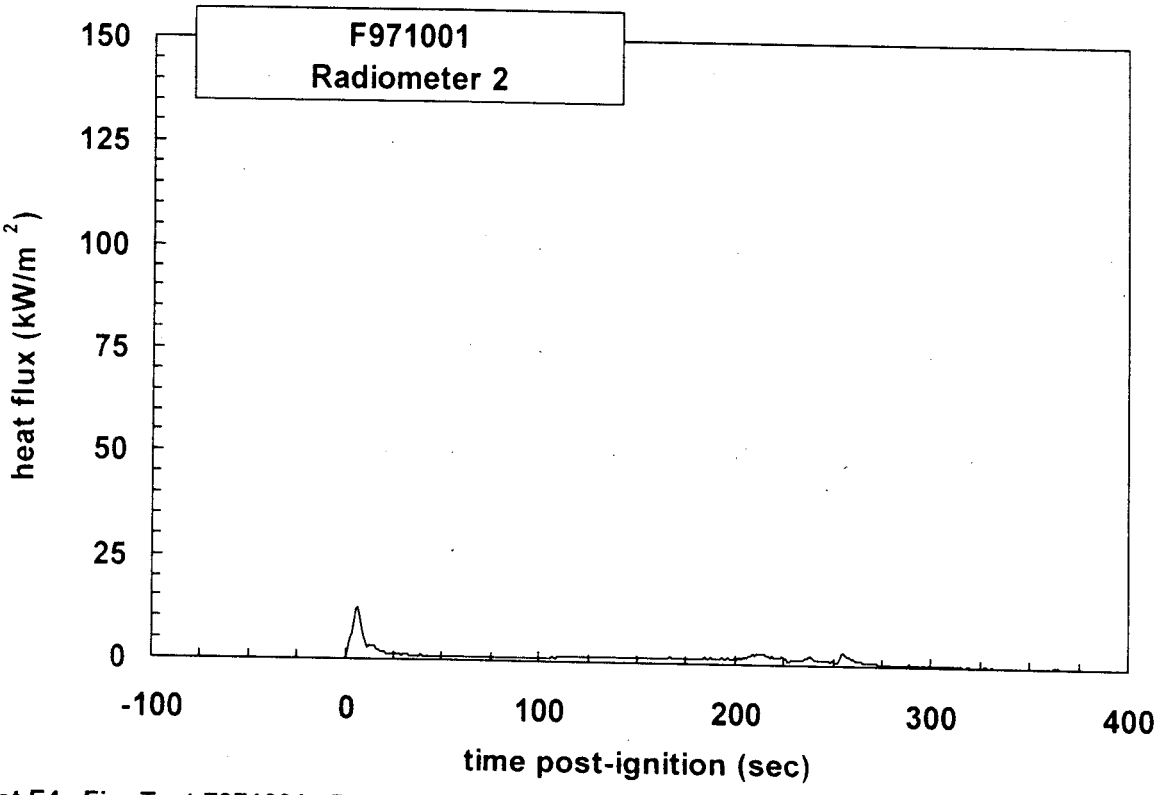

Plot E4. Fire Test F971001. Data plot from Radiometer 2.

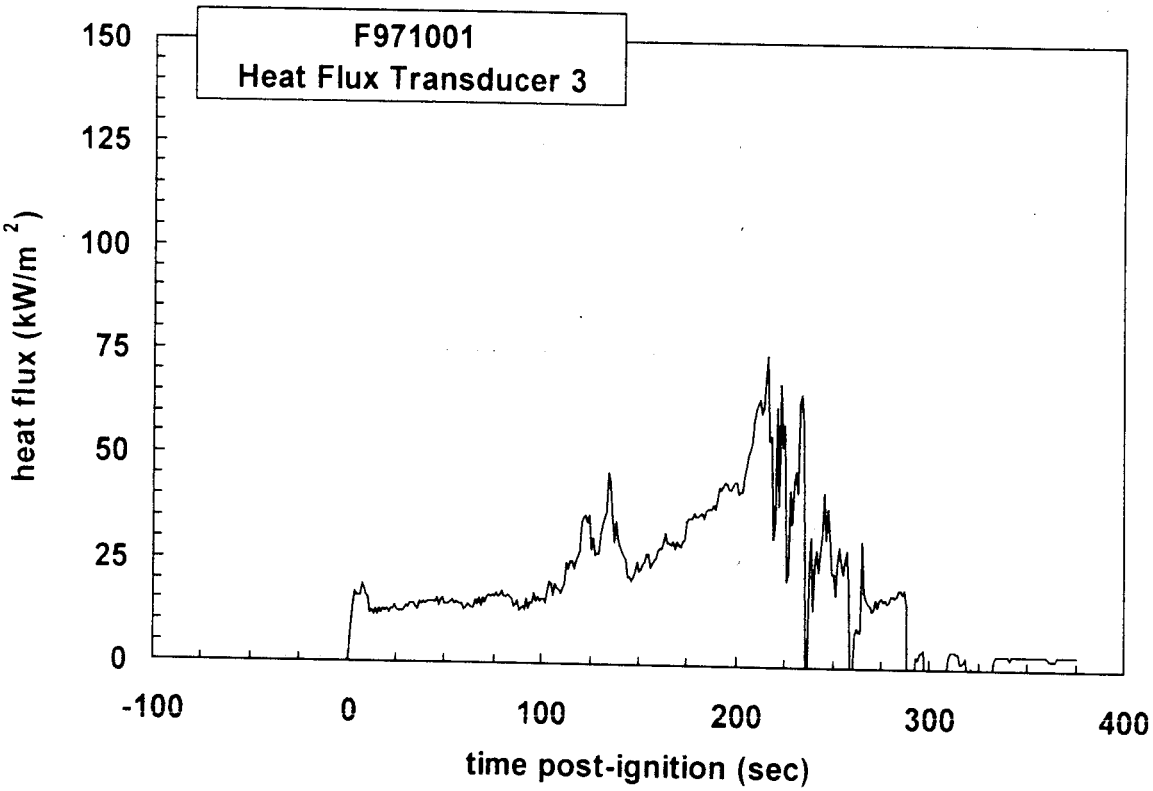

Plot E5. Fire Test F971001. Data plot from Heat Flux Transducer 3.

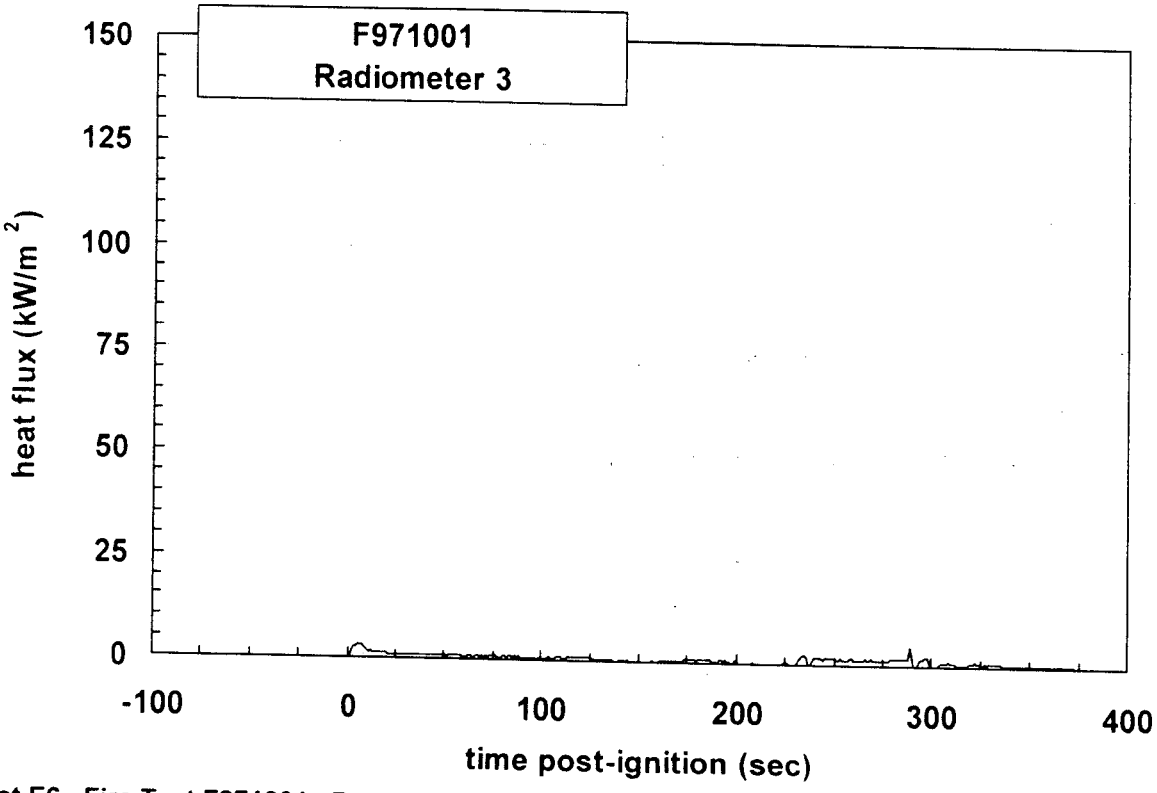

Plot E6. Fire Test F971001. Data plot from Radiometer 3.

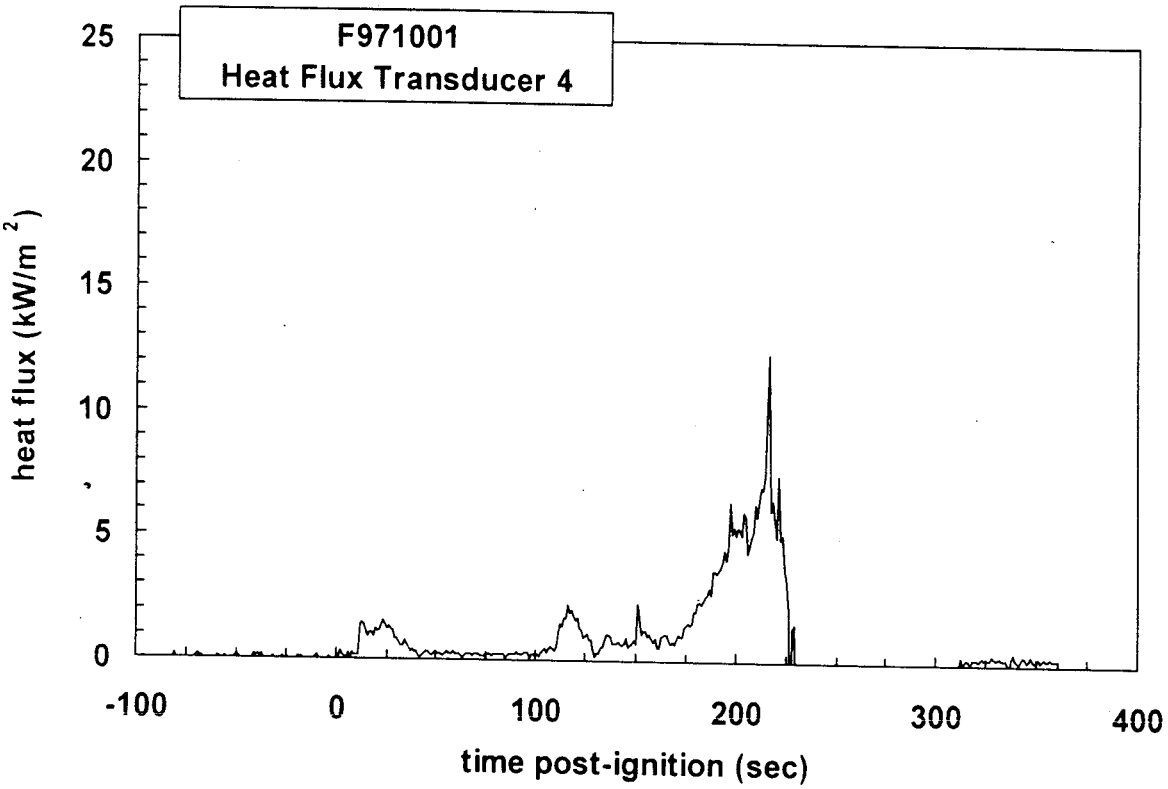

Plot E7. Fire Test F971001. Data plot from Heat Flux Transducer 4.

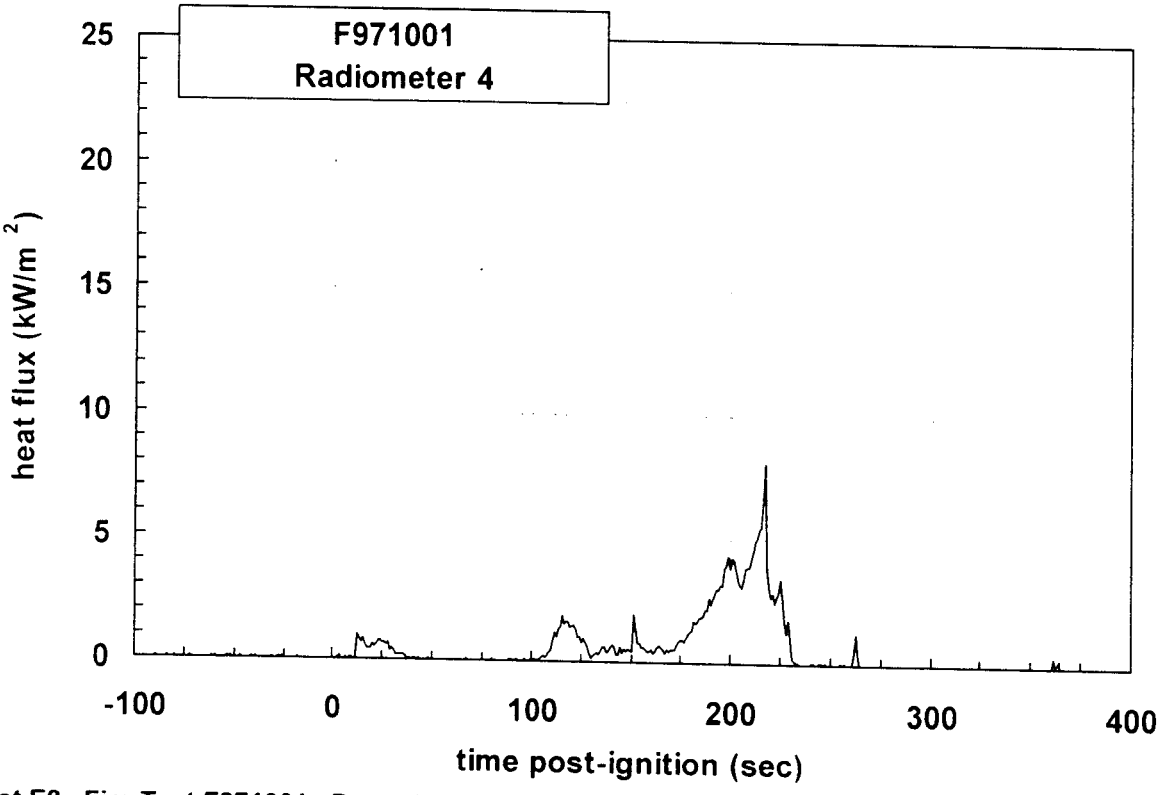

Plot E8. Fire Test F971001. Data plot from Radiometer 4.

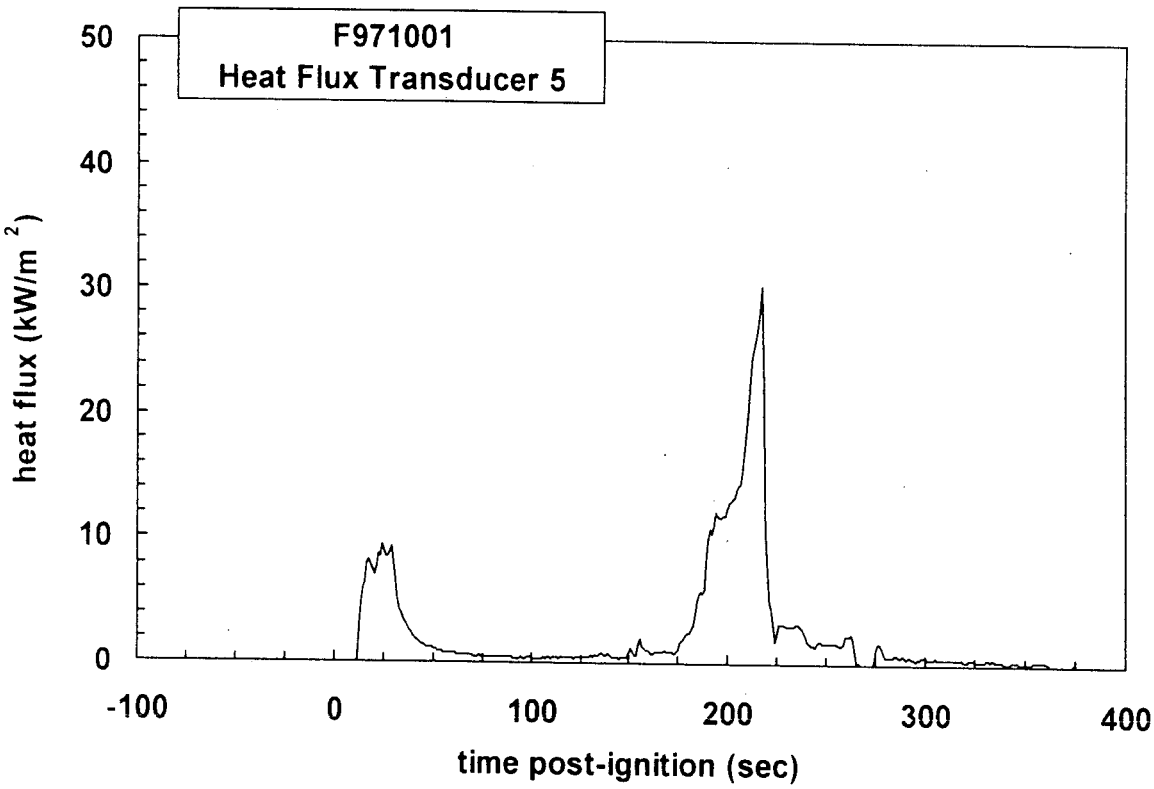

Plot E9. Fire Test F971001. Data plot from Heat Flux Transducer 5.

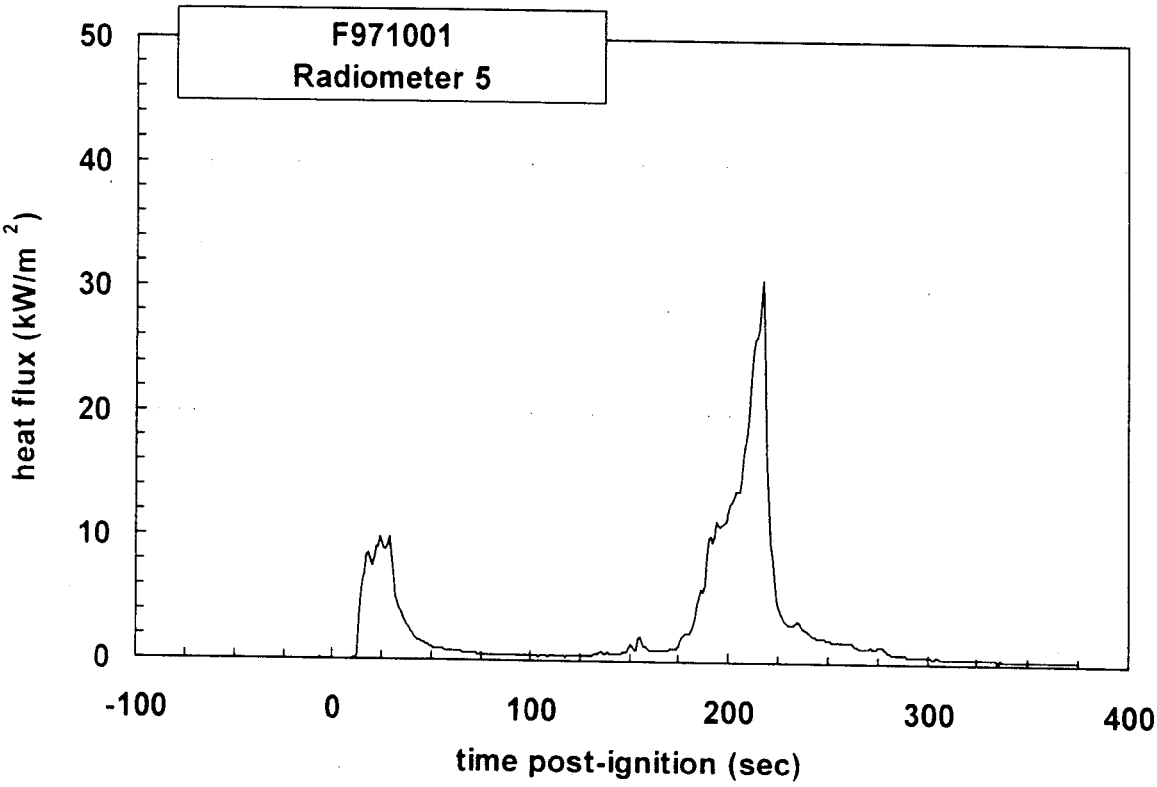

Plot E10. Fire Test F971001. Data plot from Radiometer 5.

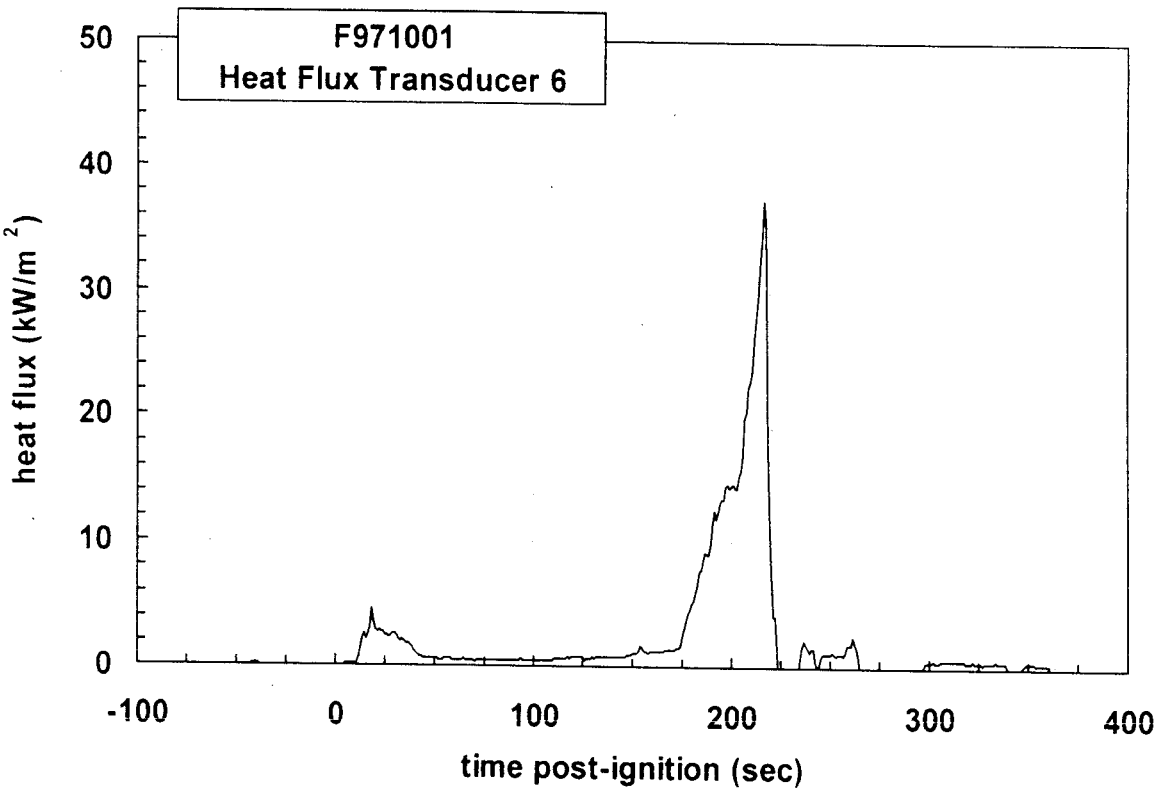

Plot E11. Fire Test F971001. Data plot from Heat Flux Transducer 6.

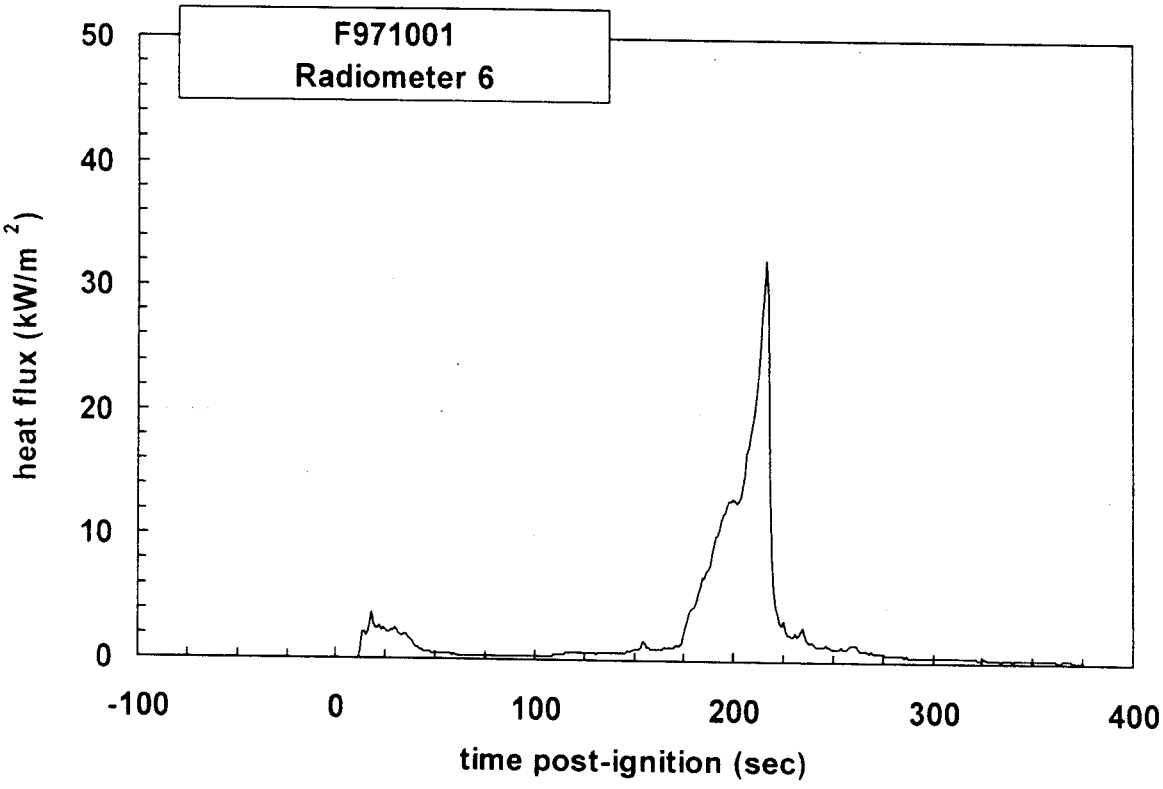

Plot E12. Fire Test F971001. Data plot from Radiometer 6.

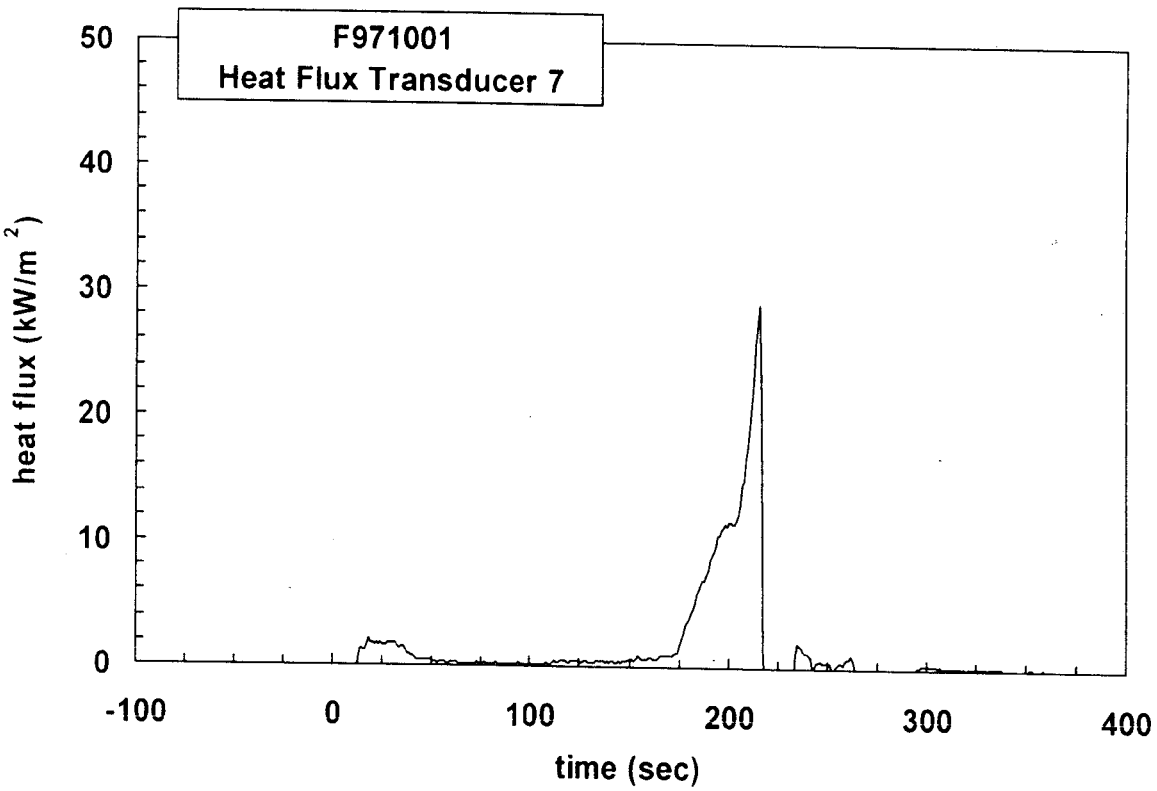

Plot E13. Fire Test F971001. Data plot from Heat Flux Transducer 7.

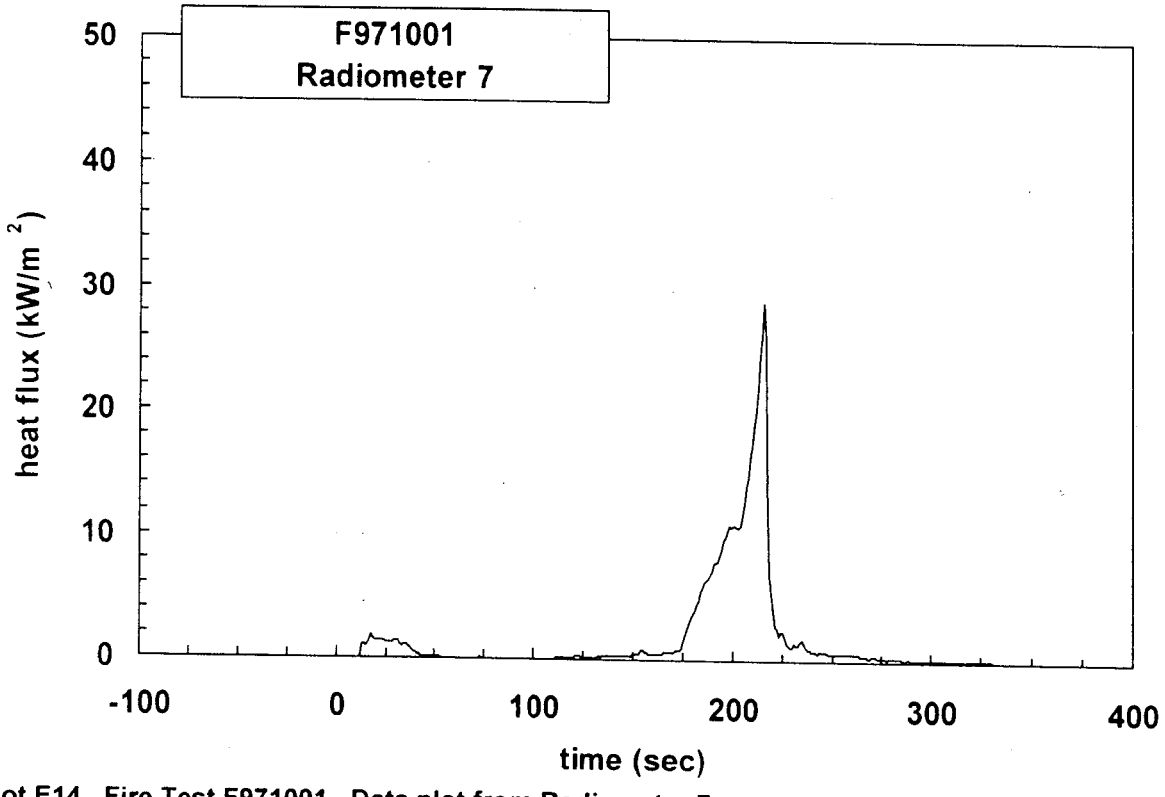

Plot E14. Fire Test F971001. Data plot from Radiometer 7.

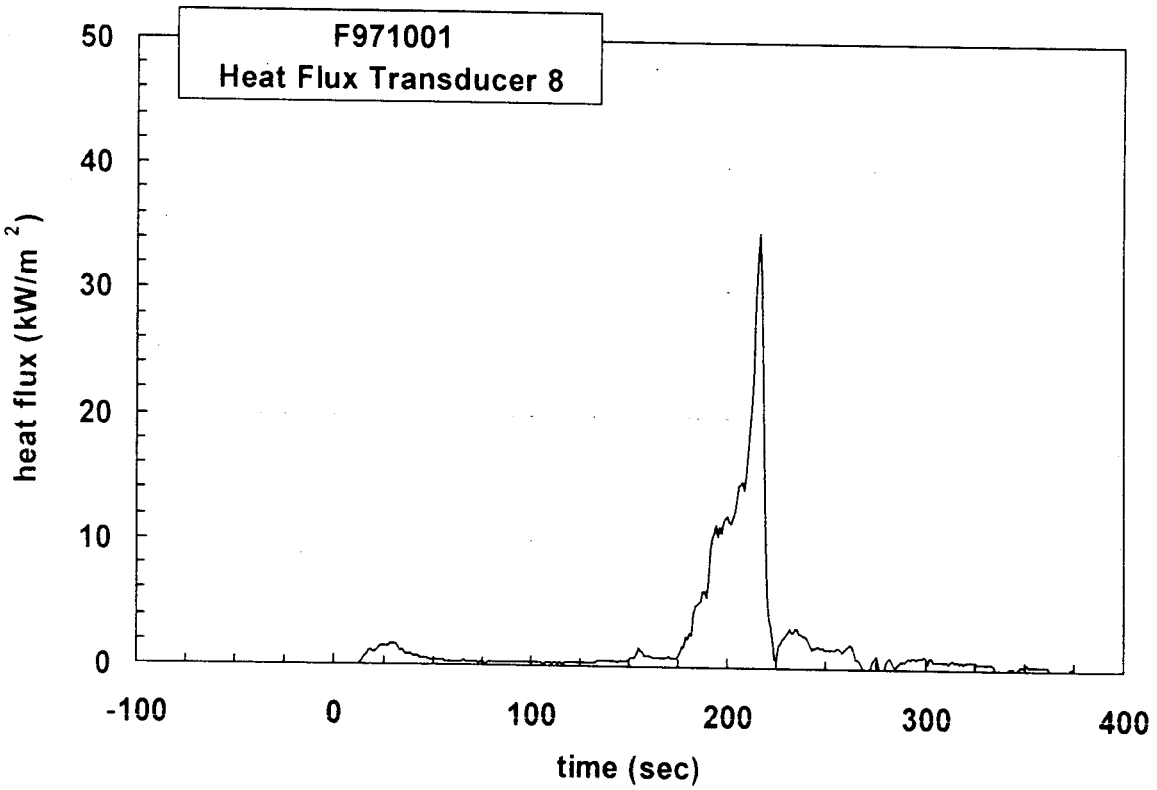

Plot E15. Fire Test F971001. Data plot from Heat Flux Transducer 8.

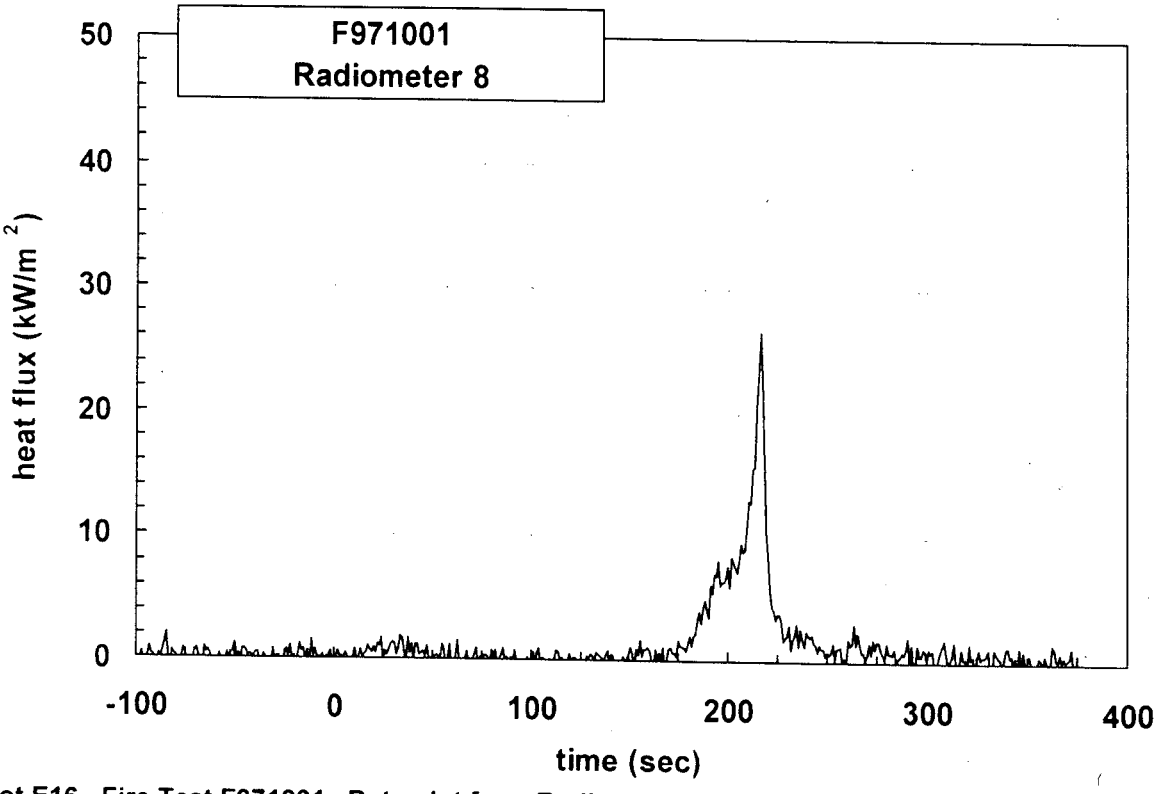

Plot E16. Fire Test F971001. Data plot from Radiometer 8.

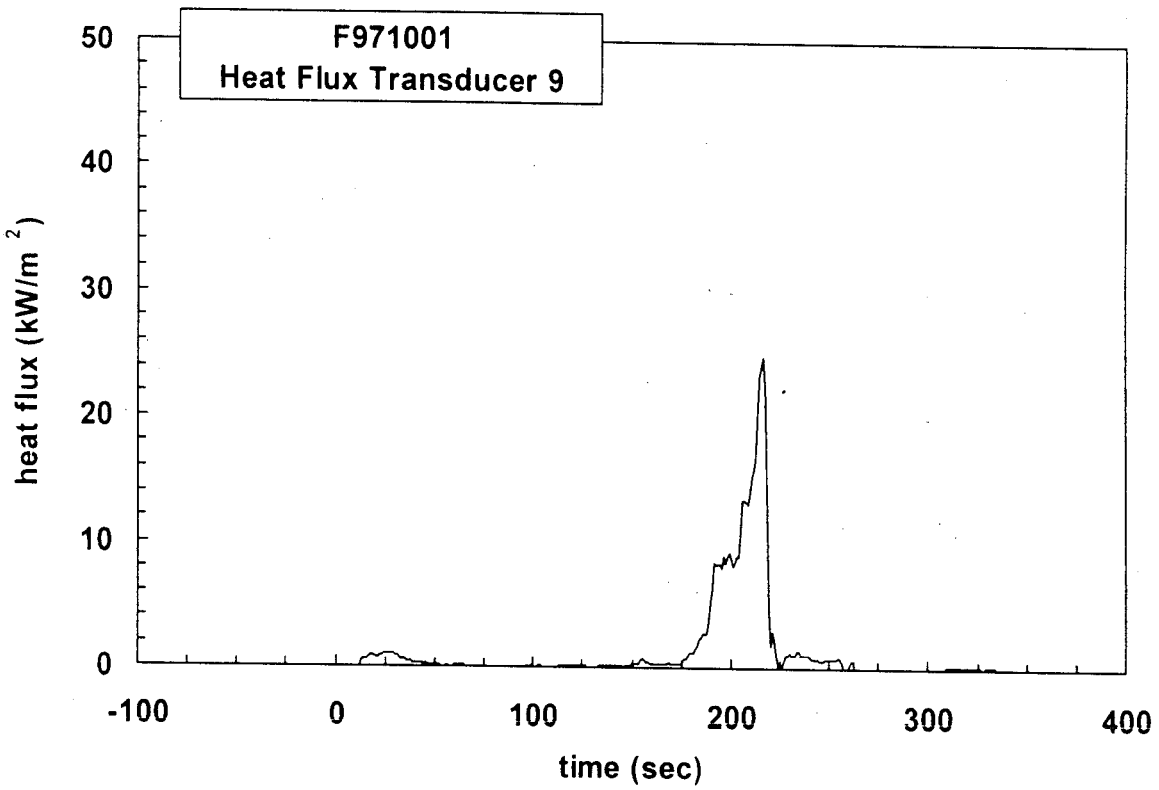

Plot E17. Fire Test F971001. Data plot from Heat Flux Transducer 9.

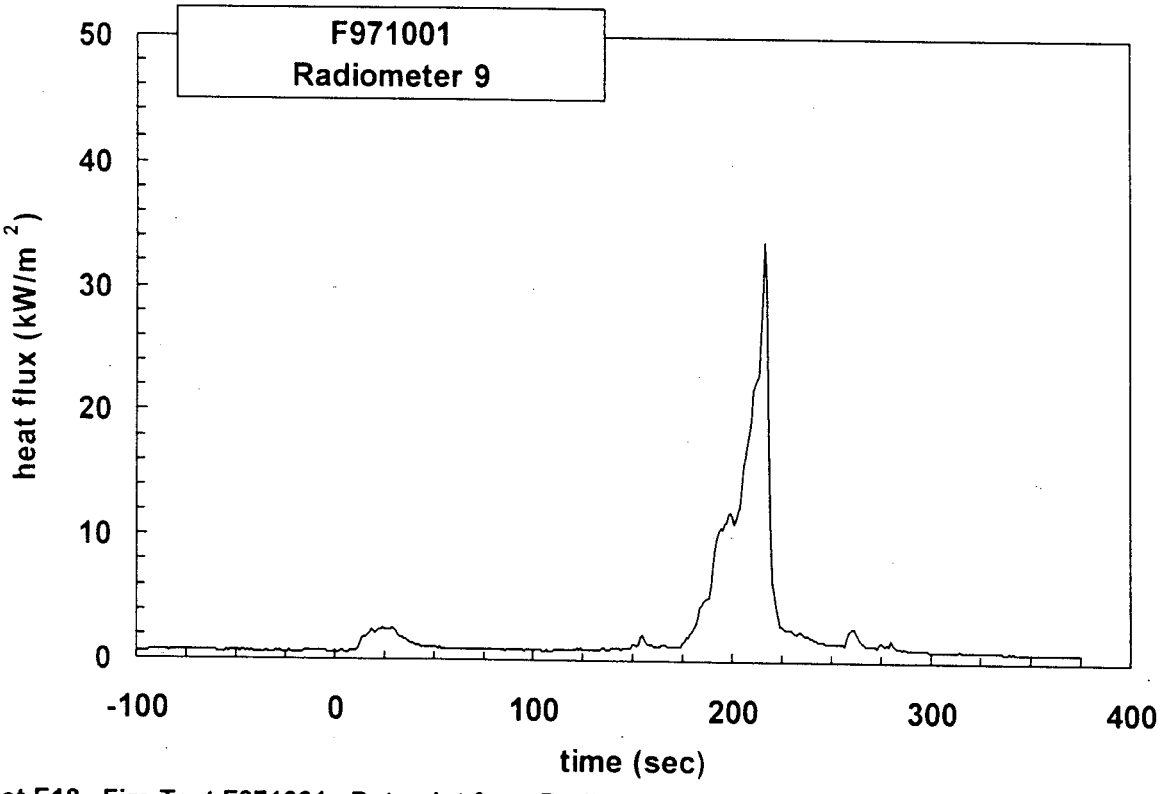

Plot E18. Fire Test F971001. Data plot from Radiometer 9.

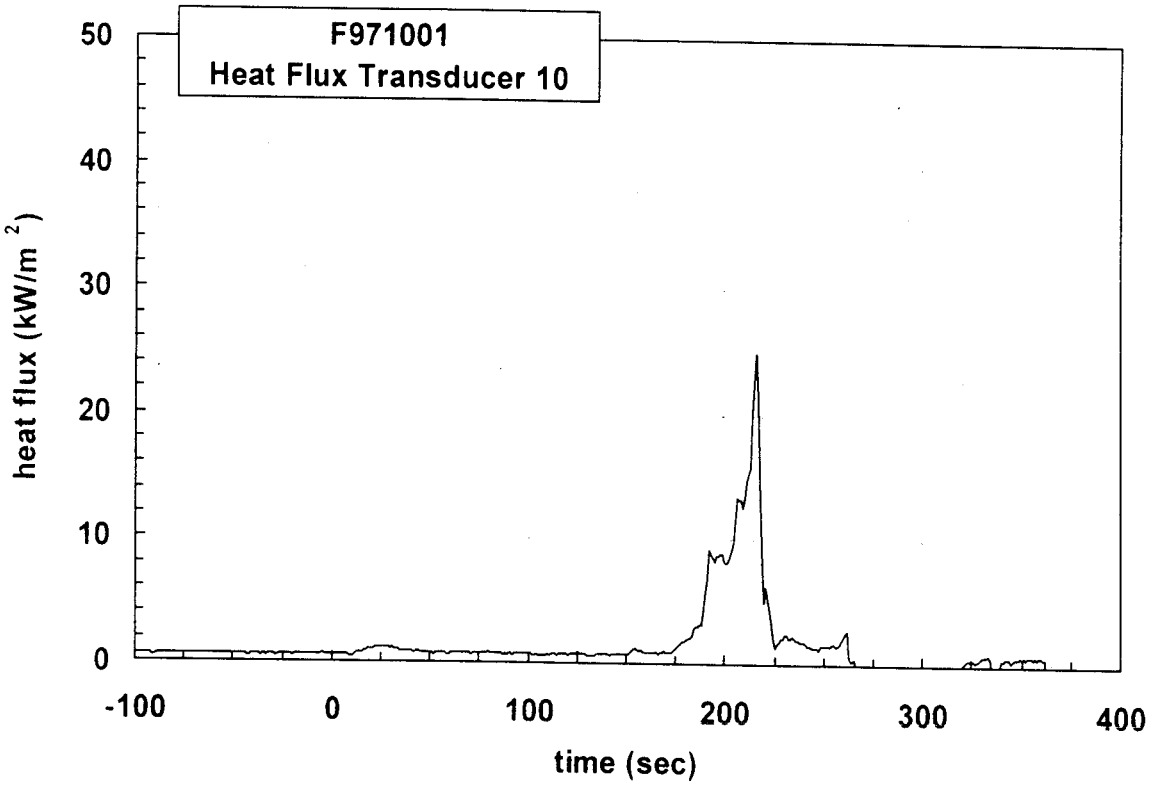

Plot E19. Fire Test F971001. Data plot from Heat Flux Transducer 10.

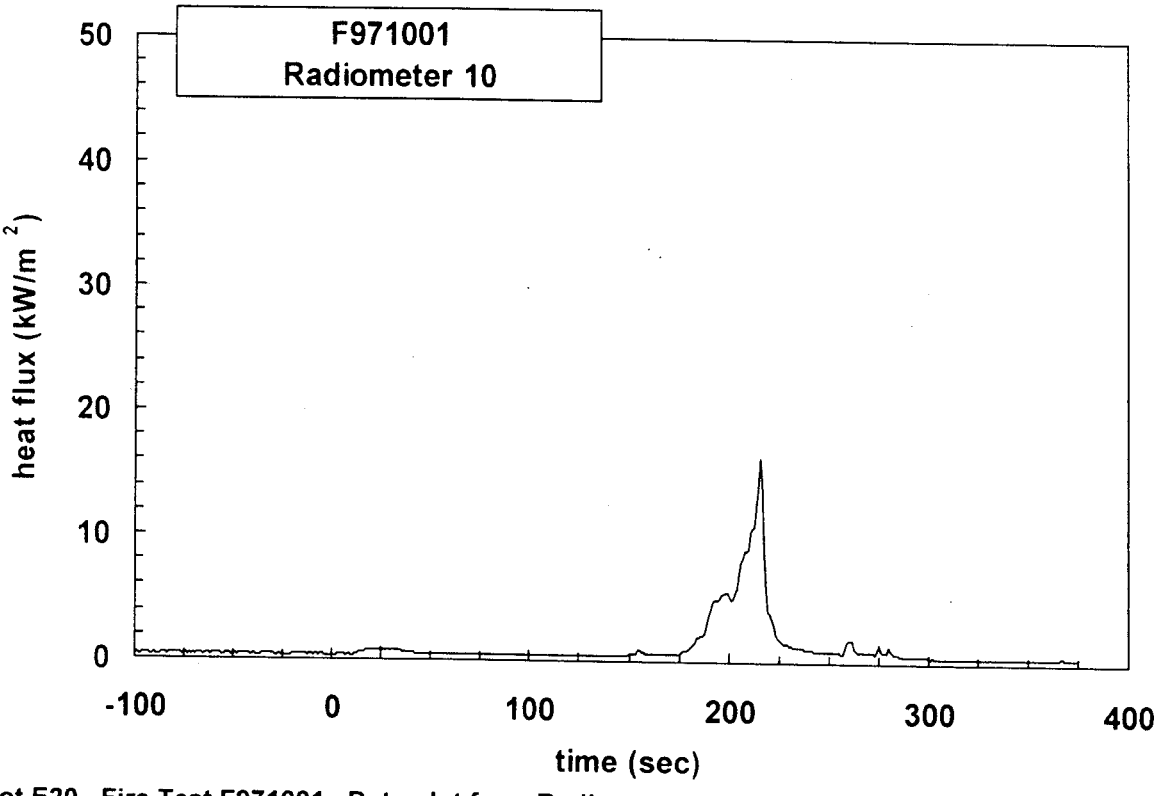

Plot E20. Fire Test F971001. Data plot from Radiometer 10.

APPENDIX F
PRESSURE AND AIRFLOW MEASUREMENTS

Figures F1 and F2 show the approximate locations of the pressure taps and bi-directional flow probe in the test vehicle.

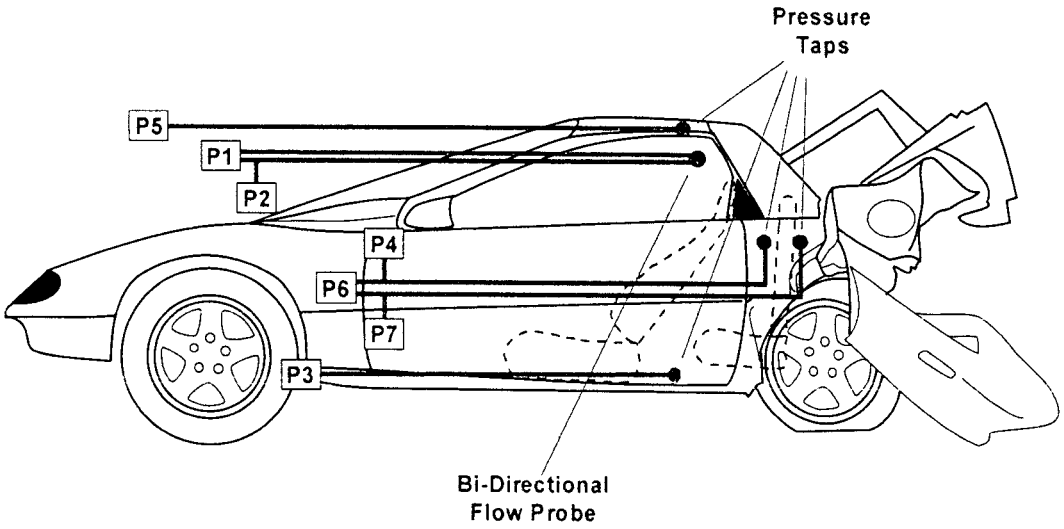

Figure F1. Fire Test F971001. Side view showing the approximate locations of the pressure taps and bi-directional flow probe in the test vehicle.

Four pressure taps were installed in the test vehicle for this test in the following locations: above the carpet in the foot area in front of the rear right seat; in front of the rear seat back, centered horizontally and approximately 10 cm below the upper edge of the sear back; rearward of the rear bulkhead in a space above the fuel tank; below the headlining above the foot area in front of the rear right seat.

Each pressure tap was constructed from stainless steel tubing (o.d. = 0.250 in.). A union-T fitting with compression-type couplings (Parker) was attached to the inlet of the stainless steel tubing, with two of the three positions in the union-T fitting were left open. The other end of stainless steel tubing was connected to a pressure gauge with solvent-resistant flexible tubing (Tygon Masterflex® 6049; i.d. = 0.250 in.; o.d. = 0.438 in.). The total length of the stainless steel and flexible tubing was approximately 10 m.

A bi-directional flow probe was located in the upper rear quadrant of the driver's door window opening (the glass was broken in the crash test) approximately 10 cm below the upper edge of the opening. This probe was used to determine the velocity and direction of airflow through the window opening during the test. The stainless steel tubes leading from the flow probe were

connected to pressure gauges with solvent-resistant resistant flexible tubing (Tygon Masterflex® 6049; i.d. = 0.250 in.; o.d. = 0.438 in.). The total length of tubing was approximately 10 m.

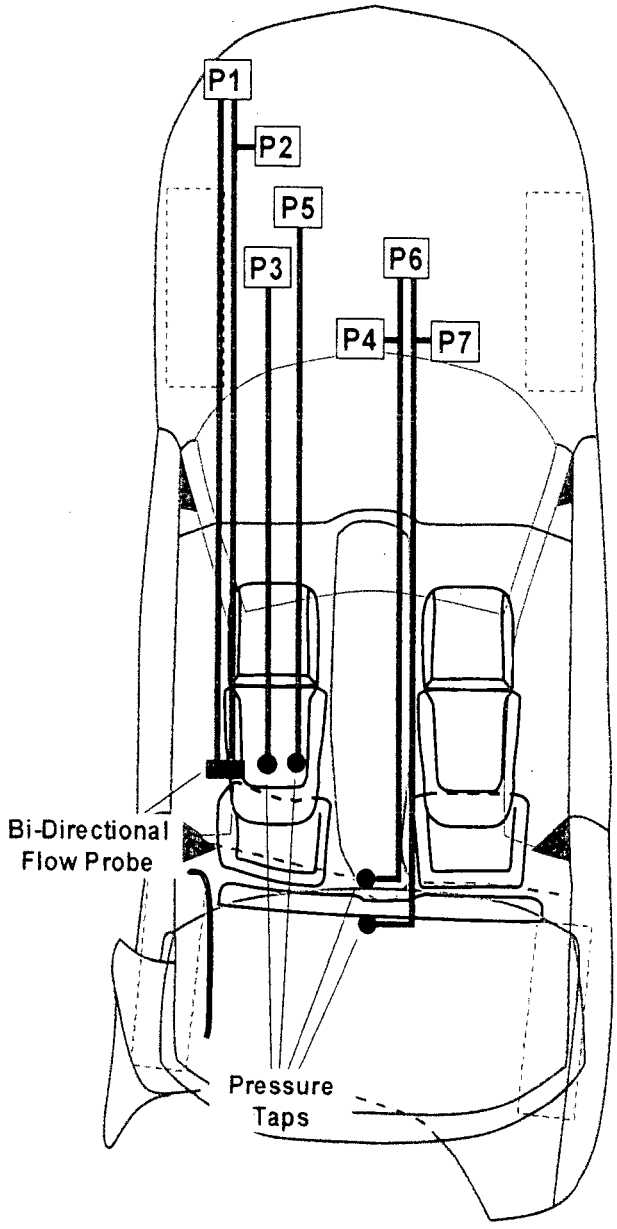

Figure F2. Fire Test F971001. Top view showing the approximate locations of pressure taps the bi-directional probe in the test vehicle.

The velocity of gas flow through the window opening in the driver's door was calculated from the pressure difference measured across the bi-directional probe using the following relationship:

$$V = 0.070\sqrt{T\Delta p} \qquad \text{(F1)}$$

where V is the gas velocity in m/s, T is the gas temperature in degrees Kelvin, and Δp is the pressure difference in Pascals (N/m^2) [F1 and F2].

Pressure gauges (Model C-264, Setra Systems, Acton, MA) with two pressure ranges were used for this test: - 0.5 to 0.5 (± 0.0013) in. W.C. (-124.5 to 124.5 Pascal) and -0.1 to 0.1 (± 0.0003) in. W.C. (-24.9 to 24.9 Pascal). Both gauges were accurate to 0.25% full scale. The gages were powered with a 24 volt non-regulated power supply (Setra Systems). Pressure Gauge P1 connected to both sides of the bi-directional flow probe. The high-pressure inlet of Pressure Gauge P2 was connected to the inboard side of the bi-directional probe, and its low-pressure inlet was left open to atmosphere. The high-pressure inlet of Pressure Gauge P3 was connected to the pressure tap located above the carpet in the foot area in front of the left rear seat, and its reference was left open to atmosphere. The high-pressure inlet of Pressure Gauge P4 was connected to the pressure tap located in front of the rear seat back, and its low-pressure inlet was left open to atmosphere. The high-pressure inlet of Pressure Gauge P5 was connected to the pressure tap located below the headlining, and its low-pressure inlet was left open to atmosphere. The high-pressure inlet of Pressure Gauge P6 was connected to the pressure tap located behind of the rear bulkhead, and its low-pressure inlet was connected to the pressure tap located in front of the rear seat back. The high-pressure inlet of Pressure Gauge P7 was connected to the pressure tap located behind the rear bulkhead, and in front of the rear seat back.

The PC-based data acquisition system described in **APPENDIX C** also was used to record the electronic signals from the pressure gauges during the test. The signal leads from the pressure gauges were plugged into panel-mounted connectors, which were hard-wired to a low-gain analog-input multiplex expansion card (DBK12, IOTech). The analog-input expansion card was interfaced to the main A/D card in the PC. The signal from each pressure gauge was sampled at a rate of 100 Hz. The analog data was stored to a data file in 100-point block-averages so that the effective sampling rate during the test was 1 Hz.

Plots of the pressures recorded with Pressure Gauges P1 through P7 are shown in Plots F1 through F7. Steam generated from the water used to extinguish the flames caused the fluctuations in the recorded pressure after about 210 seconds post-ignition observed in Figures F1 through F7.

REFERENCERS

F1. N. R. Keltner and J. L. Moya. Defining the thermal environment in fire tests. *Fire and Materials* **14**: 133-138, 1989.

F2. B. J. McCaffrey and G. A. Heskestad. Robust bidirectional low-velocity probe for flame and fire application. *Combustion and Flame* **26**: 125-127, 1976.

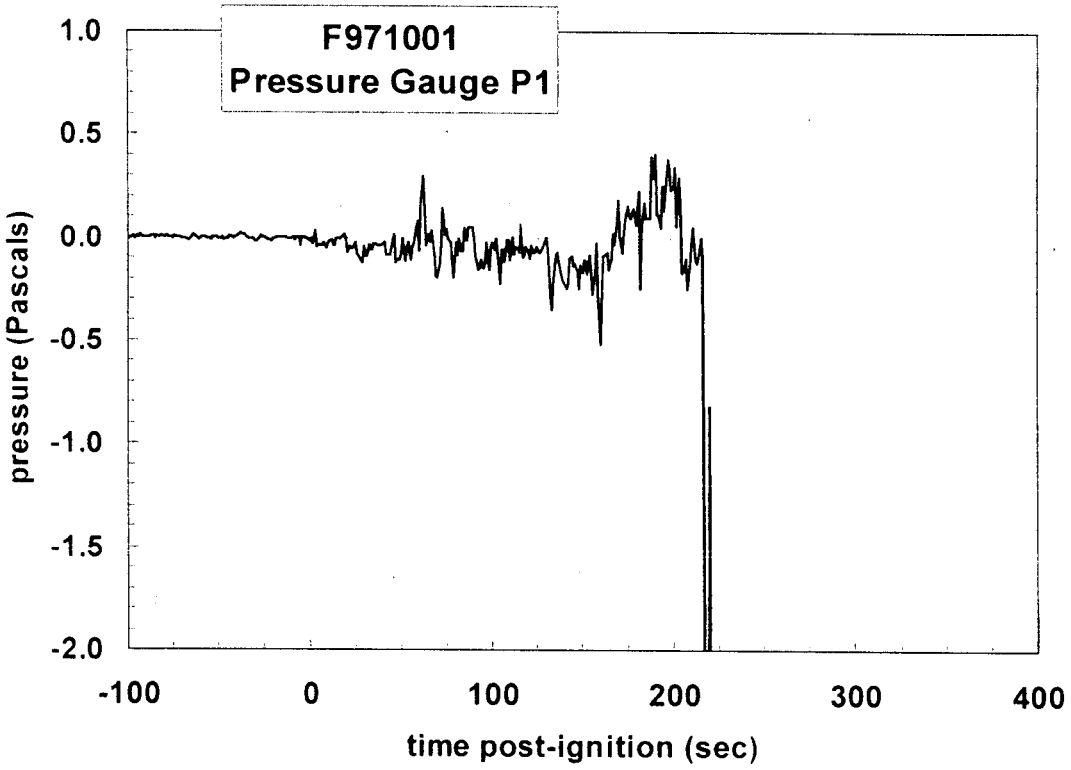

Plot F1. Fire Test F971001. Differential pressure across the bi-direction flow probe measured with P1.

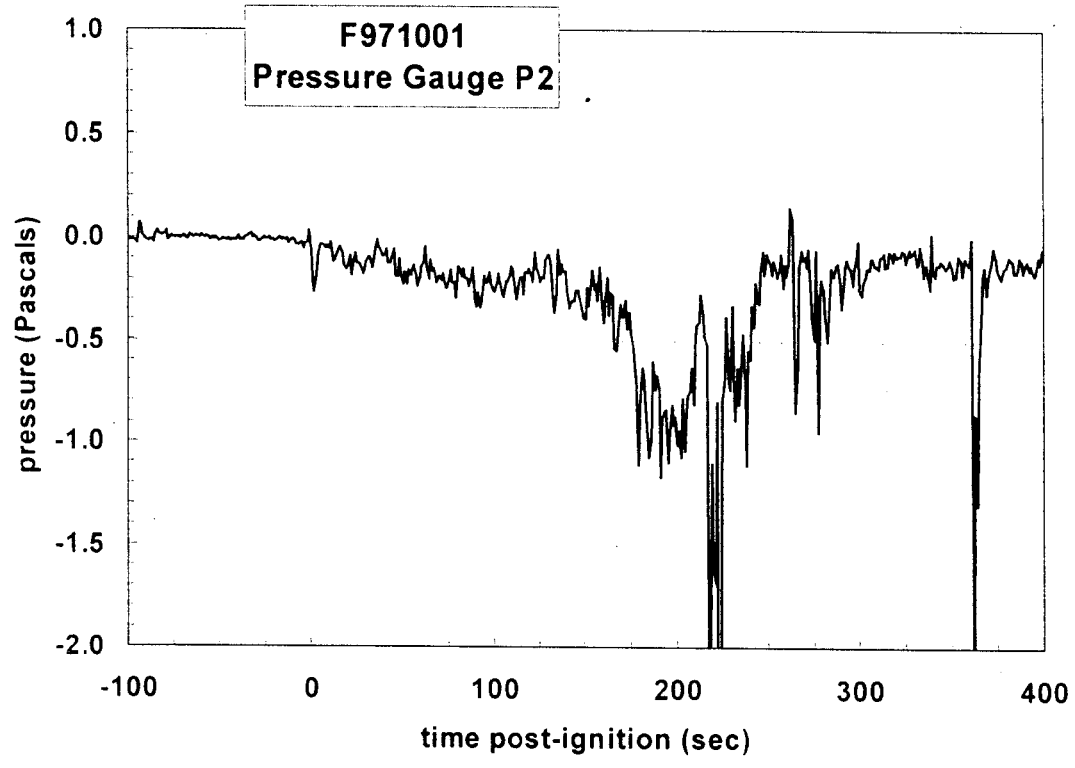

Plot F2. Fire Test F971001. Pressure at the inboard side of the bi-directional flow probe relative to atmospheric pressure measured with P2.

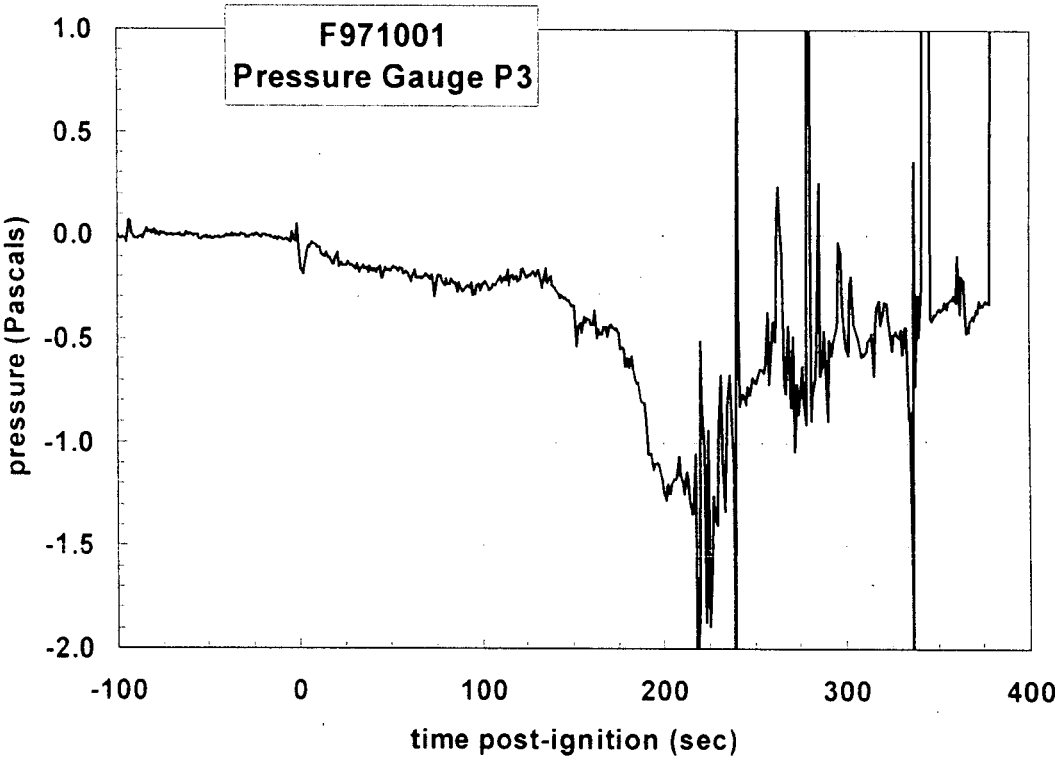

Plot F3. Fire Test F971001. Pressure above the carpet in the rear left foot area relative to atmospheric pressure measured with P3.

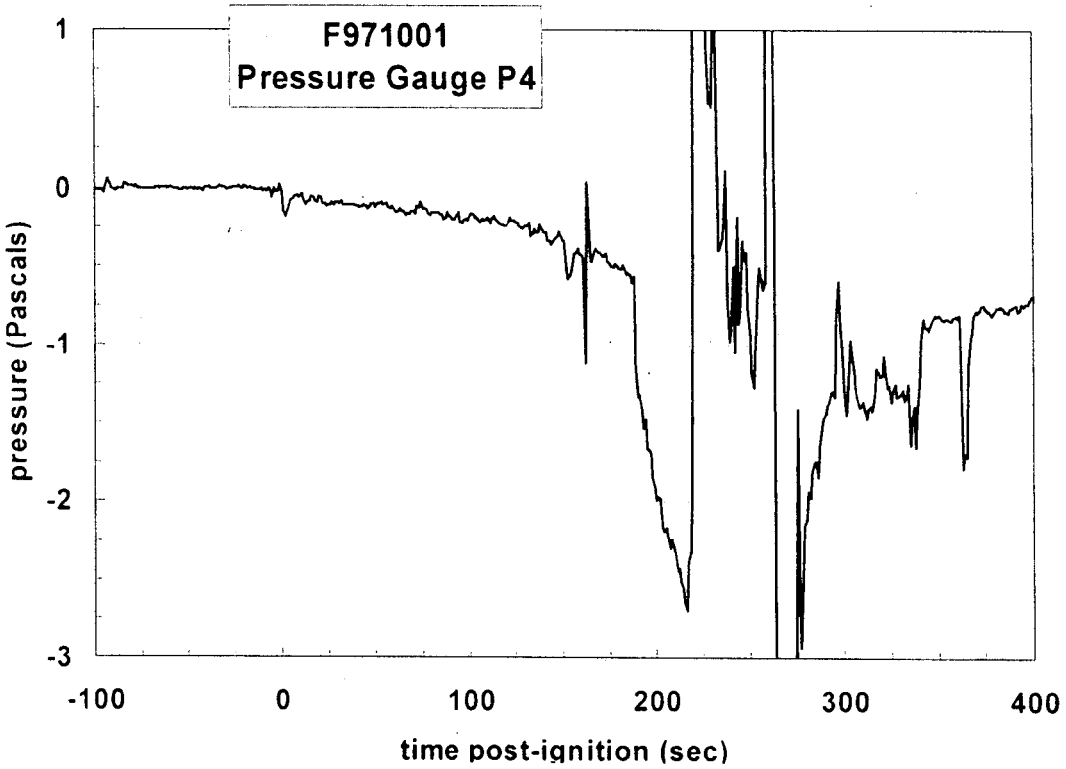

Plot F4. Fire Test F71001. Pressure in front of the rear seat back relative to atmospheric pressure measured with P4.

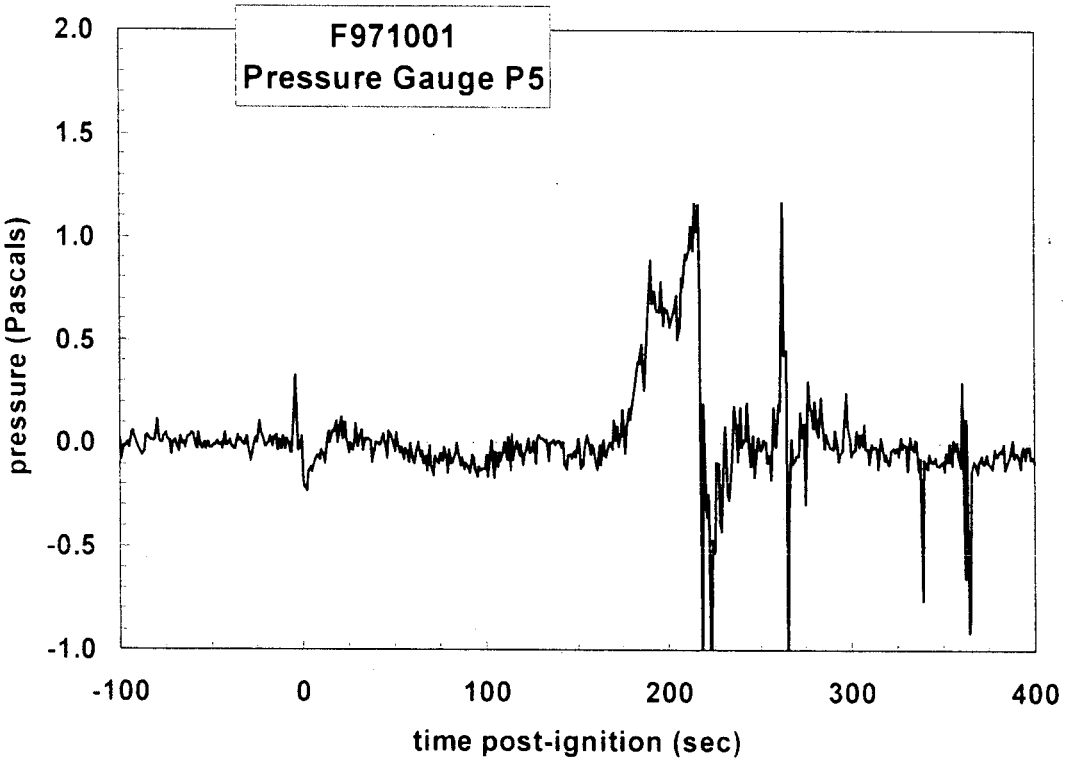

Plot F5. Fire Test F971001. Pressure below the headlining relative to atmospheric pressure measured with P5.

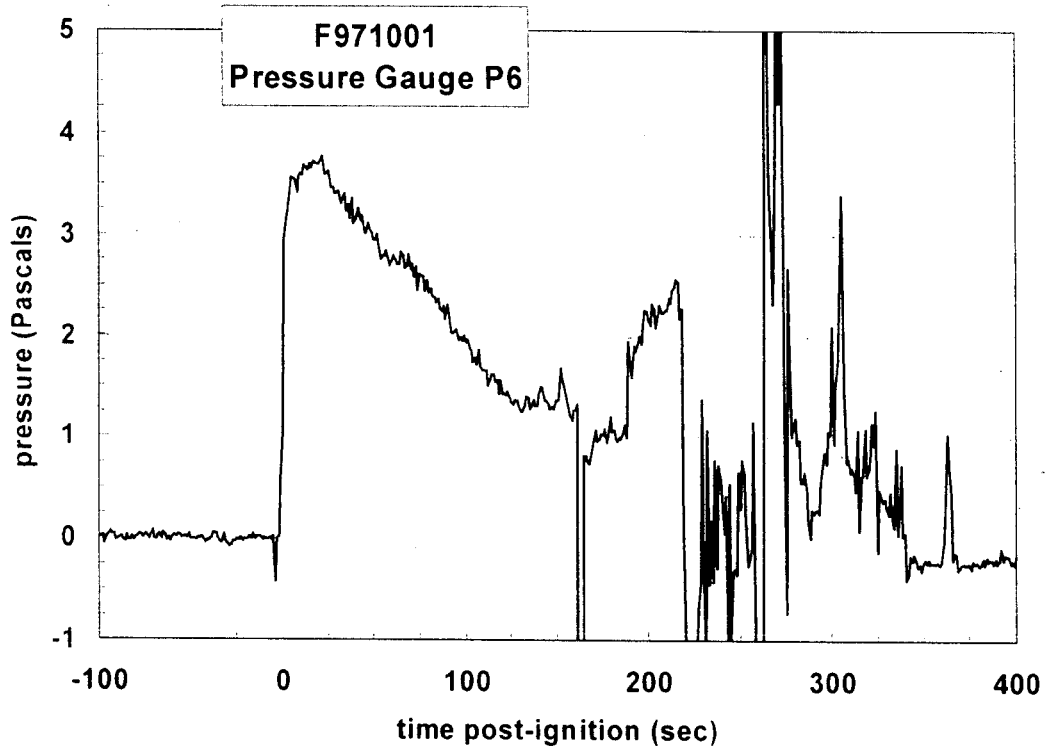

Plot F6. Fire Test F971001. Differential pressure across the rear bulkhead measured with P6.

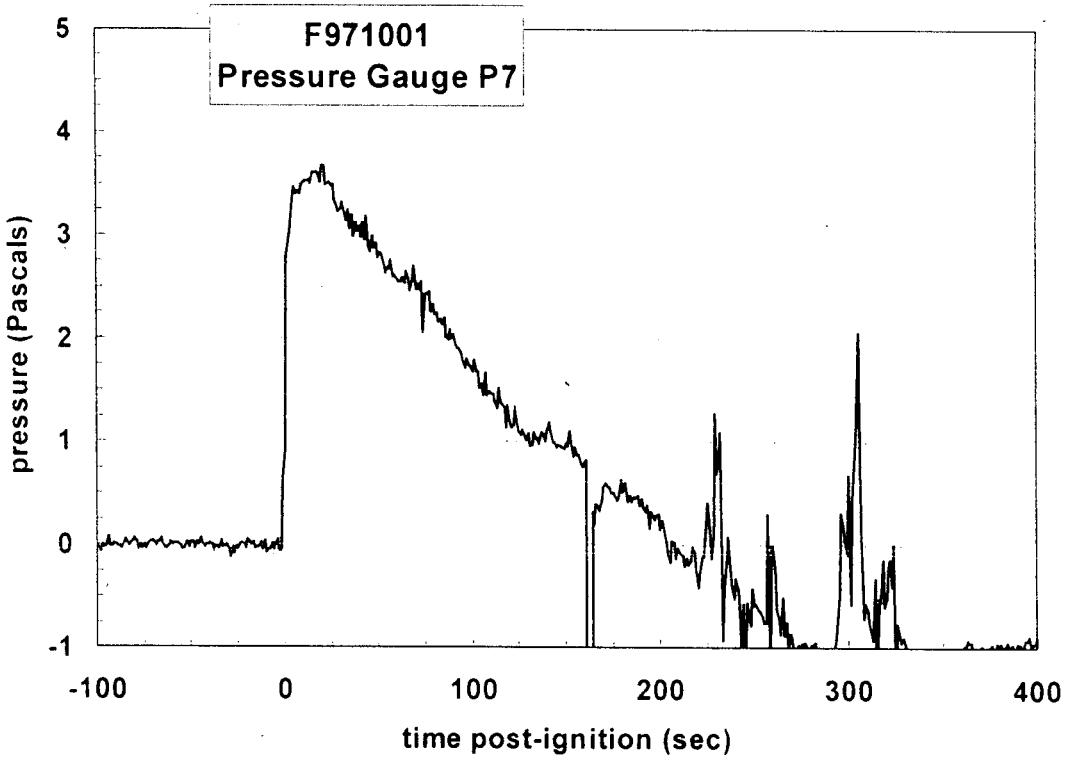

Plot F7. Fire Test F971001. Pressure behind the rear bulkhead relative to atmosphere measured with P7.

APPENDIX G
FIRE PRODUCTS COLLECTOR DATA

Scientific and technical personnel from Factory Mutual Research Corporation were primarily responsible for obtaining and analyzing data from the Fire Products Collector (FPC) at the Factory Mutual Test Center.

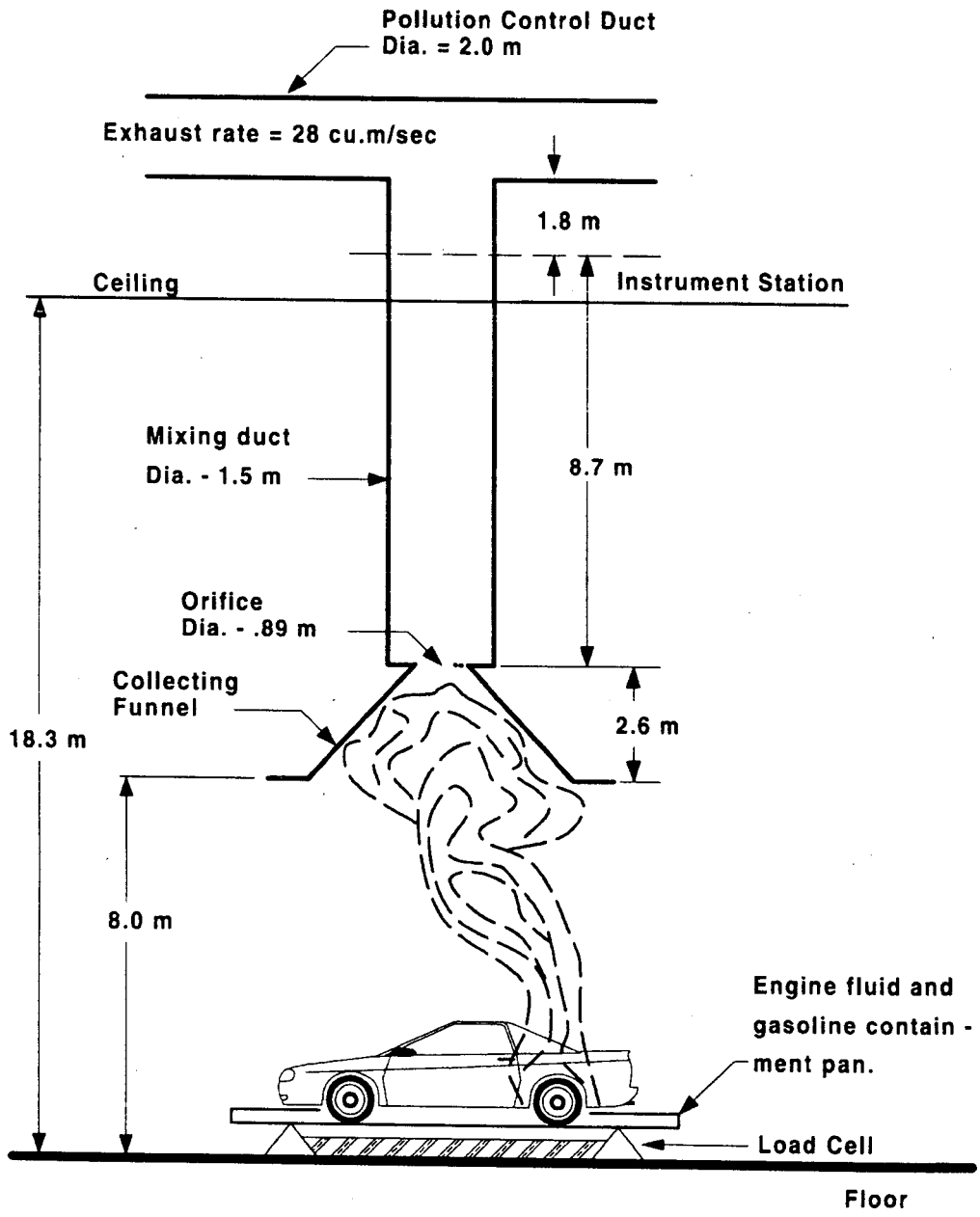

Figure G1. Fire Test F971001. Diagram of the test vehicle under the fire products collector at the Factory Mutual Test Center.

A fire products collector was used to measure heat and combustion gases generated by the burning vehicle during this test (Fig. G1). The fire products collector consisted of a collection funnel (diameter = 6.1 m), an orifice plate (hole = 0.9 m), and a vertical stainless steel sampling duct (diameter = 1.5 m). The sampling duct was connected to the air pollution control system of the Test Center. The blower of the air pollution control system induces gas flow through the sampling duct. Air enters the sampling duct via the orifice plate. The temperature, linear velocity, optical transmission, and chemical composition of the entrained gas were measured in the center of the sampling duct 8.66 m (5.7 duct diameters) downstream from the orifice plate, ensuring a flat velocity profile at the sampling location. The data acquisition system consisted of a Hewlett Packard 2313B analog-to-digital conversion sub-system interfaced to a Hewlett Packard 1000 computer.

Gas temperature in the sampling duct was measured with two Type-K thermocouples (30 gage) with exposed bead-type junctions. The thermocouple leads were housed in stainless steel tubes (o.d. = 6.4 mm). Ambient air temperature in the facility was measured by five Type-K thermocouples attached to the external surface of the duct at 2.44, 5.49, 9.14, 12.8, and 15.9 m above the floor. These thermocouples were shielded from radiation from the fire.

The linear velocity of the gas entrained in the sampling duct was measured with a Pitot ring consisting of four Pitot tubes. A static pressure tap was mounted on the inside wall of the sampling duct. The pressure difference between the Pitot ring and the static wall tap was measured with an electronic manometer (Barocel Model 1173, CGS Scientific Corporation).

The particulate concentration in the entrained air was determined from the optical transmission across the duct measured at 0.4579 μm (blue), 0.6328 μm (red), and 1.06 μm (infrared). The optical path length across the duct was 1.524 m. Gas was withdrawn from the sampling duct through a stainless steel tube (o.d. = 3.9 mm) at a flow rate of 0.17×10^{-3} m^3/s for chemical analysis. The gas flowed through a particulate filter, a water condenser, and a drying agent before entering the analyzers. Carbon dioxide (CO_2) and carbon monoxide (CO) were measured with two dedicated non-disperse infrared analyzers (Beckman Model 864 Infrared Analyzers). Oxygen (O_2) was measured with a paramagnetic oxygen analyzer (Beckman Model 755 Paramagnetic Oxygen Analyzer). Total gaseous hydrocarbons were measured with a flame ionization analyzer (Beckman Model 400 Flame Ionization Analyzer).

The rate of product release was calculated using the following relationship:

$$\left(\frac{dR_j}{dt}\right) = f_j\left(\frac{dV}{dt}\right)\rho_j = f_j\left(\frac{dW}{dt}\right)\left(\frac{\rho_j}{\rho_g}\right) \qquad \text{(G1)}$$

where $d(R_j)/dt$ is the mass release rate of product j in kg/s; f_j is the volume fraction of product j; dV/dt is the total volume flow rate of the gas entrained in the sampling duct in m^3/s; dW/dt is the total mass flow rate of the gas entrained in the sampling duct in kg/s; ρ_j is the density of product j in g/m^3; and ρ_g is the density of the gas entrained in the concentration measurements. The rate of oxygen consumption was calculated using equation (G1), where the volume fraction of oxygen consumed was substituted for f_j.

The volume fraction of smoke particulate was calculated from the following relationship:

$$f_s = \frac{D\lambda \times 10^{-6}}{\Omega} \qquad \text{(G2)}$$

where f_s is the volume fraction of smoke, λ is the wavelength of the light source, Ω is the extinction coefficient of particulate (a value of 0.7 was used in these calculations), and D is the optical density at each of the three wavelengths at which measurements were made:

$$D = \frac{\ln\left(I_0/I\right)}{L} \qquad \text{(G3)}$$

where I_0 is the intensity of light transmitted through clean air, I is the intensity of light transmitted through air containing smoke particulate, and L is the optical pathlength, which was equal to 1.524 m. A value of 1.1×10^6 g/m^3 was used for the density of smoke particulate (ρ_j) in equation (G1).

The convective heat release rate was calculated using the following relationship:

$$\left(\frac{dE_{conv}}{dt}\right) = \left(\frac{dW}{dt}\right) \times c_p \times \left(T_g - T_a\right) \qquad \text{(G4)}$$

where $d(E_{conv})/dt$ is the convective heat release rate in kW; dW/dt is the mass flow rate of the gas entrained in the sampling duct in kg/s; c_p is the heat capacity of the gas entrained in the sampling

duct at the gas temperature in kJ/(kg×K); T_g is the temperature of the gas entrained in the sampling duct in K; and T_a is the ambient air temperature in K.

The chemical heat release rate was calculated from the release rates of carbon dioxide and carbon monoxide as follows:

$$\left(\frac{dE_{ch}}{dt}\right) = \Delta H^{\bullet}_{CO_2} \times \left(\frac{dR_{CO_2}}{dt}\right) + \Delta H^{\bullet}_{CO} \times \left(\frac{dR_{CO}}{dt}\right) \qquad \text{(G5)}$$

where $d(E_{ch})/dt$ is the chemical heat release rate in kW; ΔH^* is the net heat of complete combustion per unit mass of carbon dioxide or carbon monoxide released in the fire in kJ/g; and dR/dt is the mass release rate of carbon dioxide or carbon monoxide in kg/s. Values of ΔH^* for carbon dioxide and carbon monoxide were obtained from the literature [G1 and G2].

The chemical heat release rate also was calculated from the oxygen consumption rate as follows:

$$\left(\frac{dE_{ch}}{dt}\right) = \Delta H^{\bullet}_{O}\left(\frac{dC_O}{dt}\right) \qquad \text{(G6)}$$

where $d(E_{ch})/dt$ is the chemical heat release rate in kW; ΔH^*_O is the net heat of complete combustion per unit mass of O_2 consumed in kJ/g; and $d(C_O)/dt$ is the consumption rate of oxygen in kg/s. The value for ΔH^*_O was obtained from the literature [G1 and G2].

The radiative heat release rate was the difference between the chemical heat release rate and the convective heat release rate:

$$\left(\frac{dE_{rad}}{dt}\right) = \left(\frac{dE_{ch}}{dt}\right) - \left(\frac{dE_{conv}}{dt}\right) \qquad \text{(G7)}$$

where $d(E_{rad})/dt$ is the radiative heat release rate; and $d(E_{ch})/dt$ is the average chemical heat release rate calculated using equations (G5) and (G6).

The vehicle was placed in a rectangular steel pan (length = 25 ft., width = 15 ft., height = 4 in.) to prevent spilled and leaking automotive fluids from spreading in the test facility. This fluid containment pan was fabricated from two sheets of carbon steel. Angle-braces were welded to

the under-side of the pan to keep it from flexing under the weight of the vehicle. The corners of the support frame rested on load cells. Mass loss was determined from data acquired from the load cells during the test.

The fluid containment pan was lined with a layer of fiberglass-reinforced cement construction board (DuraRock, USG Corporation). A thin layer of sand was used to level the concrete board so that the grade of the surface measured from the center to the edges along the major and minor axes was no greater than 1%. The joints between boards were sealed with latex caulking.

Mass loss from the burning vehicle and any burning fluids retained by the containment pan was measured with a load cell weigh-module system. The fluid containment pan was supported by an I-beam frame a load cell weight-module (KIS Series, BLH Electronics, Inc.) at each corner. These weight-modules contain cylindrical, double cantilever strain gauge transducers that are not generally affected by changes in mass distribution. The weight-module system wsa calibrated before this test by placing a series of standard weights on the fluid containment pan.

Data from the fire-products collector and load cell weight-module system are shown in Plots H1 through H5. The Fire Products Collector did not detect a fire plume until approximately 15 seconds after the gasoline was ignited. After the initial increase (approximately 15 to 25 seconds post-ignition), the heat release rate increased exponentially until the fire was extinguished (Plot G1). The heat release rate reached a maximum of approximately 1200 kW at 230 seconds post-ignition. The carbon dioxide release rate curve (Plot G2) was similar to the heat release rate curve. After initially increasing between 15 and 25 seconds post-ignition, the carbon monoxide release rate curve approached a value of 1.6 to 1.7 g/s asymptotically, and decreased when the fire was extinguished (Plot G3). The smoke release rate curve was similar, approaching a value of 0.5 to 0.6 mg/s before the fire was extinguished (Plot G4). Mass loss curve indicated that the vehicle lost between 2 and 3 kg as a result of material burning during this test (Plot G5). The resolution of the load cell system used to make the weight measurement was between 0.3 and 0.4 kg (between 10 to 15% of the total mass loss during the test), and was responsible for the high degree of scatter in the mass loss curve (Plot G5).

REFERENCES

G1. G. Heskestad. A Fire Products Collector for Calorimetry into the MW Range, Technical Report J.I. OC2E1.RA. Factory Mutual Research Corporation, Norwood, MA. June, 1981.

G2. Archibald Tewarson. "Generation of Heat and Chemical Compounds in Fires" Section 3/Chapter 4, SFPE Handbook of Fire Protection Engineering, 2nd Edition, 1995, pp. 3:53-124.

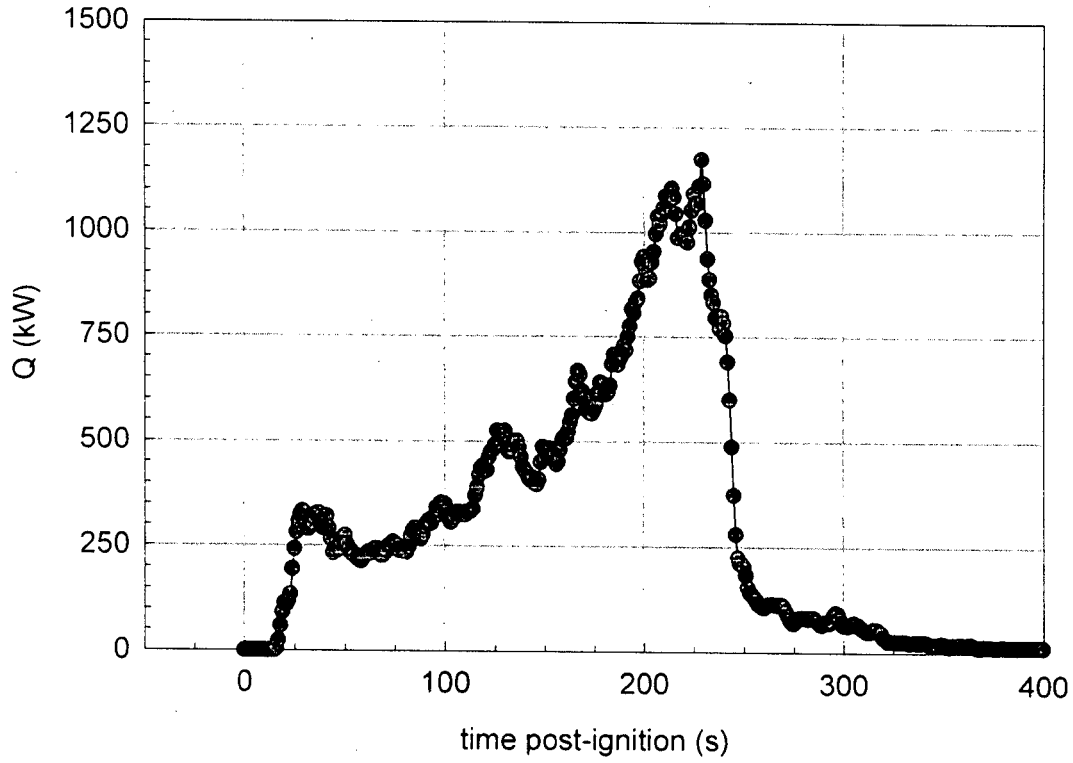

Plot G1. Fire Test F971001. Heat release rate measured using the Fire Products Collector.

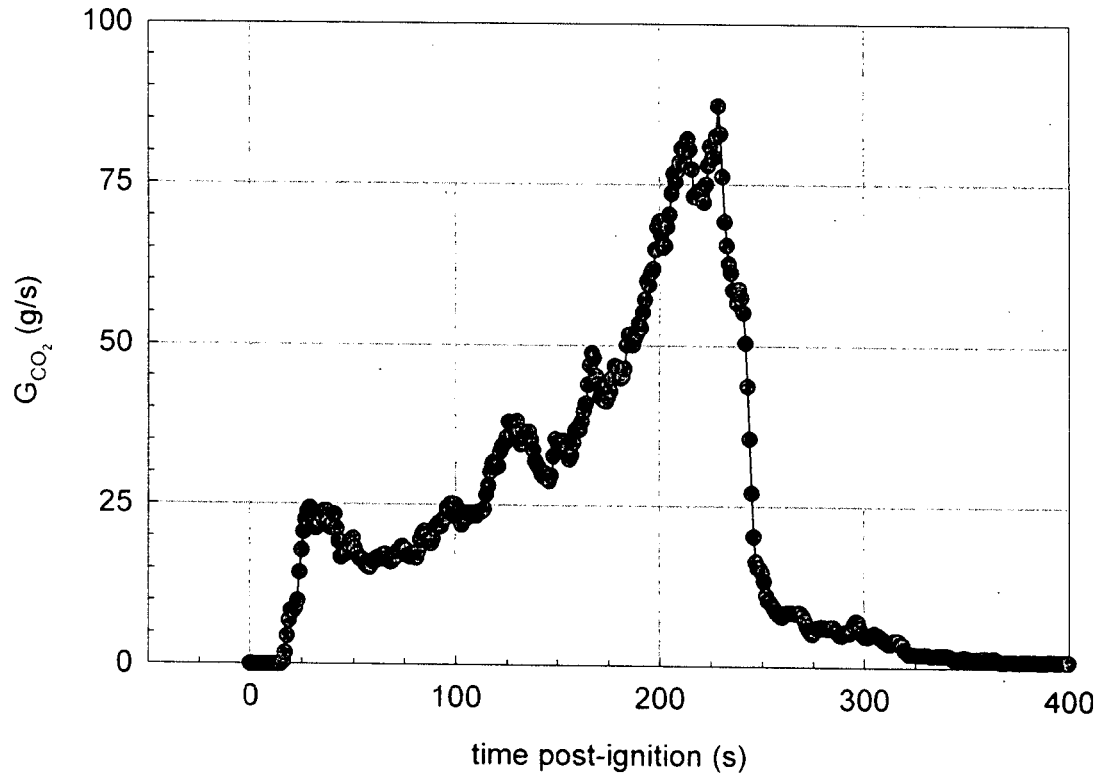

Plot G2. Fire Test F971001. Carbon dioxide release rate measured using the Fire Products Collector.

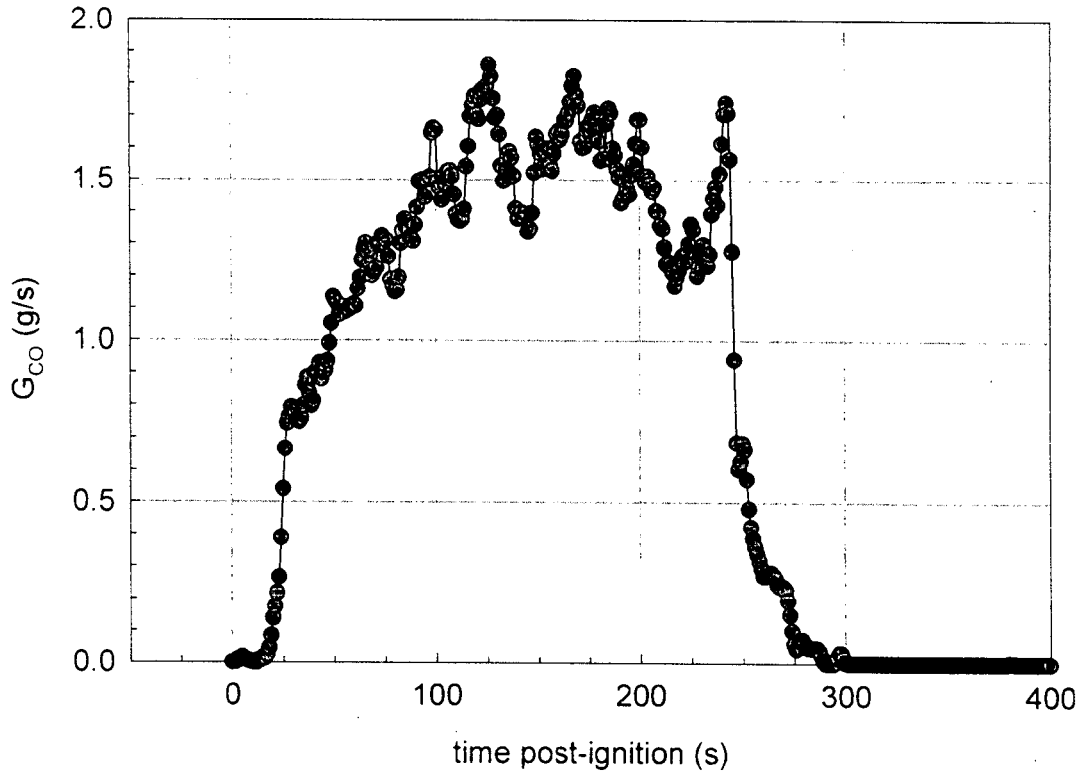

Plot G3. Fire Test F71001. Carbon monoxide release rate measured using the Fire Products Collector.

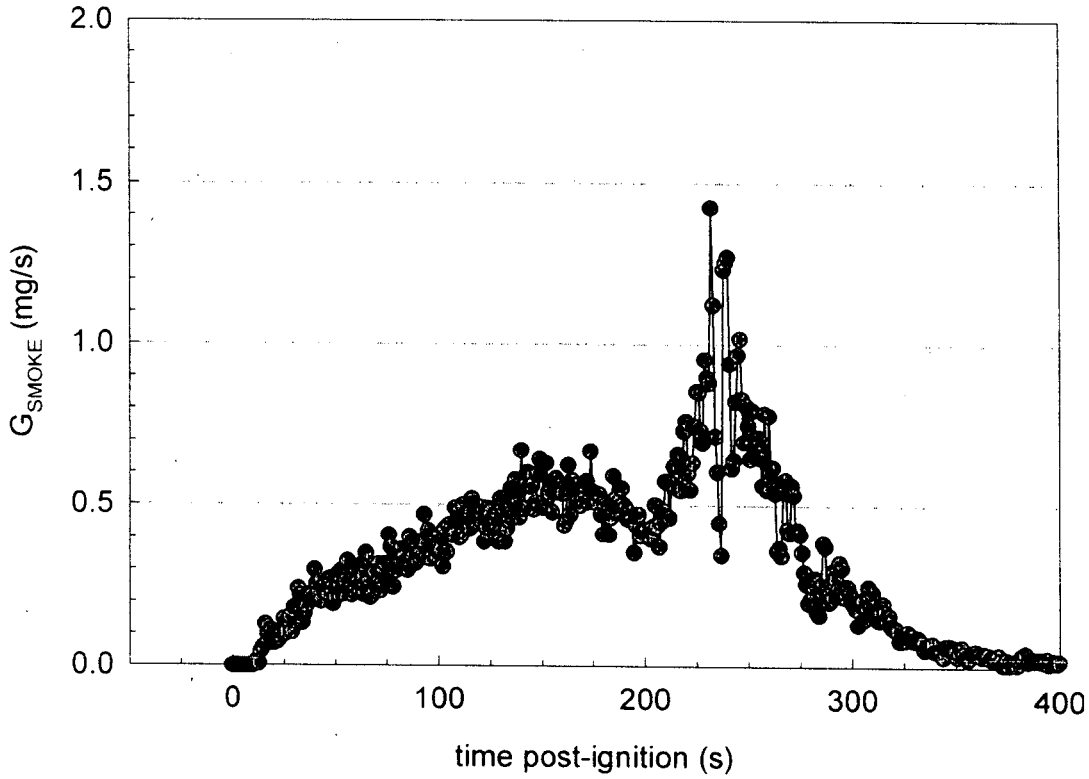

Plot G4. Fire Test F971001. Smoke release rate measured using the Fire Products Collector.

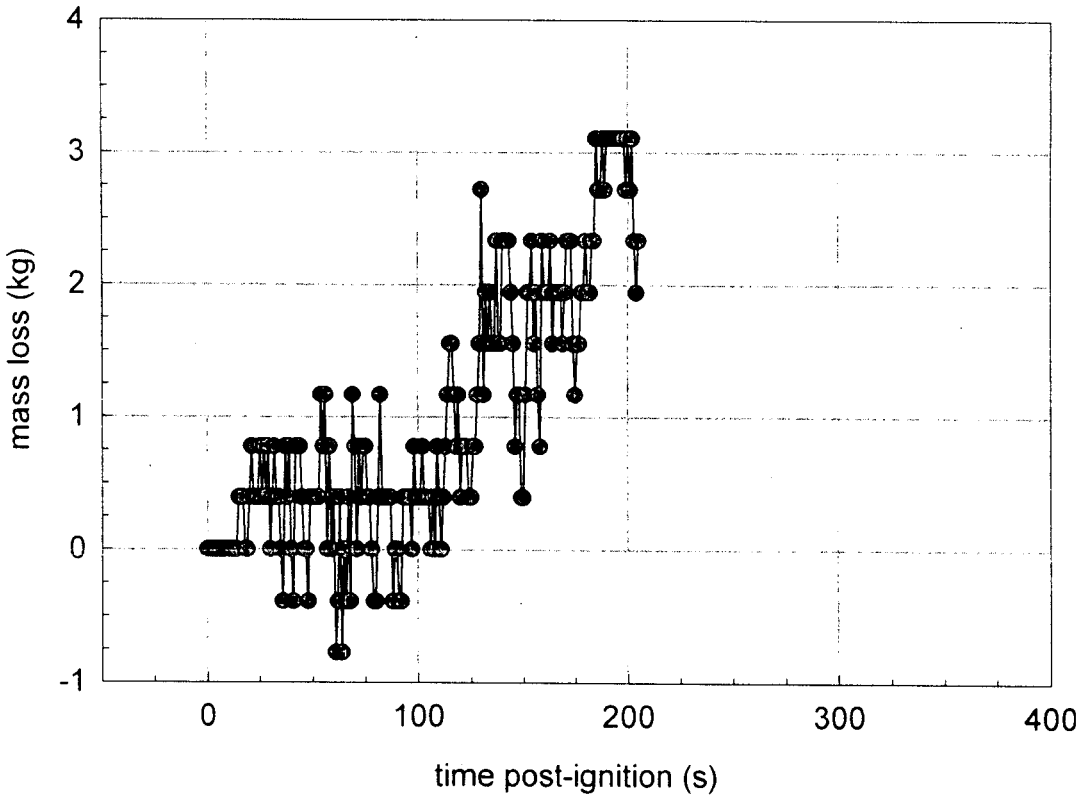

Plot G5. Fire Test F971001. Mass Loss from the test vehicle during the fire test. The mass data was not valid after 205 seconds post-ignition because test personnel stepped onto the fluid containment pan to move video equipment.

APPENDIX H
PASSENGER COMPARTMENT COMBUSTION GAS DATA
FOURIER TRANSFORM INFRARED SPECTROSCOPY
AND
OXYGEN SENSOR DATA

The sampling-line for FTIR analysis consisted of a stainless-steel tube (o.d. = 0.250 in. (6.4 mm), i.d. = 0.125 in. (3.2 mm), l = 20 ft (6.1 m)) inserted through the roof between the front seats along the longitudinal midline of the test vehicle (Fig.'s H1 and H2). The inlet of the sample-tube extended approximately 10 in. below the headlining. The tube was not heated. The outlet of the sample tube was connected to a heated Teflon® transfer-line (o.d. = 0.250 in. (6.4 mm), i.d. = 0.125 in. (3.2 mm), l = 75 ft. (23 m)), which was connected to the gas cell of the FTIR spectrometer. The transfer-line was heated to 105°C during the test to prevent condensation of water and water-soluble gases (*e.g.*, HCl, HCN, NO, and NO_2). An in-line stainless steel filter holder containing a quartz fiber filter (o.d. = 47 mm) was placed between the sample-tube and the transfer-line to prevent smoke particles from contaminating analytical instrumentation.

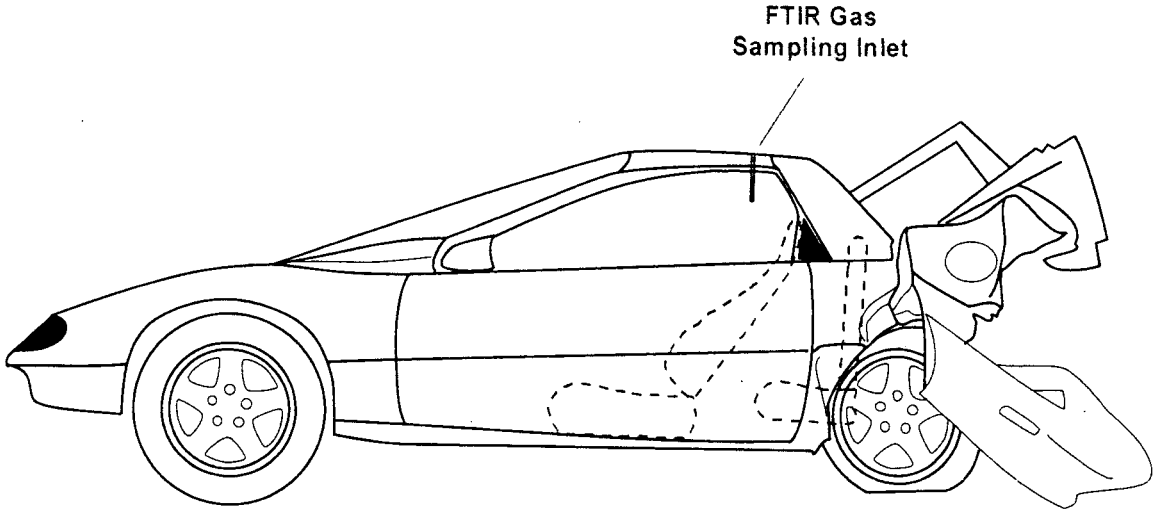

Figure H1. Fire Test F971001. Side-view of the test vehicle show the approximate location of the FTIR gas sampling inlet in the passenger compartment.

The FTIR spectrometer was a Model I-1000 Series FTIR Spectrometer (MIDAC Corporation, Riverside, California), with a KBr beam-splitter; a liquid nitrogen-cooled Mercury-Cadmium-Telluride detector; and gold-surfaced aluminum optics. This instrument was fitted with a stainless steel, multiple-reflectance gas cell (path length = 10 m) with zinc selenide windows. The gas cell was heated to 105°C. The optical bench was filled with clean, dry argon and hermetically sealed. The usable spectral range of this instrument was approximately 7400-700 cm^{-1}. Pressure in the gas cell during the fire tests was measured with a Baratron pressure gauge (MKS Instruments, Burlington, MA). The spectrometer was operated at a spectral resolution of 0.5 cm^{-1}.

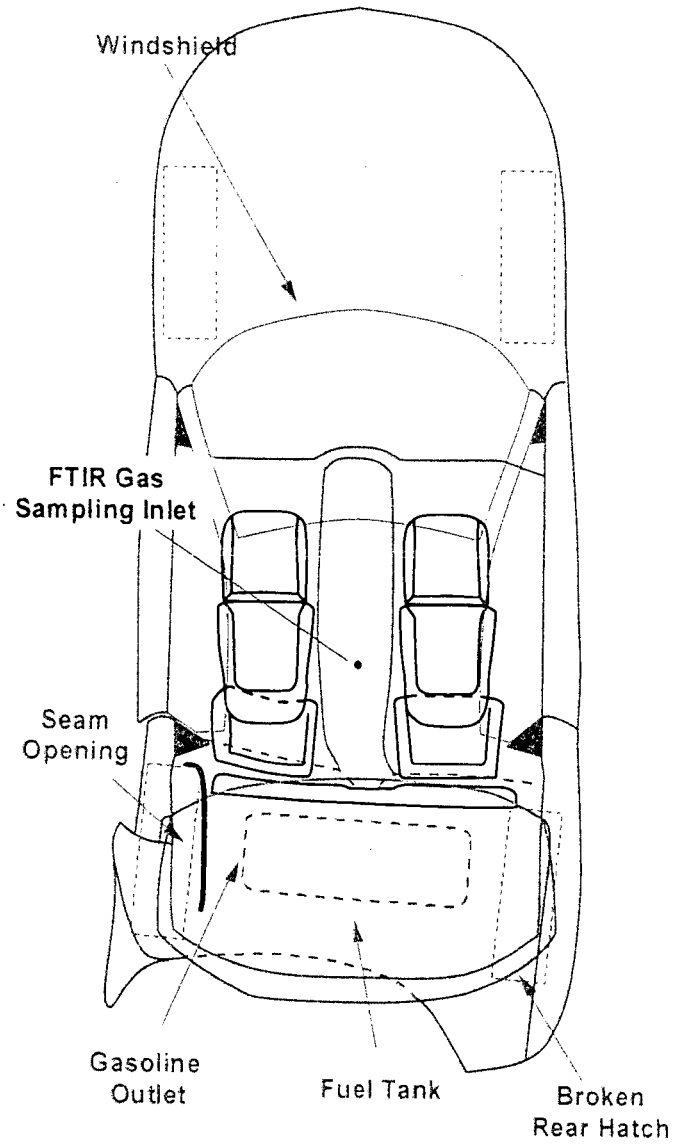

Figure H2. Fire Test F971001. Top view of the test vehicle showing the approximate location of the FTIR gas sampling inlet in the passenger compartment.

The sampling line and gas cell were equilibrated to 105°C for at least 60 minutes before sample acquisition. A reference spectrum was acquired while the gas cell was evacuated. During the fire tests, the gas cell was purged continuously with air withdrawn from the passenger compartment at a flow rate of 7 L/min. Single-scan absorbance spectra were acquired and stored to disk at intervals of 10 s. After the test, the stored spectra were analyzed using the quantitative analysis software provided by the instrument manufacturer (AutoQuant, MIDAC). This software uses a Classical Least Squares algorithm to determine gas concentrations. The method developed for analysis of combustion gases was calibrated with gas standards (Scott Specialty

Gases, Inc., Troy, MI). The standards were either NIST-traceable or produced by a gravimetric blending process.

An electrochemical oxygen sensor (Model SE-25, FIGARO USA, Inc.) was placed in the FTIR sampling line just before the FTIR gas cell. The signal from the oxygen sensor was recorded by the data acquisition system described in **APPENDIX C**. The oxygen sensor was calibrated before this test by recording its responses when purged with room air (21% O_2) and with pure nitrogen (0% O_2).

The gaseous combustion products measured by FTIR in the passenger compartment during this test included carbon dioxide, carbon monoxide, methane, ethylene, acetylene, hydrogen cyanide, nitric oxide, and hydrogen chloride (Plots H1 through H8). Except for carbon dioxide, which has a background concentration in air of approximately 0.05 %, the concentrations of all of these gases were less than their respective lower limits of detection from the start of the test to 6 minutes post-ignition.

The concentrations of carbon dioxide, carbon monoxide, methane, ethylene, and acetylene started to accumulate in the passenger compartment by 10 seconds post-ignition (Plots H1 through H5). The data in Plots H3 through H5 indicate that concentration of the hydrocarbons increased as they became more highly unsaturated. The scale of the ordinate in these plots is the same to facilitate comparison of the relative amounts of the hydrocarbons. The Infrared spectra acquired during this test also contained a broad absorbance band between 2800 and 3200 cm^{-1}, indicating the presence of a mixture of aliphatic hydrocarbons in the air samples from the passenger compartment. The intensity of this absorbance band generally followed the same time-course as that of methane (Plot H3), ethylene (Plot H4), and acetylene (Plot H5). This broad band appeared to contain absorbances from ethane, propane, and butane. However, all of the gaseous species contributing to this absorbance band could not be identified or accurately quantified.

Hydrogen cyanide (Plot H7) and nitric oxide (Plot H8) started to accumulate in the passenger compartment between 40 and 60 seconds post-ignition. Hydrogen chloride (HCl) started to accumulate in the passenger compartment between 80 and 90 seconds post-ignition (Plot H6).

The concentration oxygen in air samples from the passenger compartment during this test is shown in Plot H9. The oxygen concentration started to decrease approximately 20 seconds post-ignition, and reached a minimum of 14% at approximately 210 seconds post-ignition.

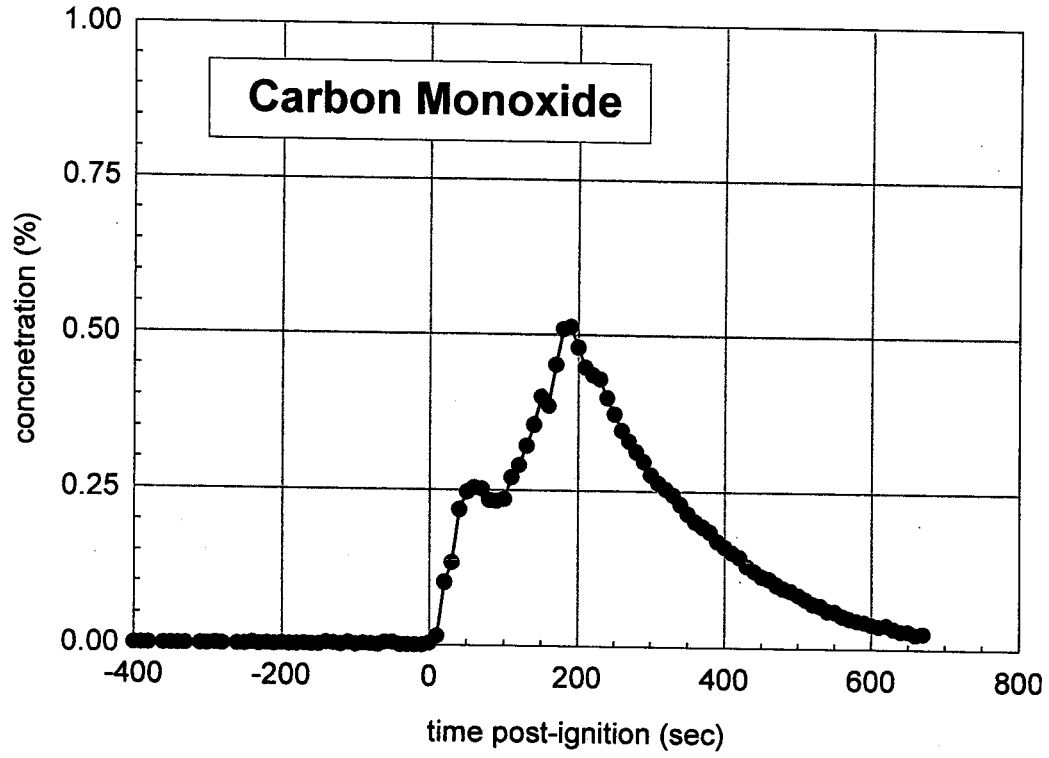

Plot H1. Fire Test F971001. Concentration of carbon monoxide (CO) in the passenger compartment determined by FTIR analysis.

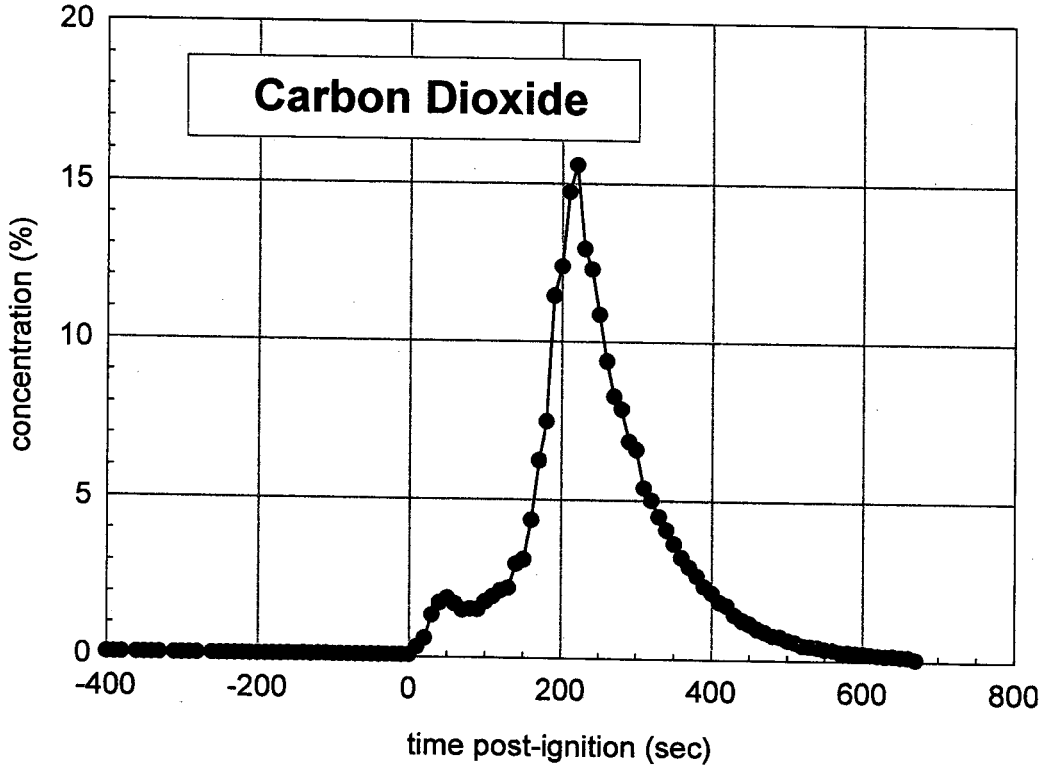

Plot H2. Fire Test F971001. Concentration of carbon dioxide (CO_2) in the passenger compartment determined by FTIR analysis.

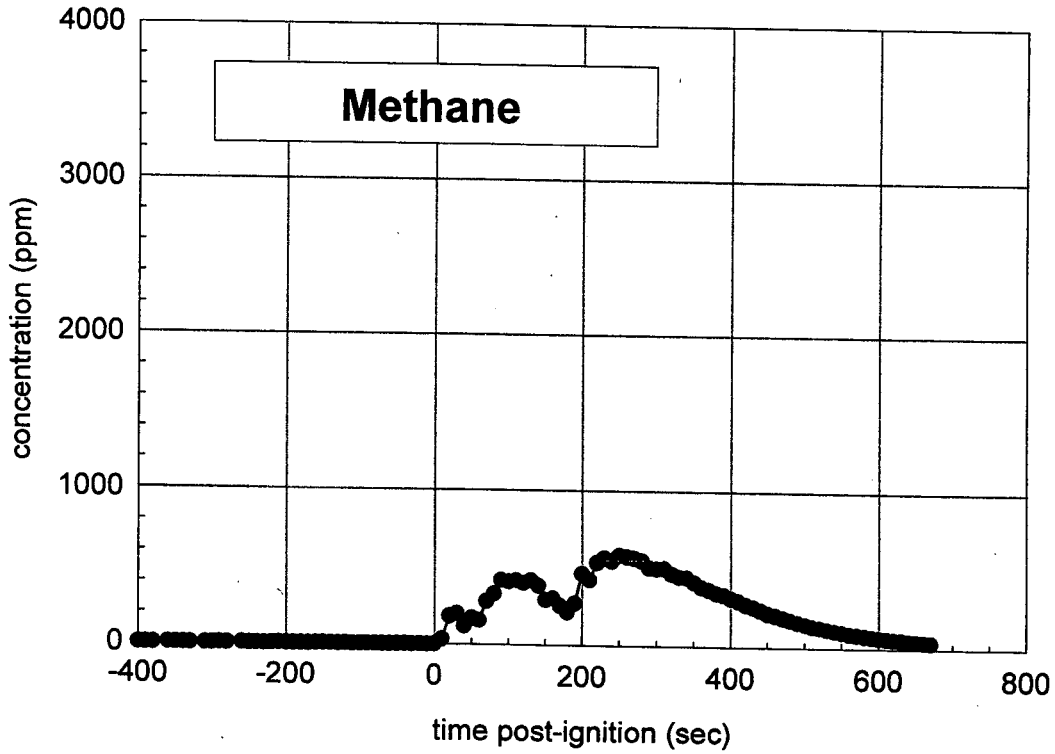

Plot H3. Fire Test F971001. Concentration of methane (CH_4) in the passenger compartment determined by FTIR analysis.

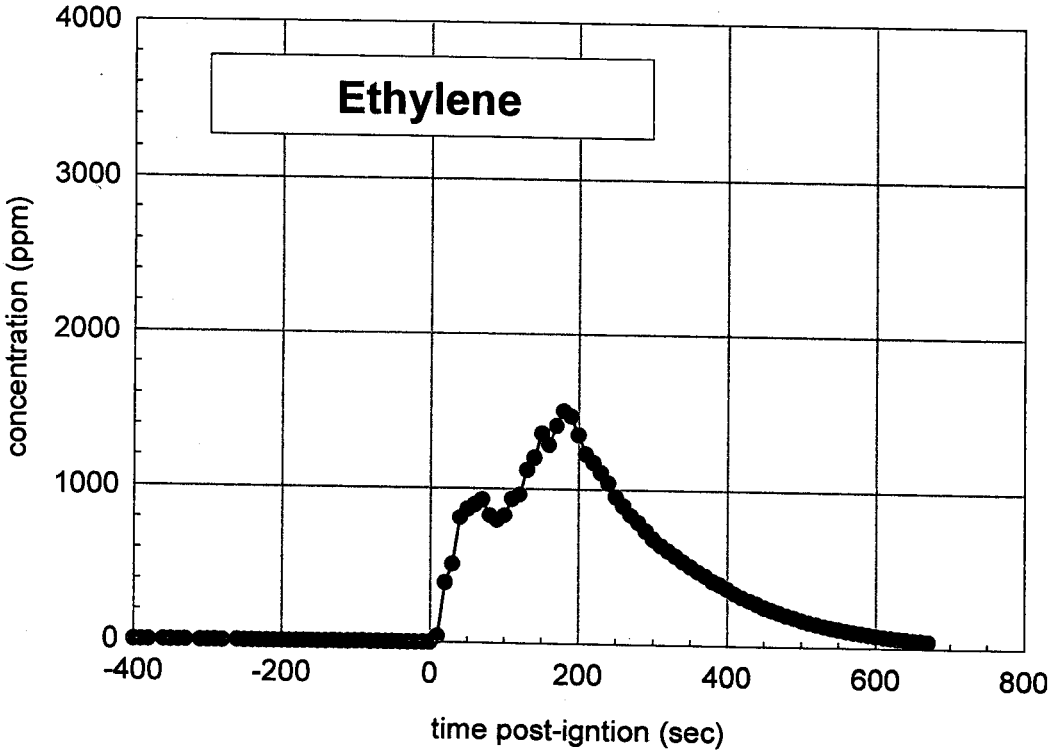

Plot H4. Fire Test F971001. Concentration of ethylene (C_2H_4) in the passenger compartment determined by FTIR analysis.

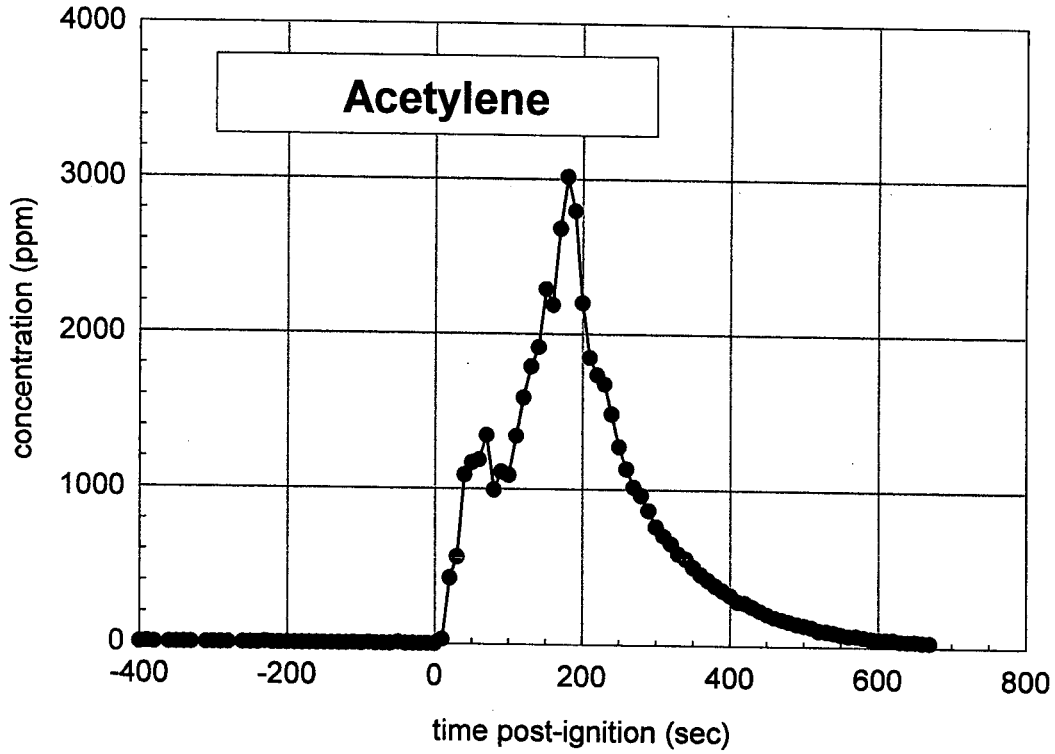

Plot H5. Fire Test F971001. Concentration of acetylene (C_2H_2) in the passenger compartment determined by FTIR analysis.

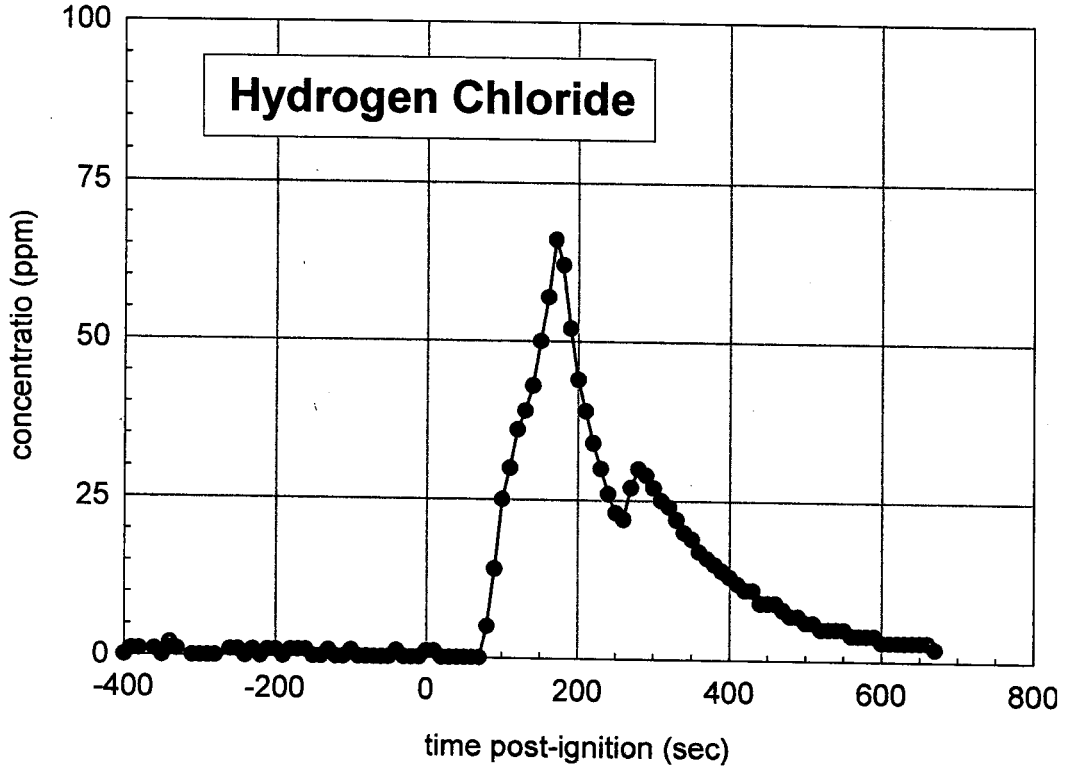

Plot H6. Fire Test F971001. Concentration of hydrogen chloride (HCl) in the passenger compartment determined by FTIR analysis.

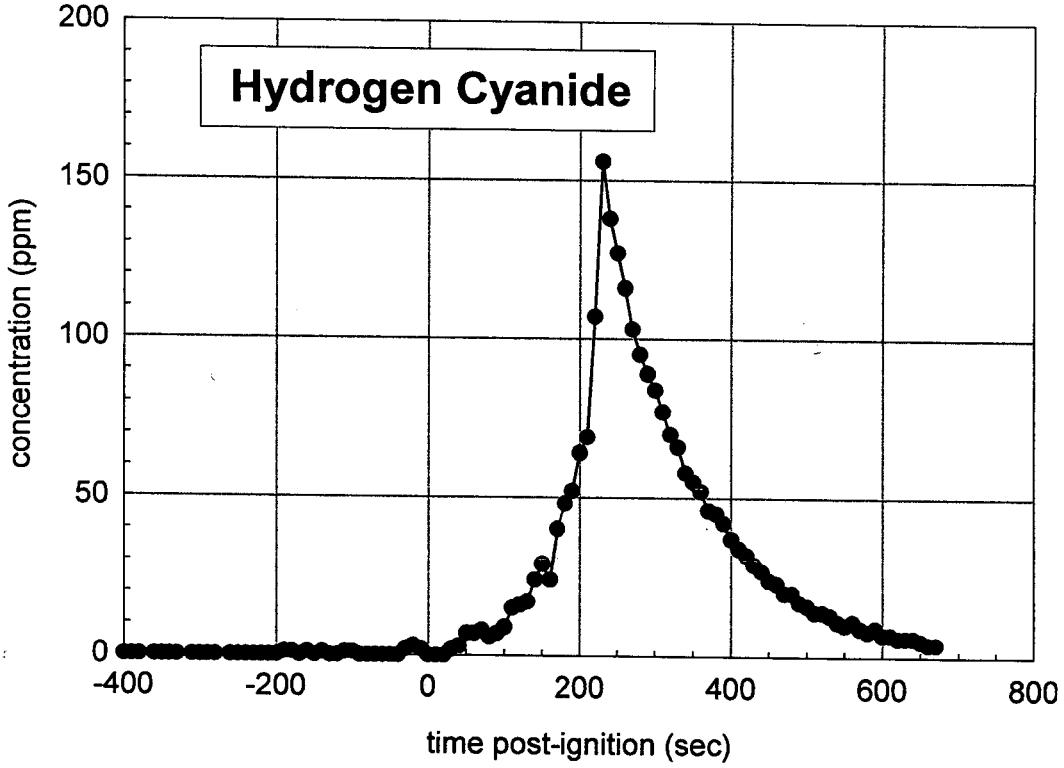

Plot H7. Fire Test F971001. Concentration of hydrogen cyanide (HCN) in the passenger compartment determined by FTIR analysis.

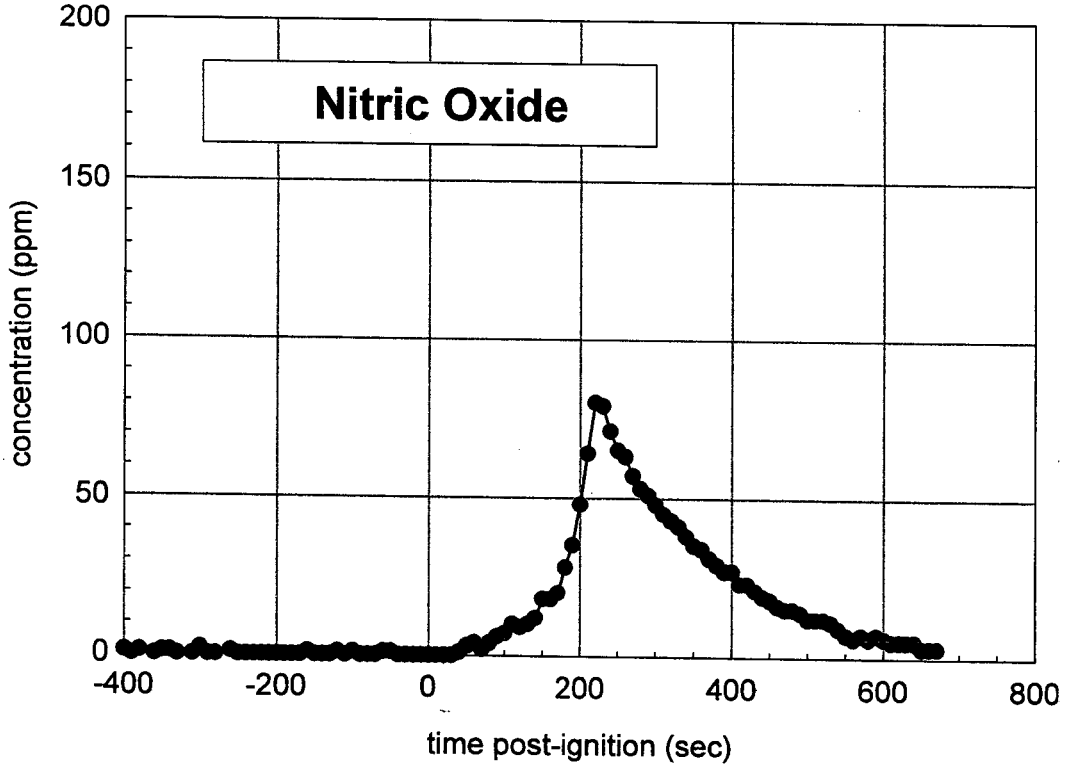

Plot H8. Fire Test F971001. Concentration of nitric oxide (NO) in the passenger compartment determined by FTIR analysis.

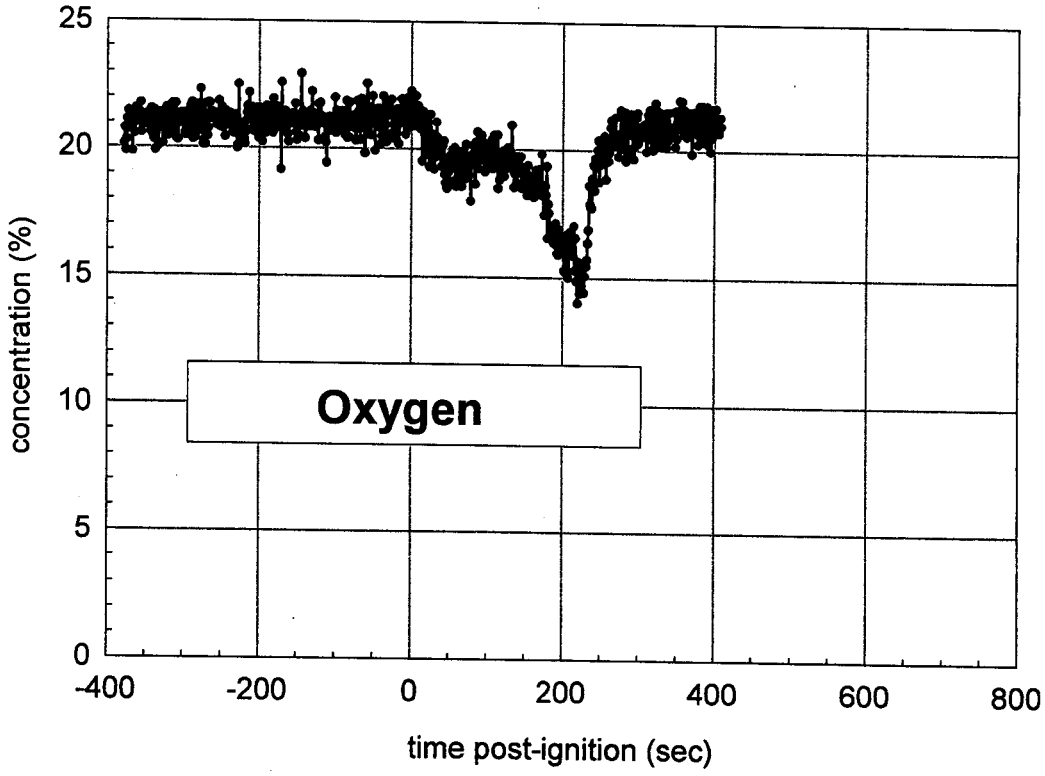

Plot H9. Fire Test F971001. Concentration of oxygen (O_2) in the passenger compartment measured with an electrochemical oxygen sensor.

APPENDIX I
PASSENGER COMPARTMENT COMBUSTION GAS DATA
GAS CHROMATOGRAPHY/MASS SPECTROSCOPY GAS ANALYSIS

The sampling-line for GC/MS samples consisted of a stainless-steel tube (o.d. = 0.250 in. (6.4 mm), i.d. = 0.125 in. (3.2 mm), l = 20 ft (6.1 m)) inserted through the roof between the front seats along the longitudinal midline of the test vehicle (Fig.'s I1 and I2). The inlet of the sample-tube extended approximately 10 in. below the headlining. The outlet of the sample tube was connected to sampling manifold by a length of stainless steel sampling tube (o.d. = ¼ in., length = 25 ft.). The sampling manifold contained five sample cartridges in parallel. Airflow was directed sequentially through the sample cartridges a solenoid-actuated gas-switching manifold. The airflow rate through the cartridges during sampling was adjusted 250 cm^3/min with a rotometer. None of the components of the GC/MS sampling line were heated.

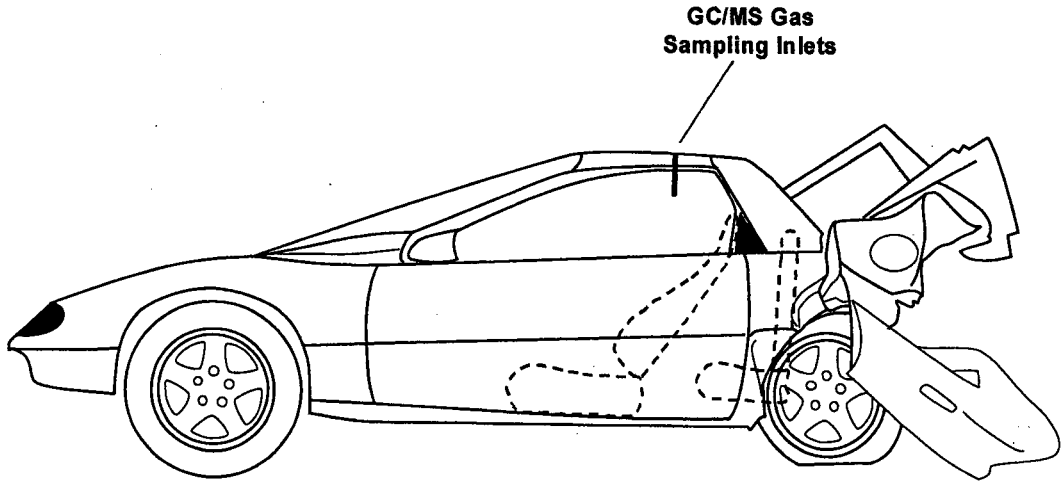

Figure I1. Fire Test F971001. Side-view of the test vehicle show the approximate locations of the FTIR gas sampling inlet and the particulate sampling inlets in the passenger compartment.

Each cartridge was a glass-lined stainless steel tube (i.d. = 4 mm; length = 10 cm; Scientific Instrument Services, Inc, Ringoes, NJ) packed with 25 mg of Carbotrap™ C Graphitized Carbon Black (Supelco, Inc.; Bellefonte, PA) in series with 15 mg of Carbotrap™ Graphitized Carbon Black (Supelco).

After the test, the sample cartridges were analyzed by thermal desorption/gas chromatography/mass spectrometry. Deuterated standards dissolved in deuterated methanol were added to each sorbent cartridge to monitor sample recovery. A modified purge-and-trap concentrator was used for thermal desorption (Model 600 Purge-and-Trap Concentrator, CDS Analytical, Oxford, PA). The gas chromatograph was a Model 5890 Series II Plus Gas Chromatograph (Hewlet Packard, Palo Alto, CA). The mass spectrometer was a Hewlet Packard Model 5989B Mass Spectrometer (Hewlett Packard). The thermal desorption unit was interfaced directly to the split/splitless injector of the gas chromatograph through a cryo-focusing unit. The

injector was operated in the split mode with a split of approximately 10 mL/min. The chromatographic column was a fused silica capillary column coated with 100% methyl silicone (HP-1 ; length = 30 m; i.d. = 0.25 mm; film thickness = 0.25 μm).

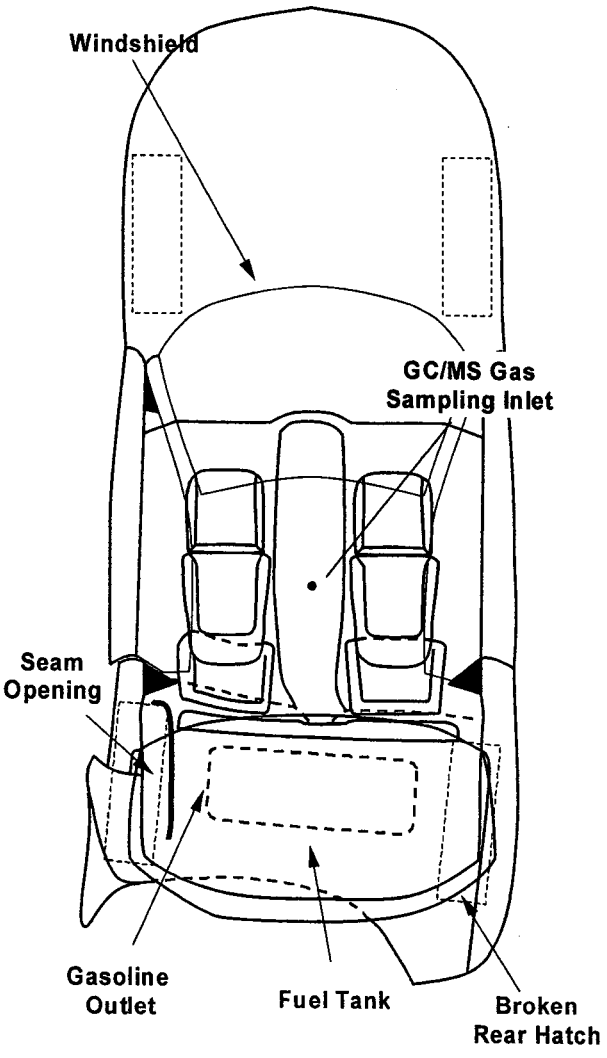

Figure I2. Fire Test F971001. Top view of the test vehicle showing the approximate locations of the GC/MS gas sampling inlet and the particulate sampling inlets in the passenger compartment.

The sample was desorbed at 320°C for 10 min, and cryofocused onto the head of the chromatographic column -80°C. The temperature of the analytical column was maintained at 0°C while the sample was desorbed and cryo-focused. To start the chromatographic analysis, the cryo-focusing unit was heated bullistically to a temperature of 320°C. The column temperature

was programmed from 0 to 325°C at a rate of 5°C/min. Mass spectra were obtained by scanning from m/z 40 to 600 at a rate of 1.2 scan/s.

Plots I1 through I6 show the mass chromatograms of the blank and samples acquired during this test. The sampling intervals in the figure captions were corrected for the time-delay for airflow through the sample-line, which was estimated to have been approximately 25 seconds.

Table I1 lists 68 components tentatively identified from analysis of the mass chromatograms of these samples. The components are listed in order of chromatographic retention time. Identifications were based on the results of a spectral search a commercial mass spectral library (Wiley 275K Mass Spectral Library). Some components were identified by interpretation of their mass spectra. The identities of all compounds listed in Table I1 were confirmed by analysis of authentic standards or comparison to thermal decomposition products from standard polymer samples.

Sample 1 through 5 contained hydrocarbons from gasoline (Plot I2 through I6, and Table I1). In addition to hydrocarbons from gasoline, Samples 2, 3, and 5 contained compounds that are characteristic of thermal decomposition of the polymeric materials in the test vehicle. For example, 2,4-dimethyl-1-heptene can be produced thermal decomposition of poly(propylene) polymers and was detected in Samples 2, 3, and 5. The presence of 2,4-dimethyl-1-heptene in these samples may indicate that some components containing poly(propylene) were thermally decomposing between 80 and 275 seconds post-ignition. Possible sources of 2,4-dimethyl-1-heptene in the test vehicle at this time include the left rear quarter inner trim finishing panel, the rear compartment lift window inner panel cover, and sections of the rear seat covers.

Traces of benzonitrile were detected in Samples 2, 3 and 5 (Plot I2 through I6, and Table I1). Benzonitrile can be produced by thermal decomposition of urethane polymers.

2-Methyl-2-propenoic acid, methyl ester also was detected in Samples 3 and 5 (Plot I3 and I6, and Table I1). 2-Methyl-2-propenoic acid, methyl ester can be produced by thermal decomposition of poly(methyl methacrylate) polymers.

A number of compounds that can be produced by thermal decomposition of poly(styrene) or styrene containing polymers were detected in Samples 2, 3, and 5 (Plot I2 through I6, and Table I1). These compounds include benzene, methylbenzene, 1,2-dimethylbenzne, 1,3-dimethylbenzene, 1,4-dimethylbenzene, ethenylbenene, ethynylbenzene, 1-methylethenyl-benzene, propylbenzene, 2-methylethenylbenzene, 2-propylenebenzene, 1-propylenebenzene, and 1,1'-(1,3-butadiyne-1,4-diyl)bis-benzene). Benzene, methylbenzene, 1,2-dimethylbenzne,

1,3-dimethylbenzene, 1,4-dimethylbenzene, ethenylbenene, and ethynylbenzene also can be produced by combustion of gasoline, and it is not impossible to determine the source of these compounds. 1-Methylethenylbenzene, propylbenzene, 2-methylethenylbenzene, 2-propylene-benzene, 1-propylenebenzene, and 1,1'-(1,3-butadiyne-1,4-diyl)bis-benzene) retain the more complex structure of the backbone of the styrene polymer. The presence of these compounds in Samples 22, 3, and 5 suggests that thermal decomposition of poly(styrene) or styrene containing polymers occurred between about 15 to 275 seconds post-ignition. Other sources of these compounds cannot be rulled-out.

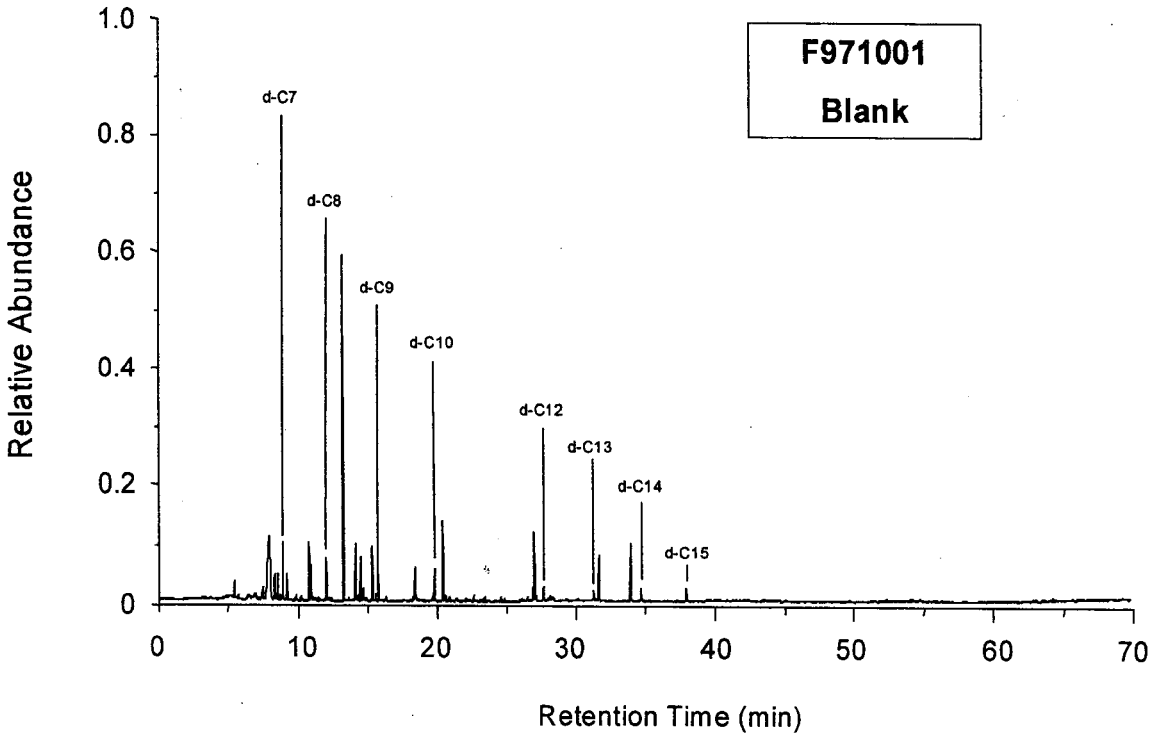

Plot I1. Fire Test F971001. Mass chromatogram from GC/MS analysis of the blank acquired before the test.

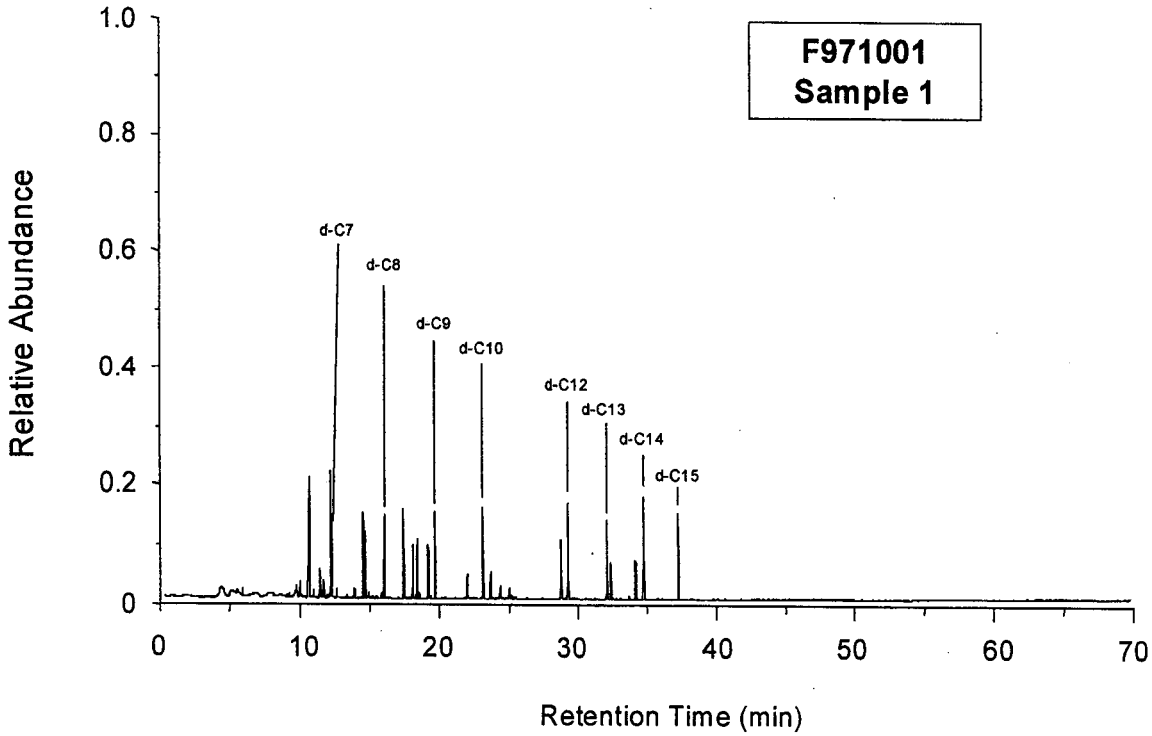

Plot I2. Fire Test F971001. Mass Chromatogram of Sample 1 acquired from -65 to +15 seconds post-ignition.

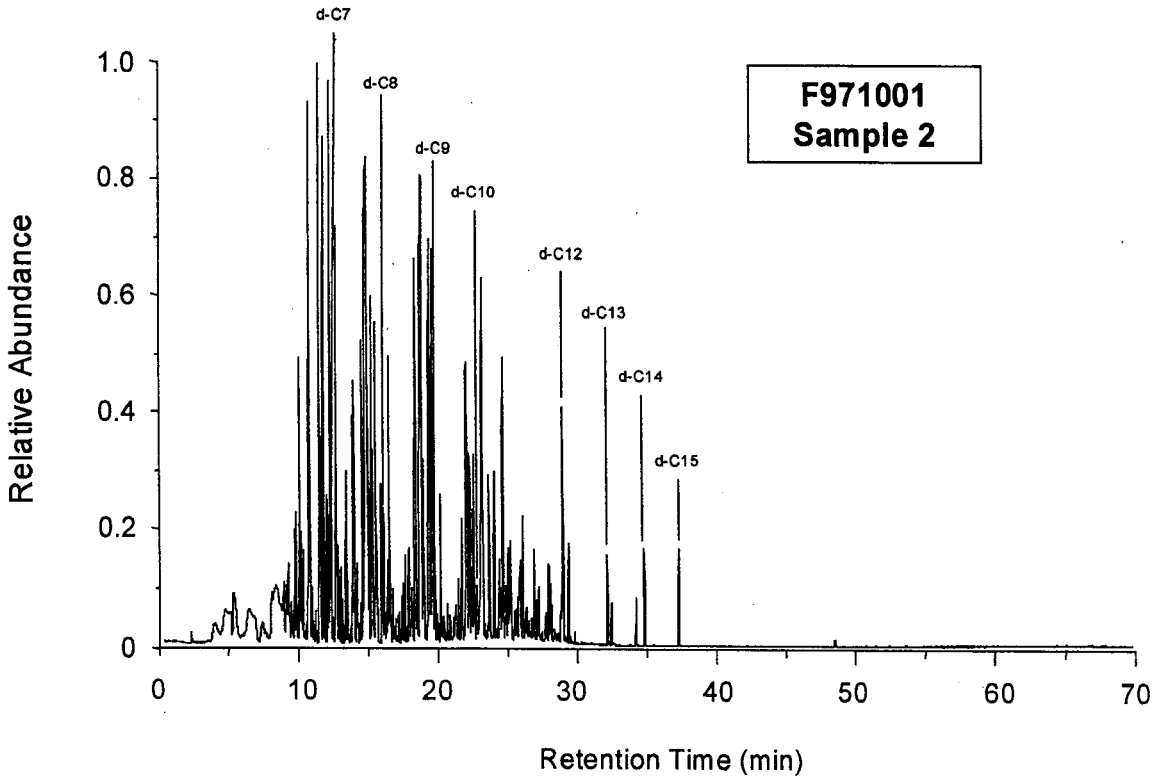

Plot I3. Fire Test F971001. Mass Chromatogram of Sample 2 acquired from +15 to +80 seconds post-ignition.

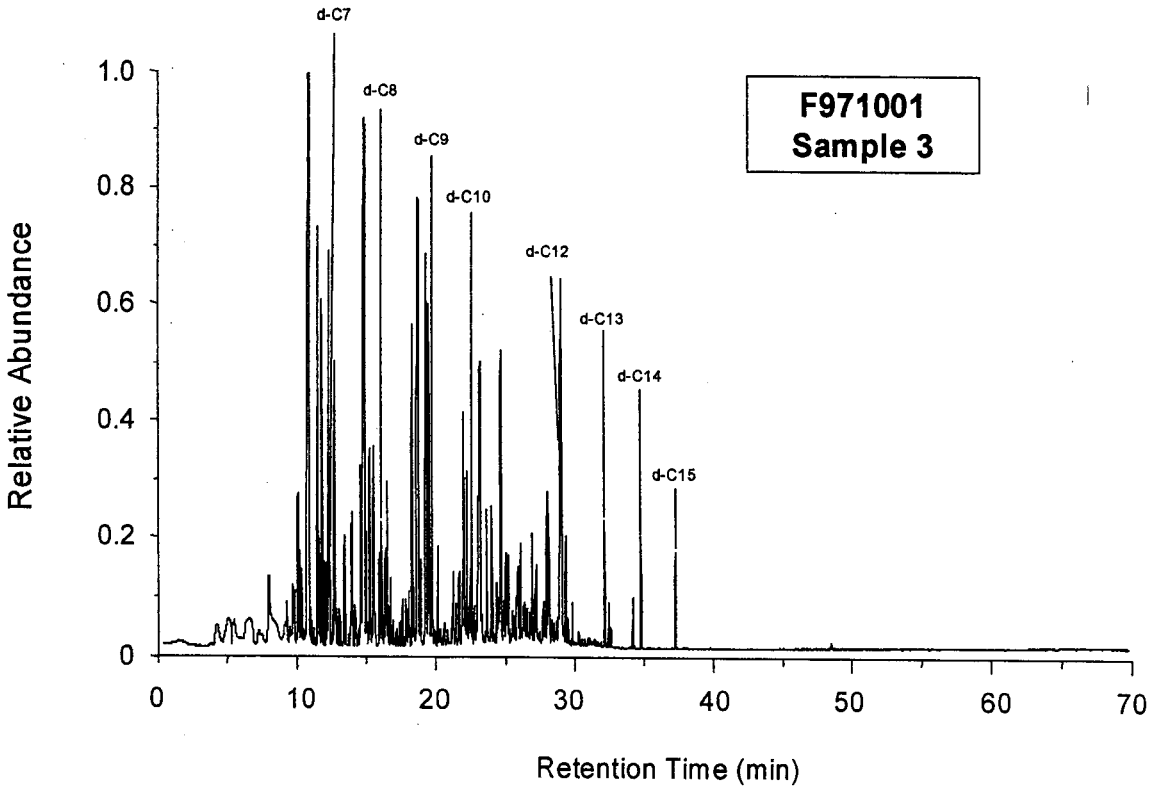

Plot I4. Fire Test F971001. Mass Chromatogram of Sample 3 acquired from +80 to +155 seconds post-ignition.

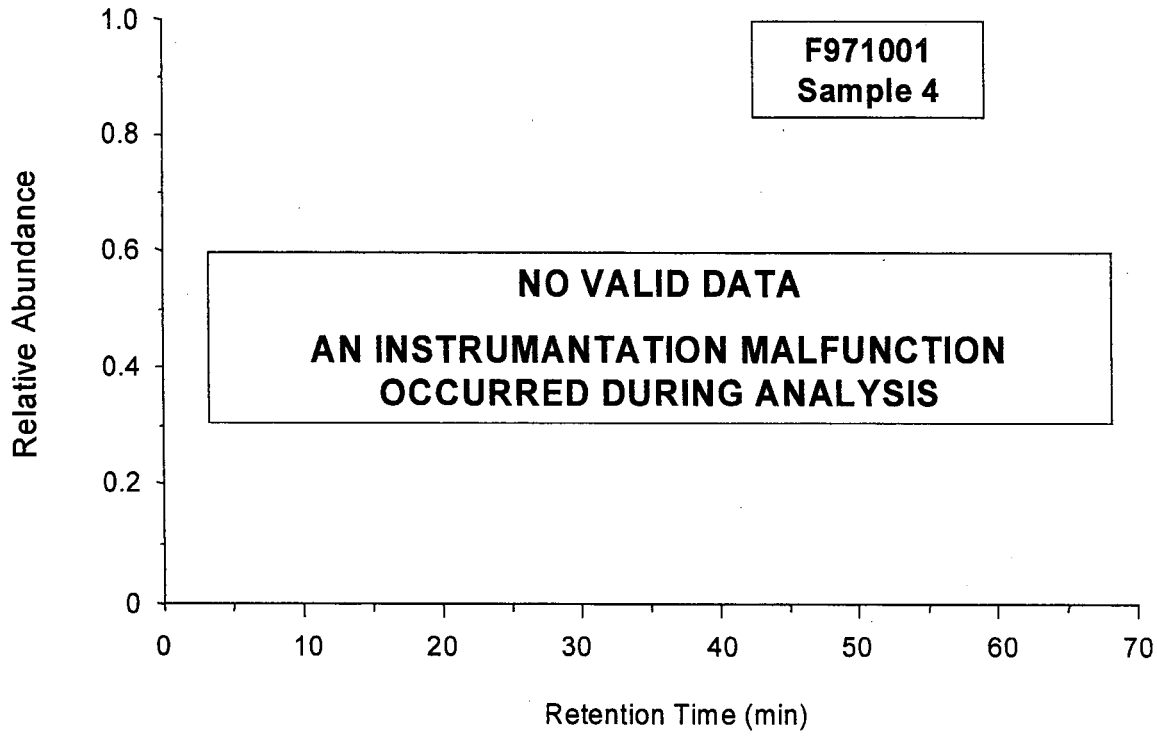

Plot I5. Fire Test F971001. Mass Chromatogram of Sample 4 acquired from +155 to +230 seconds post-ignition.

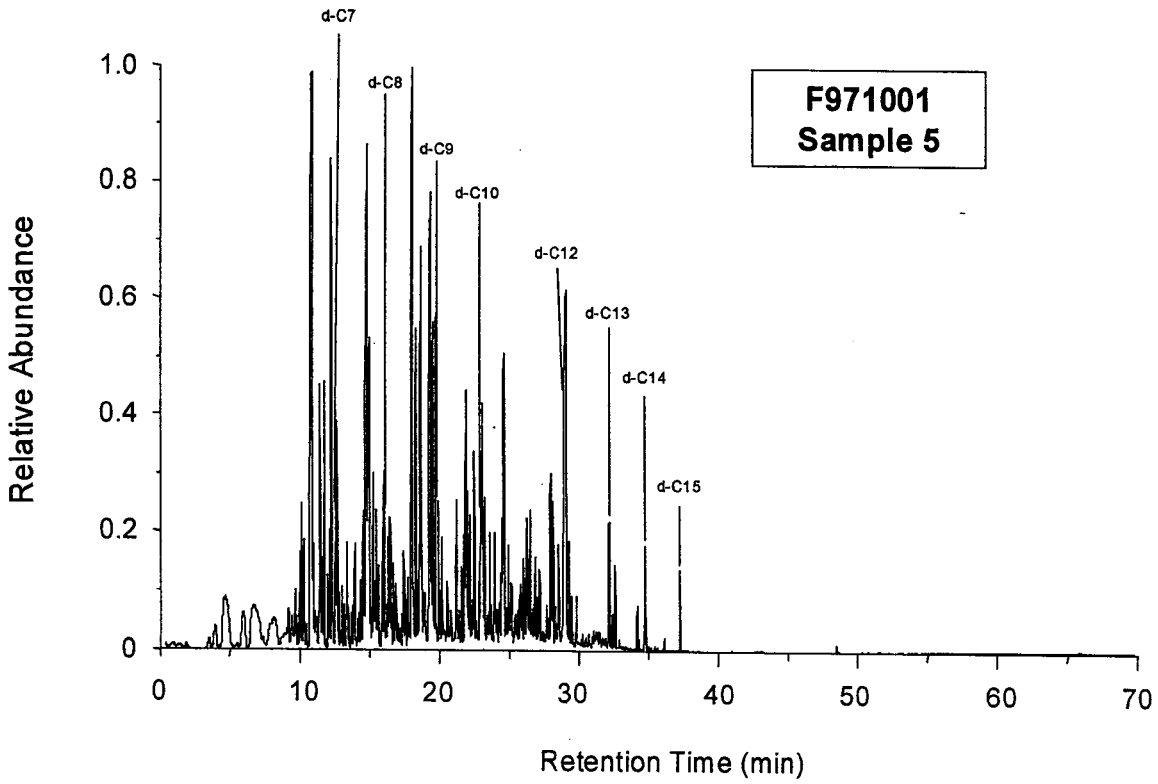

Plot I6. Fire Test F971001. Mass Chromatogram of Sample 5 acquired from +230 to +275 seconds post-ignition.

APPENDIX J
PASSENGER COMPARTMENT
AIRBORNE PARTICULATE ANALYSIS

Five samples of airborne particulate were samples from the passenger compartment during this test. The approximate locations of the inlets particulate samplers are shown in Figures J1 and J2.

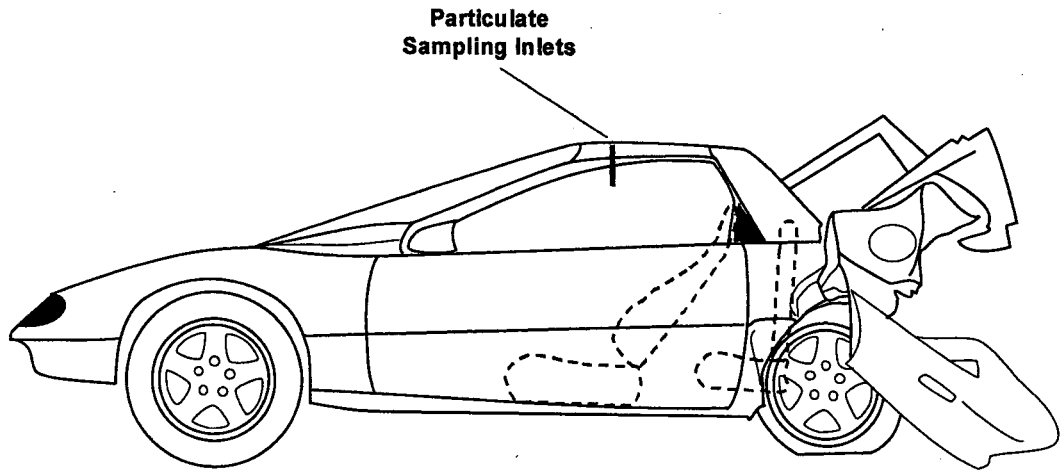

Figure J1. Fire Test F971001. Side-view of the test vehicle showing the approximate locations of the particulate sampling inlets in the passenger compartment.

Each particulate sampling apparatus consisted of an in-line stainless steel filter holder (filter diameter = 47 mm, Gelman Scientific). The inlet of each filter holder was fitted with a straight length of stainless steel tubing (o.d. = ¼ in., o.d. = $^{5}/_{16}$ in., length = 12 in.) using a compression fitting (¼ in., Swagelok). The inlet tube was inserted through the roof of the test vehicle so that it extended below the headlining approximately 10 in.. The outlet of each filer holder was connected to a vacuum manifold using flexible copper tubing (o.d. = $^{5}/_{16}$ in., length = 25 ft.). The vacuum manifold was connected to a pumping system configured to maintain constant flow through the filter holder as the pressure drop across the filter increased due to particulate loading. Qartz-fiber filters were used to collect particulate from the passenger compartment. The filters were placed in an electric furnace at 650°C in air overnight and pre-weighed. The pumping system was adjusted to maintain a volume flow rate of 30 L/min. through a single filter holder. This produced a linear velocity of approximately 29 cm/sec. of airflow perpendicular the face of the filter.

Two blanks were collected for 10 minutes before the test. Samples were collected during the test. In-line solenoid valves fitted to each port of the vacuum manifold and were actuated manually during the test to direct flow through the filter holders sequentially. The time intervals for sample acquisition were the same as those for acquiring GC/MS samples.

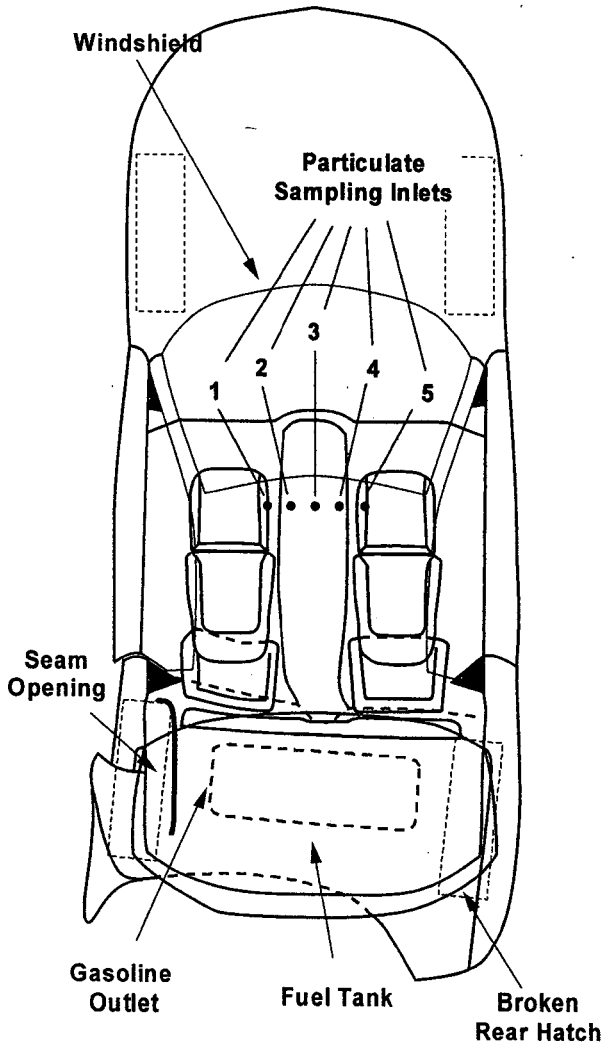

Figure J2. Fire Test F971001. Top-view of the test vehicle showing the approximate locations of the particulate sampling inlets in the passenger compartment.

After the test, the filters placed in a dissector cabinet overnight to remove water absorbed by the filter media and particulate. The weight of each filter was recorded only after constant weight was achieved. The average concentrations of airborne particulate during each sample interval ware determined from the mass of particulate collected, the volume flow rate, and the elapsed time.

A quarter was cut from each filter, weighted, and extracted for quantitative ion chromatographic analysis. The extracting solution was the mobile phase buffer. The chromatography column was an IC-Pak A HC column (Waters, Milford, MA). The mobile phase was a sodium borate/gluconate buffer at a flow rate of 1.8 mL/min [J1]. The chromatographic system consisted of a Model 616 Pump, a Model 717 Autosampler, and a Model 431 Conductivity Detector

(Waters). The following anions were measured in the ion chromatographic analysis: fluoride (F^-), bicarbonate (HCO_3^-), chloride (Cl^-), nitrite (NO_2^-), bromide (Br^-), hypochlorite ($HClO_3^-$), nitrate (NO_3^-), phosphate (HPO_4^-), sulfate (SO_4^-), and oxalate ($C_2O_4^-$).

Table JI shows the concentration of airborne particulate in the passenger compartment during this test.

Table J1
Average Airborne Particulate Concentration

Sample	Sampling Interval (sec.)	Sampling Time (sec.)	Airborne Concentration (mg/m^3)
Blank	n/a	600	0
Sample 1	-31 to +41	72	200
Sample 2	+41 to +107	66	485
Sample 3	+107 to +179	72	1030
Sample 4	+179 to +257	78	225
Sample 5	+257 to +302	45	2350

Table J2 shows the results of the average anion concentration in the airborne particulate. The results shown in Table J2 were corrected for bicarbonate, nitrate, phosphate, sulfate, and oxalate detected in the blanks. All samples contained chloride and bromide. Sample 4 also contained fluoride and hypochlorite.

Table J2

Average Anion Concentration in the Airborne Particulate

Sample	Anion Concentration in Airborne Particulate (μg/mg)[1]									
	F^-	HCO_3^-	Cl^-	NO_2^-	Br^-	$HClO_3^-$	NO_3^-	HPO_4^-	SO_4^-	$C_2O_4^-$
Sample 1	n/d[1]	n/d	36	n/d	2	n/d	n/d	n/d	n/d	n/d
Sample 2	n/d	n/d	37	n/d	2	n/d	n/d	n/d	n/d	n/d
Sample 3	n/d	n/d	32	n/d	1	n/d	n/d	n/d	n/d	n/d
Sample 4	2	n/d	105	n/d	41	2	n/d	56	n/d	n/d
Sample 5	n/d	n/d	58	n/d	6	n/d	n/d	n/d	n/d	n/d

[1] n/d = not detected

REFERENCES FOR APPENDIX J

J1. Method A-102, Waters Innovative Methods for Ion Analysis, Manual Number 22340, Waters Corporation, Milford, MA.